CRANFIELD UNIVERSITY

NICOLA ATTARD MONTALTO

THE CHARACTERISATION AND PROVENANCING OF ANCIENT OCHRES

CRANFIELD HEALTH

PHD

CRANFIELD UNIVERSITY

CRANFIELD HEALTH

TRANSLATIONAL MEDICINE

PHD THESIS

2010

NICOLA ATTARD MONTALTO

THE CHARACTERISATION AND PROVENANCING OF ANCIENT OCHRES

SUPERVISORS: PROF. K.D. ROGERS

DR A. SHORTLAND

APRIL 2010

TO MY PARENTS

ACKNOWLEDGEMENTS

There are several people who have offered me varying degrees of support throughout my PhD and to whom I would like to forward my thanks.

I am forever indebted to both my supervisors, Professor Keith Rogers and Dr Andrew Shortland, to whom I express sincere gratitude. Keith has been amongst one of the most understanding people I have met throughout the course of my PhD, and I was lucky enough to have him as my supervisor. He gave me incredible support, especially towards the end of this thesis, offering indispensible advice when all appeared bleak. I have had the pleasure of working with Andrew since my MSc days in Cardiff, and he has been an inspiring tutor, supervisor and mentor, offering me help and guidance when needed. Thanks to both supervisors for all their incessant support, tutoring, and invaluable help.

I would also like to forward thanks to Dr Mike Edwards from my thesis committee and to all the individuals and organisations, who helped me acquire the archaeological and geological samples for this study, both locally and abroad. Thanks therefore to the Superintendence of Cultural Heritage (Malta), and to Heritage Malta; particularly to Nathaniel Cutajar from the SCH and to Sharon Sultana, Reuben Grima, Prof JoAnn Cassar, Katya Stroud and Mario Galea from HM. Thanks to Tom Hardwick from Bolton Museum for allowing me to sample from their collection of ancient Amarna ochres. I am also indebted to Dr Ruth Siddall, who gave me invaluable assistance with my PLM investigations, and who also provided me with geological material to help in my research. I am grateful to the other members of the Pigmentum Project: Dr Nicholas Eastaugh and Ms Valentine Walsh, who loaned me a large number of earth pigments for this project, as well as further access to the collection. Thanks also to Ian Wright from Shotover Wildlife and to Dr Saviour Scerri from the University of Malta, for helping me acquire geological samples from UK and Malta respectively. I would also like to extend my gratitude to Dr Ian Donaldson from the Royal Society of Chemistry for donating a series of geological samples of banded iron-formations and other iron-rich samples to this project for general observation, and to the Maltese Soil

Information System (MALSIS) group in Malta, for allowing me to sample their collection of soils. Thanks to Peter Tandy from the Natural History Museum in London, for sending me ochre samples from their geology collection for use in my PhD. Thanks also to Tanmay and Mr Tipnis for providing me with my Indian ochre.

Special gratitude ought to be forwarded to all those who assisted me with my laboratory work and statistical analysis. Thanks therefore to Dr Jon Painter and Dr John Rock for their help with the SEM-EDS, and again to Dr Rock with some DSC experiments. Thanks also to Prof Rogers for his help with the XRD, to Jenny Lovell with the FT-IR, Dr Xiao Fang on the Raman spectrometer, Mike Sellwood for his assistance with the PIXE, Dr Dave Lane for our attempts at magnetic testing, and Dr Nick Walsh for the ICP-AES analysis. Special thanks to Dr Trevor Ringrose and his invaluable assistance with Minitab, and to Iain McKay who helped me get hold of most of the literature for this project. Many thanks to my colleagues, work mates and the staff and at Cranfield University, for all the ways they have assisted me.

My gratitude is also extended to those who helped fund my project: The Malta Government Scholarship Scheme (MGSS), my department (DASSR), and School, Cranfield Health. Thanks to Innov-X and to Andrew Clarke for loaning me the handheld XRF for the *in situ* investigations in this project.

I would also like to thank my parents for their invaluable support throughout, especially to my wonderful mother, who proof-read my thesis, helped me with several tedious tasks and provided me with moral support when it was needed the most. Heartfelt thanks to Dan for all his encouragement, advice, for being there for me and for helping me get through this difficult and emotional journey with a smile on my face.

I would like to conclude this lengthy set of acknowledgements by thanking Keith and Andrew, once again, for all they have done for me these past few years.

TABLE OF CONTENTS

LIST OF FIGURES

LIST OF TABLES

LIST OF APPENDICES

ABBREVIATIONS

AAS	Atomic absorption spectroscopy
AES	Atomic emission spectroscopy
AMN	Amarna samples donated
BLN	Amarna samples obtained from Bolton
BSE	Backscattered electron images
CR	Calcitic reds (Malta geological sample group)
Cwa	Cirkewwa (Malta geological samples)
EC	Sia (Cyprus) samples (Pilot Study 1)
EDS	Energy dispersive X-ray spectroscopy
FTIR	Fourier transform infrared spectroscopy
G	Gelmus (Malta geological samples)
Gh	Ghadira (Malta geological samples)
GMA	Gozo Museum of Archaeology
Gr	Greensands (Malta geological sample group)
GTA	Ggantija temples (XRF readings)
GT	Ghajn Tuffieha (Malta geological samples)
GTG	Ghajn Tuffieha Greensands (Malta geological samples)
HYP	Hal-Saflieni Hypogeum (XRF readings)
ICP	Inductively coupled plasma
LIBS	Laser induced breakdown spectroscopy
MC	Margi (Cyprus) samples (Pilot Study 1)
MG	Mgarr (Malta geological samples)
MS	Mass spectrometry
Mv	Mistra village (Malta geological samples)
N	Norfolk samples (Pilot Study 1)
NAA	Neutron activation analysis
NMA	National Museum of Archaeology
O	Ooids (Malta geological sample group)
PC	Principle components
PIGE	Particle induced gamma emission
PIXE	Particle induced X-ray emission
PLM	Polarising light microscopy
PPL	Plane polarised light
RB	Ramla l-Hamra (Malta geological samples)
RBS	Rutherford backscattering spectroscopy
REE	Rare earth elements
RI	Refractive index
S	Shotover samples
SE	Secondary electron
SEM	Scanning electron microscopy
SKB	Skorba (XRF readings)
STA V	Santa Verna (XRF readings)
TAR	Tarxien (XRF readings)
TR	Terra rossae (Malta geological sample group)
XRF	X-ray fluorescence spectroscopy
XRD	X-ray diffraction
XPL	Cross polarised light
XSC	Xaghra Stone Circle (XRF readings)

ABSTRACT

This thesis focuses on the analysis of iron oxides/hydroxides (ochre) for provenancing purposes. It explores the composition of red and yellow ochres used by the Neolithic Maltese through a series of carefully selected optical, structural and chemical methods. These instrumental techniques are defined in an analytical methodology established for this project through a series of pilot studies. A comparative study with ancient ochre from Amarna supports the methodology adopted and outlines the limitations of the sourcing method. Results from the analyses and subsequent statistical tests carried out on data indicate that certain element 'signatures' strongly link the majority of the Maltese archaeological pigments to local sources. These results therefore suggest that, contrary to popular belief, the Maltese archipelago was the likely source for Neolithic ochre. The study disproves the argument for contact with Europe based on ochre trade, therefore indicating that biogeography stands as the most compelling argument for the observed divergence from cultural habits during this Neolithic era.

INTRODUCTION

Ochres are common, yet highly valued pigments and have been used for several thousands of years by numerous ancient cultures across the continents (Herbst 2004). Archaeological evidence clearly indicates that prehistoric man was attracted to the pleasant tones and outstanding properties of these widely available earth colours, which were predominantly extracted from local deposits. Ochres have, in fact, been used for a broad range of purposes, including artistic, ceremonial and medicinal purposes; as colouring materials, body paints, as food and wood preservatives, insect repellents, in tanning processes for hides, for rituals and in funerary contexts (Helwig, 2007; Erlandson, 1999).

This study focuses on the provenancing of ancient ochres through material analysis. Here the chemistry of these archaeological pigments is investigated with the aim of giving supporting evidence that could corroborate and/or challenge current archaeological debates regarding trade between countries. The main case study investigated in this thesis explores the ochres used by the Neolithic Maltese as embellishing and symbolic media during the Temple period. It aims to establish (1) whether there are any possible sources of ochre on the Maltese islands; (2) whether these sources can satisfy the provenancing postulate hypothesis, and therefore be linked to the remaining prehistoric ochre, using a set analytical methodology; and (3) potentially prove/disprove ochre as being the presupposed trade product which definitively proved that exchange between neighbouring countries took place in Neolithic times. This thesis also (4) looks at ancient pigments from the ephemeral

Egyptian city of Amarna as a comparative study, which also serves to validate and examine the limitations of the provenancing methodology used.

Chapter outline

The chapters in this thesis can be summarised in the following outline. Chapter 1 introduces ochres by describing their formation, their use as pigments throughout the course of time, and their properties. This chapter also outlines the principles of sourcing, and the provenancing postulate theory. Chapter 2 provides a description of the geology and Neolithic/Temple period of the Maltese archipelago and therefore focuses on giving an overview of the various aspects of the main case study of this provenancing project. It gives a description of the iron-rich formations on the islands and highlights the importance of this study by describing assumptions made involving ochre and trade between the islands and mainland Europe in the Neolithic era. Chapter 3 focuses on establishing which characterisation methods are best for use in pigment and ochre analysis.

Chapter 4 defines the methodology for characterising ochre, and presents a series of pilot studies implemented for this purpose. It also describes the acquisition of the Maltese geological and archaeological samples; as well as the Amarna samples, and concludes by outlining the statistical methods employed in this provnenacing study. The fifth and sixth chapters are the results and discussion chapters respectively. Chapter 5 therefore underlines the results and data examination for both the Malta and the Amarna projects through a series of descriptive and statistical operations; whereas both Chapter 6 and the Conclusion show the implications of these observations.

Chapter 1.

Ochres: Formation, composition and properties

1.1. An introduction to ochres

A wide variety of materials have arrested human attention throughout history because of their visual characteristics and aesthetic appeal. Their exploitation for use as artistic media has often preceded the discovery of and overall use as materials based on their functional properties (Stafford, Frison et al., 2003). This concept is illustrated exceptionally well through the iron oxides, namely the ores of hematite and goethite, which have been used as ochre pigments for thousands of years (Marsden, 1990; Rapp, 2002).

The term "ochre" is derived from the Greek word *ochros*, meaning pale yellow. It refers to a group of pigments containing a mixture of accessory and/or host phases, and colouring components (Cornell and Schwetmann, 2003: 512). The amount of accessory materials and/or host minerals associated with the natural ochre depends on its source and degree of processing, with all the associated minerals affecting the final tone of the pigment in question (Hradil, 2003). However, iron minerals, especially the oxides and/or hydroxides, are the most important constituents of these ochres, as they are the main colorant agents of these pigments. Their formation within rocks is therefore considered to be important in providing an overall understanding to how ochres form, and how these colouring materials are an overall product of their surrounding environment; an association that is retained even after extraction.

Figures 1-1a, b. Modern yellow ochre beds in Roussillon, France (Krijgsman, 2009)

1.2. The formation of iron ores within rocks

Iron is the third most abundant cationic element on the earth's crust after silicon and aluminium. It is ubiquitous in nature, present in all rock groups, and is therefore constantly channelled in varying forms and degrees of abundance into the global cycle of elements (Maynard, 1983: 10). Iron constitutes about 5% of the earth's upper crust, but is rarely found as a free metal in nature as it readily combines with oxygen, sulphur and other anions (Rapp, 2002: 139, 161). The most common iron ores are iron oxides and, to a slightly lesser extent, iron hydroxides. Sources of these primary (hypogene) ores can also be enriched, chiefly by metamorphism, and by precipitation, dissolution and reprecipitation during rock weathering (Clout, 2006). The alteration stimulators include pH, temperature and water activity; therefore different iron oxides may serve as indicators of the type of environment in which they were formed (Cornell and Schwertmann, 2003: 409).

1.2.1. Formation within igneous and metamorphic rocks

The presence of iron oxides in igneous and metamorphic rocks is of minor importance as their occurrence within these rock formations is limited. Iron oxides fundamentally form as decomposition and/or exsolution products from titomanetites (Fe-Ti oxides) and ilmenites in magmatic rocks. Conversely, the iron-rich minerals in metamorphic rocks are formed from metamorphised sedimentary iron-formations, metabasites, aerobic clay rocks and metamorphosed manganiferous rocks (Cornell and Schwertmann, 2003: 409-412)

Eon	Era	Time-frame	Start (mya)
Phanerozoic	**Cenozoic**	Holocene	0.01
		Pleistocene	1.64
		Pliocene	5.2
		Miocene	23.3
		Oligocene	35.4
		Eocene	56.5
		Paleocene	65
	Meso-zoic	Cretaceous	145.6
		Jurassic	208
		Triassic	245
	Paleozoic	Permian	290
		Carboniferous	362.5
		Devonian	408.5
		Silurian	439
		Ordovician	510
		Cambrian	570
Precambrian	**Proterozoic**		2500
	Archaean		4000
Hadean			4600

Table 1-1. Earth's geological time scale

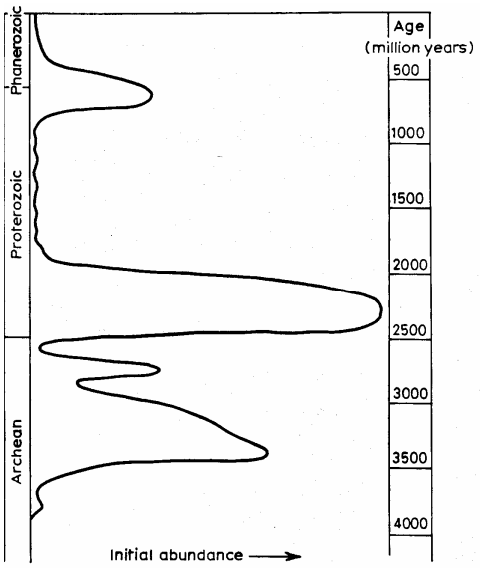

Figure 1-2. Estimated abundance of iron-formation deposited through geological time. Horizontal scale is non-linear, approximately logarithmic; range 0-10 tonnes (from Edwards and Atkinson, 1986: 320)

1.2.2. Formation within sedimentary rocks

Sedimentary rocks are the principal sources of iron and contain both minor and major amounts of Fe ores, with iron-rich sediments containing in excess of 15% Fe. A list of the range of iron minerals present in sedimentary rocks is given on P.10. The classification of iron-rich deposits is rather subjective and is also dependant on the country's geology. It is, however, generally agreed upon that red beds and sedimentary iron ores nominally constitute the more important of the iron oxide sediments (Cornell and Schwertmann, 2003: 412). The majority of these were formed under marine conditions; consequently these rocks often include traces of marine fossils (Tucker, 2001: 182).

The red beds are fairly widespread and mostly belong to the late Palaeozoic, Early Mesozoic and Late Cenozoic periods. They owe their remarkable red colour to the presence of hematite, which is typically formed from the oxidation of magnetite (Fe_3O_4), biotite ($K(Mg, Fe)_3AlSi_3O_{10}(F, OH)_2$), ilmenite ($FeTiO_3$) and goethite (α-FeOOH) (Cornell and Schwertmann 2003: 413). In the latter case, the transformation appears to be diagenetic and favoured with increasing temperature and increasing burial depth (Weibel and Grobety, 1999). Varying grain size of hematite also affects colour, with an overall transformation from red to purple beds as the size of the hematite crystals gets larger (Cornell and Schwertmann, 2003: 414). Goethite is also one of the main iron-bearing minerals in red beds, and is abundant in younger deposits, which have a distinctive yellow-brown appearance (Gualtieri and Venturelli, 1999)

There are two main groups of sedimentary iron ores, the early to middle Precambrian iron formations and the Phanerozoic ironstones.

The iron formations or banded iron formations (BIF), are characterised by their regular layered banding of iron minerals (>15%: usually hematite or magnetite), interbedded with chert and/or quartz (Edwards and Atkinson, 1986: 316; Rapp, 2002: 72-73). The banding may range from a few millimetres to several centimetres in thickness (typically 0.5 – 3 cm thick), and examples of three recognised banding scales in Western Australia are described in Edwards and Atkinson (1986: 322). The four important BIF facies identified are summarised below.

Facies Type	Description
Oxide	Most important, consists of gradations of hematite, magnetite and chert. Carbonate may be present. Typically ~30-35% Fe in rocks. The simplest and commonest BIF consists of alternating layers of hematite and chert
Carbonate	Bands consist of chert, siderite or ankerite and sometimes sulphides. 25-30% Fe
Silicate	Layers of alternating iron silicates (greenalite, stilpnomelane, minnesotaite), magnetite, siderite and chert. 25-30% Fe
Sulphide	Chiefly pyritic (~37%), thinly banded with organic matter and carbon constituting to about 7-8% of the formation.

Table 1-2. An overview of the identified facies in BIF (Evans 1993: 253)

A possible subdivision of the Precambrian BIF has been suggested for the iron formations in North America. Though not satisfactorily fitting for other basins, they have divided them into the Superior (/Lake Superior) and Algoma types; associated with near-shore environments and volcanics respectively (Maynard, 1983: 9; Evans, 1993: 254). The itabirites are a further sub-class to the BIF, and are laminated, metamorphosized, oxide-type BIF (Edwards and Atkinson, 1986: 317). Sometimes 'itabirites' is also used as another term used for BIF, along with jaspillite, hematite-quartzite and specularite (Marsden, 1990: 50; Evans, 1993: 253). Another relatively important sedimentary iron ore occurs in skarns, which are fundamentally a type of Archean age gangue formation (Cornell and Schwertmann, 2003: 417). The great bulk of the iron formations were laid down in a particularly short period of time of 600 years, approximately 2,500-1,900 million years ago (Maynard, 1983: 11; Evans, 1993: 253). It is assumed that their deposition resulted from the combined effect of structural, geological and biological factors, as will be described later.

Group	Mineral	Occurrence	Formula and Description
Oxides	Hematite	Precambrian iron-formations and Phanerozoic ironstones	α-Fe_2O_3 Thin red beds and laminae in the iron formations, also occurs as large, peloidal and oolitic forms, associated with quartz and chert. In ironstones is present as ooids.
	Magnetite	Common in Precambrian iron-formations, found in Phanerozoic ironstones	Fe_3O_4 Grey, interlaminated with chert in iron-formations, forms crystals or granules within oolitic ironstones
	Goethite	Mesozoic and Phanerozoic iron deposits	α-FeO.OH Forms yellow-brown spherical ooids, also can occur with berthierine
	Limonite	Weathering product of, and thus associated with, iron oxides	FeO.OH.nH_2O Poorly defined form of hydrated iron oxide. Contains goethite, other materials such as clay and adsorbed water
Carbonate	Siderite	Major constituent of Precambrian and Phanerozoic iron deposits	$FeCO_3$ Cement to many oolites, is common in non-marine, organic-rich mudrocks as crystals or as nodules, yellow-brown
Silicates	Berthierine	In most Jurassic ironstones	$(Fe_4^{2+}Al_2)(Si_2Al_2)O_{10}(OH)_8$ Occurs as ooids, flakes; commonly distorted, is a green, early diagenetic mineral
	Chamosite	Found in most Palaeozoic ironstones	$(Fe_5^{2+}Al)(Si_3Al)O_{10}(OH)_8$ Forms from berthierine, similar structure, cemented by siderite or calcite
	Greenalite	Precambrian iron deposits	$Fe_6^{2+}Si_4O_{10}(OH)_8$ Rounded to subangular green pellets, with little internal structure
	Glauconite	Form greensands, ancient and modern	$KMg(FeAl)(SiO_3)_6.3H_2O$ Green, pellets and aggregates up to 1mm diameter
Sulphides	Pyrite	Common in many iron-rich sediments, but they rarely form the major part	FeS_2 Grains and cubic crystals, may form spherical aggregates (framboids), yellow crystals
	Marcasite	Rare, associated with pyrite	FeS_2 Dimorph of pyrite, forms nodules in chalk

Table 1-3. The common iron minerals in sedimentary rocks (adapted from Marsden, 1990: 48 and Tucker, 2001: 182-188)

The second group of iron ores are the ironstones. These date back to the Phanerozoic era and cover the time span between the Ordovican and Tertiary eras (Cornell and Schwertmann, 2003: 417). The main minerals contained in these ores are usually goethite, chamosite, hematite, berthierine and siderite, which, in contrast to the iron formations, are intimately mixed. They also contain less SiO_2 and more Al and P than the BIF, and in places the chamosite has been observed to grade into kaolinite (Maynard, 1983: 9, 20, 50). Ironstones are predominantly oolithic in character, consisting of spheroids of Fe accumulations that suggest (an almost) concentric precipitation of the iron and/or iron oxide, often around a detrital core (Cornell and Schwertmann, 2003: 419). The oolith bodies are typically hardened, and are either perfectly rounded, or encompass a slightly off-centre nucleus, which makes them irregularly shaped. These are termed concentric- and eccentric-type ooliths respectively (Maynard, 1983: 50). The ironstones are sometimes further sub-categorized into Clinton and Minette types based on their internal constituents (Evans, 1993: 257; Clout, 2006).

1.2.3. Formation and transportation of iron

There are no modern analogues for the formation of iron-deposits; hence suggested methods for formation and transportation of iron are purely hypothetical (Tucker, 2001: 182). Speculations suggest a combination of structural, geochemical and biological factors, which include processes of continental weathering and volcanic-hydrothermal activities, as explained below.

The Lower Proterozoic was marked by a series of structural changes, which led to the development of shallow intercontinental troughs and marginal basins that provided numerous sites for the deposition of iron formations (Edwards and Atkinson, 1986: 317). The incipient iron is presumed to have originated from sub-aquatic volcanic activity, or from continental landmasses, and was then carried to the sea through rivers. Because of its low solubility in natural waters due to the pH and Eh ranges present, the iron was transported as the highly insoluble ferric hydroxide [$Fe(OH)_3$] either: (i) as a colloidal suspension, stabilized in the presence of organic matter, or (ii) by adsorption and chelation onto organic matter or (iii) by transportation on clay minerals, either as part of the clay structure, or as oxide films on the surface of clays (Tucker, 2001: 182).

Although many queries still need to be resolved, it is believed that formation of the principal iron minerals hematite and goethite involved the diagenetic transformation of iron from its trivalent ferric state as $Fe(OH)_3$ to its divalent, ferrous (Fe^{2+}) form. This process is to a large extent dependant on changes in the pH and the Eh of the surface and diagenetic environments, the concentration and activity of carbonate and sulphide ions in solution, and the presence of organic matter (Tucker, 2001: 182). The ferric hydroxide precursor is stable at the higher pH levels under more oxidising conditions such as those experienced in natural environments; whereas Fe^{2+} is stable under more acidic and more reducing conditions. Organic matter considerably affects the Eh in natural aqueous environments by promoting oxygen consumption by photosynthetic bacteria. These subsequently create favourable oxidising conditions for the depositing of the ferric (Fe^{3+}) hydroxide.

The ensuing oxidation/reduction breakdown processes therefore result in the precipitation of iron oxides and other iron minerals, which is strongly dependant on the chemistry of the contiguous environment, the oxygen content and the water-sediment depth. This scheme thus summarises the formation of the Precambrian iron formations, which were formed by seasonal precipitation from sediments rich in silicon, iron and organic matter at particular redox potentials and water depths. Here, the metastable phases (such as ferrihydrite and chert) were converted to hematite by bacterial action and diagenesis (Cornell and Schwertmann, 2003: 417). Thermodynamic plots (Figure 1-3) suggest that hematite is the most likely mineral to be formed (most stable) in a moderately to strongly oxidising environment and low original organic content conditions; hence in shallow, well-oxygenated water (Edwards and Atkinson 1986: 321).

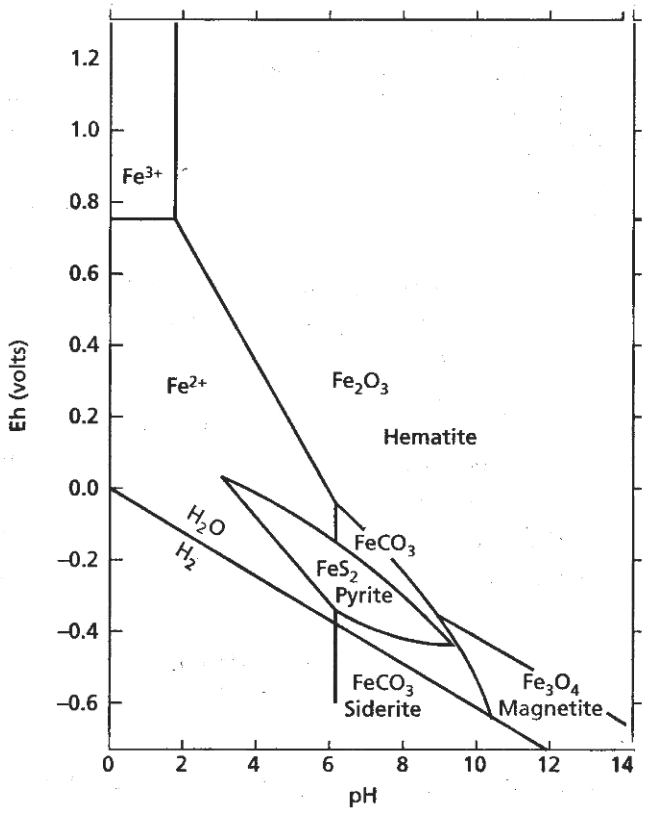

Figure 1-3. Eh-pH diagram for iron oxides and iron ores. This shows that hematite is stable in moderately to strongly oxidising environments, whereas the other minerals are stable in reducing environments and are dependant on the concentrations of carbonate and sulphide in solution (from Tucker, 2001: 185)

Environment	Characteristic Phases
Oxic	Hematite, goethite, MnO_2-type minerals, no organic matter
Anoxic 1) Sulphidic	Pyrite, marcasite, rhodochrosite, organic matter
2) Non-sulphidic a. Post-oxic	Glauconite, berthierine, no sulphide ores, minor organic matter (also siderite, vivianite, rhodochrosite)
b. methanic	Siderite, vivianite, rhodochrosite, earilier formed sulphide minerals, organic matter

Table 1-4. Characteristic phases formed in early diagenetic environments

While goethite is formed directly from the dehydration of $Fe(OH)_3$ by heating and/or ageing (Maynard, 1983: 22), it can be seen that the formation of the ferrous minerals pyrite, siderite and magnetite is strongly dependant on reducing conditions and on the carbonate and sulphide ions present in solution. This implies that the minerals are formed during early diagenesis where the Fe^{2+} is liberated by bacterial activity in the sediment. A negative Eh also prevails in this environment, owing to bacterial decomposition of the organic matter present, therefore promoting this reaction. The ferrous minerals consequently form as follows (from Tucker, 2001: 185):

1) *Pyrite* (FeS_2): Sulphate present in solution (common in seawater) is reduced by bacteria present in sediments to H_2S. This reacts with the liberated Fe^{2+} to form metastable iron sulphides: *mackinawite* and *greigite*, which are eventually transformed to pyrite during diagenesis. Pyrite can also form in association with the bacterial reduction of sulphate in gypsum.

2) *Siderite* ($FeCO_3$): Precipitates when high carbonate and low sulphate levels are present (in a methanic environment). It is more common in non-marine sediments which contain less sulphates.

3) *Magnetite* (Fe_3O_4): Formed when carbonate and sulphide levels are low and with negative Eh and neutral pH conditions. Since such an environment is rare, magnetite precipitation in this manner is uncommon.

4) *Iron silicate minerals*: These include berthierine, chamosite, greenalite, glauconite; precipitation is not completely understood, but could occur in reductive, post-oxic, diagenetic environments.

These sedimentary iron ores may be further modified by both metamorphism when exposed to high temperatures, and by oxidation and/or weathering when exposed to atmospheric conditions (Maynard, 1983: 15). This results in the formation of a "gossan" (aka "gozzan" or "iron-hat": refer to Figure 1-4 below), an oxidised outcrop iron ore deposit, a layer that is often used as an indicator of a buried ore deposit (Cornell and Schwertmann, 2003: 420). Goethite in ironstones, for example, may have resulted from the oxidation of siderite or other ferrous minerals on exposure to ambient conditions (Equation 1-1 below), even from specular hematite through dissolution or reprecipitation. Hematite, though generally a primary mineral, can also be synsedimentary and be formed in berthierine after exposure of the grains to a more oxidising environment (Tucker, 2001: 186).

$$4FeS_2 + 15O_2 + 10H_2O \rightarrow 4FeOOH + 8H_2SO_4$$

The weathering of pyrite, resulting in the formation of goethite as a gossan. Sulphuric acid also forms, termed "acid mine drainage"

Equation 1-1. The oxidation of siderite

1.2.4. Supergene enrichment

It is assumed that the superior-quality ochre deposits form by a process known as supergene enrichment of the iron orebodies, typically from the sedimentary iron formations. The process involves the uplift and mobilization of gangue material (e.g. silicates and silica) from the iron-rich sediments by means of hydrothermal solutions (Maynard, 1983: 16), or by circulating and/or downward-moving ground waters via basinal de-watering (Carney and Mienie, 2003; Clout, 2006).

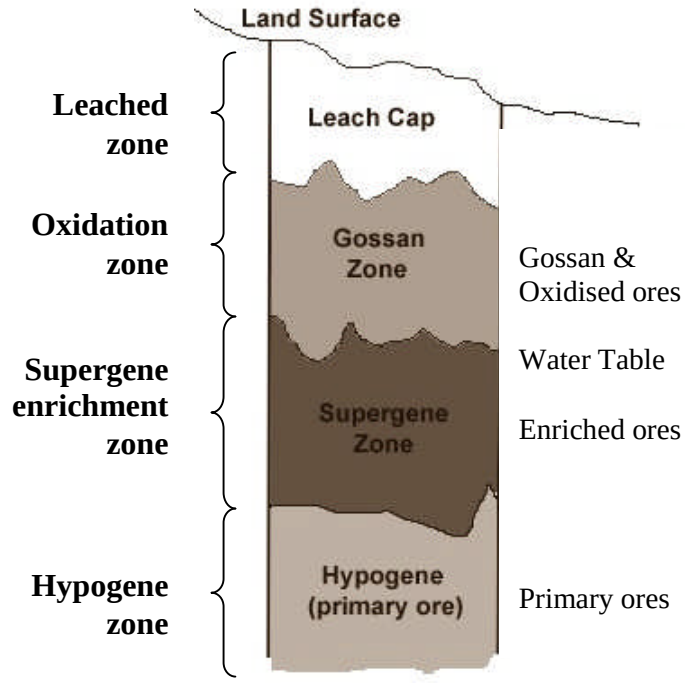

Figure 1-4. Overview of the supergene enrichment process (adapted from Rapp, 2002: 177; Clout, 2006)

Consequently soluble gangue material and lower-grade, porous iron minerals are leached out of the iron formations and flushed through the regional stratigraphy (a process intensified if the BIF is underlain by impervious formations), resulting in a considerable enrichment in metal values. The ensuing voids are characteristically filled by iron minerals, typically hematite, leaving a compact, purer, high grade iron-rich sediment of low porosity (Evans, 1993: 39, 267; Clout, 2006). Other metals such

as Cu, Ni, Co, Zn and Pb are also dissolved and usually co-precipitate with the Fe compounds via isomorphous substitution (Oliveira, Imbernon et al., 1996). Over time, voids would develop and overlying strata could collapse into these cavities, leaving the enriched ore preserved in deep sinkholes (Carney and Mienie, 2003). Further gradients in the redox potential, usually along continental shelves in shallower waters stimulate the formation of ironstones. These ooids also require mobile Fe^{2+} ions as a source of iron and are therefore said to be exclusively of supergene origin with foreign elements present reflecting the growth environment (Cornell and Schwertmann, 2003: 418; Evans, 1993)

The essential conditions for the genesis of supergene iron ore involve:

1) Iron-rich deposits (e.g. BIF) as a source of iron and as a target for enrichment;
2) Imperpeable/poorly permeable beds e.g. shales, above and below iron-rich deposits;
3) Suitable open structures, such as plunging synclines, together with deep-water access through e.g. fracture zones to initiate the system of enrichment;
4) Suitable geochemical conditions, including exposure to the atmosphere;
5) Suitable electrochemical conditions to achieve desired redox potential gradients;
6) Stable tectonic conditions for extended periods of time (Morris, 1998).

Examples of BIF sites that experienced such enrichment processes have been discussed in Evans (1993), and include the Hamersley Basin (Edwards and Atkinson, 1986: 326) and Mount Tom Price in Western Australia (Clout, 2006; Thorne, 2006), Cerro Bolivar in Venezuela, with the richest Fe-source being the N4E Mine in the

Carajas region of Brazil (Evans, 1993: 270). Another recognised mine for commercial-scale exploitation of hematite is the Sishen Iron Ore Mine in Southern Africa, which has been in use since 2,000 B.C. (Carney and Mienie, 2003). One of the largest iron ore mines in the world (BIF: hematite and goethite) is Mount Whaleback in the Pilbara district of Western Australia (Clout, 2006).

Many iron ore deposits are therefore residual deposits, which are subjected to further weathering throughout the course of time. These weathering processes continually remove the more soluble minerals within the formations, and the ferric iron oxides and hydroxides remain as residual deposits. Ferric oxide content is said to be indicative of the quality of these pigments and typically varies between 15 – 70 % (Helwig, 2007). The main mineral within these more recent deposits is most often goethite, FeOOH, which was probably the first iron ore to be exploited as ochre (Rapp, 2002: 55).

Ochres have been used abundantly by mankind throughout the course of time. There are relatively few ochre beds specially recommended as sources in historical records, yet existing evidence indicates probable trading of iron oxide pigments between ancient groups, undoubtedly because certain high-quality red ochres were especially valued by these peoples (Scott and Hyder, 1993; Rapp, 2002: 162). Both archaeological and ethnographic data also suggest that high-quality red ochres were quarried systematically at a limited number of discrete regions because these peoples were conscious of the superiority of certain ochres and thus sought out particular varieties for their specific characteristics (Rapp, 2002: 199).

1.3. Use of ochre throughout history

"Prehistory has produced evidence for two meaningful regularities in human evolution: tool making and the collection and use of ochre" (Wreschner, 1980: 631)

Ochre has played an important role in early human activities, having been used for several thousands of years by peoples all over the world. Though its frequency of use was never consistent, it is a recurring archaeological theme, with a transcultural character of exploitation that has remained relatively consistent throughout the course of time. The mineral pigment was used in social and cultural activities, as a material that infused the dull surfaces it was applied to with a colourful, visual appeal. Ochre is therefore associated with cultural expression through its use in the art, customs, rituals, magic, symbolic behaviour and the religious beliefs of man from the Upper Palaeolithic through to the contemporary world and present day (Taçon, 2004: 37).

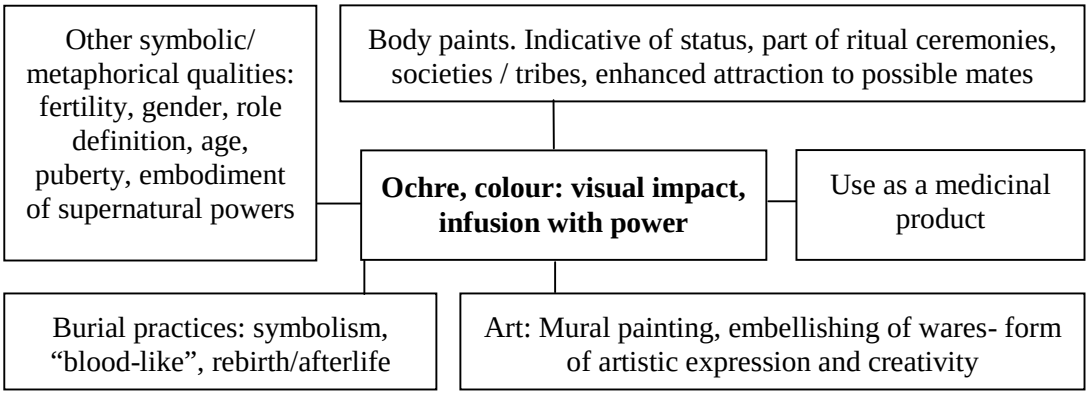

Figure 1-5. Possible uses of ochre (adapted from Boivin 2004)

Although it is debatable as to whether ochre associated with the lower Palaeolithic actually implied use, the earliest possible evidence for ochre exploitation is thought to be at Olduvai in a context dating from more than 498,000 B.C. (Rapp, 2002: 199).

Prehistoric man was undoubtedly attracted to the iron ore it for its colour, and collected and transported it for use over large distances (Wreschner, 1980; Helwig, 2007: 47). The discoveries at the site of la Chapelle aux Saints in France indicate that ochre must have played an important role in burial customs for the Neanderthal man. Several pieces of the mineral were found in a grave dating back to the Mousterian culture (c.70,000 – 40,000 B.C.), which also contained many funerary items, therefore probably having a key role in the man's survival in an afterlife (Schmandt-Besserat, 1980: 128). It also appears that pieces of ochre were collected and prepared by deliberate shaping of the ends for use as 'pencils' or 'crayons' for a facilitated application of colour directly onto a surface. The ochre 'crayons', some found with worn out tips marking unquestionable evidence of use, ranged from red to yellow to red-brown, possibly also indicating colour manipulation through heating of the mineral; an impressive achievement so early on in the history of mankind (Wreschner, 1976; Tacon, 2004: 32).

Event timeline	Culture	Period B.C.
Middle Palaeolithic	Mousterian (Neanderthal man)	70,000 – 40,000
Upper Palaeolithic	Châtelperronian	40,000 – 29,000
	Aurignacian	29,000 – 22,000
	Gravettian	22,000 – 18,000
	Solutrean	18, 000 – 15,000
	Magdalenian	15,000 – 10,000
Epipalaeolithic/Mesolithic		12,000 – 8000
Neolithic	Pre-Pottery Neolithic A (PPNA)	10000 – 8500
	Pre-Pottery Neolithic B (PPNB)	8500 – 6500
	Pottery Neolithic (PN)	6500 – 3500

Table 1-5. Stone age timeline (adapted from Schmandt-Besserat, 1980)

Although it is still uncertain as to why ochre was considered to be an important material for survival in life after death, it is generally thought that the intense red colour symbolised blood, the analogy of life; possibly rebirth and a continued existence in this or another world (Stafford, Frison et al., 2003; Tilley, 2004: 140). This supposition is especially favoured as red ochre was preferred over the yellow equivalent of the pigment, and because the red colour was often used in connection with fertility symbols deposited with the dead in the Palaeolithic (Wreschner, 1976; Vassallo, 2007). Although ochre was not ubiquitous amongst grave goods in all burials, the material has been found in fifteen other sites reminiscent of this Mousterian culture (Wreschner, 1980; Schmandt-Besserat, 1980: 128). As in Terra Amata, the proof that the ochre fragments were used as colouring media is evidenced by the worn/smooth and/or pointed or shaped ends. Other ochre pieces bear traces of having been scratched into with pointed tools, undoubtedly for exploitation of the extracted powder as a pigment, as shown in Figure 1-6 (Hovers, Ilani et al., 2003).

The earliest phase of the Upper Palaeolithic, the Châtelperronian period in Europe (c. 40,000 – 29,000 B.C.) indicated that ochre began to play a predominant role in human society, where it was extensively used in burials and rituals, and in human settlements. Evidence also shows effort put into pigment preparation (such as at the site of Arcy-sur-Cure near Paris), with traces of ochre visible on slabs and pestles indicating grinding. Further preparation is observed in ochre found associated with hearths and camp fires, implying calcination for colour manipulation (see later). Other discoveries include the apparent development of palettes for colour mixing, and balls of ochre containing and/or intermixed with flint or bone (Schmandt-Besserat, 1980: 129-130).

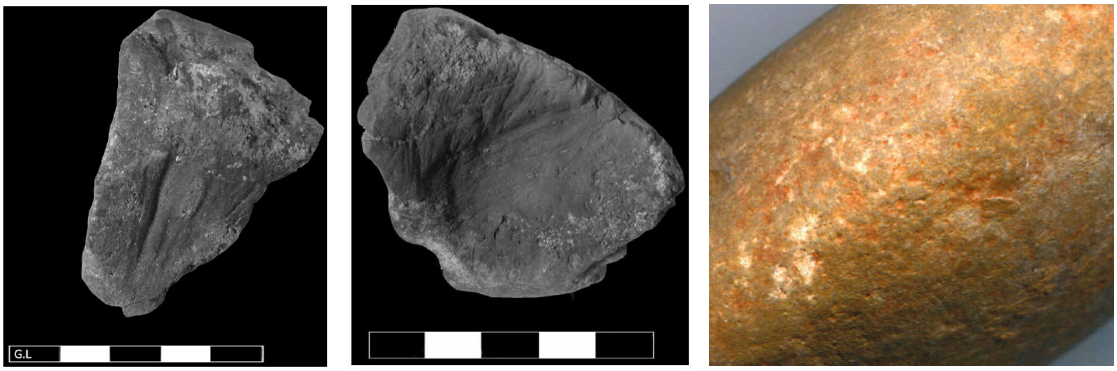

Figures 1-6 a-c. Two views of an ochre piece from Qafzeh Cave showing striations indicative of heavy scraping off the lump (Hovers, Ilani et al., 2003), and a grinding stone from Slovenian Late Paleolithic sites (Ciganska jama, Lukenjska jama) indicating pigment preparation (from Petru, 2006): size not given

Figures 1-7 a-c. Red ochre found in graves of three infants uncovered just over two years ago in the ~27,000 B.C. Stone Age camp of Krems-Wachtberg in Lower Austria. Scale rules marked in 5 cm (a, b) and 1 cm (c) (Einwögerer, Friesinger et al., 2006)

The earliest definite intended use of ochre in the first type of figurative art, namely in rock-art paintings, was experienced with the Aurignacian culture (29,000 – 22,000 B.C.), the period in which the presence of the *Homo sapiens* is fully attested. Famous examples include those at the sites of La Ferrassie and Abri Castanet, and the first human representations appear later in the Gravettian culture (c. 22,000 – 18,000), which also shows an abundance of ochre associated with Upper Palaeolithic burials extending from England, through Europe, all the way to Russia (Schmandt-Besserat, 1980: 131-133).

Although there appears to have been a decrease in the use of ochre associated with the Solutrean culture between 18,000 – 15,000 B.C., the Magdalenian period (15,000 – 10,000 B.C.) saw the culmination of the mastery of use of this pigment by Palaeolithic man. This is especially evident in the caves at Lascaux (France) and Altamira (Spain), with impressive animal representations of horses, bison and cattle, painted in a wide range of colours including blacks, yellows, yellow-browns, browns, and various intensities of reds. The wall paintings realise astounding effects through the naturalistic depictions and intense, expertly applied colour (Hradil, Grygara et al., 2003).

Figures 1-8 a, b. A cave painting in Lascaux, France (c 15,000 BC) and another in the vicinity of the village of Vallon - Pont-d'Arc in southern France (Lewis, 1995; Davis, 2004)

Ochre use in Europe predated use of the pigment anywhere else across the globe, and use in Australia, for example, dates back to at least 63,000 to 41,000 B.C. at sites including Malakunanja II, Nauwalabila in Laladu National Park and in western New South Wales, where the pigment was used as 'crayons' and in burial practices (Taçon, 2004: 32). The Levantine North African contemporaries of the upper Palaeolithic also used red pigments, albeit on a much smaller scale. In sharp contrast, the Natufians (the original black Africans of Israel) were more sedentary; resulting in the introduction of

novel activities, and painting in ochre appears to have been one of them (Weinstein-Evron and Ilani, 1994). Red ochre once again appears to have been used in burials, with lumps, painted skulls and even painted plaster flooring unearthed in certain burial pits found associated with these cultures (Wreschner, 1980).

Period	Location	Use
298,000 – 228,000 B.C.	Terra Amata, near Nice, France (Schmandt-Besserat, 1980), and from the Lare Acheulican sites of Ambrona	Earliest evidence of use in Europe
Paleolithic period Before 10,000 B.C.	Chumash Indians of California Chinese and Japanese graves (Robinson, 2004), Egypt	Extensive use for artistic, burial and ritual purposes: quite well documented. Red ochre was commonly used to colour skeletons, sometimes cinnabar was applied to the skulls.
Neolithic Period Start 10,000 B.C.	Catal Hüyük, Turkey (Schmandt-Besserat, 1980), China and Japan	
Unified Silla period ~668 – 935 A.D.	Korea (Winter, 1989)	
Ayurvedic period ~ 520 B.C.	India (Ray, 1956)	Synthetic production in the context of medicinal materials
Roman Empire 510 B.C. – 476 A.D.	E.g. Pompeii, Italy	Red earth most commonly used red pigment for wall decorations
Middle ages to today Start ~500 A.D.	Worldwide, particularly mentioned in treatises for Italian artists (Theophilus, Cennini)	Typically used for flesh tones, preparatory drawings in frescoes, as base colours, in mordants and in bole for water gilding. Also synthetically produced from iron for enamel and glass décor

Table 1-6. History of use of ochre pigments (from Helwig, 2007: 46-52)

In the Neolithic period, which started in Europe c. 8000 B.C., ochre was clearly regarded as a popular, prominent colouring material, and was applied in vast quantities. It was has also been found in cosmetic sets of many women's graves, either as compressed pigment in shells or mixed with fat for use as rouge. This period saw workshops designated to pigment preparation by grinding and storing in cake-like

lumps, as seen in the prehistoric towns of Beidha (Jordan, 7,200 – 6,500 B.C.) and Ali Kosh (Iran, 6600 to 6000 B.C.).

Ochre continued to dominate in pigment use for mural painting and pottery decorations throughout history as is summarised in Table 1-6. These iron ores, were, however, only the start to the discovery of a whole new world of pigments which were exploited by our predecessors to varying extents and at various periods throughout the course of time. Ochre nevertheless remains an "index fossil" for evolution (Wreschner, 1976), being a direct, remaining record of human development and an abstract representation of behaviour.

1.3.1. Other Pigments commonly associated with Ochre

Analysis of finds and documentation in artists' manuals has shown that ochres have been used in conjunction with certain other pigment varieties, either for certain ritualistic purposes, or merely to imitate some other colour. The more important pigments are listed below:

- *Cinnabar* – is the native form of red mercury (II) sulphide (HgS). This pigment has been used with red ochre in various Paleolithic and Neolithic tombs in Turkey, Korea, Japan and China to colour skeletons – sometimes cinnabar was used to colour the head, whereas the ochre was used to cover the rest of the body (Helwig, 2007: 47). Mercuric sulphide has also been used in association with the ochres by the Egyptians, but only after the seventh century B.C. (Colinart, Delange et al., 1996). It has also been interchanged with red ochre by Roman artists, though the ochre was preferred because of its lower cost and higher stability.

- *Jarosite* $KFe_3(SO_4)2(OH)_6$ and *natrojarosite* (with Na substituting the K), a yellow pigment commonly found in Egyptian wall paintings, is naturally occurring and at times used as an ochre substitute as the colours are similar.
- The earliest significant exploitation of *galena* (PbS) in North America occurred in the 2nd millennium B.C. where small pieces were placed in burials together with red ochre (Rapp 2002: 174).
- *Vermillion* is also mercury (II) sulphide, but a synthetic variety. It has been recommended as a chief component for flesh tones (with lime and red earth) in Thompson's (1960) artist's manual.
- *Red Lead* – Lead (II,IV)-oxide, or *minium* - is found mixed with red ochre in murals in the Mogao grottoes near Dunhuang, China. It has also been recorded by Pliny to have been used in conjunction with the ochre to produce *sandyx*/*syricum*, a cheaper cinnabar-like colour which could be used on classical frescoes without any colour alteration.

1.3.2. Painting in ancient Egypt

The artistic capabilities of the ancient Egyptians have always been well recognised. Their skill is represented in the vast majority of their remaining art works; which show an outstanding degree of creativity (Petrie, 1996: 9).

Though the most characteristic form of art pertaining to the ancient Egyptians is exhibited by their stonework, these peoples also strove to embellish surfaces through the application of pigments (James, 1979: 188). It is suspected that painting was the earliest form of art in Egypt (Lucas and Harris, 1999: 338; Petrie, 1996: 55). This

form of art is particularly well represented from the Dynastic period, and was used extensively to decorate papyri, plaster, leather, pottery, stone, wood and sometimes linen (James, 1979: 204-205). The later eighteenth and nineteenth Dynasties are moreover popularly described as the 'age of the art', as they indicate a flourishing in painting techniques. This was observed in several remaining eighteenth Dynasty paintings (James, 1979: 206) and described, for example, by Flanders Petrie (1894) in the palace and temple of the ancient city of Amarna (Petrie, 1996: 18).

The pigments exploited by these Egyptian artists included a wide range of naturally sourced and artificially prepared colours which have been outlined in the table below. Both pigments and painting techniques showed the remarkable acuity and knowledge these peoples had about materials and their properties (Lucas and Harris, 1999: 133, 352; Davies, 2001: 22-24; James, 1979: 205).

Colour	Pigment (and chemical formula)
Black	Carbon black/soot/charcoal (C), bone black ($Ca_3[PO_4]_2$ + $CaCO_3$ +C), pyrolusite (MnO_2)
White	Calcite ($CaCO_3$), gypsum ($CaSO_4.2H_2O$), huntite ($CaMg_3[CO_3]_4$)
Yellow	Yellow ochre (FeOOH), orpiment (As_2S_3), massicot (PbO), jarosite ($KFe_3[OH]_6[SO_4]_2$), natrojarosite ($NaFe_3[OH]_6[SO_4]_2$) and organic yellows
Red	Red ochre (Fe_2O_3), red lead (Pb_3O_4)
Blue	Azurite (2 $CuCO_3$. $Cu[OH]_2$), Egyptian blue (frit- $CaCuSi_4O_{10}$)
Brown	Ochre (Fe_2O_3 / FeOOH)
Green	Malachite (2 $CuCO_3$. $Cu[OH]_2$), Egyptian green (frit- $CaCuSi_4O_{10}$ + vegetable yellow)

Table 1-7. A summary of the pigments used in ancient Egypt (adapted from Lucas and Harris, 1999; Davies, 2001)

The ancient city of Amarna: a historical overview

Amarna, sometimes also (incorrectly) referred to as Tell el-Amarna, is the name given to an extensive archaeological site that represents the remains of an ephemeral capital city constructed and abandoned within about fifteen years in the eighteenth Dynasty by King Akhenaten,; approximately between 1347 and 1332 BC. It is located on the eastern bank of the Nile, approximately 200 km south of Cairo; roughly halfway between Cairo and Luxor (or Memphis and Thebes) at the border of Middle and Upper Egypt (Redford, 1992).

The surviving remains of site serve as an ideal reference to the study of this brief Amarna period, therefore also providing a good insight into this particular timeframe of the history of Egyptian civilisation. It was also considered as a complementary case to this project owing to its definite start and end date, implying that all materials found at the site were representative of the eighteenth dynasty. Excavations following discovery started in 1891 by W. M. Flinders Petrie, and several teams have continued to excavate, survey and study this unique site ever since (Kemp, Garfi et al., 1993; Petrie, 1894; Nicholson, 2007). The paintings in particular, have been described as "…the most complete and striking remains found in the present excavations" (Petrie, 1894: 12). Amarna is known to hold amongst the most beautiful examples of mural paintings on clay plaster in both the palaces of the king as well as in private houses (Lucas and Harris, 1999: 354).

1.4. Properties and preparation techniques of ochre

The preparation and application of pigments is considered to be a rather complicated process, and has been regarded as a greater achievement of prehistoric peoples than tool making (Wreschner, 1976). The outline below substantiates this by describing all the methods involved from sourcing of the ore to application of the pigment.

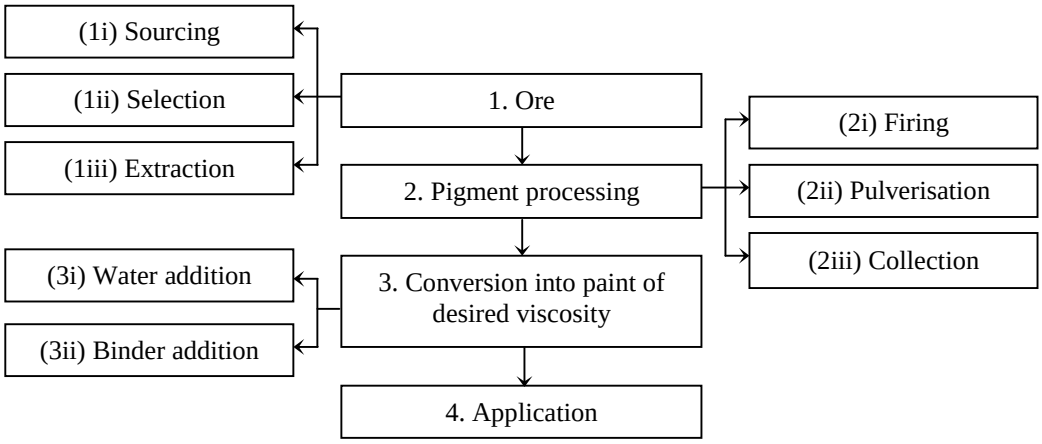

Figure 1-9. Outline of pigment production from natural ochre

1.4.1. Ochre production: Extraction and processing

Though little is known about the procurement of ochre by ancient peoples, historical sources mention the mines in Athens and other mainland sites in Greece, particularly in Attica (Wilson, 2006: 166) and Analfi (Vaughn, Grados et al., 2007). The red ochre from the island of Ceos, Greece, was exported as early as the 4th century B.C. and this apparently significant site is also mentioned by Theophrastus (Caley and Richards, 1956). Hematite was also mined in the Chalchihuites area in Zacatecas, Mexico, around 200 – 500 A.D. (Rapp, 2002: 59). Roman writers describe Egypt as being a source of high-quality red earth (Colinart, Delange et al., 1996, Lucas and Harris, 1999), whist the documented sources of ochre quarried by the Native Americans in the US include the Sunrise Mine in Wyoming and the Red Rock Quarry in California (Tankersley, Tankersley et al., 1995; Stafford, Frison et al., 2003).

Certain iron-based pigments appear to have been processed to some extent following extraction (Chalmin, Menu et al., 2003). Ochres were ground on quartz cobbles to improve the grain size, for example. It is also thought that minerals such as biotite and feldspar were intentionally mixed with the pigments, and that different recipes were used at different times by prehistoric peoples (Clottes, Menu et al., 1990). Ethnographic evidence also suggests that the Chumash Indians of California distinguished between the varieties of red earth, giving each type a specific name and use (Helwig, 2007: 68).

Colour manipulation through heating was practiced as early as 298,000 B.C. (mentioned previously), showing the advancement of these peoples. The method of synthetic ochre production involved the irreversible process of calcination, or heating, of raw yellow earth to produce a range of hues, such as orange, red, brown and mid-tones of these colours. This process involved the dehydroxylation of hydrated iron oxides to the oxide, with the final colour being dependant on the original material, the temperatures and/or the duration of the heat treatment involved. Even the hematite-based ochres were at times roasted to produce more intense red hues, as was observed from the remains in the Châtelperronian site at Arcy-sur-Cure (Schmandt-Besserat, 1980: 129).

$$\underset{\substack{\text{Iron hydroxide (goethite)}\\ \text{Yellow/yellow-brown}}}{2FeOOH\ (s)} \xrightarrow[\text{Dehydroxylation}]{\text{Heat (260-300°C)}} \underset{\substack{\text{Iron oxide (hematite)}\\ \text{Red/brown}}}{Fe_2O_3\ (s)} + \underset{\substack{\text{Water of}\\ \text{hydration}}}{H_2O\ (g)}$$

Equation 1-2. The calcination of iron hydroxide

Calcination of the iron ores remained and probably still is the most popular technique employed for synthetic red ochre production throughout the course of time, even though several other methods were developed. The calcination of iron sulphates to temperatures between 500°C and 750°C, for example, was another technique that was practiced, and dates back to the end of the Five Dynasties (960 A.D.) in China (Helwig, 2007: 47). This technique was later described by Theopharastus, and eventually by Vitruvius and Pliny, and is referred to as *colcothar* by various medieval craftsmen and alchemists (Hawthorne and Smith, 1979). By the early sixteenth century, the red oxide product was also generally known as burnt vitriol (Thompson, 1936). From around the fifth or sixth millennium B.C., raw ochres were also reduced to a black pigment by briefly heating vessels, to which a layer of ochre had been applied, at 800°C in a sealed kiln/furnace. This reduction technique was particularly important in Mesopotamia and Minoan Crete.

Methods for producing synthetic medicinal iron oxides by roasting iron filings with various salts were known in India from early times, even dating back to the Ayurvedic period c.600 B.C. – 800 A..D. Seventeenth and eighteenth century alchemical treatises and writings on enamel and glass also describe a related artificial iron oxide, referred to as *croccis martis*, made by intentionally oxidizing metallic iron or steel. Synthesis by solid state transformation through the heating of iron ores and/or iron salts (such as iron sulphates $FeSO_4.7H_2O$, iron chlorides $FeCl_2$ and $FeCl_3$, iron hydroxides FeOOH, iron carbonate, Fe_2CO_3 and magnetite) in an oxidizing atmosphere probably remains one of the most practised methods of synthetic ochre production (Helwig, 2007: 49).

1.4.2. Application

The methods employed in prehistory to enable the adhesion of a pigment to a surface include 1) fluid application by means of the combination of a solvent and/or a binder to the material; 2) through the utilisation of ochre with a high proportion of clay in its composition, 3) by the preparation of a pigment with an extremely fine grain size. The latter form was achieved by thoroughly grinding the pigment as no evidence for other methods, such as levigation (a process which involves the suspension of ochre grains in a water-filled vessel) has been found to date. It is assumed that the pigment particles were fine enough to stain the walls by infusing themselves into the pores of the rock (Stafford, Frison et al., 2003).

A fluid paint generally consists of two to three components, namely the colouring material, which in this case would be the ochre; a solvent/dispersant, typically a liquid which has the ability to disperse the pigment particles making the colour easier to apply and manipulate; and the binding medium, a component which binds the pigment particles together and to a surface, thus allowing both cohesion and adhesion. In the case of natural ochres, the proportion of clayey matter in the composition of the pigment is sometimes high enough to act as a binder, which explains the exploitation of the ochre pieces as 'crayons', and why in some cases it is suspected that the ochre was merely mixed with a solvent, such as water, to ease application. Nevertheless, it is suspected that sometimes urine, fat, vegetal matter/juices and blood were also added to the paint mixture, though few traces of these organic materials have survived environmental degradation since prehistoric times (Wreschner, 1976). An example of burned vegetal matter combined with red ochre was identified among pigments found

at Herod's palace in Jericho (Rapp, 2002: 212). Taçon (2004: 33-34) also forms interesting, and possibly quite apt parallels between ochre exploitation by the aboriginals in Aurstralia to its use by our ancestors in prehistory. Several extracts quoted in his text describe how red and/or yellow ochre was mixed with fat and daubed over bodies for self adornment, and how the said mineral was ground, mixed with a fluid, characteristically water, and sometimes also the binding agents saliva or blood for use in artistic depictions.

It is assumed that various methods of application depended on the material to be embellished with ochre, as well as on the time period involved and the ensuing preferred technique by the cultures in question. Some other simple methods appeared to entail blowing the pigment onto the wall through a tube, as well as finger painting using the ochre-solvent-medium mix to trace outlines onto a surface. Other scenarios saw people using makeshift brushes, which were made out of fibrous or vegetal material, such as a pad of moss; out of tufts of animal hair or by using the shredded end of a reed (Rogers and Rogers, 1985: 29-31).

1.4.3. Structure, substitutions and transformations

Whether naturally occurring or manufactured synthetically, the colour of ochre is characteristically a product of its constituent iron oxides/hydroxides. Though fourteen iron oxides, oxide hydroxides and hydroxides have been identified to date (Table 1-8 below); goethite (α-FeOOH: iron hydroxide) and hematite (α-Fe_2O_3: iron oxide) are the most thermodynamically stable under aerobic conditions (Carbone, Benedetto et al., 2005; Mazeina and Navrotsky, 2007). They are therefore the most widespread in

nature and are the iron mineral varieties customarily found in ochre pigments. Other phases may also be present, and include the minerals lepidocrocite and magnetite (Eastaugh, Walsh et al., 2004: 363).

Hydroxides/oxyhydroxides			Oxides		
	Formula	*Mineral*		*Formula*	*Mineral*
1	α-FeOOH	Goethite	5	$Fe_5HO_8.\ 4H_2O$	Ferrihydrite
2	β-FeOOH	Akaganéite	6	α-Fe_2O_3	Hematite
3	γ-FeOOH	Lepidocrocite	7	γ-Fe_2O_3	Maghemite
4	δ'-FeOOH	Feroxyhyte	8	Fe_3O_4	Magnetite
9	$Fe(OH)_2$		12	FeO	Wüstite
10	FeOOH	High-pressure	13	β-Fe_2O_3	
11	$Fe(OH)_3.nH_2O$	Bernalite	14	ε-Fe_2O_3	
Salts					
Oxy-hydroxy salts			**Hydroxy salts**		
15	$Fe_{16}O_{16}(OH)_y(SO_4)_z.$ n H_2O	Schwertmannite	17	$Fe^{II,\ III}$	Green Rusts
16	Oxyhydroxy nitrate				

Table 1-8. Iron oxides, oxyhydroxides and salts known to date (Schwetmann and Cornell, 2003)

The structures of the two iron hydroxides/oxides goethite and hematite are very similar: both have hexagonal close-packed structures and are termed alpha phases. The close structural relationship suggests a topotactic transformation in which the oxygen sub-lattice is preserved. The stability of the two minerals is controlled by thermodynamics with transformation being affected by pressure, relative humidity, temperature and grain size (Goss, 1987).

The structure of goethite is based on an arrangement of O atoms in an orthorhombic unit cell: a = 0.9956 nm, b = 0.30215 nm, c = 0.4608 nm (Cornell and Schwertmann, 2003). The Fe(III) atoms are arranged in two rows to form double chains of octahedra alternating with double chains of vacant sites, ultimately leading to the orthorhombic symmetry. The chains run the length of the *c*-axis in the *b*–*c* plane (Helwig, 2007: 59).

All the bonds within the double chains are covalent with each octahedron sharing four of its edges with neighbouring octahedra, whereas all the bonds between these chains consist of relatively weak hydrogen bonds (Frost, Ding et al. 2003). Goethite has a number of polymorphs, namely lepidocrocite (γ-FeOOH) and akaganéite (β-FeOOH). Hematite has a hexagonal unit cell (a = 0.5034, c = 1.375), although it is sometimes described as belonging to the rhombohedral crystal system. While in goethite half the octahedral interstices are filled with Fe^{3+}, in hematite two thirds are filled. The framework of hematite is regarded as a set of O and Fe layers, arranged normal to the threefold axis (Gualtieri and Venturelli, 1999).

These natural iron oxides/hydroxides also have the tendency to exhibit isomorphous substitution of the ferric ion by other cations and are often referred to as "sinks" for trace and heavy metals which tend to substitute for Fe on the octahedral sites (Wells, Fitzpatrick et al., 2006). Al is the most common substitution cation in both goethite and hematite (Friedel and Schwertmann, 1996), and small amounts of transition metals and trace elements including Ni, Co, Cr, Ga, V, Sc, Ge, Mn, Cu, Zn, Cd and Pb are also reported to associate with natural and synthetic goethite (Wells, Fitzpatrick et al., 2006). Cr, Mn, Rh, Ga, In, Nd, Ni, Cu, Ge, Sn, Si and Ti are noted as substitution metal ions in hematite (Cornell and Schwertmann, 2003: 47). This partial cation substitution also results in colour variation, resulting in pigment shades which may range from yellow through to brown and purple (Helwig, 2007: 39).

The effect of aluminium, the most frequent element that substitutes for Fe, on the unit cell parameters of goethite and hematite is given as illustrated in the tables below

(Grave, Bowen et al., 1982; Amarasiriwardena, DeGrave et al., 1986; Friedel and Schwertmann, 1996; van-San, Grave et al., 2001; Vandenberghe, San et al., 2001; Wells, Fitzpatrick et al., 2006; Alvarez, Rueda et al., 2007).

Goethite	***Unit cell parameters (nm)***		
	a	***b***	***c***
Mean	0.4634	0.9945	0.3021
Mean Unit cell volume $Å^3$	138.67		
Al-substituted goethite	***a***	***b***	***c***
2.1 Mol.%	0.4635	0.9921	0.3012
3.0 Mol.%	0.4609	0.9930	0.3015
3.8 Mol.%	0.4632	0.9910	0.3011
4.6 Mol.%	0.4617	0.9913	0.3010

Hematite	***a***	***c***
Mean value	0.5036	1.3760
Mean Unit cell volume $Å^3$	302.235	
Al-substituted hematite	***a***	***c***
5 Mol.%	0.5023	1.3732
10 Mol.%	0.5016	1.3716
15 Mol.%	0.5011	1.3720
20 Mol.%	0.5008	1.3692

Tables 1-9a,b. The effects structural Al on the unit-cell parameters at various molar concentrations with respect to the non-substituted Fe oxide for goethite and hematite

Thermal transformations involving the dehydroxylation of goethite to hematite occurs after natural and managed thermal transformations when the iron hydroxide is subjected to heat or mechanical stress (Ruan and Gilkes, 1995). Understanding this transformation is of importance in the study of colorants used in antiquity, primarily because calcination was used by ancient peoples to modify the colour of their iron oxide/hydroxide-based pigments (Pomies, Menu et al., 1999; Chalmin, Vignaud et al., 2004). Appreciating changes experienced by the ochre following this thermal treatment is important to assert that the material does not experience any change in elemental composition that could potentially affect the accuracy of this provenancing project.

When heated, hydroxo-bonds are therefore replaced by oxo-bonds and face sharing between octahedral (absent in FeOOH structures) develops and leads to a denser structure: The (100), (010) and (001) directions in goethite become the (001), (110) and (111) directions in the trigonal haematite cell (Özdemir and Dunlop, 2005). As only one half of the interstices are filled with cations, some movement of Fe atoms during the transformation is required to achieve the two thirds occupancy found in hematite (Frost, Ding et al., 2003).

The goethite-hematite phase transformation has been widely investigated and several structural relationships and mechanisms of solid-state transformation of goethite to hematite have been suggested, with many points remaining unclear and debated. (Watari, Delavignette et al., 1983; Goss, 1987; Wolska and Schwertmann, 1989; Gualtieri and Venturelli, 1999; Walter, Buxbaum et al., 2001; Cornell and Schwertmann, 2003: 369). Relatively recent thermal kinetic studies carried out by Gualtieri and Venturelli, (1999) and Fan, Song et al. (2006) have carefully investigated microstructural changes and the transformation kinetics of synthetic goethite. The results have suggested that the dehydration of goethite during calcination involves a three-dimensional diffusion process which does not appear to involve any alteration in composition, apart from the observed dehydration, which is described below.

Since iron oxides are known to have a particularly high affinity for water, adsorbing up to one mole of excess water per mole of iron oxide (Mazeina and Navrotsky, 2007), the initial dehydration process therefore involved loss of surface water (Fan, Song et al., 2006). The next phase, beginning at approximately 473 K, involved the formation

of non-stoichiometric hematite, which was described as the intermediate "protohematite" $Fe_{2-x/3}(OH)_xO_{3-x}$, in certain publications (Wolska and Schwertmann, 1989).

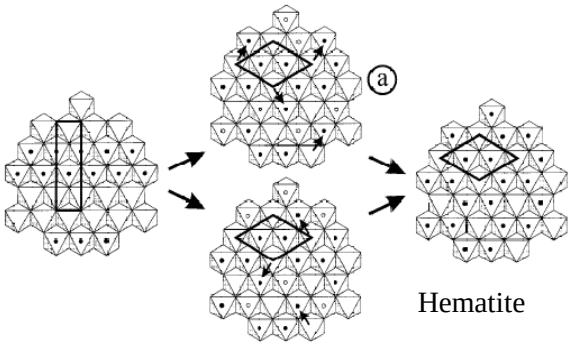

Figure 1-10. The two most probable ordering schemes of iron during the goethite-protohematite phase transformation and final transformation to hematite (Gualtieri and Venturelli, 1999)

Fan, Song et al. (2006) observed the formation of hematite on the surfaces of goethite, which started preferentially in areas with a large surface-are-to-volume ratio, such as edges. Other observations included the delay of further oxidation by this hematite 'film', which appeared to act as a protective layer to the enclosed goethite.

The dissociative water was then produced through further diffusion of hydrogen or hydroxyl groups at a relatively high temperature, making the rate-determining step an interface reaction process and not long-range diffusion. This endothermic reaction proceeded until recrystallization into hematite fully occurred (Fan, Song et al., 2006). A small amount of water was found to be left in the product, even when only hematite peaks were observed, i.e. the final product was able to support some OH-ions (Goss, 1987).

1.4.4. General properties of ochre

It has already been established that ochre is a universally exploited material and was primarily used throughout history as a pigment for its colour, which it derives from its constituent components. There are, in fact, several factors that affect the final tone of the pigment in question, and these have been aptly outlined by Bednarik (1994), who attributes the varying colours to the states of hydration, oxidation, reduction, hydrolysis, adsorption, grain shape and size/size distribution of the various components within the pigments.

It is commonly accepted that the degree of hydration of the pigment, which is analogous to the quantities of the two main ochre-colouring minerals present (namely the ratio of hematite to goethite), is the major factor influencing colour (Mortimore, Marshall et al., 2003). Purple and red shades therefore show a prevalence of anhydrous oxides (hematite) within the pigment. The lighter tones conversely indicate some degree of hydration, with goethite as the main ferrous colorant present. The darker ochres contain various phases of manganese oxides as well as the iron hydroxides and/or oxides. If the manganese oxide quantity exceeds five percent of the total colorant matter within the pigment, these are termed brown earths and umbers, which are often described as ochre variants (Chalmin, Vignaud et al., 2004). Their overall characteristics and composition, however, reflect otherwise (Robertson, 1976). The umbers in particular contain between five to twenty percent manganese oxides, which tend to have a significant effect on the physical properties of the pigment.

Accessory minerals also affect ochre properties, besides colour, occasionally in a negative way. Examples of accessory minerals present in ochres include quartz, feldspars, calcite, dolomite and other carbonate minerals; various clay minerals and possibly gypsum (Carbone, Benedetto et al., 2005). Ochres still exhibit outstanding pigment characteristics, including non-toxicity, excellent hiding power and good tinting strength (Cornell and Schwertmann, 2003).

Siennas, pigments mined from Siena in Italy, and often also referred to as natural varieties of yellow ochre, are exceptions to this. Their relative transparency has been commented about in artist's manuals since the eighteenth century (Merrifield, 2003), and this property was eventually ascribed to the atypically small particle size of the goethite in the pigment (Helwig, 2007). Particle size may therefore also affect pigment characteristics: goethite is reputedly the end member of many transformations; unless its particle size is less than 0.1 mm, whereupon it becomes thermodynamically more unstable than hematite (Prasad, Prasad et al., 2006).

Mineral	Particle Size	Colour
Goethite α-FeOOH	~1 μm 0.05 μm	Yellow Brown
Hematite α-Fe_2O_3	1 – 5 μm 0.1 – 0.2 μm	Blue-red to purple Bright red

Table 1-10. The relationship between mineral, particle size and colour (Cornell and Schwertmann, 2003)

The continuous and extensive history of application of ochres can therefore be attributed to a variety of factors, including abundance in nature, relatively simple methods of preparation, and suitable optical and handling characteristics. These pigments are also amongst the most permanent of pigments available to date,

exhibiting excellent resistance to light, water, fluctuating environmental conditions, alkali and dilute acid attack (Clarke, 1976; Bikiaris, Daniilia et al., 2000). Ochres are also absorbers of ultraviolet light and therefore tend to protect their binding medium from deterioration, thus increasing the overall permanence of the paint they constitute (Cornell and Schwetmann, 2003: 511). It appears that even aboriginals judged the suitability of ochres by their purity, consistency, opacity and texture (Clarke, 1976; Taçon, 2004: 34).

Ochres therefore bear evidence to the aptitudes of age-old cultures, and to the way these peoples sourced the material for artistic and symbolic use. The durability of ochre has also allowed us to observe and appreciate this form of cultural expression thousands of centuries later. Though little is known about the procurement of these pigments, current characterisation studies show the potential benefits of linking ochres to their sources. Determining their provenance may therefore be key to understanding ancient technologies, and, more importantly, to establish trade routes and communication between ancient civilizations (Popelka-Filcoff, Robertson et al., 2007). The second point is of particular interest in this study because of the implications associated with ancient exchange that tally with the aims of this thesis, and is described below.

1.5. Provenancing techniques

The capacity for gaining fresh insight to regional interconnections in prehistory by means of provenance research has been recognized by archaeologists for several decades. Provenancing has assumed great importance in the field of archaeological

studies for a number of reasons, including: the understanding of the interrelationships between material transactions and social organizations, the recognition of the movement of goods and of peoples and thus the social and evolutionary significance of exchange, as well as the appreciation of mobility patterns of prehistoric peoples (Earle and Ericson, 1977).

Provenance research involves the acquisition of evidence by means of quantitative analysis of the constituents of archaeological items and/or materials and their potential sources. Although the main methodology used for provenancing entails the acquisition of compositional profiles through element/chemical characterisation methods, other forms also comprise descriptive modeling, application of ethnographic and ethnohistorical research, systemic modeling, and several others (Earle and Ericson, 1977: 4). Chemistry-based provenancing is, however, the most exploited and more recognized technique, and its principles have been understood since the early 1970s (Glascock and Neff, 2003). Research in this field has grown rapidly over the past few decades, and has experienced an increase in the number of implemented techniques for analysis, as well as a better examination of data by means of suitably applied statistical methods. The ultimate aim is to potentially link the individual artefacts to their place of origin, as has been described by Weigand, Harbottle et al. (1977) by means of the 'provenance postulate' theory.

This theory requisites differences in composition between natural sources that exceed, in some recognizable way, differences observed within a given source. The raw material can therefore be linked to its source through chemical analysis as long as the

inter-source variation between different sources is greater than the intra-source variation within one source. If the elemental signatures of the artefact source groups follow the provenance postulate, then elemental analysis may be used to source the artefacts if all possible sources are known, and as long as significant numbers of datasets are obtained to ensure suitability of results and to establish appropriate conclusions (Glascock and Neff 2003).

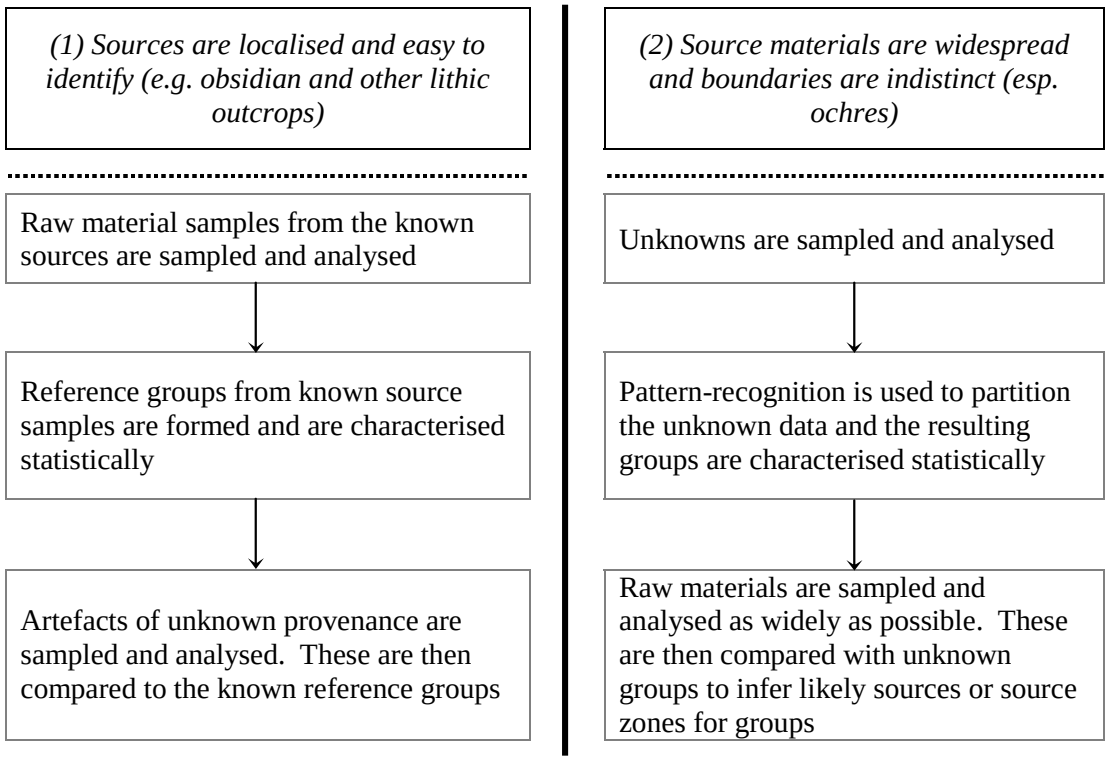

Figure 1-11. The two approaches to provenancing of materials (Glascock and Neff, 2003)

Sourcing based on this provenance postulate theory can therefore follow one of two separate paths, as shown in Figure 1-11: (1) The raw materials from localized and relatively distinguishable sources are analysed in conjunction with the materials/artefacts of unknown provenance. Statistical analysis can then be used to determine whether the composition profiles fit into any of the source groups. (2) Conversely, when sources are more widespread, as is usually true in the case in ochre

provenancing, characterisation of all individual sources is virtually impossible. Provenancing therefore begins with the characterisation of the artefact/material composition, resulting in the generation of reference groups. Individual raw materials are then compared to these groups and the range of variation is evaluated (Glascock and Neff, 2003).

Since iron is ubiquitous in the environment, establishing the likely sources of these iron-based ochres is often rather challenging as sources are usually widespread and indefinite, and have not been elementally characterised as extensively as other materials used in provenancing, such as ceramics and obsidian. The provenance approach adopted in this thesis therefore utilizes a combination of the two paths suggested above to facilitate the study and substantiate the results. It involves restricting the area examined to the Maltese islands, which means that the iron-rich sources, although never explored for provenancing purposes before, are quite well defined (refer to Chapter 5). These were established through a thorough understanding the geology of the archipelago, and will be described in section 2.1. The Maltese islands are also particularly rich in Neolithic remains that show evidence of heavy ochre use (refer to section 2.2), therefore implying that the acquisition of a representative sample group of archaeological ochre to link the Neolithic pigment to potential local sources was possible.

Provenancing of these pigments, however, also presents another set of challenges, which are discussed in Chapters 5 and 6. These include the fact that (1) ochre applied to archaeological artefacts consists of relatively thin layers, making sample recovery and/or analysis difficult and (2) the addition of other materials (such as binders and/or

other pigments) is likely, and these may have an effect on the chemical signature of the ochre (Hall, Meiklejohn et al., 2007).

Chemical characterisation of materials for provenancing purposes therefore necessitates the undertaking a number of procedures, which have been summarized in the list below. These steps were also used to formulate the outline of this thesis.

(1) The identification of the artefact/material that needs to be sourced, including its main components/raw materials

(2) Establishing of the area/region for research into potential sources for the identified raw materials

(3) The execution of a geological survey across the area/region, with a representative number of reference materials taken from each source. Samples must also be sufficient to account for intra- and inter- source variation.

(4) Characterisation of the material chemistry through instrumental analysis from both the archaeological material as well as the source groups.

(5) Statistical evaluation of the data obtained to determine source homogeneity, grouping and chemical "fingerprinting" of both the artefact material as well as the raw material sources, thus isolating the characteristic composition for each. Differences between sources must be clearly distinguishable and samples from different geological sources must fall into discrete clusters.

(6) Establishing whether the data satisfies the provenance postulate theory, and whether the chemical signatures or 'fingerprints' from the archaeological material fit in any of the discrete source groups (Popelka-Filcoff, Robertson et al., 2007).

Chapter 2.
Malta: Its geology and prehistory

2.1. An overview of the geology of the Maltese islands

The Maltese archipelago is located in the centre of the Mediterranean Sea, 96 km to the east of the Sicilian coast and 290 km off the North African coast. It lies along a main navigational seaway in the Sicily channel, which connects the basins of the Eastern and Western Mediterranean sea (Pedley, Clarke et al., 2002: 14).

Location:	
Latitude: 35°48'28" – 36°05'00" North	Longitude: 14°11'04" – 14°34'37" East
96 km south of Sicily (Italy)	1836 km from Gibraltar
290 km from North Africa (Libyan coast)	1519 km from Alexandria (Egypt)
Islands:	
Malta: 245.7 km^2	Gozo: 67.1 km^2
Comino: 2.8 km^2	St. Paul's Islands: 10.1 ha
Cominotto: 9.9 ha	Filfla: 2.0 ha
Fungus Rock: 0.7 ha	

Table 2-1. Maltese geography (Schembri, 1993)

Figure 2-1. The Maltese islands (Carr, 2010)

Although centrally located, the entire archipelago totals a mere 316 square kilometres, with Malta and Gozo (Ghawdex) being the two main inhabited islands. Malta is the largest of the group, followed by Gozo, which lies North West of Malta (Tilley, 2004: 93). The location of the Maltese islands, coupled with the abundance of the particularly fine, natural harbours they encompass, have made the islands of particular importance throughout history, despite their tiny size (Pedley, Clarke et al., 2002: 13).

2.1.1. The formation of the Maltese islands

The rocks forming the archipelago were initially sheets of marine sediment that were deposited on the sea bed of the Pelagian spur some thirty to five million years ago during the Oligocene and Miocene epochs in the Tertiary period of the Earth's geological timeframe. A collision of the African continental plate into the Eurasian plate ten million years ago led to a partial subduction of the African foreland beneath the European plate, resulting in an exertion of pressure and an uplift of marine sediments to levels above sea level. This resulted in rock formation and the emergence of the archipelago by the processes of sediment induration. The Maltese islands were thus formed and were originally linked to Sicily and Europe by a land bridge that emerged during this uplift (Gardiner, Grasso et al., 1995). The eventual split from the rest of Europe occurred during the Holocene, which led to a rise in the sea level of the Atlantic Ocean, causing it to spill out into the Mediterranean Sea. The next Ice Age that was experienced two million years ago resulted in a wetter climate that also affected the topography of the archipelago, leading to the formation of river valleys in the islands (Pedley, Clarke et al., 2002: 18-29).

2.1.2. The rock formations of the archipelago

The geology of the Maltese archipelago is therefore relatively young, consisting solely of Tertiary formations, with all the rock types being sedimentary and limestone-dominant (Tilley, 2004: 94). Geophysically, the archipelago and the Ragusa peninsula of southeast Sicily belong to the African plate, hence the rock types of the Maltese islands are similar to those of both south-eastern Sicily as well as to the coastal areas of Tunisia (Schembri, 1993: 28). They fundamentally encompass a large number of lime-

rich skeletal remains of marine flora and fauna whose skeletons are majorly calcitic (Fenech, 2007: 6). There is, however, a subsidiary portion of clays and marls within the limestones, which originate from water-borne clay minerals and/or fine (volcanic) dust blown by the wind from distant land sources. A few bands in the limestone are also significantly rich in metallic ions, such as iron (described below) and aluminium. Some areas are also distinctly abundant in cemented calcium phosphate (Pedley, Clarke et al., 2002: 41).

The geological sequence of rocks falls into four/five distinct layers of uneven thickness and which lie almost horizontally over one another. These are: Lower Coralline Limestone (LCL), Globigerina Limestone (GL), Blue Clay formation, Greensand and the Upper Coralline Limestone (UCL) They are characterised by differing mineral properties; including hardness and resistance to environmental weathering (Spratt, 1854: 5), and are summarised in Table 2-2 below. Together with the geological fault lines, the different formations dictate the overall surface topology, which varies considerably between the islands (Pedley, Clarke et al., 2002: 21, 35; Tilley, 2004: 94).

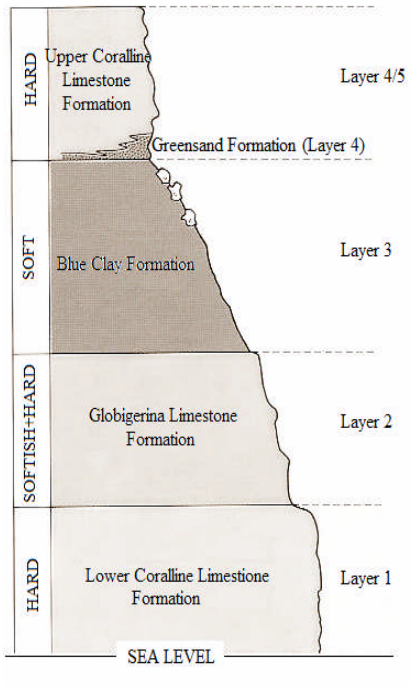

Figure 2-2 . A section through the rock layers of the Maltese islands, adapted from Pedley, Clarke et al., 2002: 35, 36

Layer	Unit	Maltese Name	Thickness (~m)	Formation and properties
4/5	**Upper Coralline Limestone**	Qawwi ta` Fuq / il-Qawwi	30 – 162	Topmost, youngest formation, a hard, pale grey limestone unit, resembling the LCL in both structure and chemistry, indicating a similar deposition in shallow waters. Some layers are completely crystalline and others are highly fossiliferous.
(4)	**Greensand**	Ramli / Il-Gebla Safra	0 – 16	A thin and sometimes absent fossiliferous sandy formation, rich in organic matter. Contains glauconite, which gives the rock its distinctive green/orange/brown colour. Also consists of bioclastic limestones and brown, phosphatic grains. Represents a long period of submarine erosion and sediment winnowing, followed by a final shallowing.
3	**Blue Clay**	Tafli / Tafal	< 75	Soft, bluish-grey, kaolinite-dominant and rich in lime and marl, of varying composition. Very fine-grained sediment dominated by skeletal material from planktonic organisms, with clay content originating from a land source, possibly volcanic ash from the north of Sicily, yet deposition may have occurred in open muddy water environments. Additional components comprise quartz, augite, feldspar and tourmaline. Has a large number of inclusions that appear through weathering of the darker clay beds, e.g. spherical concretions of iron-rich ooids.
2	**Globigerina Limestone**	Il-Gebla tal-Franka	20 – 250	Fine-grained rock-type, widely exposed in the south-eastern part of Malta, and extending over two-thirds of the island's surface. Believed to have been of a bluish-grey when deposited but now has a honey-brown/yellow shade owing to oxidation of its constituent iron sulphides to hydroxides by percolating rainwater. Contains planktonic fossils and Globigerina shells. Has high phosphate levels that suggest that the water streaming over this shallowed surface was rising from greater depths as an "upwelling" current.
1	**Lower Coralline Limestone**	Qawwi ta` Isfel: Zonqor	Exposed: 120	The oldest rock formation of the islands, forming most of Malta's southern and south-western sheer coastline and outcropping inland along fault lines. Consists of hard, resistant, pale grey limestone, containing limestone beds with debris derived from skeletal remains of fossil corals and other calcareous algae. Grading and sorting indicates shallow marine deposition, probably in an agitated, gulf environment, though younger beds show deposition in more open marine conditions.

Table 2-2. Rock formations of the Maltese islands: Adapted from Zammit-Maempel, 1977; Pedley, Clarke et al., 2002; Tilley, 2004; Fenech, 2007

The formations therefore reflect the changes that took place in the Pelagean Platform millions of years ago, with the current rock sequence reflecting changes in water depth. The outcrop geology of Gozo is more varied than that of Malta, and the various rock outcrops that predominate on Malta include GL appearing in the central and south-eastern portion of Malta, and the UCL outcropping in the northern and north-western regions of the island (Pedley, Clarke et al., 2002: 63).

2.1.3. Soils

The rocks are overlain by terrestrial, aeolian and alluvial deposits laid down subsequent to the surfacing of the Maltese islands and their exposure to weathering and erosion (Conklin, 2005). These soils are normally bright red and fertile, and are all characterised by their close similarity to the parent rock material from which they originate (Trump, 2008: 16). They are rich in calcite, clay, oxides of iron and manganese and other mineral particles (Oertel, 1961; Fenech, 2007: 21). Since pedological processes are slow in calcareous soils the deposits are relatively immature (Vella, 2006: 171). Maltese soils have long been classified into three main types following the Kubiena classification system (after Lang, 1960), depending on their age and site of formation. These include the more mature and weathered Terra Soils, formed during the Pleistocene; the Xerorendzinas (Globigerina deposits) and the Carbonate Raw Soils, which are both immature soil groups with a high amount of calcium carbonate and a low organic matter content (Schembri, 1993). A recent MALSIS (Maltese Soil Information System) study undertaken in 2004-2006 has further subdivided the soils into seven types, as described in Table 2-3 below.

Soil Type	Characteristics
Calcisols	Dominant soil group on the Maltese islands, rich in lime and secondary $CaCO_3$ Divided into Endoleptic Calcisols, Epileptic Calcisols, and Hypocalcic Calcisols
Leptosols	Shallow soils in garigue areas Are calcari-lithic soils
Vertisols	Clay soils, therefore are limited to the Blue Clay outcrop Crack and degrade easily
Luvisols	Relicts of different environments as formed under climatic conditions different to those of the present age: All reddish, clayey and containing secondary $CaCO_3$ Divided into Chromi-Calci-Epileptic Luvisols (shallow) Endolepti-Chromi-Calci Luvisols and Chromi-Calcic Luvisols (deep)
Cambisols	Still incipient formations, but very fertile soils for agricultural purposes Vary from browner to redder soils (latter are richer in ferric ions)
Regosols	Also incipient formations, therefore weakly developed Classed as the 'other' soils, as all outliers fall into this group
Arenosols	Sandy soils, therefore quartz-rich, beach deposits, relatively localised

Table 2-3. Maltese soil types (from MALSIS, 2006)

2.1.4. Overview of the geological iron-rich sources on the Maltese islands

Though the geology of the Maltese archipelago mainly consists of limestones which lack significant iron deposits, such as beds (and/or caves) of iron formations, various areas have been identified as being abundant in metallic elements, particularly in iron, and could therefore be potential sources of ochre. Four such sources were identified through a thorough literature survey and through consultation with Maltese geologists. These were: the red veins, or *'Calcitic red'* limestones, the *'Greensands'* formation, the *'Ooid'* group, and the soils, termed *'Terra rossa(e)'*.

The first of the iron-rich deposits are known to originate from the formation of 'mineral-veins' within the sedimentary bedrock; particularly from the occurrence of what are known as 'veins of replacement' in the UCL. These occur through the deposition of a mineral mass, such as soil, in rock fractures, which sometimes cut through the entire stratgraphical sequence of the limestone. This process is promoted by the passage of water through the soil and then through upper rock layers; encouraging mineral substitution and enrichment in certain materials, such as iron oxides, within the rock. Subsequent solution, redeposition and burial, coupled with the action of time, result in the formation of hardened iron-calcitic palaeosols; the alleged *'Calcitic reds'* (Scott, 1921), which are predominantly present in outcrops towards the north of Malta, mainly at Cirkewwa and Ghadira.

The invariable presence of the mica mineral glauconite is one of the major distinguishing features of the fossiliferous *'Greensands'* formation. The composition of glauconite depends on its structure and degree of ordering, but it essentially is a potassium/sodium/calcium-iron aluminosilicate of chemical formula $[(K,Na,Ca)_{1.2\text{-}2.0}(Fe^{3+},Al,Fe^{2+},Mg)_{4.0}[Si_{7\text{-}7.6}Al_{1\text{-}0.4}O_{20}](OH)_4.n(H_2O)]$ (Deer, Howie et al., 1966: 207). Greensand is a sedimentary sandstone, forming by marine diagenesis in shallow water under moderately reducing conditions; probably in the anoxic, non-sulphidic, post-oxic diagenetic environment, thus explaining the high Fe^{3+}/Fe^{2+} ratio with respect to the rest of the geology. The glauconite itself forms by clay mineral transformation and by crystallite growth within substrate pores (Tucker, 2001). This Greensands formation and is generally referred to as the Ghajn Melel member of the UCL, and is widespread in Gozo and found in selected locations in Malta; at Dingli Cliffs and Ghajn Znuber Mellieha, for example (Pedley, Clarke et al., 2002: 56).

Figures 2-3 a, b. Heated greensand rock in a shallow cave in Gelmus, Gozo (Photos: author)

The Blue Clay layer underlies Greensands in the stratigraphy of the Maltese archipelago, and outcrops at many coastal regions. It is known to host irregular, though often spherical concretions, nodules, or 'Ooids', that are significantly rich in iron (Zammit-Maempel, 1977: 26; Spratt, 1854: 7). Although the actual route of formation of these minerals is not completely understood, it is hypothesized that these Ooids were formed through weathering reactions, such as repeated winnowing and reworking, of fine-grained iron minerals in shallow water. The clay/mud cover is thought to have provided the required reducing conditions to the sediment (Spratt, 1854: 7; Zammit-Maempel, 1977: 26; Einsel, 2000: 253).

The alluvial, unconsolidated deposits on the Maltese islands were also considered to be likely sources of iron oxides, mainly because of the high percentage of iron minerals they contain. Their very name, *'Terra Rossa'*, or red Mediterranean soil, denotes this factor (Priori, Costantini et al., 2008). Although it is probable that these soils have altered somewhat in composition since prehistoric times, undoubtedly with the concentration of impurities increasing proportionally to the ever-growing increase in population, human activity, urbanisation and development throughout the ages, it is this very factor that has strengthened the belief that these deposits could have been

sources of ochre (Vella, 2006). It was also assumed that chemical signatures within these soils would have remained unaltered, and therefore links to the parent material and earlier alluvial deposits would be demonstrable by means of chemical analysis. Of the seven soil types established by the MALSIS Maltese Soil Information System, certain reference groups were considered to be more likely candidates as ochre sources than others, namely the leptosols and the luvisols.

Little of the geology is thought to have changed since the first settlers set foot on the Maltese islands (Fenech, 2007). Some land has been lost to cliff erosion in the south and west, and a little more through subsidence of the land towards the north and east. The topography, on the other hand, has suffered extensively subsequent to human habitation and interference, with an extensive depletion of trees, mainly pine and evergreen oak, which were felled from as early as the Bronze Age (post 2500 B.C.) to clear the land for farming and cattle grazing. Stripping the land of its tree cover consequently led to soil erosion; and settler interference has led to a complete change in the topography of the islands because of the construction works as well as the resulting pollution which has clearly affected the chemical composition of the soils (Trump, 2008: 14–15). The islands were therefore limited in resources for human habitation. Although providing inhabitants with fertile land, water, seafood and some chert for tools; the restricted size of the archipelago, coupled with the lack of game, locally available hard-stones, metal ores and inadequate amounts of timber, probably made the islands rather difficult to live on; and near-impossible to do so without some form of contact with mainland Europe (Trump, 2008: 19–20).

2.2. Malta: Its prehistory and temples

Radiocarbon dating carried out on ancient deposits has shown that the relatively isolated islands of Malta and Gozo were originally colonized around 5200 B.C., probably by settlers from Sicily (Bonanno, 1991; Vassallo, 2007: 59). Archaeological evidence mainly based on pottery styles indicates that the ancient customs adopted on the archipelago retained their ties with the cultures from southern Italy and Sicily for the next couple of millennia, possibly indicating that Malta was part of a network of societies that stretched across to these countries (Bonanno, 1986; Zammit, 1994).

A major drift or 'schismogenesis' (Robb, 2001) was observed in the course of the fourth millennium, around 3600 B.C., when the Neolithic Maltese created a unique society whose cultural disparity is clearly exhibited through the Megalithic temples that were built on the islands over the next two millennia, and, although to a lesser extent, by their new ceramic repertoire. The temples were the climax of the islands' prehistory and remain unique to date. They are reputed to be the earliest surviving free-standing, though now ruinous, existing stone structures, since at the time they were being built it appears that no-one else was raising self-supporting roofed stone buildings elsewhere in the world (Trump, 1999: 93; Hoskin, 2001: 23; Evans, 1953; Stoddart, 1999; Bonnano, 1996; Tilley, 2004: 87; Vassallo, 2007: 6). The temples show the unique advancement in the art and architecture of this Neolithic Maltese society, and the sophistication and technical achievement of these structures defy all preconceived ideas of primitivism associated with these ancient peoples (Vella, 2007).

Period	Phase	Time (B.C.)
Neolithic	Ghar Dalam	c5200 - 4500
	Grey Skorba	4500 - 4400
	Red Skorba	4400 - 4100
Neolithic: "Temple Period"	Zebbug	4100 - 3800
	Mgarr	3800 - 3600
	Ggantija	3600 - 3000
	Saflieni	c. 4000 - 2500
	Tarxien	c. 3000 - 2500
Bronze and Iron Age	Tarxien Cemetery	2500 - 1500
	Borg in-Nadur	c. 1500 - 725
	Bahrija	c. 900 - 725

Table 2-4. The chronological sequence of Maltese Prehistory. Classification based on pottery typology and radiocarbon dating (from Pace, 2004)

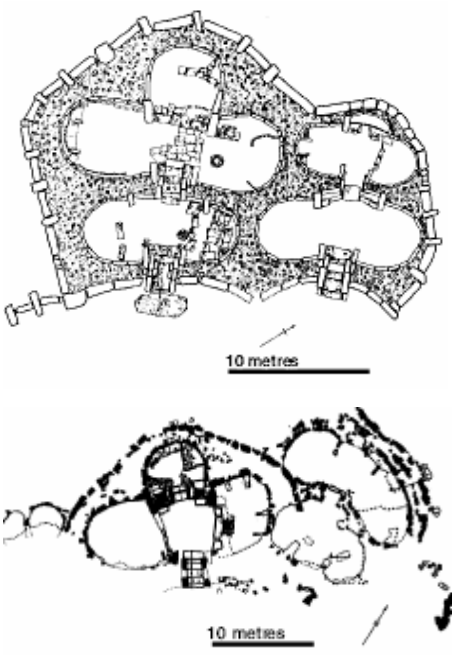

Figures 2-4 a, b. Temple plans of Ggantija (above) and Skorba (from Trump, 1966 and Robb, 2001)

Although this period included other ritual sites, burial sites and habitations, very little evidence has survived the ravages of time, with remains of habitation sites today almost entirely lost to environmental decay. The village of Skorba, found towards the north-west of Malta, is the last surviving site known to date and has allowed for the radiocarbon ^{14}C dating of material deposits. This study, coupled with the classification of pottery typology, has enabled the establishment of the most commonly accepted chronological sequence given above (Trump, 1966: 48).

What remains today are therefore mere vestiges of what the architecture in the Neolithic and Temple Period must have looked like some 5500 years ago. Albeit in ruins, the temples are still recognized as architectural wonders, representing incredible building capabilities for the once presumed 'primitive' society of this period. Stipulations as to what these structures must have looked like are based on what is left,

on a few temple models and on what has been best preserved (Trump, 2008: 192). The Hal-Saflieni Hypogeum burial complex, for example, is an underground, multi-level necropolis, located close to a mega-temple complex, Tarxien (Figure 2-7), and which was developed between 4000 – 2500 B.C. both for burial and temple purposes (Zammit, 1925). It is important because it is the only remaining prehistoric site that has not suffered as extensively to the ravages of time as the other temples have, and is therefore our only insight into what the temple structures above ground must have looked like (Ridley, 1976; Mifsud and Ventura, 1999: 5). This underground site is architecture in the negative and was majorly used as a funerary site, therefore its 'construction' and functionality were clearly different to that of the temples above ground, however, structural parallels with the over-ground architectural structures are obvious. The Hypogeum is set on three different levels and has been decorated with replicas of temple architecture, with surviving details that include megalithic interiors, corbelled roofing and several ochre wall paintings (Pace, 2000: 16; Pace, 2004; Morana, 2003).

2.2.1. Structural layout and general description of the temples

The temples are generally low, intricate, expansive, stone structures, with a physical form mimetic of the surrounding landscape, yet are also visually prominent (Robb, 2001). Each contain between four and twenty spaces, enclosed within a substantially thick wall enclosing a labyrinth of rooms and a forecourt, possibly left unroofed, for public assembly (Trump, 1999: 98). Temples first consisted of lobed structures with trefoil floor plans, arranged around a central axis (Bonanno, 1996). The structures were then elaborated and sometimes modified to form increasingly complex multi-

apsed buildings of varied sizes, generally consisting of around four to six hemispherical chambers branching off a narrow entrance path (Trump, 1966: 47; Trump, 2008: 69–76). The façade was built of orthostats (rows of large stone slabs), with taller cornerstones intentionally positioned at either end. The side and rear walls were also constructed from sets of orthostats, laid in a slightly different manner to and generally taller than the façade itself (Zammit, 1994). The primary axis of orientation of the entrances for most temples was on a north-west to south-east line, arguably orientated in such a manner for the implied astronomical significance and solar alignments involved (Trump, 1999: 92; Zammit, 1994: 6-12; Hoskin, 2001).

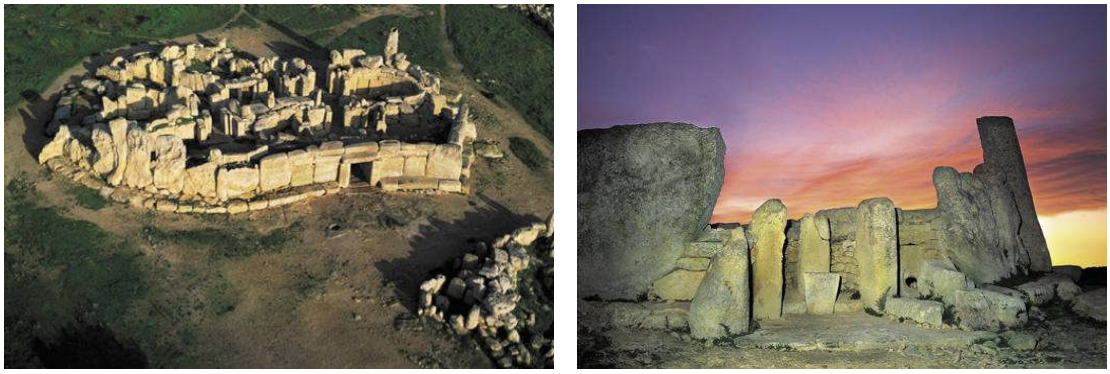

Figures 2-5a, b. An aerial view and (b) the outside of the main shrine of Hagar Qim temples, south of Malta (Pictures courtesy of Heritage Malta)

Temple construction materials consisted of huge blocks of both coralline and globigerina limestone (Table 2-5). The tough coralline stones tended to crack naturally, hence these broken off blocks were selected for use as structural elements and carried to the chosen location in the temple without being modified. The softer globigerina stone was, on the other hand, standardized to taste, therefore potentially looking relatively smooth and new in comparison to the coralline blocks (Trump, 2008: 6, 71). Typical architectural components were also carved from the latter

globigerina stone and examples include the incomplete dome, the horizontal arch, the orthostats and post-and-lintel trilithon (literally meaning 'three stones'). Some elements were decorated with drill holes and other surfaces embellished with relief representations of fish, domestic animals and spirals (Tilley, 2004: 94, 112, 136).

Characteristics	Temple examples	Rock availability
Coralline limestone dominant	Ggantija temple (~ 3600-3000 B.C.)	Close proximity
	Kordin III temple (~ 3600 B.C.)	Carried over from a distance
Globigerina limestone dominant	Tarxien temple (~ 3000-2500 B.C.), Hagar Qim temple (~ 2600 B.C.)	Close proximity
	Mgarr temple (~ 3600-3000 B.C.), Skorba temples (~ 4100B.C.)	Carried over from a distance
Coralline: external walls, globigerina: internal walls	Mnajdra temple (~ 3200 B.C.)	Coralline stone used was carried over from a distance

Table 2-5. Dominant rock used for building of the temples (from Cassar and Vannucci, 2001; Trump, 2008: 79)

Figures 2-6a, b. An aerial view and (b) the middle axis of the Mnajdra temples, south of Malta (Photographs courtesy of Heritage Malta)

While the temple exteriors were composed of a series of megalithic blocks, it is assumed that the rough surfaces of some of the internal walls and floors were entirely smoothened, plastered or paved over either in clay or in a cement-like plaster known as *torba*. The latter cement mix was a tough and durable material made from crushed

limestone paste, and was sometimes spread over a rubble foundation when used as flooring. The material was purposely applied to conceal rock contours and surface textures, and was consistently used as flooring in the temple apses (Trump, 2008: 72, 77). Various flagstones seem to have paved other floor areas and rope holes across entrances could indicate that different parts of the internal space may have been cordoned off depending on the occasion (Tilley, 2004: 118). Oracle holes were also a key part to the interior design of some temples, probably providing the means for the priestly elite to communicate with the congregation (Trump, 2008: 111). Apart from the relief / pitted decorations and the built-in, sometimes elaborately carved stone tables assumed to have been altars; little evidence of embellishing is left, though it is likely that the interiors may have been decorated with a series if ochre paintings. Other internal décor may have included doors, partitions and other furnishings made from organic raw materials which have long since disappeared (Evans, 1971: 175; Trump, 2008: 77; Tilley, 2004: 102). Finds within the temples comprise a wide variety of stone (sometimes polished), chert and some obsidian tools (mainly sacrificial knives); amulets and a large range of pottery, the production of which appeared to have flourished incredibly during this period (Bonanno, 1986). Spindle whorls, phalli and figurines which are dominantly female and other rather sexless or animal-shaped were also unearthed on excavation; clearly exhibiting an ancient population that was agricultural-based with a cult involving the adoration of a corpulent fertility deity (Bonanno, 1986; Robb, 2001; Trump, 2008: 75).

The temples within the archipelago therefore have similar architectural characteristics, yet the construction appears to have been 'base' controlled as methods and architectural details vary between temples; indisputably reflecting a division of the

local population into cultural groups (Robb, 2001). The temples themselves appear to be distributed into six clusters of two or three temples, which could be indicative of the territorial centres of various chiefdoms, each probably with a preferred, specialized priesthood; undoubtedly an element of secular competition rather than religious fervour. Consequently, the temples/temple clusters were not just religious centres but could have also served as administrative centres with communal leaders making decisions for the internal community (Bonanno, 1986; Trump, 2008: 89). Certain repetitive features also appear to be shared by a number of temples, and therefore giving some insight to the mindsets of these Neolithic cultures. Firstly, several temples seem to be associated with seasonal watercourses, the sea and/or with the small, off-shore islets. Only two temple sites occupy high points, indicating that sites were not chosen for high visibility; yet larger temple locales were probably intervisible. (Tilley, 2004: 91-92; Trump, 2008: 198) Pairs of temple sites may also be related in terms of locations in the landscape (Table 2-6 below).

Although today the temples are roofless structures exposed to the elements, the walls are estimated to have reached varying heights depending on the roofing system employed. Overall interior volumes are, nevertheless, estimated to have been limited; thus when still in use the temples must have been dark and confined, probably amplifying internal sounds and smells, creating an ethereal, unworldly experience for any congregation of believers (Trump, 1999: 96). The resulting effect that most of the temples presented was a deceivingly solid, static exterior with a mobile, convoluted, organic interior intended to confound. The passageways within the temples were probably opened or blocked at will to endorse this confusion, and the construction itself also induced

changes in body posture through careful manipulation of roof height and overall space. This created an almost bewilderingly complex interior, aimed at disorientating those ancient peoples visiting the temples; thus advocating fear and awe of the priesthood elite and/or chiefs, who stood as the sole intermediaries between the general population and the gods within these prehistoric societies (Tilley, 2004: 130). The temples, therefore, purport a hierarchical culture whereas burials, surprisingly, do not. This class distinction theory within the temples is further supported by the fact that the internal space was too limited to cater for a large group of people, and because the inner sections of some temples (such as Tarxien) and the 'Holy of Holies' in the Hypogeum suggested selective access (Bonanno, 1986; Robb, 2001). A brief description of some of the more important temples and burial complexes (which will also be mentioned later in the text) is given in Table 2-7.

That the temples were ritual monuments is therefore beyond doubt (Robb, 2001). Physical evidence indicates that worship included animal sacrifice on rectangular-cut altar stone slabs, but beyond this, little is known about the rites and rituals that took place in them (Vella, 2007: 63). It is assumed the underlying reason for the construction of these temples and the execution of sacrificial rites lies with the fact that the Neolithic Maltese were farmers who felt the necessity to build the temple structures primarily as loci for ritual and worship to either a priestly elite, or to the figurative 'mother goddess' (/'goddess of fertility') whose obese symbolic form features in many archaeological sites around the archipelago. It has also been suggested that the temples themselves were modeled on the form of the 'goddess of fertility' statues (Trump, 2008: 88).

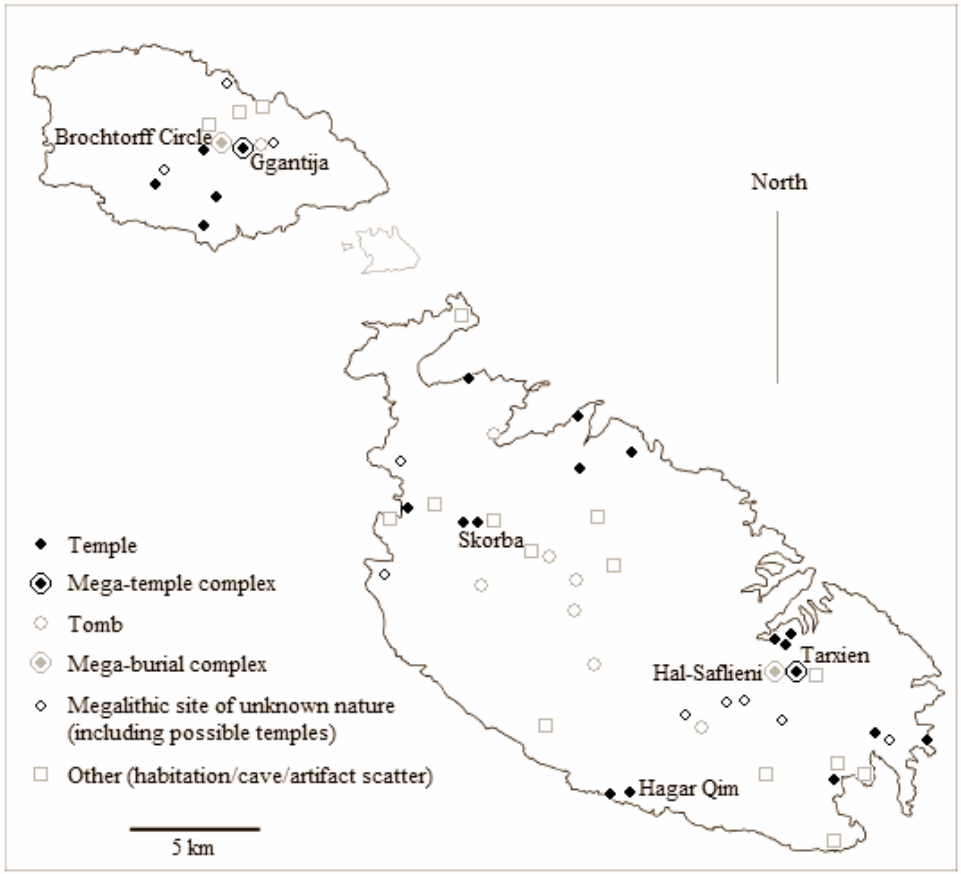

Figure 2-7. The location of the Maltese temples and other prehistoric sites (adapted from Robb, 2001)

Characteristics	Temple examples
Associated with watercourses	1. Borg in-Nadur 2. Hagar Qim and Mnajdra 3. Kuncizzjoni temple site
Associated with harbours	1. Kordin temples 2. Borg-in-Nadur 3. Hagar Qim and Mnajdra 4. Bugibba temple
Associated with the sea and islets	1. Hagar Qim and Mnajdra: Filfla island 2. Bugibba temple: St Paul's island
Occupying high points	1. Hagar Qim 2. Tas-Silg
Intervisible groups	1. Hagar Qim and Mnajdra 2. Ggantija, and Santa Verna and Xewkija 3. Borg-in-Nadur and Tas-Silg 4. Tarxien and Kordin 5. Skorba and Ta Hagrat
Landscape pairs	1. Skorba and Ta Hagrat 2. Hagar Qim and Mnajdra 3. Tarxien and Kordin

Table 2-6. Common characteristics between temples and temple groups (from Tilley, 2004: 91–92)

Site	~ Date B.C.	Brief Description
Malta		
Skorba (SKB)	5000-2500	Settlement complex with two temples, excavation began in 1937. Several artefacts were found, including figurines, pottery and evidence of use and development of site for many years (Neolithic to early Bronze age)
Tarxien temples (TAR)	3000-1500	Discovered in 1913, found here was "the earliest colossal statue in the world" (Vassallo, 2007: 129). The statue and temple complex were partly destroyed by farmers before a formal excavation was undertaken. The complex was still very rich in Temple period remains, which were found beneath a Bronze Age crematorium
Hal-Saflieni Hypogeum (HYP)	4000-2500	Discovered in 1902. Brief description given in text: underground necropolis, burial and temple site, sculpted in the rock. Consists of three levels: Upper level used for burials during 3600-3000 B.C., Middle and Lower levels cut during Tarxien Phase (3000-2500 B.C.), contains about 7000 secondary burials
Gozo		
Ggantija temples (GTA)	Started 3600	'Gigantic' temples, considered as being the oldest free standing structures in the world Massive walls, probably were ~10m high, though today the highest point is 6m: roofing is a mystery Excavated in 1826 (by convicts!) Structure began as one trefoil, which was extended Evidence found of sacrificial offerings and rites
Xaghra (or Gozo) Stone Circle, also referred to as Brochtorff's Circle (XSC),	Between 4100-1500	The burial site for the Ggantija builders Cleared ~1820-1822, but was partially destroyed between 1834-1835 by treasure seekers. Further 20th century excavations unearthed an underground complex of caves, with many finds (~200,000 bones and other artefacts) showing usage from after 4100 (Zebbug Phase) till <1500 B.C. (Bronze Age)
Santa Verna (STA V)	Started 5000	Excavated in 1911, found to have first been a habitation site in the early Neolithic, converted to a temple, used during all periods of Gozitan archaeology. Finds included numerous sherds

Table 2-7. Overview of the temples/sites/habitation sites mentioned in this thesis (from Cope, 2004 and Vassallo, 2007)

2.2.2. Ochre use in Neolithic Malta

One of the more prominent materials used during the Neolithic in Malta was red ochre. Sprinkling liberal amounts of the pigment over bones of the deceased was presumably part of common burial practice in the prehistoric tombs. Quantities used were such that the bones associated with this material were described as being "soaked in blood" by workmen who inadvertently came across them when clearing the sites, horrified at the notion of having discovered some "bloody murder" (Evans, 1971; Trump, 2008: 211). This scenario has been described in the 1910-11 annual report (: 3-4), when a mass of bones were discovered in a prehistoric well-tomb between Buqana and Ta'Qali (Evans, 1953). In the Hal-Saflieni and Xaghra Stone Circle burial sites, it appears that the funerary rituals involved exposing the bodies or burying them until the flesh had decomposed and fallen off completely, with the bones then reburied in a vast ossuary and sprinkled with vast amounts of ochre, possibly mixed with water (Stodart, 1999: 183; Vassallo, 2007: 69)

Ochre was also used to decorate the walls of the Hypogeum and probably the temple walls (Robb, 2001). Though only traces of pigment appear in the temple sites, primarily as dabs of colour on pieces of plaster, very few of which remain *in situ* (Evans, 1959, 1971) (Figure 2-8 below), the elaborate designs in the Hypogeum have survived environmental degradation and are therefore the only surviving examples of wall paintings executed during the prehistoric times on the Maltese islands (Zammit, 1994). Here, it appears that the ochre was ground and mixed with water and possibly some organic binder to form a deep-red coloured paste.

Figures 2-8a, b. The only two remaining pieces of wall *torba* coloured with red ochre. (a) measures approx 5 x 5 cm, whereas the longer ends of (b) measure 10 x 5 cm. Both pieces were found at Ggantija temples in Gozo (Photos: author)

The wall decorations in the Hypogeum include block colour applied to the walls of whole sections throughout the necropolis (as can be observed in Chambers 4, 6, 17, 20 and 23), as well as a variety of other more organic and intricate designs (Bonanno, 1996). These were probably applied for both aural as well as visual effects and comprise a couple of rows of spirals, with free bifurcated ends, connected to polygonal/honeycomb forms by means of a series of vertical lines and applied to the walls and ceiling of the decorated/painted room (Chamber 20, Figure 2-9: Ridley 1976). Other designs include several interconnecting spirals, circles, swirls, curvilinear paintings and other circular designs; such as the three circles in the oracle niche in the oracle chamber, C18 (Pace, 2000: 12; Evans, 1971: 51). Although the curvilinear forms and polygonal designs can be linked to the naturalistic reliefs from Bugibba, Hagar Qim and Tarxien temples, it is interesting that the circle was painted in such abundance in the 'Oracle room', as the use of this shape was exceptionally rare in Maltese prehistory (Ridley, 1976: 22)

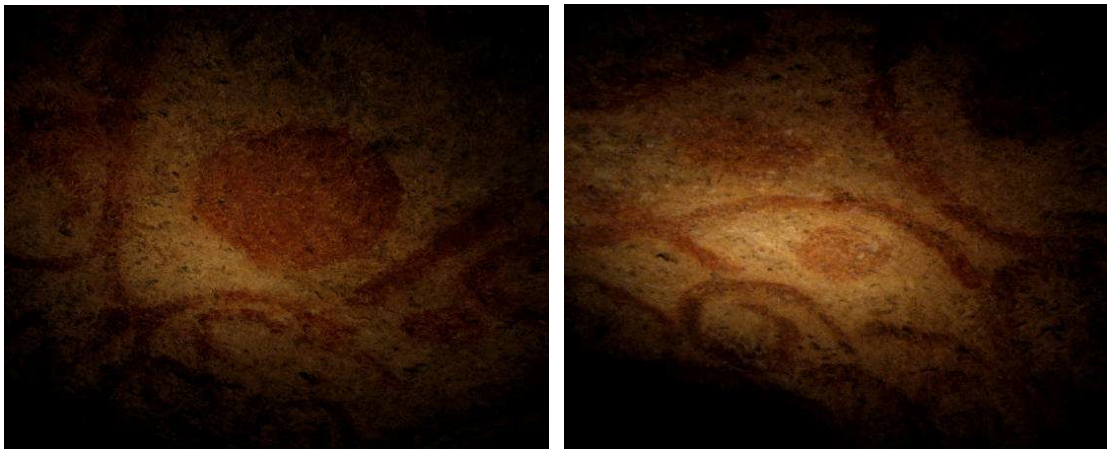

Figures 2-9a, b. Decoration in the underground necropolis of the Hal-Saflieni Hypogeum, Malta. Pictured: Spiral and circular designs from the Oracle chamber (Photos: author)

Ochre was also used to paint several figurines, to encrust and highlight the scratched designs on ceramic ware and probably also as body paints and cosmetics during various rituals and/or on special occasions (Figures 2-10, 2-11). It is also suspected to have been used more profusely as, for instance, a background to the relief spirals on some of the altars and on the torba flooring in Skorba, for example (Trump, 1966: 8; Trump, 2008: 211). It has been assumed that the ochre, albeit used in such copious amounts, was completely imported from Sicily, perhaps in special vessels from the Agrigento area in southern Sicily (Trump, 2008: 211), as it is of common belief that 'none occurs on the islands' (Tilley, 2004: 140).

Although the definite reasons for the designs in the Hypogeum and the use of this pigment in Malta still elude scholars, it is likely that ochre was probably used for its symbolic properties (Pace, 2004). In the temples it is associated with cults for the living, perhaps being an invocation of the semantic properties of the colour red; whereas in burial practices its symbolism is associated with the dead, suggesting an initiation from life towards death, perhaps towards another life (Tilley, 2004: 140).

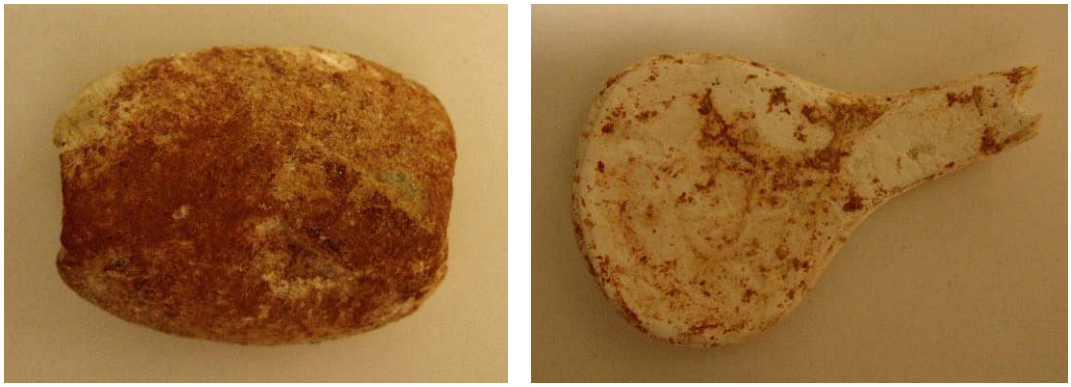

Figures 2-10a, b. Ochre on various stone materials, including a large bead (left) and a spoon (from Gozo, Museum of Archaeology. Photos: author))

Figures 2-11a, b. More ochre-doused material, including the very famous 'Twin Seated' figurines carved out of globigerina (a) and ochre on bone in (b) (Photos: author)

2.2.3. Contact and trade

This temple-building period and exploitation lasted for over a millennium, and around thirty such temples were built on Malta and Gozo, though others may have once existed (Figure 2-7: Tilley, 2004). Though their mass construction may have been spurred by cultural groups and regional priesthood distributions, the massive size and complexity of the temples, their abundance on two tiny islands and the fact that the temples remain without any convincing parallels elsewhere, has made these architectural wonders a point of fascination amongst archaeologists and antiquarians since as early as the sixteenth century (Vella, 2007: 62; Trump, 2008: 6).

There is no simple explanation as to why the Temple period civilization in Malta supported complex art and architecture far more advanced than those of its nearer or distant neighbours, and why none of the contemporaries of the Neolithic Maltese built similar megalithic structures of any kind. This is, in fact, an ongoing debate which has centred on the economic and social set-up of Maltese society in prehistory. Although some authorities consider that the Maltese islands must have been an international centre where foreign cultures combined, producing the temple society as a result; archaeological evidence from places like Skorba for instance, strongly suggest the development to be local, as "No large numbers of visitors, pilgrims, or traders, could have passed through Malta leaving so little trace." (Trump, 1966: 51)

Two relatively plausible hypotheses proposed to describe the unique character of the temples are based on the local environment. The most generally accepted explanation emphasizes biogeography: because the Maltese islands were isolated and relatively insular, the civilizations living there experienced an inevitable drift from the cultures of mainland Europe. The second argument stresses the fragile ecosystem and potential of environmental vulnerability on the archipelago, where increasingly scarce natural resources led to impossible economic problems for the population, invoking a heightened need for fertility rites, which resulted in this mass temple construction (Tilley, 2004: 87). Unfortunately, no concrete evidence for environmental deterioration during the Neolithic exists; hence this latter point is purely hypothetical. The temples have therefore been described time and time again as being a product of cultural isolation, rejecting contact with the external world (Evans, 1953: 80; 1959; Bonnano, 1996; Tilley, 2004: 87). Nevertheless, the problem still stands: how isolated were the islands in actual fact? Did they not form part of a network of societies

stretching across southern Italy and Sicily? Why was there this sudden apparent divergence in cultural habits? The question regarding isolation has in fact been a topic invoking several heated debates between groups of antiquarians for a relatively long period of time.

Many compelling arguments have been purported for and against the presumed isolation hypothesis. The argument for isolation is based on the unique character of the temples (Evans, 1953), and on other archaeological evidence, mainly on the sharp decrease in the quantities of imported products such as obsidian (which was obtained from southern Italy) and pottery, and on the significant differences between temple-period ceramics and contemporary Sicilian and Italian pottery (Evans, 1953: 76, 81, 83). It is also surprising that none of the metallurgical technology was imported to the islands during this period (Bonanno, 1991). Robb, 2001 however, challenged the interpretations based on this 'evidence', insisting that "Malta's apparent isolation at least partially reflects archaeologists looking at Malta in isolation". He pointed out that Malta was not as isolated as claimed but was linked to the rest of Europe through a wide regional network. Robb supported his argument by drawing parallels between the circles of standing stones like those at the Brochtorff Circle to some from Sardinia, and also found similarities between the Hal Saflieni Hypogeum and a 35-room rock-cut hypogeum at Calaforno in Sicily and a smaller one at Malpasso (Vassallo, 2007). Even Bonanno (1986, 1991) drew parallels of the tomb architecture with those of the *Ozieri* culture of Sardinia. Ceremonial rituals also appeared to have been similar (Robb, 2001). Robb also aptly pointed out that the decline in trade of obsidian and pottery was a regional decline, and not a local factor. Moreover, it appears that most pottery dating from this period across Sicily and southern Italy also exhibited regional

differences that emphasized local identities; hence differences were not just a trait being experienced on the Maltese islands. He argued that the unique character of the temples was deliberate action to create cultural differences and maintain their identity.

Robb stressed this claim further by providing arguments and evidence for contact, which rests on the fact that it was relatively easy to cross the 100 km separating Malta and Sicily, a journey that could have been undertaken between one to three days in calm waters (Tilley, 2004). Possible evidence of trade is present, with imports, albeit relatively few, that include high-quality flint, hardstones, polished stone axes and/or amulets, lava rock for grind stones, as well as alabaster and some semi-precious stones which were used as beads (Trump, 1966: 49). Other potentially limited resources that must have necessitated import include timber and fuel (Bonanno, 1986; Robb, 2001). The chief apparent import, however, appeared to have been ochre, which, as has been detailed previously, was used extensively and lavishly throughout this period. Since it has been claimed that there are no ochre sources on the islands this pigment has been used as the definitive proof for contact between the islands and mainland Europe (Evans, 1959; 1971; Bonnanno, 1986; Robb, 2001).

People are still searching for answers to questions relating to these Neolithic inhabitants of Malta who ceased their temple construction 'frenzy' and vanished, as mysteriously as they had first appeared, sometime around 2500 B.C. (Zammit, 1994: 6). It is still a mystery as to why this sophisticated culture collapsed, and/or why the culture was suddenly uprooted as there is no evidence pointing towards a sudden catastrophe (Evans, 1953: 84). It appears that the temples were abandoned abruptly and totally, although a select few were used for other purposes: the Tarxien temple, for

example, was converted into a cemetery (Bonanno, 1986). Speculations include a wipe out of the population through war or pestilence; though it is unlikely that either of these would kill off an entire population.

The most accepted suggestion returns to the probable economic problems associated with islands, including rapid depletion and ensuing lack of resources or a probable draught, which consequently made the archipelago unfit to be lived upon (Trump, 1966: 51). Competition between territorial centres could also have led to social collapse, or the Neolithic Maltese peoples may have been led to think that the islands were accursed by the gods and needed to be abandoned. Suggestive evidence of Maltese influence has been observed in Sardinia (Bonanno, 1986), but little else accounts for the 200 year gap observed before the arrival of the Bronze Age people from southern Italy or the Cyclades (Vassallo, 2007: 60). Whatever the situation was, no evidence exists to disprove any of the theories proposed; yet the temples have always been shrouded in mystery, since nothing as remotely as spectacular has ever succeeded the Temple-phase on the Maltese islands, at least, not for several millennia (Trump, 2008: 241).

Imported Items	Used for	Found at	Originated from
Flint	Tools	Many sites	Monti Iblei, near Syracuse; others from further afield
Obsidian	Tools	Many sites	Major source Lipari, another was Pantelleria
Pumice	Grinding bone instruments	One block found at Skorba	Etna region or on Lipari (?)
Lava quernstones	Cereal grinding	Tarxien	Etna
Red ochre	Ritual, decoration	Many sites	Different sites in Sicily (?)
Polished metamorphic / igneous rocks	Stone axes	Skorba	Various: behind Messina and in the Sila of Calabria
Green stone	Axe amulets	Tarxien	Calabria, probably Sila
Alabaster	Miniatures	Various sites	Argrigentino or northern Calabria
Foodstuffs?			No archaeological trace

Table 2-8. Imported material from Sicily/Italy to Malta: Imports were not that plentiful, and exports are impossible to identify (Trump, 1966: 49-50; Bonanno, 1986)

Figures 2-12a, b. Lower walls at Mnajdra, and a view of the main hall in the Hal-Saflieni Hypogeum (Pictures courtesy of Heritage Malta)

Chapter 3.

Characterisation methods

3.1. Overview of characterisation methods used in the analysis of pigments

As the aim of this project was to assess whether or not the Maltese islands may have been the ultimate source of these abundantly used ancient ochres, it was necessary to establish which techniques were appropriate for characterisation and provenancing purposes; specifically applied to the analysis of pigments, as will be described below.

The techniques selected for the determination of the chemistry of materials therefore depend on a number of issues, including the quantity and quality of the materials to be analysed, the type of information/results required, the availability, suitability and efficiency of the instrument and its operators, the cost-limitations of the study, the accuracy, precision, value and validity of the data, as well as the sample sizes and sampling limitations imposed by the case in question.

Numerous techniques are being studied, implemented, improved upon and made available for the study of objects, for the observation of their condition, fabrication technology, for constituent characterisation and for provenancing purposes. The range of equipment ranges from simple microscopy and chemical methods, to the more precise and innovative instrumental methods, which can be non-invasive, non-destructive and completely destructive; where sampling may or may not be required for the analytical investigation. In the case of non-invasive methodologies, results can be obtained without sampling, and are therefore particularly appealing for archaeometric studies. Non-destructive techniques conversely involve the acquisition of samples, though these samples can be re-used if stored carefully after the

investigation. Destructive techniques on the other hand necessitate complete 'consumption' of an extracted sample for the analytical process involved (Crown, 1968). Although 'classical' wet methods and 'traditional' techniques are still being employed for material chemistry studies, analysis by means of the generally faster and more reliable instrumental techniques is now preferred, especially for provenancing studies because of the ever increasing potential and accuracy exhibited by these techniques. Relatively simple methods like polarising light microscopy (PLM), for example, that uses visible light to observe the optical properties of materials in transmission and/or reflection is still a rather popular technique that is often implemented in the analysis of pigment dispersions (Eastaugh, Walsh et. al., 2006).

The majority of these instrumental methods work on a similar principle. They essentially utilize a source, which may be collimated and resolved before being allowed to interact with a surface, artefact or with an appropriately prepared and/or activated sample. The interaction generally results in some sort of emission, which is then detected, and the overall data output can be interpreted. Comparing the results obtained with supplementary data from complementary techniques is usually necessary for a more comprehensive investigation; which can thus be used to satisfy the aim(s) of the enquiry. Literature studies pertaining to pigment analysis and provenancing studies have shown the potential of a wide range of instrumental techniques, as will be described in the following section, while further instrumental details are supplied in Appendix I. However it is generally observed that:

'There is no one method that is the most suitable for solving all problems…each analytical method has its own particular advantages and limitations' (Brill, 1999)

3.1.1. Analysis of inorganic materials

X-rays have been applied extensively in the analysis of coloured materials. A regularly used non-destructive X-ray technique is XRF spectroscopy, a method that was first implemented in the early 1970s (Moioli and Seccaroni, 2000). It has now become one of the most powerful tools for qualitative and semi-quantitative investigations of cultural materials (Scott, 2001; Hahn, Oltrogge et al., 2004) and is often used in ochre studies, though chiefly in conjunction with other techniques (Calza, Anjos et al., 2008; Ramos, Ruisánchez et al., 2008). Improved portable XRF models additionally allow *in situ* analysis in field studies or in galleries, museums or private collections (Szokefalvi-Nagy, Demeter et al., 2004). The importance of this non-destructive technique has been highlighted in numerous publications (Klockenkamper, von Bohlen et al., 2000; Scott, 2001; Hahn, 2004), and other case studies use this X-ray method to *help* establish the provenance of painted artworks (Aloupi, Karydas et al., 2000) and to authenticate several paintings through pigment analysis (Klockenkamper, von Bohlen et al., 2000; Szokefalvi-Nagy, Demeter et al., 2004). XRF, nevertheless, has its limitations and is generally used as a preliminary investigative technique or employed with complementary analytical or physico-chemical methodologies to allow for an exhaustive knowledge of all the components present in the different pigments (Moioli and Seccaroni, 2000). Although it provides quick and relatively reliable results (Moioli and Seccaroni, 2000; Samek, Injuk et al., 2002) it is a surface technique that does not give any stratigraphical information (Cesareo, Castellano et al., 2004).

PIXE is another widely used non-destructive X-ray technique, implemented rather frequently in the examination of cultural works of art. Like XRF, the advantages of using PIXE with an external air path include few sample size restrictions, improved heat conduction and less charge build-up (Mando, 1994; Moser, Bubb et al., 1998). Its detection is likewise limited to medium and heavier elements, but PIXE can be coupled with other techniques including PIGE to simultaneously analyse the light elements (Reiche, Britzke et al., 2005), and Rutherford backscattering spectroscopy, RBS, for profiling heavy elements (Uda, Demortier et al., 2005, Salamanca et al., 2000). Its lower beam deflection moreover allows for quantitative analysis of materials when appropriately calibrated. PIXE and PIGE applications are similar to those of XRF; hence these techniques have been used to identify inorganic paint constituents on a wide range of substrates and as a result provide historical information about the artefact for authentication, dating and provenancing purposes (Moser, Bubb et al., 1998; Brenner, Lill et al., 2004; Reiche, Britzke et al., 2005; Uda, Demortier et al., 2005; Rivero-Torres et al., 2008; Pappalardo et al., 2008). PIXE is therefore preferable when the non-destructive elemental characterisation of small, well-defined regions is important. However, the technique necessitates transportation of the objects into the accelerator laboratory, which, besides being rather costly, may also result in limitations in its use (Neelmeijer, Brissaud et al., 2000).

The conventional SEM-EDS, on the other hand, remains one of the most prominent techniques used for compositional analysis; mainly due to its relatively low operating costs and its adequate detection limits. The chief advantage of this technique is the coupling of the electron microscope with a dispersive spectrometer. These jointly

provide high-quality magnified images, morphological data, stratigraphical information (if cross sections are prepared), as well as elemental information (San Andres, Baez et al., 1997; Colombini, Giachi et al., 2003; Damiani, Gliozzo et al., 2003; Ponting, 2004; Mazzeo, Joseph et al., 2006). It is often used in conjunction with the PLM for imaging. The EDS is in fact probably '*one of the mostly accepted physical techniques for elemental analysis'* (Szokefalvi-Nagy, Demeter et al., 2004). Though ENVAC modes now allow examination of small objects under environmental temperature and pressure, the SEM-EDS is generally classified as an invasive, but non-destructive technique. Constant calibration is also necessary due to repeated fluctuations of the electron beam.

XRD has an unmistakable advantage over the aforementioned elemental techniques. It is able to give qualitative phase analysis of crystalline, polycrystalline or partially crystalline organic and inorganic molecules (Silbilia, 1996), thus identifying the *compound* rather than giving a peak chart of elements. Powder diffraction is nevertheless considered to be the most reliable way of achieving satisfactory data from an array of crystallites and has been exploited in several ochre analysis studies (Krekel and Polborn, 2003; Rendle, 2003; Pradell, Salvado et al., 2006). Here, it is rarely used alone but is typically exploited in conjunction with other elemental/molecular identification methods, especially as naturally occurring goethite and hematite are poorly crystalline materials (Schwertmann and Cornell, 2000). The potential of XRD, however, lies in its ability to identify the composition, distributions, structural imperfections and relative proportions of the mineral phases associated with the ochre (Murad, 1979; Dold and Fontbote, 2002; Chalmin, Menu et al., 2003; Mortimore,

Marshall et al., 2003). XRD has also been used in several thermal transformation studies of ochres (Przepiera and Przepiera, 2001; Loffler and Mader, 2006; Manasse and Mellini, 2006; Prasad, Prasad et al., 2006). Powder diffraction, however, makes the technique invasive and thus less desirable when compared to the non-destructive XRF or PIXE/PIGE methods.

Several other techniques have been exploited to varying extents for pigment analysis. Mössbauer spectroscopy, for instance, is a technique based on the energy level transitions experienced in nuclei of solids associated with the emission and/or absorption of gamma rays; and has also been used in pigment analysis. It has been found to be especially useful in the observation of iron-containing pigments, mainly to discriminate between lattice structures and co-ordination geometries and to identify oxidation states for iron. It is, however, conventionally also used in conjunction with other complementary methods, yet provides useful supplementary information about the iron content in the materials (Murad, 1979; Casellato, Vigato et al., 2000).

Examples of other useful and routinely implemented techniques include laser induced breakdown spectroscopy, or LIBS, inductively coupled plasma (ICP), sometimes coupled with mass spectrometry (MS), atomic absorption/emission spectroscopy (AAS and AES). All these techniques entail volatizing a sample to plasma, whose constituent particles or elements, existing in an excited state, are subsequently identified by means of a detector/system. The majority of these instrumental methods, the ICP coupled techniques in particular, are very sensitive and hence are ideal for quantitative analysis. Their high sensitivity generates data values of elements present

in materials down to the parts per million range (ppm), and has consequently resulted in the exploitation of these ICP plasma-based techniques in various provenancing studies. Here, when coupled with suitably targeted statistics, some elements present in trace quantities have proven to be geological markers and are therefore exceptionally useful in the successful sourcing of materials, as has been observed in numerous publications (Jarvis, 1989; Kato, Ohta et al., 1998; Lawrence, Greig et al., 2006; Marmolejo-Rodríguez, Prego et al., 2007; Iriarte, Foyo et al., 2008). These techniques are, however, only used in specialized studies as (i) sample preparation can be rather challenging and labour costs can be significant, (ii) the sample is completely consumed during the analysis and (iii) excess data is equally superfluous; consequently these highly-sensitive techniques are rarely used for general material characterisation purposes (Glascock and Neff, 2003).

Neutron activation analysis (NAA) is another technique being implemented in elemental characterisation studies. It involves sample irradiation with neutrons or another neutron source, and results in radioactive emission from the sample, resulting in radiation spectra with peaks characteristic to the elements present within the sample (Glascock and Neff, 2003). Although other techniques, such as the ICP-coupled techniques, have superseded this method in terms of practicality (a neutron source is costly), this method is still being employed in pioneering ochre provenancing studies to date (Popelka-Filcoff, Robertson et al., 2007; Popelka-Filcoff, Miksa et al., 2008).

3.1.2. Molecular methods

FTIR and Raman spectroscopy both utilize the interaction of infrared rays (IR) with materials to gain information about organic and inorganic molecular bonds, and are therefore useful tools in the molecular characterisation of materials. Although both are powerful techniques, they are generally combined with other complementary methods to corroborate results (Wilkinson, Perry et al., 2002). This is mainly because these methods are qualitative rather than quantitative, as too many factors influence the peak heights; which are typically proportional to concentration within a given sample. Resultant spectra can also be confusing, bands may overlap, and absorbance and/or fluorescence may be experienced in critical regions of the spectrum, masking the presence of weaker, yet possibly significant peaks (Drake and Moore, 2006).

Semi-destructive transmission FTIR using a KBr 'window' has often been used as a quick, cheap and relatively satisfactory way of identifying materials: In conservation, for example it has been used for successful identification of both pigments and binding media (Derrick, Stulik et al., 1999; Coates, 2000; Learner, 2004; Drake and Moore, 2006). It has also been found to be a useful method in earth pigment characterisation studies, generally in conjunction with SEM-EDS and XRD (Bikaris, Danila et al., 2000; Genestar and Pons, 2005) and has also been used to observe the molecular structure of ochres and the ensuing changes in molecular composition upon calcination (Cambier, 1986; Betancur, Barrero et al., 2004; Prasad, Prasad et al., 2006). Attempts are still being made to make the technique completely non-destructive by attaching microscopes to the spectrometer and using reflectance methods (van der Weerd, Heeren et al., 2004).

Raman spectroscopy is a completely non-destructive technique that requires little or no sample preparation. It has a wider spectral range in comparison to conventional FTIR (de Gelder, Vandenabeele et al., 2005), and is thus preferred for rapid, *in situ* detection and identification of numerous materials (Rosalie David, Edwards et al., 2001). Raman and micro-Raman have been studied extensively and the techniques have been implemented widely in the analysis of organic and inorganic pigments (Davey, Gardiner et al., 1994; Scardova, Lottici et al., 2002; Smith, Derbyshire et al., 2002; Perez and Esteve-Tebar, 2004; Suzuki and McDermot, 2006). FTIR is, however, generally preferred in ochre studies as it gives more information about the clay fraction within the ochre in comparison to Raman methods, and thus is a better method for ochre/earth pigment differentiation. Several interesting studies have been carried out, however, using Raman as one of the major techniques of analysis, and include spectroscopic studies of natural and archaeological pigments (Edwards, Brooke et al., 1997; Edwards, Drummond et al., 1999; Fremout, Saverwyns et al., 2006). A critical drawback of the technique is the possible aforementioned fluorescence, which seriously interferes with the Raman signals. Though ways of mitigating this problem are being explored (Bartick, 2002; Macdonald and Wyeth, 2006), analogous techniques such as FTIR (Smith and Clark, 2001; Hernanz, Mas et al., 2006; Edwards et al., 1998; Daniilia et al., 2008); or complementary techniques including XRF (Centeno, Mahon et al., 2004; Ricci, Borgia et al., 2004, Sawczak et al., 2008, Ramos et al., 2008) or PIXE (Vandenabeele, 2004) are generally implemented to qualify the components of the material in question. A comparative table of the most useful techniques is provided on P.88.

Chapter 4.
Methodology

4.1. Analytical methodology and pilot studies

4.1.1. Overview

The aim of this section of the project was to explore the methods described in Chapter 3 used for pigment and ochre analysis, and identify which techniques were more efficient at characterising/differentiating between ochres and potentially link them to their source(s). Although recent ochre studies have already suggested the implementation of certain techniques such as NAA and XRF spectroscopy (Popelka-Filcoff, Robertson et al., 2007; Popelka-Filcoff, Miksa et al., 2008), instrument availability and the possible potential benefits of experimenting with other techniques necessitated this part of the study. Two pilot studies were therefore implemented in an attempt to establish a methodology to differentiate between ochres.

The first study, Pilot Study 1, exploited a combination of the complementary and analogous analytical techniques to characterise natural and synthetic ochres, and to assess the reliability in generating data suitable for provenancing. These methods include polarising light microscopy (PLM), scanning electron microscopy (SEM) coupled energy dispersive X-ray spectroscopy (EDS), X-ray diffraction (XRD), X-ray fluorescence spectroscopy (XRF), particle induced X-ray emission (PIXE), inductively coupled plasma – atomic emission spectroscopy (ICP-AES), Fourier transform infrared (FTIR), and Raman spectroscopy. The techniques were used to determine the visible particle morphologies (surface), mineral structures, chemical composition (major, minor and trace elements), and molecular bonds present. An overview of these methods is supplied in Appendix I. Experimentation was also attempted with other

techniques but when results failed to contribute to satisfying the aim of the project further analysis was deemed unnecessary.

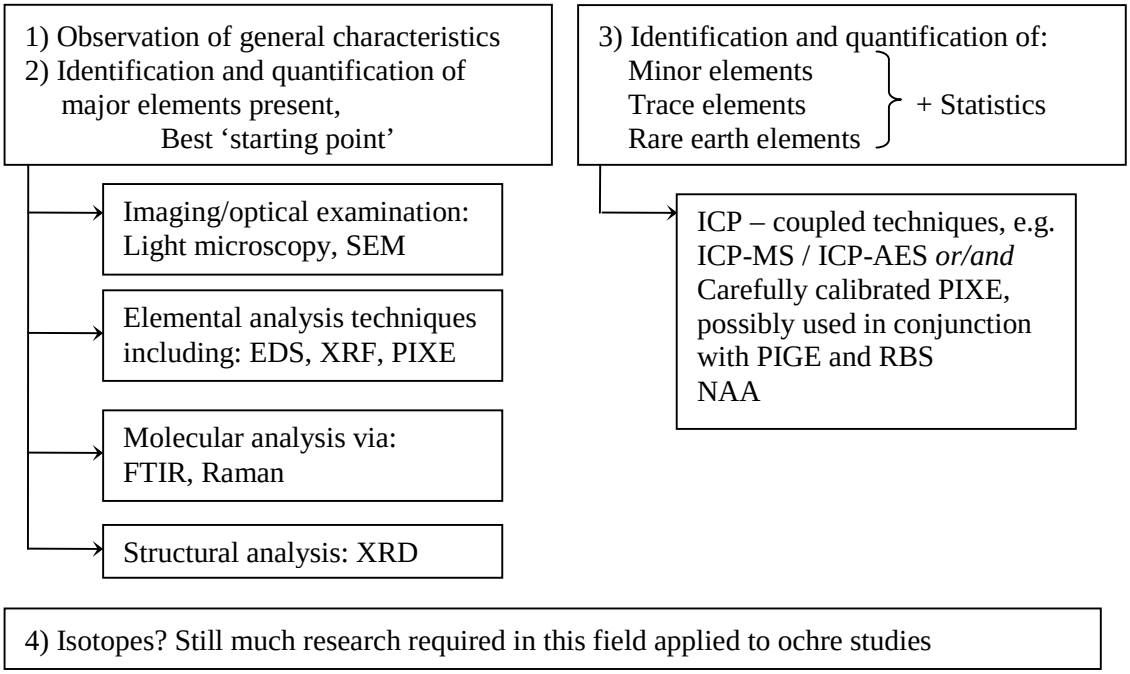

Figure 4-1. The scheme suggested for provenancing studies

The second study, Pilot Study 2, was a sub-study that focused on two of the methods described in Pilot Study 1 that showed debatable benefits for this ochre project; namely XRD and FTIR. The aims and objectives of each study will be outlined in further detail in their respective sub-sections.

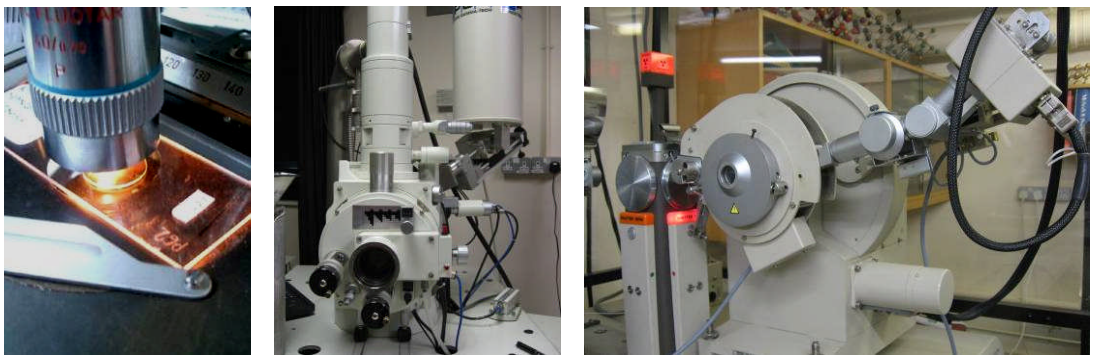

Figures 4-2a-c. *(a)* Observing a dispersed sample *(b)* The SEM-EDS and *(c)* an XRD (Photos: author)

Technique	Pros	Cons
SEM -EDS	Non-destructive, very useful for simultaneous imaging and chemical analysis	Sampling required, and preparation of embedded cross sections if required can be relatively time consuming
XRF	Non-invasive, low penetration depth, quick, no sample preparation required, qualitative and semi-quantitative elemental analysis of a particular area of the sample	Surface sensitive, careful calibration is necessary, irregularities and distance from object might lead to inaccurate results, no stratigraphical information and cannot detect light elements
PIXE	Sensitive elemental technique, non-destructive, can also be non-invasive if an air-path is used/sample is mounted outside the chamber. Profiling through multiple paint layers is also possible by varying the energy of the incident beam	Expensive to run and operate, sample needs to be transported to the accelerator facility, quantification is only possible if the 'dark matrix' i.e. the matrix of the invisible elements (generally of low Z) is known (Pappalardo, Sanoit et al. 2007). Detection is limited to medium and heavier elements
XRD	Establishes chemical identity of materials rather than their elemental composition, also used to measure crystallinity (via XRD line widths), order and particle size (coherently diffracting domain size). Sample preparation is relatively easy, results obtained are both qualitative and quantitative	Only useful for materials with repeating structural unit (crystalline phases). Library of diffractograms and reference material required to establish material identities. Powder diffraction also necessitates sampling, and detection limits can be an issue
ICP-AES	Very sensitive technique for elemental analysis: major, minor, trace and rare earth elements are identified	Complex and time consuming (sometimes dangerous) sample preparation, sample is consumed during analysis
FTIR	Molecular characterisation, small quantity of sample required, quick and relatively simple sample preparation, short analysis time. Also allows for the simultaneous study of organic and inorganic species, crystalline or amorphous compounds, and in some cases, even provides mineralogical information	Quantitative analysis is virtually impossible, spectra interpretation can be very difficult because of overlapping bands, grain size affects results, spectral interferences are not uncommon
Raman	Non-invasive, low penetration depth, no sample preparation required, provides information regarding the molecular structure and crystal lattice vibrations and hence is sensitive to the composition, chemical environment and crystalline structure of the material analysed	Fluorescence may mask several if not all peaks, surface sensitive, too high power may burn material, matrix effects, bands may overlap if mixtures are present, weaker peaks may be masked

Table 4-1. Pros and cons of the instrumental techniques used in this pilot study (from Lyman, 1990; Brundle, Evans et al., 1992; Silbilia, 1996; Skoog, Holler et al., 1998; Rouessac and Rouessac, 2000; Action, 2004; Adriaens, 2005; Sackler, 2005)

4.1.2. Sample selection for pilot studies

The samples for Pilot Study 1 were acquired from a variety of sources. Pieces of raw yellow ochre were collected from a once popular, now disused ochre deposit at Shotover hill, Oxfordshire. A total of four areas were selected, S 1001 – S 1004, with multiple samples extracted from both the surface and the core were obtained from each. Another group of geological ochres were donated to this project and consisted of four different lumps of ochre acquired from the well-known ochre mines in Margi (MC 1001) and Sia (EC 1001 – EC 1003), in Cyprus. Another large block of red-chalk ochre was obtained from Norfolk (N 1001). Two final sets of samples of natural and synthetic red ochre were also acquired from a paint plant factory in Mumbai, India, for comparative purposes and were used as controls (NI 1001, SI 1001).

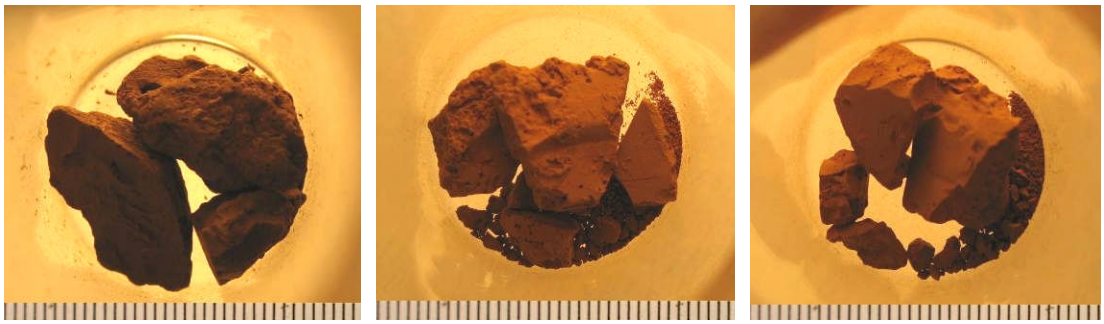

Figures 4-3a-c. Examples of samples gathered (Photos: author)

The group collected for Pilot Study 2 consisted of a large set of earth pigments which were provided by the Pigmentum Project. These included a range of forty different varieties of ochres, siennas, green earths and umbers, with shades ranging from yellow to red, green to brown, all collected for comparative purposes. The country of origin was known in most cases, and all known details were documented (refer to Pilot Study 2 for a comprehensive list of the pigments, their colours and sources).

4.1.3. Sample preparation

Technique	Samples Prepared
(a) PLM	Preparation of dispersion sample by dispersing the pigment particles in thermoplastic resin on a slide mounted on a hot plate. The permanent slide was sealed with a coverslip while the resin was still hot
(b) SEM-EDX	Particles were dispersed on a stub, attached by means of double-sided sticky carbon tabs. These were carbon coated twice for examination in certain experiments (SEM-EDS 1)
(c) XRF	No sample preparation was required. This method was only used in experiments in Chapter 5
(d) PIXE	Tests were carried out using approximately 0.3 g of sample, which was pressed into 10 mm ∅ pellets and was mounted on a graphite holder. Carbon paths were traced along the edges of the pellets
(e) ICP-AES	Samples (~ 0.3g) were dissolved and analysed at the Royal Holloway College Geology Labs in Surrey
(f) XRD	Around 0.006 g of sample was ground and placed in the middle of an XRD sample holder
(g) FT-IR	Powdered samples (0.004 g) were pressed into discs with 0.132 g of potassium bromide (KBr)
(h) Raman	Various tests carried out, with varying acquisition times and distances on both the mineral and ground pigment

Table 4-2. A table summarising sample preparation

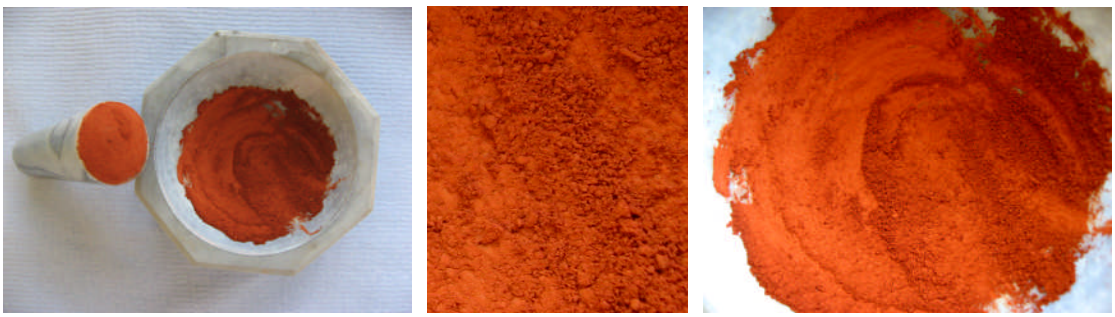

Figures 4-4 a-c. Pigment preparation: grinding (Photos: author)

4.1.4. Instrumental set-up

PLM: The PLM used was a Polyvar MET microscope, equipped with a Polaroid camera for quick capture. Various magnifications were used for observation of the properties of the sample, including an objective lens of X100 which necessitated oil immersion.

SEM-EDS: Two SEM-EDS instruments were used for this pilot study. Samples were powdered and adhered to a stub for both machines. The first SEM was a JEOL JSM – 840A, which was operated at an accelerating voltage of 15 kV under high vacuum. The powdered samples examined under this SEM were coated in a conductive layer of carbon to prevent negative charge build-up on the surface. Backscattered electron images (BSE) of each sample were obtained and both major and minor elements were detected at a working distance of 15 mm using the attached PGT Princeton Gamma – Tech Si(Li) detector (EDS). This was regulated to collect a spectrum at approximately 300 seconds livetime.

The second SEM was a LEO 435VP variable pressure microscope with the potential of working in near environmental (EnVac) conditions. This EnVac mode was operated at 20kV and was used for examining the samples, thus precluding carbon coating required for high vacuum conditions. Observations were carried out with a backscattered electron detector (BSE). Analysis was carried out by means of an attached GENESIS EDAX INC. advanced microanalysis solutions energy analyser, which was regulated to collect a spectrum at approximately 200 seconds livetime and at a working distance of 24 mm. Quantitative oxide concentrations in weight % were calculated by stoichiometry from element percentages generated by the EDS software.

XRF: An Innov-X Alpha Series was loaned for the non-invasive analysis of selected samples in this project. It had an X-ray tube excitation source, and a high resolution, thermo-electrically cooled SiPiN diode detector. The XRF was operated at 40 kV, 9 μA, at approximately 40 seconds livetime. The instrument was suspended ~ 5mm from the surface of the object.

PIXE: The samples were attached to a graphite holder by means of conductive carbon cement. Paths of this cement were also traced along the edges of the sample. The PIXE was equipped with a Van der Graaf accelerator source and a PGT Princeton Gamma-tech Si(Li) detector, operated at 2MeV and 10 nA.

ICP-AES: 0.3 g of the sample was powdered finely. 0.2g of the powdered sample was then weighed into a Teflon beaker. 4 ml of hydrogen fluoride (HF), 2 ml of perchloric acid ($HClO_4$) and 1 ml of nitric acid (HNO_3) were added to the sample and the mixture evaporated to dryness on a hotplate. After cooling, the samples were dissolved in 10% hydrochloric acid, warmed and after cooling diluted to 20mls. The prepared solutions were then analysed using the Perkin Elmer 3300RL ICP optical spectrometer for the range of major and trace elements. Major elements were quoted as weight percent oxide and trace elements as parts per million (ppm) of the element. Both acid dissolution and analysis was carried out at the Royal Holloway College.

XRD: The XRD profiles of the powdered samples were obtained using a Kristalloflex 810 Siemens powder diffractometer equipped with a Cu Kα radiation source. The accelerating voltage and the electric current at the Cu anode were 40 kV and 30 mA (1200W) respectively. A range of 10 – 80° 2θ was scanned at a step size of 0.02° and at a count time of five seconds per step. All data was compared to reference data from Crystallographica Search-Match. Further analysis was carried out at a later date on a separate X'Pert PRO PANalytical powder diffractometer, operated at 40 kV and 40 mA and a Cu Kα source. The angular range was also set at 10 – 80° at a step size of 0.013° and scanning s peed of 0.022 s.

FTIR: Sample preparation involved pressing the powdered samples into 10 mm diameter discs (pressure 10 t) using the compressed alkali metal halide pellet method (also known as the KBr pellet or disk method). A typical disc was prepared by combining the sample with the salt in an approximate ratio of 1:33. A total weight of 0.055 g made the pellet of appropriate thickness for effective transmission. Generally 0.004 g of sample was mixed with 0.132 g of KBr, thus two pellets were run off the same sample to corroborate results. A background scan was also made to preclude environmental interferences, and the KBr pellet was prepared just before it was due to be analysed.

The sample pellet was placed in the infrared beam path of a Bruker Vector 22 FTIR spectrometer and data collection time was run over a period of 100 seconds. Some charts distortions, exhibited as slightly sloping baselines and low percentage totals that possibly represented energy loss by scattering and/or diffraction of the IR beam, were found to be impossible to rectify and consequently necessitated the application of the baseline correction system and y-axis scaling to facilitate peak evaluation.

Raman: The instrument used was an Ocean Optics R-3000 Raman spectrometer, with an incident beam wavelength of 785 nm and a output power of 250 mW. The dynamic usable range was between 200 – 1800 R cm^{-1}. White light background correction was performed prior to the acquisition of every spectrum, and integration times were set at 5, 10, 20 and 30 seconds

4.1.5. Pilot Study 1

An overview of the aims of this study therefore included the following:

i. To test the instrumental techniques used in pigment analysis, namely PLM, SEM-EDS, PIXE, XRD, ICP-AES, FTIR, Raman.

ii. To establish how useful, adequate and/or complementary the methodologies were to differentiate between ochres.

iii. To observe whether different groups may actually be differentiated, and how these relate to their sources, colorant etc.

iv. To establish which methodology provided the most valuable information for this project; i.e. which results obtained were the more useful for the characterization and provenancing of ochres.

v. To determine whether any unanswered query would require further investigation in an auxiliary study.

Sample		Description	
N$^{o.}$	**Name**	**Source**	**Colour**
1	S 1001	Shotover, Oxford, UK	Yellow-brown
2	S 1002	Shotover, Oxford, UK	Yellow-brown
3	S 1003	Shotover, Oxford, UK	Yellow-brown
4	S 1004	Shotover, Oxford, UK	Yellow-brown
5	MC 1001	Margi, Cyprus	Bright yellow
6	EC 1001	Sia, Cyprus	Yellow-brown
7	EC 1002	Sia, Cyprus	Dirty-brown
8	EC 1003	Sia, Cyprus	Red
9	N 1001	Norfolk, UK	Reddish -white
10	NI 1001	Paint plant, India	Red (natural)
11	SI 1001	Paint plant, India	Red (synthetic)

Table 4-3. The samples analysed in this study

PLM results. PLM data from the examined Shotover dispersion samples showed a large number of quartz grains and goethite. The goethite consisted of fine, translucent, rounded, yellow-brown crystals of approximately 1.5 µm (though variable) diameter, and which tended to clump together and to the quartz grains (Figure 4-5b). The quartz particles varied in size but were characteristically much larger than goethite; with a vitreous, angular and transparent appearance. S 1003 had fewer quartz grains in comparison to the other Shotover samples (Gribble and Hall, 1992: 40).

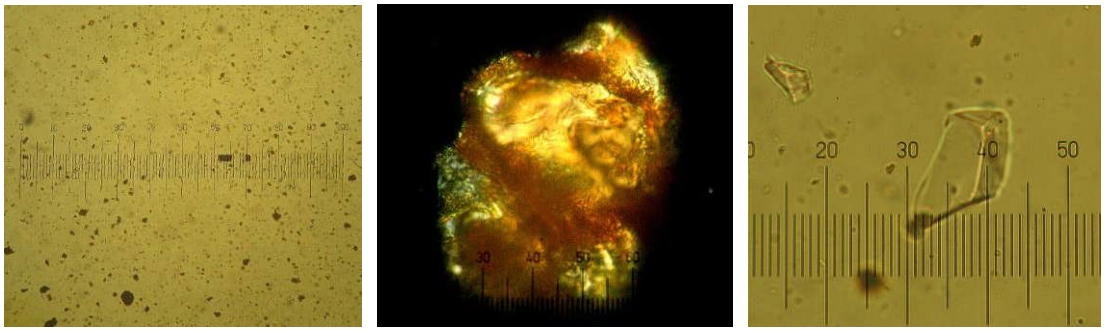

Figures 4-5a-c. Characteristic Shotover dispersion samples under the PLM: Mag. X200 of clumps of goethite grains in S 1001 (a) and goethite on a large particle of quartz at Mag. x1000 in oil immersion of S 1002 under crossed polars (XPL) (b) Quartz grain (X1000) in S 1001 (c)

Observation of the particles in MC 1001 showed that the pigment was not an ochre. Comparison to previous studies of documented optical properties of pigments under plane and cross-polarized light (XPL) indicated that the main colorant was probably a material known as jarosite or natorjarosite, of composition $KFe_3(SO_4)_2(OH)_6$ and $NaFe_3(SO_4)_2(OH)_6$ respectively (Eastaugh, Walsh et al., 2004: 150). The main distinguishing features included the particle shape and size: while goethite and hematite were rounded particles with a distinctive yellow or red colour, jarosite-based particles were generally hexagonal with a yellow to greenish tinge (Figure 4-6c). An even more marked distinguishing feature was the high birefringence experienced under XPL.

The EC 1001 – EC 1003 dispersion samples were similar to those from Shotover, as can be seen in Figure 4-6c. Here goethite appears as clumps on a quartz grain. These samples appeared to be quartz dominant with varying proportions of goethite-to-hematite. Hematite crystals observed were more abundant in EC 1003 and appeared near-identical to goethite particles under both plane and crossed polarized light; only differing, as expected, in colour. The EC samples differed from the Shotover group as they appeared to have a greater pigment to-accessory mineral ratio, and thus were 'purer' (Chapter 1).

N 1001 consisted of hematite granules clumped onto particles of calcite. The calcite itself was present in large quantities and was clearly distinguishable from quartz grains (which did not feature anywhere in N 1001) due to its high level of birefringence with third order interference colours (Figure 4-7a). Pleochroism of the same calcite particles was also visible under plane polarized light (PPL).

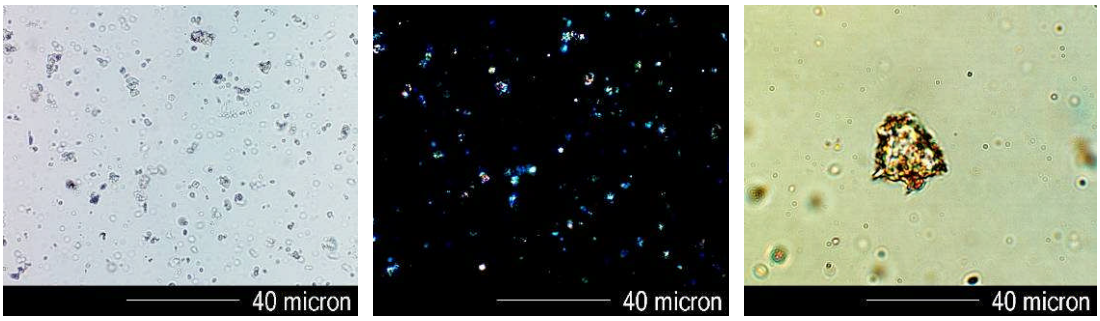

Figures 4-6a-c. (a) MC 1001 samples PPL, (b) MC 1001 under XPL and (c) EC 1002 showing ochre particles clumped on a grain of quartz. Mag X400 in all images.

Lastly, the samples obtained from the paint plant in India appeared to consist solely of pure hematite, both as separate, minute, grains and as clumps. Although there were no very noticeable differences between the natural and synthetic varieties, the synthetic

ochre consisted of particularly small rounded particles, a characteristic of a synthetic method of manufacture, whereas the so called 'natural' variety seemed to have some grains with a sub-angular/less rounded appearance.

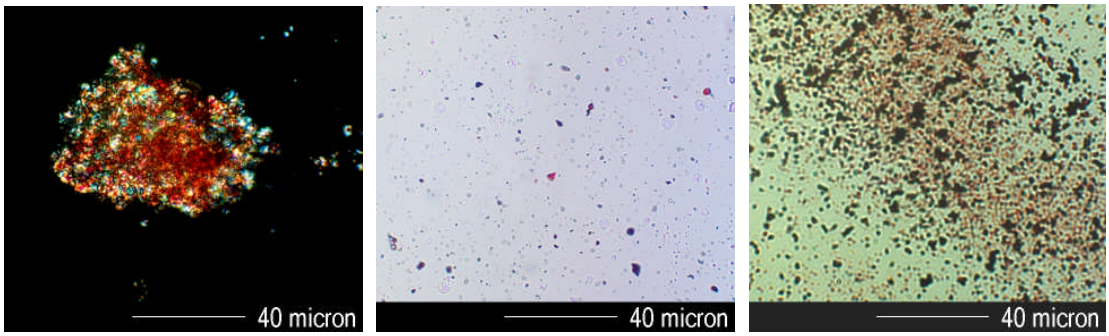

Figures 4-7a-c. (a) Particles of ochre clumped onto a large, birefringent calcite particle in N 1001, viewed under XPL, (b) NI 1001 and (c) SI 1001. All were viewed under Mag. of X400

SEM-EDS results. Below are some examples of the secondary electron (SE) images taken of a selected few of the samples in question. Particle size varied, with grain dimensions of the larger (quartz) particles differing between grains on the same stub. EDS analysis was majorly qualitative and partially quantitiative as the JEOL JSM-840A-PGT Princeton Gamma-Tech EDS spectrometer used was inadequate for fully or even semi-quantitative results. The particles were also irregular, making it difficult to obtain accurate elemental counts. The major and minor constituents of the pigment particles in each case were evaluated by calculating ratios of the abundance of elements present in proportion to their peak heights. Analysis for the Cyprus samples was repeated on the LEO 435VP - GENESIS EDAX INC SEM-EDS (more accurate).

Optical observations under the SEM merely confirmed PLM observations, revealing pigment particles clumped together or around the more angular quartz grains. The latter observation was especially featured in the Shotover samples, whereas the Cyprus samples predominantly appeared to clump together. The accessory mineral in N 1001

was calcite, whose particle sizes were significantly smaller (~20 μm) in comparison to the quartz grains. The paint plant pigment from India purely consisted of small pigment grains and negligible amounts of material other than the iron oxide.

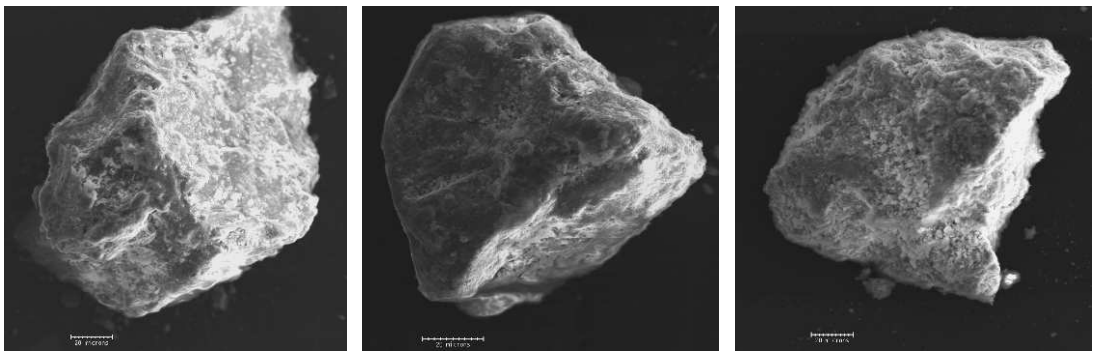

Figures 4-8a-c. SE images of examples of the Shotover samples (scale bar: 20 μm)

Qualitative results and comparisons between the major elements present in averaged semi-quantitative readings enabled the division of most samples into their (expected) groups, namely Shotover, Sia, India. The data indicated that both Shotover and Sia natural ochres predominantly consisted of silicon dioxide, iron oxide and aluminum oxide, while the paint plant India ochres were chiefly hematite based. The Margi and Norfolk samples fell into categories of their own, with the Margi ochre being sulphur and iron dominant, whilst the Norfolk sample was very calcitic.

Partially-quantitative results are given below, displayed in oxide wt-% as is conventional for EDS analysis. These results also gave inter-group differences, with S 1003, for example, having a much higher concentration of Fe in comparison with the other three samples, indicating that the ochre was of better quality than the other Shotover samples. Comparison between minor elements present enabled a more efficient sample distinction, and confirmed the discrepancy between these samples. S 1001, S 1002 and S 1004 had a similar composition containing small quantities of

potassium and titanium, whereas S 1003 conversely contained traces of phosphorous and lead.

	Samples			
Oxide %	MC 1001	EC 1001	EC 1002	EC 1003
Na_2O	3	0	0.2	0.5
MgO	0	0.3	0.5	1.7
Al_2O_3	1.2	5.1	3.3	12
SiO_2	8.3	20	20	41
SO_2	26	0.6	5.5	1
K_2O	0.4	0.3	0.5	0.8
CaO	0	0	0.3	1
TiO_2	0	0.7	0	1.2
Fe_2O_3	62	73	69	41

Table 4-4. Oxide % values of samples from Cyprus

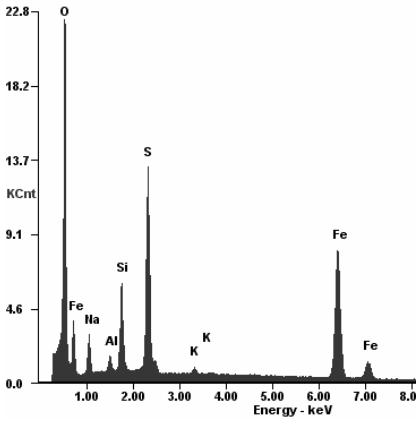

Figure 4-9. EDS spectrum of MC 1001

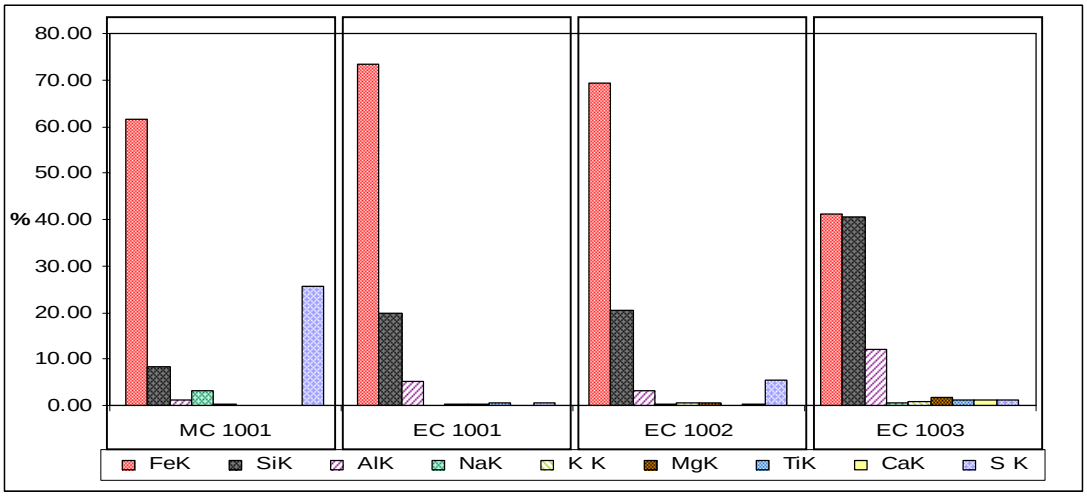

Figure 4-10. Comparison between oxide% in MC and EC samples (Error at 20%). K (in FeK/SiK etc.) refers to the K lines representing electron shell transitions in the EDS

EDS measurements of the Cyprus samples showed that MC 1001 were of different composition to the EC samples. They had comparatively high sulphur levels; though the other (minor) elements present indicated formation in similar silicaceous (rather than calcitic) environments. Differences within the same Sia ochre group were also apparent, therefore indicating inter-site variation. EDS analysis is therefore useful for characterisation studies, although a much larger sample group is necessary to assess whether inter-site variation was significant.

PIXE results. Tests results showed that the PIXE had potential, but needed to be re-calibrated. Nevertheless, a poor signal-to-noise ratio and a low count rate were observed for each sample, though the deadtime was fairly satisfactory. Results were preliminary and somewhat unsuitable, and further testing at a later stage gave similar results.

XRD Results. The XRD results both corroborated and, in some cases, complemented the SEM-EDS results, giving structural identities of the major materials present rather than giving mere elemental compositions. The colorant in MC 1001, for example was found to be natrojarosite, with molecular formula $NaFe_3[SO_4]_2[OH]_6$. This therefore confirmed and accounted for the predominance of sulphur in the EDS spectrum, confirming the PLM and the SEM-EDS investigations.

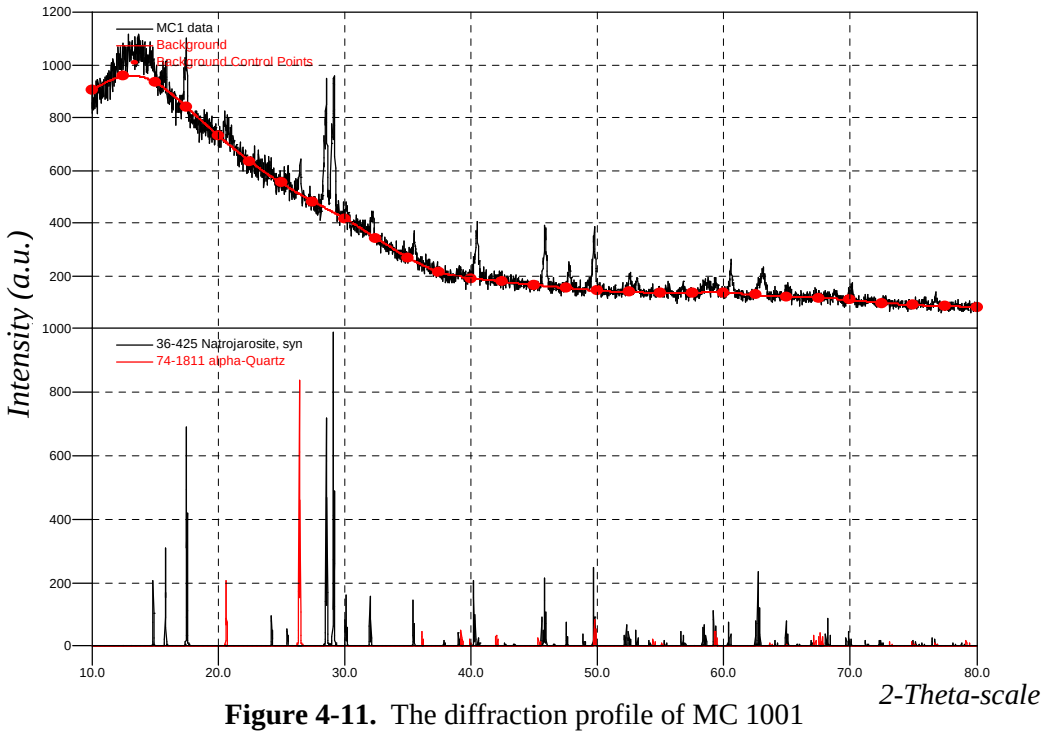

Figure 4-11. The diffraction profile of MC 1001

Distinct diffraction profiles were obtained whenever quartz or calcite were present, as observed in the Shotover and Cyprus samples (quartz dominant), and the Norfolk samples (calcite dominant). Iron oxide profiles gave a poor signal-to-noise ratio as the material was poorly crystalline (typical problem) and/or was present in very low quantities, thus giving almost no peak visible above the background.

When iron oxide was present in quantities above detection limits, it was identified as goethite in sample S 1003 and hematite as in both the EC samples and in the paint plant samples from India. In the latter example, the natural ochre gave a more defined diffractograms, possibly showing that the iron oxide here was more crystalline than its synthetic counterpart. Higher counts also indicated a higher proportion of crystalline material, as in S 1002. A blank slide was run as a control and showed that the broad swell observed between the 10 – 20^{o}2θ was attributable to the support.

Figure 4-12. Poorly crystalline goethite which was distinguishable in S 1003

Overlaying the diffractograms obtained per sample (Figure 4-13 below) also showed obvious correlations between materials obtained from the same site in comparison to those obtained from different sites. In the latter (b) example, for instance, EC samples had near-identical diffraction profiles, whereas it is obvious that MC 1001 fell into an entirely different pigment category.

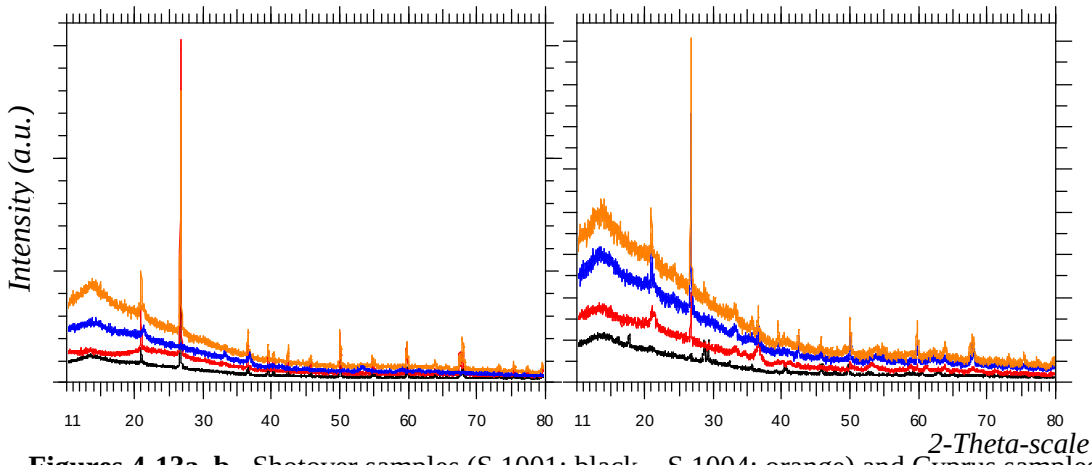

Figures 4-13a, b. Shotover samples (S 1001: black – S 1004: orange) and Cyprus samples (MC 1001: black, EC 1001: red – EC 1003: orange)

ICP-AES results. Not all the samples were analysed by means of dissolution ICP-AES due to the cost incurred per sample; hence representative samples, namely S 1001 – S 1003, N 1001, MC 1001 and EC 1001 – EC 1003, were selected for analysis. This ICP-AES method was the most sensitive of the selected techniques in these pilot studies and is probably amongst the most sensitive of methods available for elemental analysis to date. The average detection limit was given as 1 ppm, though this varied slightly per element: consequently all data will be reproduced to 2 significant figures. The data obtained was exceptionally useful at discriminating between the samples, showing both site similarities and disparities. All the results obtained have been tabulated on the following pages, and various charts have been plotted to observe relationships between data.

A considerable amount of information was acquired from the data. The plots below (Figures 4-14a, b), for example, show the variation and correlation between the major and minor elements in the samples. Observations included a significantly higher Na_2O wt-% in MC 1001 in comparison to all the other samples: therefore corroborating all evidence and proving the pigment was natrojarosite. TiO_2% in MC 1001 was much lower (8x lower) than average, and also appeared to be indirectly proportional to Al_2O_3% in Cyprus data, though not in UK data. The Cyprus results also show that the Ba and Cu (ppm) content was higher than in any other sample group.

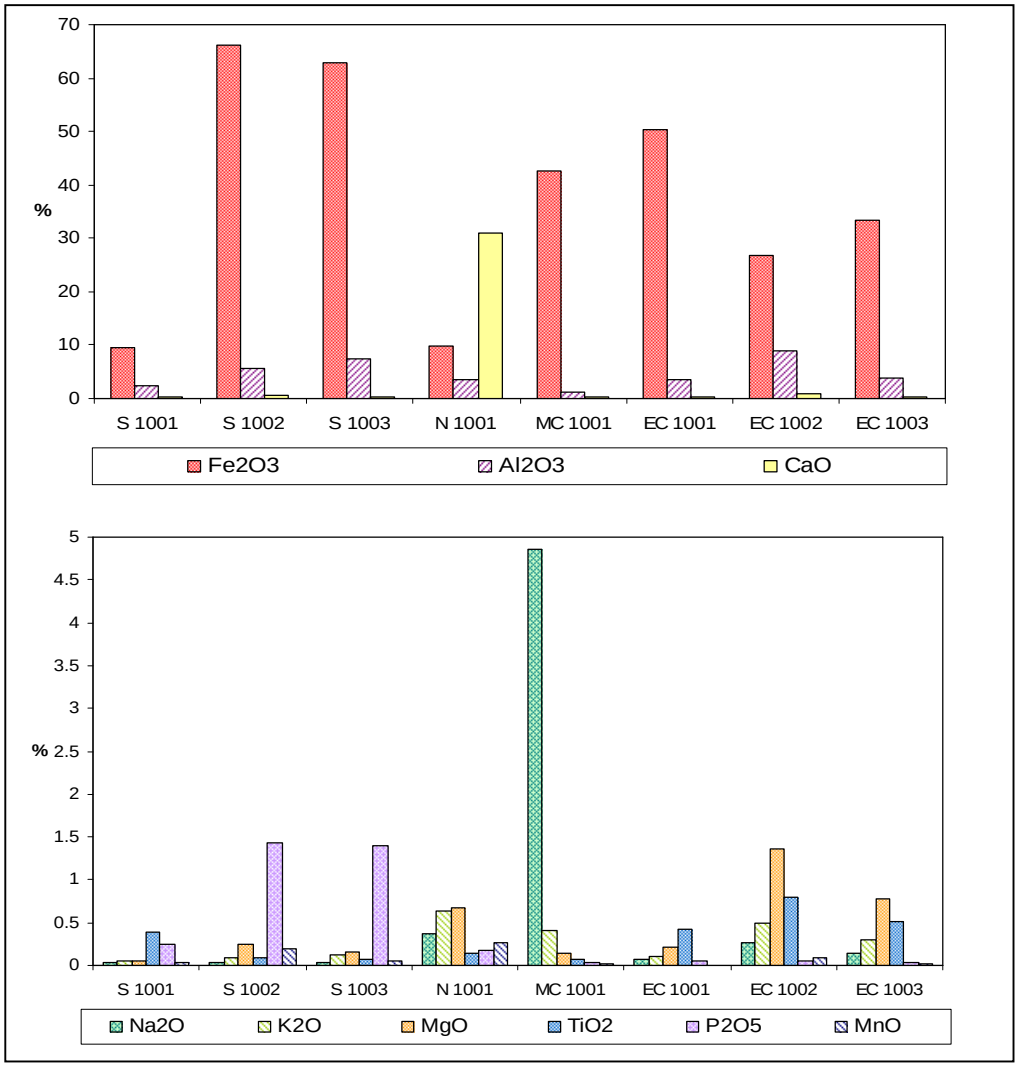

Figures 4-14a, b. Bar charts showing the oxide percent variations of Fe, Ca and Al between samples (a) and of the minor elements present in the samples (b)

	%	%	%	%	%	%	%	%	%	(ppm)	(ppm)	(ppm)	(ppm)	(ppm)	(ppm)	(ppm)
sample	**Al2O3**	**Fe2O3**	**MgO**	**CaO**	**Na2O**	**K2O**	**TiO2**	**P2O5**	**MnO**	**Ba**	**Co**	**Cr**	**Cu**	**Li**	**Ni**	**Sc**
S 1001	2.4	9.4	0.06	0.21	0.04	0.06	0.39	0.24	0.04	48	7	104	6	12	34	3
S 1002	5.7	66	0.24	0.45	0.04	0.09	0.09	1.4	0.2	26	73	200	23	4	283	11
S 1003	7.3	63	0.16	0.41	0.04	0.13	0.07	1.4	0.05	44	26	190	38	8	137	11
MC 1001	1.05	43	0.14	0.31	4.9	0.40	0.07	0.03	0.01	190	1	0	57	2	1	3
EC 1001	3.7	50	0.22	0.36	0.07	0.10	0.42	0.05	0.005	66	5	2	870	1	0	11
EC 1002	8.9	27	1.4	0.86	0.27	0.50	0.79	0.05	0.08	430	11	69	1600	3	23	27
EC 1003	3.8	33	0.77	0.40	0.15	0.30	0.51	0.03	0.02	260	9	21	46	2	5	15
N 1001	3.6	9.9	0.67	31	0.37	0.64	0.15	0.17	0.26	59	9	92	25	23	252	6

	(ppm)	(ppm)	(ppm)	(ppm)	(ppm)	(ppm)	(ppm)	(ppm)	(ppm)	(ppm)	(ppm)	(ppm)	(ppm)	(ppm)	(ppm)
sample	**Sr**	**Zr**	**U**	**Th**	**Rb**	**Nb**	**Cs**	**Y**	**La**	**Ce**	**Pr**	**Nd**	**Sm**	**Eu**	**Gd**
S 1001	24	78	2.6	1.7	6	0.8	0.28	14	7.7	14	2.1	10	2.3	0.53	2.2
S 1002	14	140	14	16	8	3.6	0.40	44	14	40	5.5	26	8.9	2.0	8.03
S 1003	32	80	19	6.1	9	4.3	1.3	47	21.4	62	8.4	42	14	3.0	12
MC 1001	76	14	0.12	0.12	5	0.2	0.04	2	0.4	0.6	0.1	0.5	0.22	0.17	0.16
EC 1001	6	28	0.17	0.16	2	0.8	0.04	3	0.5	1.0	0.1	0.7	0.36	0.15	0.33
EC 1002	39	37	0.69	0.46	6	1.6	0.15	6	2.3	4.4	0.6	2.8	0.82	0.47	0.72
EC 1003	21	25	0.14	0.18	4	1.0	0.05	3	0.6	1.1	0.2	1.0	0.47	0.24	0.38
N 1001	207	59	0.51	5.03	24	15.4	1.28	18	19.2	33	4.9	22	4.8	0.93	4.3

	(ppm)	(ppm)	(ppm)	(ppm)	(ppm)	(ppm)	(ppm)	(ppm)	(ppm)	(ppm)	(ppm)	(ppm)	(ppm)	(ppm)	(ppm)
sample	**Tb**	**Dy**	**Ho**	**Er**	**Tm**	**Yb**	**Lu**	**As**	**Pb**	**Cd**	**Tl**	**Mo**	**Sb**	**Bi**	**Sn**
S 1001	0.37	2.0	0.39	1.02	0.15	0.86	0.12	57	6	0.1	0.04	0.7	0.6	0.2	0
S 1002	1.6	9.6	1.9	5.4	0.89	5.7	0.80	170	106	1.0	0.07	1.5	3.8	2.3	1
S 1003	2.4	13	2.4	6.6	1.06	6.7	0.95	890	150	0.4	0.17	22	15	1.8	2
MC 1001	0.07	0.21	0.07	0.42	0.04	0.14	0.02	106	33	0.1	1.9	4.1	1.3	1.0	1
EC 1001	0.07	0.64	0.11	0.40	0.06	0.39	0.05	24	10	0.3	0.10	0.7	1.1	0.2	2
EC 1002	0.15	0.98	0.25	0.76	0.10	0.70	0.11	300	72	1.9	1.3	5.2	16	1.7	4
EC 1003	0.09	0.48	0.12	0.32	0.07	0.53	0.06	23	7	0.1	0.09	4.2	1.9	0.7	1
N 1001	0.6	3.1	0.62	1.7	0.24	1.5	0.23	103	15	0.3	0.17	1.5	4.1	0.6	1

Table 4-5a-c. ICP-AES data for Pilot Study 1: the major elements are given as the conventional oxide wt-%, while all the other data is given in ppm. Data has been rounded off to 2 significant figures

The main component of all samples was undoubtedly iron, although the accessory mineral that predominated in the majority of the samples, namely quartz (as was determined by means of SEM-EDS and XRD analysis), could not be measured by this analytical technique. Relative proportions of iron oxide in the samples have been plotted (Figure 4-15), and show that if the iron oxide was the main colorant material and denotes pigment quality, it may be assumed that both the Shotover (S) and Cyprus sites are good ochre sources, with certain areas within the stated sources being better than others (S 1003).

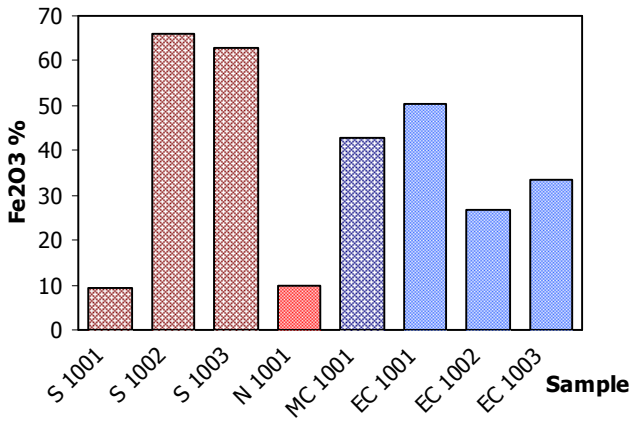

Figure 4-15. Oxide percent of iron (oxide) in the samples showing clear variation in proportions of iron in samples from the same source

It is apparent that the iron oxide concentration varied per sample, even markedly within a same source; hence analysis of results for the purpose of source discrimination (comparative purposes) necessitated treating the iron as a dilution factor for the other components. This involved examining the elements as log-10 ratios to the iron in a series of bivariate plots to validate this discrepancy and enable efficient comparison of concentration ratio values (refer to section 4-3). A considerable number of graphs were plotted to observe inter- and intra-source variation, with only the most representative being reproduced in this brief report. These include four examples of bivariate plots used to compare the concentrations of examples of rare earth elements (REE) present within the materials to show sample grouping in UK vs. Cyprus samples.

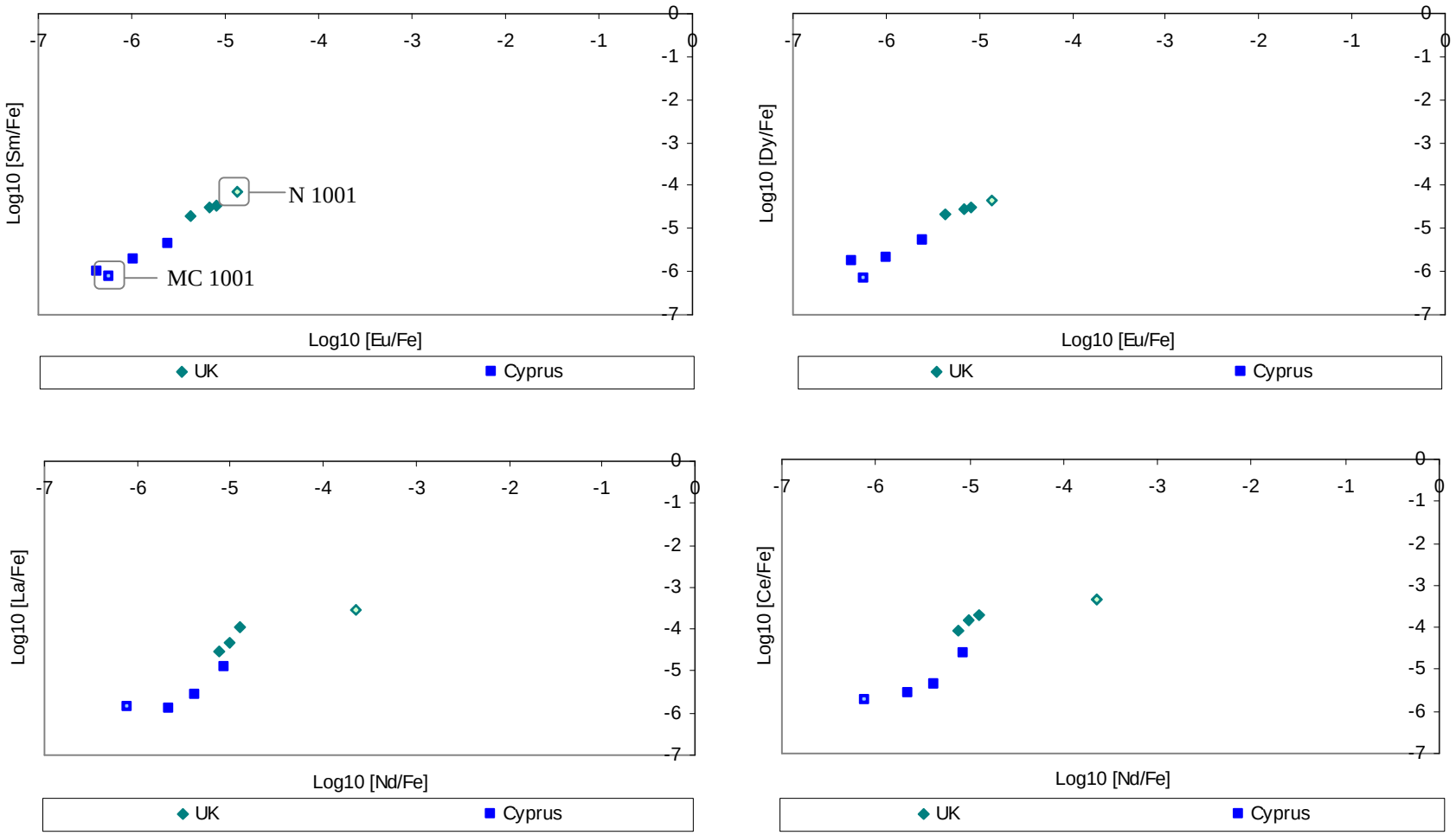

Figures 4-16a-d. Examples of bivariate plots of REE showing the distinct groups corresponding to different geographical origins. A slight variation in the REE signature also corresponds to the different source within the same country

This was also important to evaluate the sub-groups identified during the previous sets of analyses based on the disparate identities of their primary constituents. Essentially, the UK samples were divided into the Shotover group, which were goethite and quartz-dominant; and the Norfolk sample, which was calcite-rich, also containing some hematite. The same feature had been observed with the Cyprus ochres, whereby the Margi sample, natrojarosite, had a completely different composition to the hematite-based Sia ochres. Although these 'odd' (Norfolk N 1001 and Margi MC 1001) samples were also somewhat distinguishable from the rest of the UK and Cyprus groups in the bivariate REE plots, these plots also showed that they form a part of the same group.

Raman Results. The Raman data was poor, because the excitation wavelength of the laser beam on the said instrument was found to be inappropriate for the analysis of pigments. No matter how short the acquisition time, the detector appeared to be repeatedly flooded with reflected light and/or fluorescence when analysing a solid sample (mineral/ground form). This was because of both the extremely high count rates (4000 counts) and due to the ensuing lack of peaks in the resulting charts (*a* in the spectrum Figure 4-17 below). A preliminary test was carried out by dispersing the pigment, namely the NtI 1001, in methylated spirit at an acquisition time of six seconds to check whether future attempts at using this Raman spectrometer were futile. Peaks, however, did appear and were potentially in right region of the spectrum, but the number of counts was nevertheless low and peak-to-noise ratio poor. Increasing the acquisition time and focusing the beam on the sample clearly improved the quality of the final spectrum, proving that analysis could be achieved using this preparation

technique. The advantage of Raman spectroscopy for sourcing is, nonetheless, debatable, especially with the Raman spectrometer available for use which gave poor qualitative data during these tests.

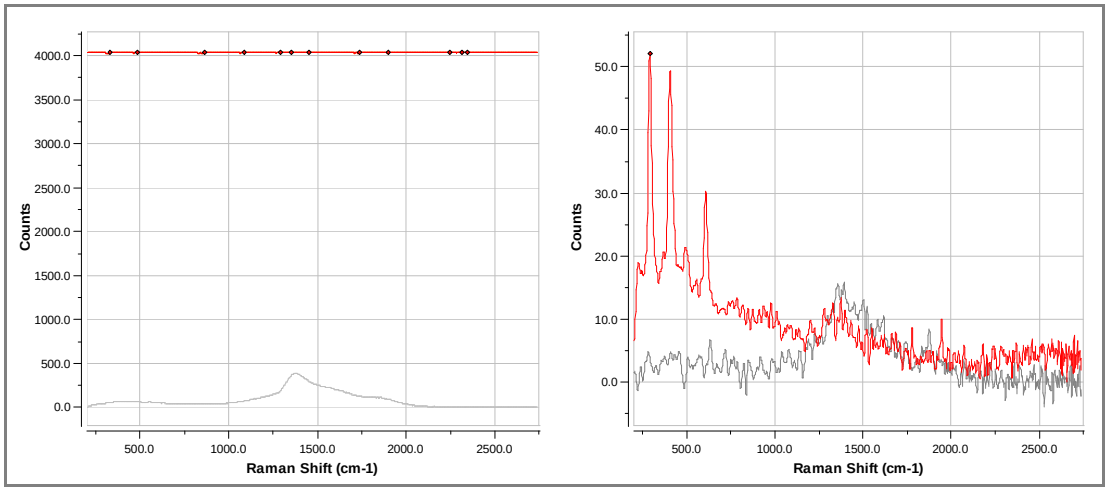

Figures 4-17a, b. Raman spectra for NtI 1001. Powdered sample at an acquisition time of 1 s (a), the dispersion in methylated spirit at 6 s (b) [Background: glass slide]

FTIR results. This technique was used to observe the preferential absorption of infrared radiation frequencies in an attempt to identify the molecular bonds within the pigments. The IR results were compared to reference data and the peaks observed appeared to compare well. Comparative studies and data interpretation with these standards and published results are given in the second pilot study.

Initial analysis also indicated that the IR frequencies from a particular site were similar, though a few peak discrepancies, such as slightly shifted absorbance peaks or broader bands were sometimes noted. This was observed in S 1001 – S 1004, which were quartz- and goethite-rich. The latter feature was determined by the hydroxyl stretching bands at ~3150 cm^{-1}. It however appeared that there was no significant

difference between S 1003 and the other spectra from Shotover, even though XRD data showed that this sample contained a larger proportion of goethite.

Similar frequency charts were also observed for samples EC 1002 – EC 1003. The large 3104 cm^{-1}, 893 cm^{-1} and 796 cm^{-1} bands showed that EC 1001 was goethite-dominant, whereas the other two Sia ochres contained hematite. The recurrent 1034 cm^{-1} absorption band was attributed to the silicate. MC 1001 was clearly of a completely different composition, as can be observed in Figure 4-20 below. Comparison of the spectrum to the IR chart for natrojarosite resulted in a good peak match. N 1001 was also distinguishable from all the other samples due to its high proportion of calcite, which was identified from the large C – O stretching band in the 1428 cm^{-1} region.

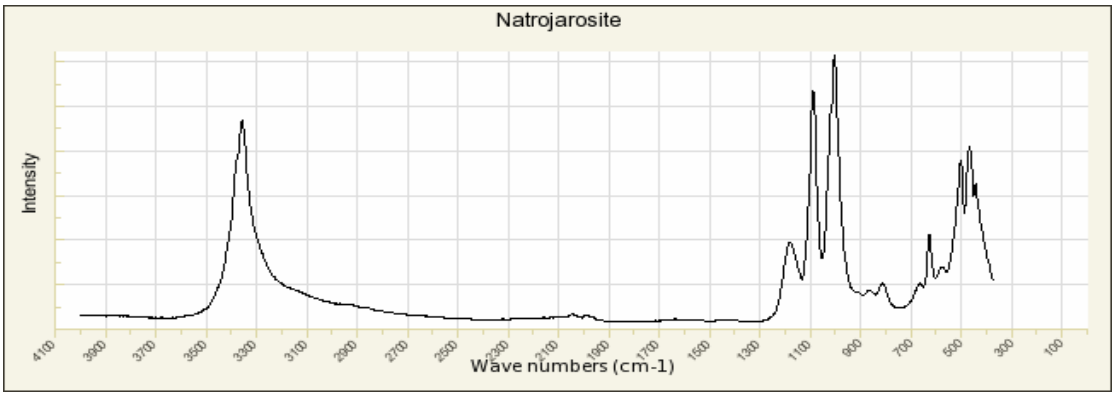

Figure 4-18. % Absorbance reference chart of natrojarosite (Downs, 2006)

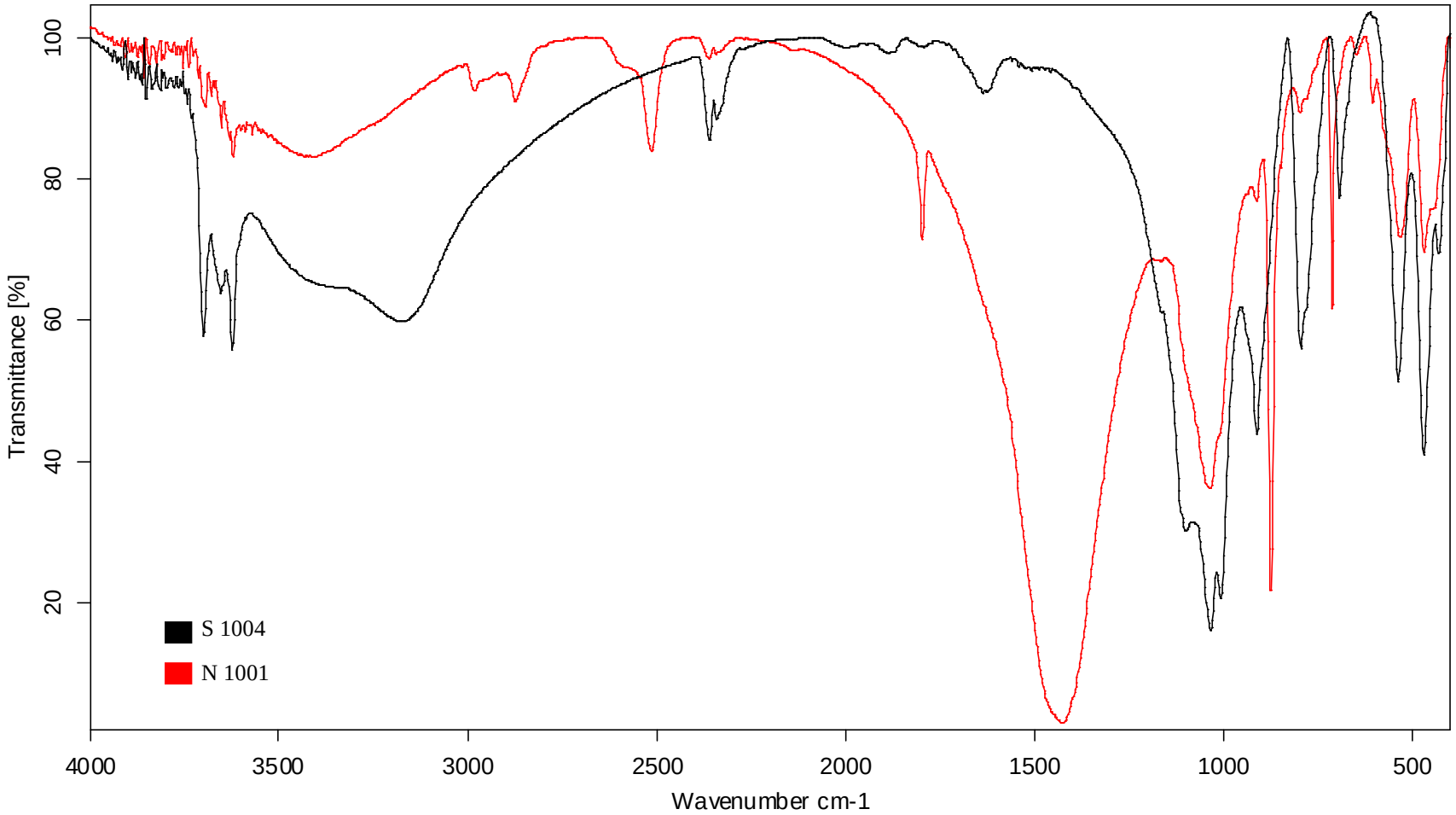

Figure 4-19. The FTIR spectra of an example of a sample from Shotover (S 1004), and the calcitic N 1001

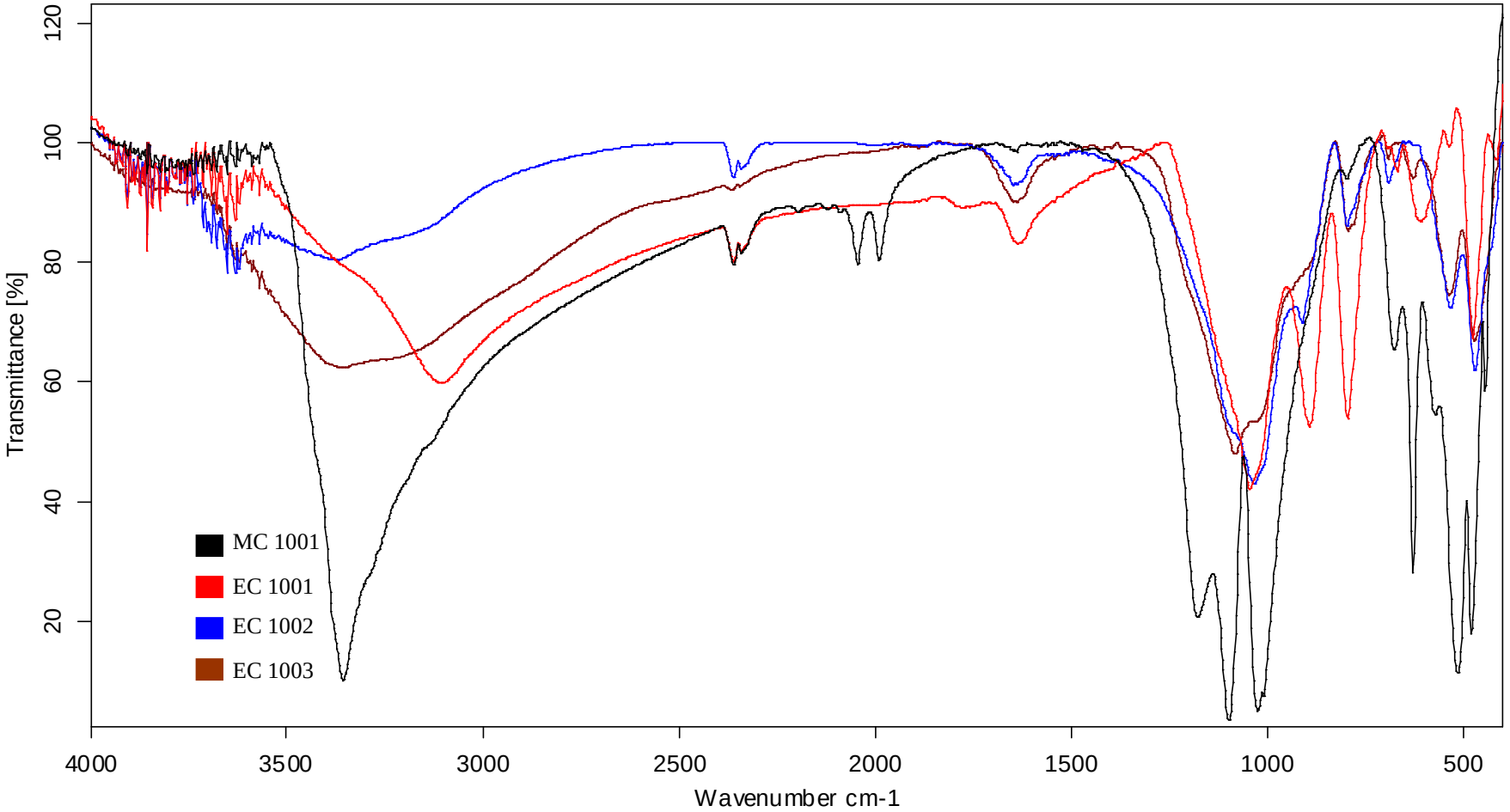

Figure 4-20. FTIR spectra of the Cyprus samples

Conclusion for Pilot Study 1

It appeared that obtaining optical, elemental, structural and molecular information off these samples was ideal for a fully comprehensive investigation of ochres. PLM studies were undoubtedly useful for preliminary investigations, with an observed advantage of this method being the small sample size, implying that little sample of the possibly limited material is necessary for the preparation of a dispersion (permanent) slide. This characteristic, however also serves as a disadvantage: Since only a few grains of the material are required, these may not be entirely representative of the whole sample, and certain observations may reflect impurities. PLM observations are also very subjective, with inferences made being entirely dependant on the prepared dispersion, the examiner and his/her experience. Relative proportions of certain minerals within a particular dispersion slide therefore are only indications of what is present and must not be taken as definite proof of, for example, the prevalence of a material over another, implying that it is necessary to couple the interpretations of this technique with data off other methods before reaching any conclusions about the identity of the material in question.

Overlap of data and unnecessary experimentation would be experienced if SEM-EDS and PIXE analysis were to be carried out in conjunction with the ICP-AES studies. It appears that the latter methodology is undoubtedly the most successful method for distinguishing between ochres and relating the materials to their sources owing to the large number of data obtained and the excellent detection limits (<1 ppm for most elements) exhibited. It is proposed therefore, that the less sensitive SEM-EDS method (~20% error per reading) will only be used as a substitute for ICP-AES when sample

quantities are limited, as only a few mg of sample are required in this non-desctructive elemental technique: ICP-AES, although very sensitive, necessitates the complete consumption of 0.3 g of sample. It is also estimated that the statistical tests described later towards the end of this chapter (4.3) will be used on future, larger quantities of elemental data sets to help identify clusters, patterns and/or groups non-subjectively. Furthermore, if these element signatures fit into clusters of geological datasets which satisfy the provenance postulate theory, then it is estimated that this method, namely ICP-AES coupled with statistical analysis, will be the ideal system to efficiently source ochre. Moreover, samples from both the core and exterior of the natural ochre lumps indicated that there were no observable differences in composition that might reflect alteration or changes in the environment.

While it was concluded that the Raman spectrometer available for use is unsuitable for this ochre provenancing study, it is also debatable how useful XRD and FTIR methods are, with the limiting factors of both methods being their poor sensitivity (~15-20%) and difficult peak interpretation. This query will be addressed in Pilot Study 2 below.

4.1.6. Pilot Study 2

Subsequent to the conclusions drawn from the first pilot study, this second study aimed at establishing whether the two techniques that appeared to have potential for differentiating between ochres based on different (non-elemental) aspects of the material, were suitable for characterising ochres for provenancing purposes. The techniques were XRD, which enabled structural characterization of the ochre constituents, and FTIR, which identified the molecular groups present. The pigments analysed were obtained from the Pigmentum project and are listed below.

Sample		Description	
Nº	**Proj. Nº.**	**Country**	**Colour**
1	51_P1897	Czech paint plant	Burnt yellow ochre: bright orange
2	52_P1898		Bohemian green earth: green-white
4	46_P1892	Leningrad Paint Plant during the late Soviet Union era, Russia	Yellow ochre: yellow
5	47_P1893		Orange ochre: yellow (darker)
6	48_P1894		Red ochre: bright orange
7	30_P056	Siena, Italy	Terra di Siena: yellow brown
8	31_P057		Terra di Siena: red
9	44_P1890	Le Marche, Italy	Pale grey earth: whitish-brown
10	45_P1891	Pesaro, Italy	Sandstone : yellow white
11	49_P1895	Warksworth, Derbyshire	Brown ochre: yellow-brown
12	43_P1889	Parys Mountain, Anglesey, N Wales	Calcined umber: bright orange
13	50_P1896		White-brownish (lumpy)
14	53_P1899	Bacup, Lancashire	Brown lumps
15	55_P1901	Near Burnley, Lancashire	Yellowish (lumpy)
16	54_P1900	Cloud Hill Quarry, Breedon on the Hill, Leicestershire	Bright red (lumpy)
17	56_P1902		Dark yellow (lumpy)
18	57_P1903	Sand, the Needles, Isle of Wight	Whitish-red
19	58_P1904		Whitish-yellow
20	59_P1905		Whitish-brown
21	60_P1906		White, little brown
22	61_P1907		Whitish-yellow
23	62_P1908		Whitish-brown
24	63_P1909		Yellow
25	64_P1910		Red-orange
26	65_P1911		White, little brown
27	26_P051	France	Yellow
28	27_P052	France	Orangey-red
29	28_P053	Germany	Yellow (darker than 26_P051)
30	29_P054	Italy	Yellow (Brighter than 26_P051)

Synthetic
Natural
Unknown

Table 4-6. The pigments analysed in this study (Green earth included for comparative purposes)

XRD results. Some examples of the XRD diffractograms obtained are shown below. In several cases it was observed that the background was rather high and/or there was a large swell present in the lower 2θ angles, which led to peak masking, poor peak detection and low confidence levels with both auto and manual peak search settings. This affected data interpretation and left some peaks impossible to qualify. Although it was difficult to determine why this inadequacy occurred, previous studies have shown that XRD of goethite (and of other iron oxides, Cornell and Schwertmann, 2003: 176) resulted in a noisy spectrum as the iron hydroxide present appeared to be poorly crystalline (Figure 4-12, 4-21).

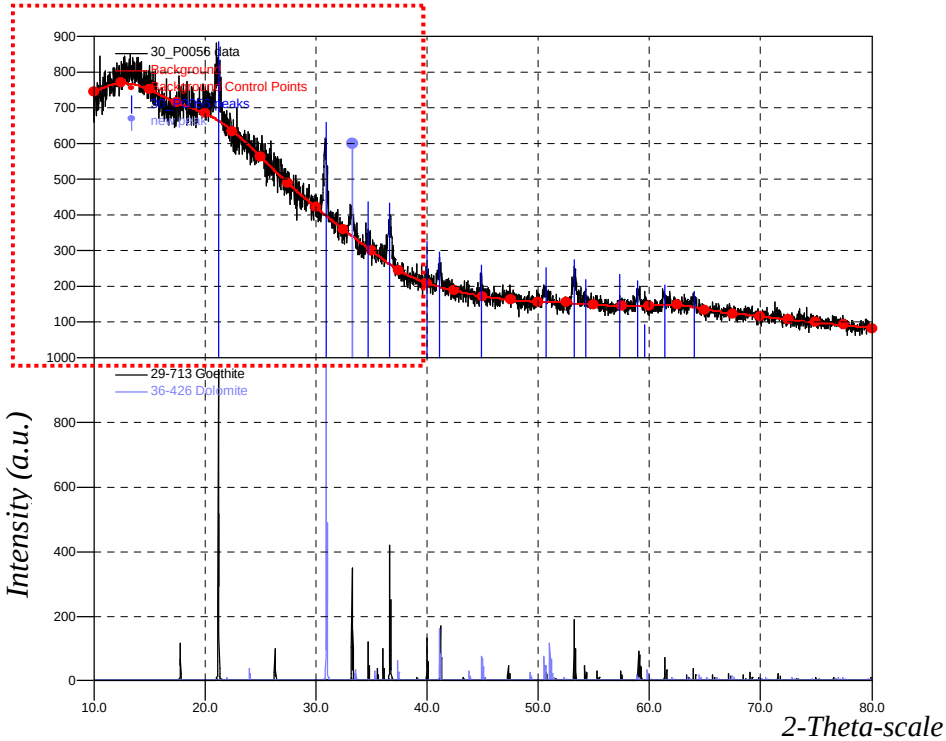

Figure 4-21. An example of the high background (highlighted), observed in sample 30_P056

Several diffractograms were of remarkably good quality, but this generally occurred when the samples were significantly rich in highly crystalline accessory phases, which majorly consisted of quartz or calcite. Data comparison illustrated the predominance

of certain accessory minerals in particular countries: primarily quartz in the Northern European countries (France, Germany, UK, Czech and Russia) and calcium-based carbonates and sulphates in samples from Italy.

Sample	Components	Sample	Components
France		**Czech**	
26_P051	A Quartz SiO_2 B Goethite Fe +3O(OH) C Hematite Fe_2O_3	51_P1987	A Quartz, alpha SiO_2 B Hematite, syn Fe_2O_3
27_P052	A Quartz SiO_2 B Some organic dye (?) C Goethite Fe +3 O(OH) D. Hematite Fe_2O_3	52_P1898	A Quartz, alpha SiO_2 B. Chromium Oxide CrO C. Manganese Vanadium Oxide Mn1.5 V1.5 O4
United Kingdom		**Italy**	
57_P1903 58_P1904 59_P1905 60_P1906 61_P1907 62_P1908 63_P1909 64_P1910	A Quartz Si O_2 A Quartz Si O_2 A Quartz Si O_2 A Quartz Si O_2 A Quartz Si O_2 A Quartz Si O_2 A Quartz Si O_2 A Quartz Si O_2	29_P054	A Gypsum $CaSO4.2\ H_2O$ B Anhydrite $Ca(SO_4)$ C Goethite, syn FeO(OH)
		30_P056	A Goethite Fe +3 O(OH) B Dolomite Ca Mg $(CO_3)_2$
Soviet Union		31_P057	A Hematite Fe_2O_3 B Dolomite Ca Mg $(CO_3)_2$
46_P1892 47_P1893	A Quartz, syn Si O_2 B Goethite Fe +3 O (OH)		
48_P1894	A Quartz, syn Si O_2 B Hematite, syn $Fe_2 O_3$ C Goethite Fe +3 O (OH)	44_P1890	A Calcite Ca CO_3 B Goethite Fe +3 O (OH)
Germany		45_P1891	A Quartz alpha SiO_2 B Calcite $CaCO_3$ C Dolomite Ca Mg $(CO_3)_2$ D Goethite Fe +3 O(OH)
28_P053	A Quartz Si O_2 B Goethite Fe +3 O (OH)		

Table 4-7. XRD analysis of some Group 2 pigments

Some results have been tabulated above. It was observed that the detected colorant (iron oxide/hydroxide) correlated with the overall colour of the particular ochre (red/yellow). Although the benefits of XRD testing include rapid analysis and relatively simple characterisation of material constituents, the technique was therefore found to have equally significant drawbacks. Essentially, XRD was found to be inadequate for a fully accurate determination of the constituents beyond the

identification of the major minerals present, namely the accessory mineral(s) and the (typically) iron-based colorant(s) when these were present in concentrations of >20%. As has already been noted, in several cases it was also difficult to detect the latter. Quantitative measurements by means of the Rietveld method were also not viable because of the overall poor diffraction signals experienced off the iron oxides and hydroxides in relation to the accessory minerals (Prasad, Prasad et al., 2006).

FTIR results. FTIR appears to have been a useful tool in the identification of iron oxides in literature and in published studies, though differentiation between sets of pigments from various sources has been met with limited success (Bikiaris, Daniilia et al., 2000; Prasad, Prasad et al., 2006). The FTIR spectra obtained for the Pigmentum ochres in this study gave interesting albeit somewhat limited results, which were found to majorly corroborate the XRD data. The frequency charts obtained were also compared to previous infrared runs carried out on an attenuated total reflectance spectrometer (ATR) by scientists at the Pigmentum Project. A summary of the observations are given below:

- Most spectra gave unusually high noise, generally between the higher 4000 and 3500 cm^{-1} region of the frequency chart. This was attributed to adsorbed water in the ochre samples.
- The FTIR spectra obtained for this study were similar to those obtained from the Pigmentum project, though the percentage transmittance (overall peak signal) was much better for the transmission spectra obtained for this study, hence were better for differentiation purposes as smaller peaks were also discernable.

- In some cases the spectra were of poor quality with a low %T, possibly because of reduced transmittance relating to the small particle size, as was experienced in samples 30_P056 and 31_P057 [Siena samples] (Figure 4-24 below). It is debatable as to whether this could be a characteristic of Terra di Siena ochres: a larger sample group is necessary to ascertain whether the 'noise' perceived is actually inherent to this particular source, although previous research has indicated that small particle size is actually a feature of Siena ochres (Chapter 1).
- Frequency charts were evaluated on the basis of both material source and pigment colour. The latter were divided into yellow, red, orange and brown samples. Peak differences for each consecutive group are briefly described in Table 4-8.
- The main peaks were satisfactory matches to published ochre spectra, though differences were noted on cross comparison between the various FTIR charts.
- Difficulties were encountered on trying to distinguish between red and yellow ochres, mainly because: 1) the spectra are known to be relatively similar, 2) hematite is found to differ from goethite in wavenumbers beyond the detection limits of the FTIR (500 – 300 cm^{-1}); and 3) several samples comprised mixtures of the two colorants, making differentiation even more complicated.

The Soviet Union samples 46_P1892, 47_P1893, and 48_P1894 were a good example of how difficult differentiation between goethite and hematite-dominant samples can be (Figure 4-22). XRD data indicated that, besides containing quartz, these samples consisted of goethite, a goethite-hematite mixture, and hematite respectively. The resulting FTIR spectra were found to be very similar, with the minor differences exhibited in peak shapes rather than differing peak positions. Variations mainly included the broadness of the 3450 cm^{-1} peak: this was more prominent in the

46_P1892, 47_P1893 samples, as was expected; and in the position of the ~1032 cm^{-1} peak, which appeared to be skewed towards a higher wavenumber in the hematite-rich sample. Consequently, although some discrepancies are observable, they are not distinct enough for accurate differentiation.

The results obtained have been summarized in Table 4-8 below.

Colour	Sample N$^{o.}$	Locality	Frequency chart description	
			Conforms to expected spectrum?	Differences
Yellow	26_P051	France	Yes	N/A
	28_P053	Germany	Yes	Very large swell at 3161cm^{-1}
	29_P054	Italy	Refer to notes for Italy samples: different spectra due to distinct calcitic peaks. Odd spectrum was 29_P054 as it was a calcium sulphate based sample	
	30_P056	Italy		
	45_P1891	Italy		
	46_P1892	Russia	Yes	N/A
	47_P1893	Russia	Yes	N/A
	55_P1901	Lancashire	Samples contained a lot of adsorbed water and gave a broad, distinctive peak around 3100 cm^{-1}.	
	56_P1902	Leicestershire		
Red	27_P052	France	Yes	Some goethite also present
	31_P057	Italy	Refer to notes for Italy samples	
	54_P1900	Leicestershire	No	Fewer peaks
Orange	43_P1889	N Wales	Yes, majorly hematite-based	Lack kaolinite peaks, interestingly similar spectra
	48_P1894	Russia		
Brown	44_P1890	Italy	All spectra were significantly different, possibly because all samples were different shades of brown	
	49_P1895	Derbyshire		
	50_P1896	N Wales		
	53_P1899	Lancashire		

Table 4-8. An outline of the properties and IR chart observations of some of the analysed Pigmentum samples

The sensitivity of the method is therefore a factor to be taken into consideration, as well as the difficulties encountered in results interpretation owing to the overlapping peaks (which were also observed in Pilot Study 1) and reduced transmittance in certain samples. An obvious flaw to the technique is the similarity between hematite, goethite and kaolinite spectra; all of which generally tend to be present in varying proportions in ochre frequency charts. This study therefore illustrates how FTIR must be used with caution, if used at all, in ochre studies; and that although potential differences within spectra may be inherent to the material, there are (a) too many variables

involved, hence a larger sample set for each country/source is necessary, and (b) the technique itself appears to be unsuitable for provenancing and even differentiation purposes as there are too many errors to be considered when using this analytical method.

Conclusion for Pilot Study 2

In conclusion, both techniques show potential for qualitative analysis, but are inadequate for quantitative measurements. FTIR data is complicated to interpret beyond identity recognition, mainly because of overlapping peaks and similarities exhibited between spectra, making it impossible to reach any definite conclusions without making (possibly wrong) assumptions. The main disadvantages of XRD seem to be related to the limitations implied by poor crystallinity of key ochre colorants. This method, however, was clearly useful to identify of the mineral phases of the major constituents and for giving an indication to the amount of disorder in the crystalline iron oxide/hydroxide phases. It was therefore concluded that XRD gave complementary information to this study and could be implemented in the provenancing study if samples are available in sufficient amounts.

These pilot studies therefore showed that the methods implemented should include PLM for optical investigations, XRD for phase identification if sample quantities are sufficient, and ICP-AES for elemental analysis. If not enough sample (g) is available for the latter method, SEM-EDS is to be used. Later investigations showed that sampling was not possible in a variety of cases (unethical), therefore the non-invasive XRF elemental technique was employed.

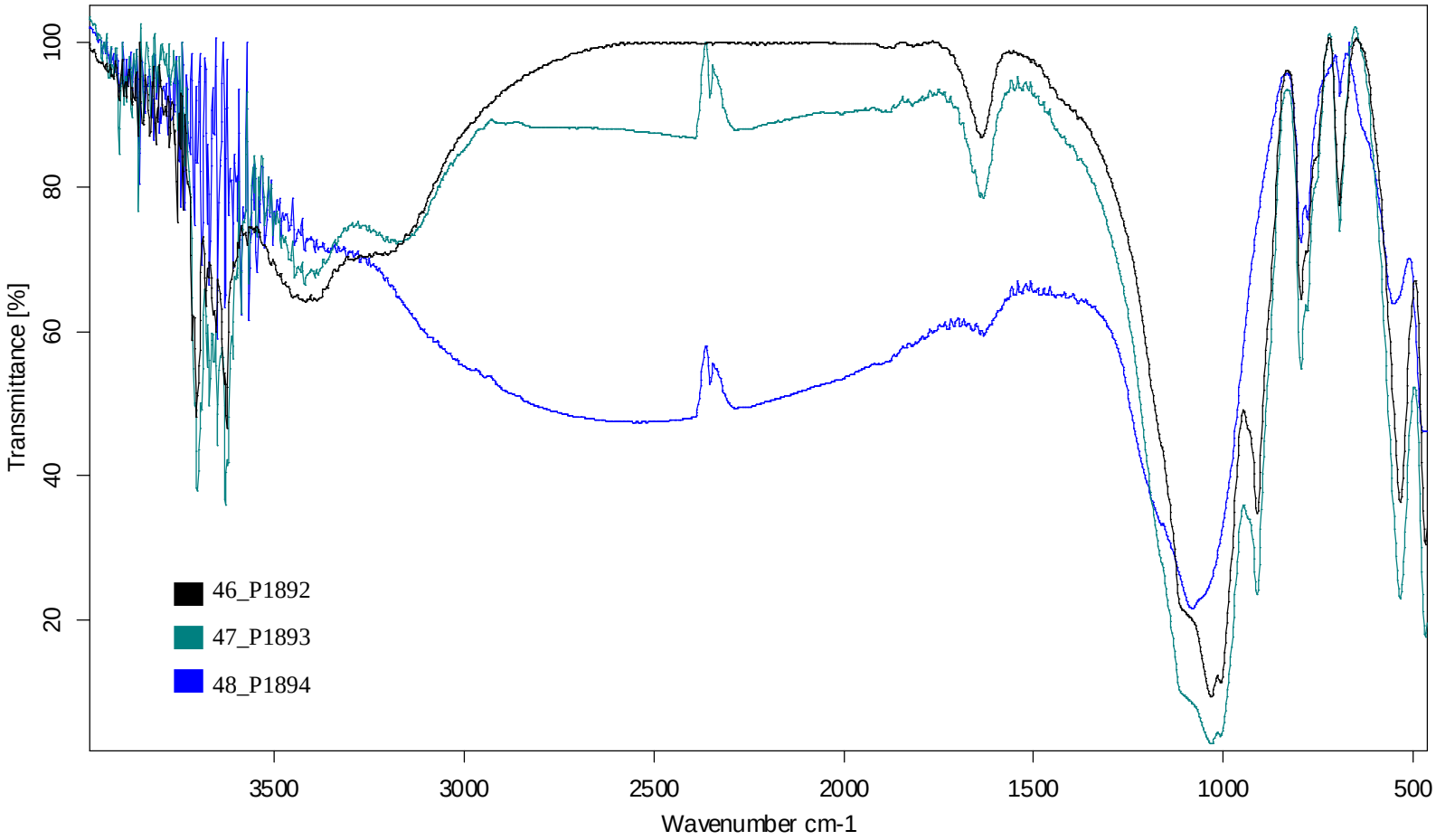

Figure 4-22. FTIR spectra of the Soviet Union samples 46_P1892, 47_P1893, and 48_P1894

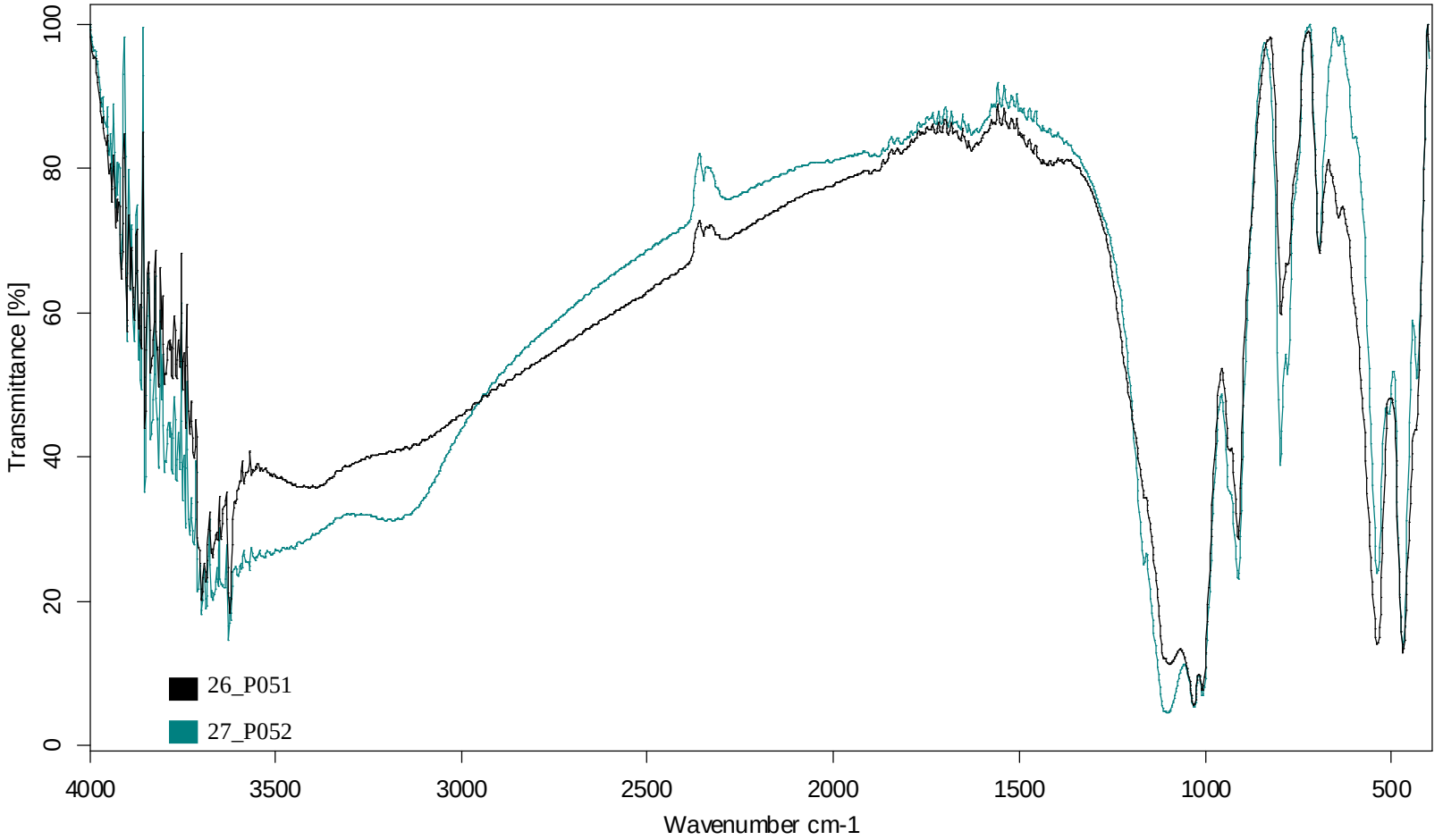

Figure 4-23. FTIR spectra of the French samples 26_P051, 27_P052

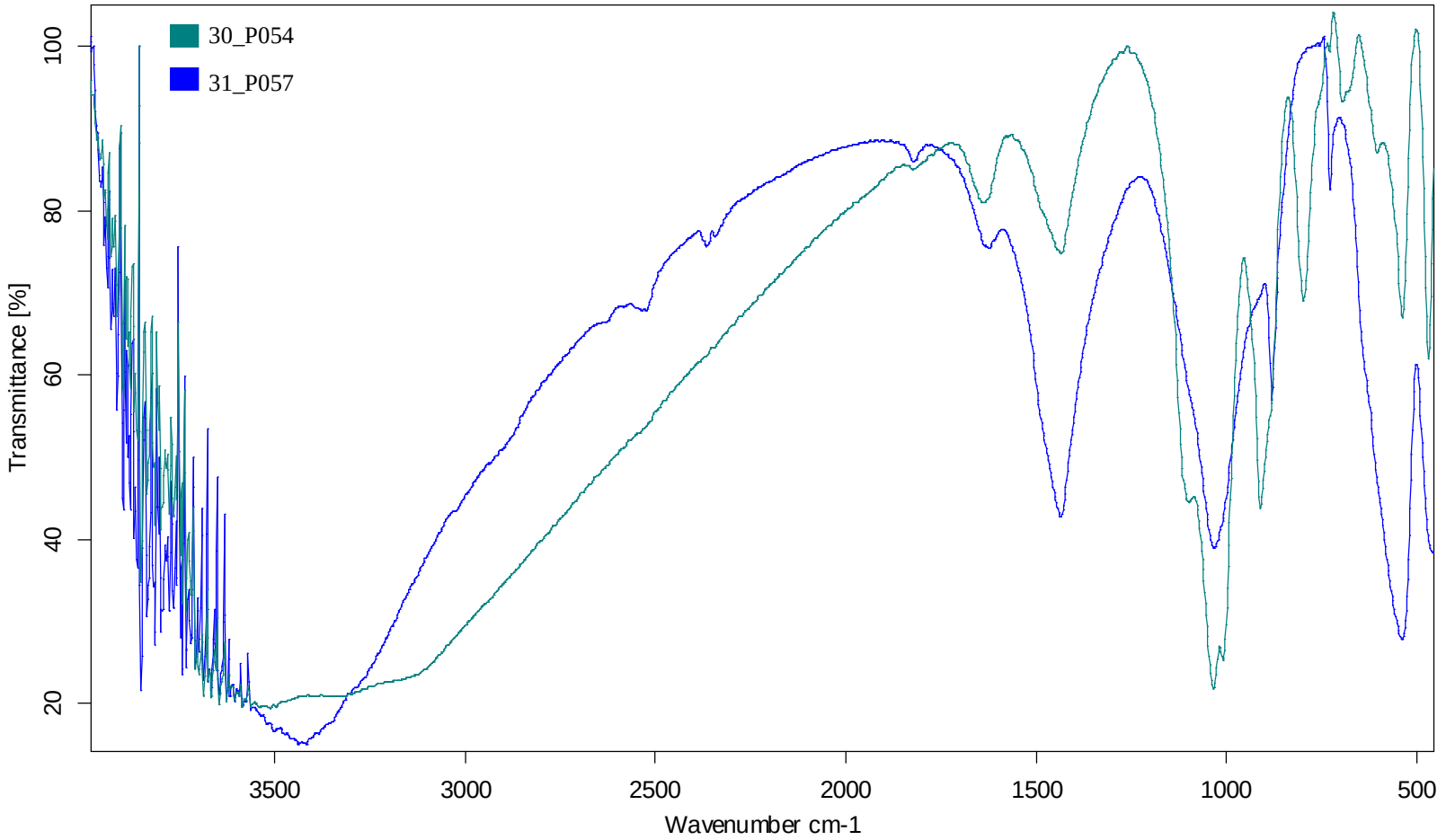

Figure 4-24. FTIR spectra of the Siena (Italy) samples 30_P054, 31_P057

4.2. Sampling, sample extraction and analysis for the case studies

After having established which analytical techniques to adopt for efficient sourcing of ochre, it was possible to investigate the ochres in the main study of this project, those of Maltese islands and its prehistoric temples, and those in the comparative study, the ochres of Amarna. This involved systematic sampling of the geological and archaeological samples, as will be described below.

4.2.1. Maltese geological samples

The geological samples analysed were collected from a number of localities (Figure 4-26). The Calcitic reds were collected from sourced areas of hardened palaeosols in the Cirkewwa (Cwa) and Ghadira (Gh) Bay areas, and from fractures through the Upper Coralline Limestone at Mistra village (Mv) and Mgarr (MG), where the desired rock had been exposed. A large number of Greensands samples, including some fully oxidised material (Figure 2-3), were collected from Gelmus (G), in Gozo. This area was an elevated landform or butte that largely consisted of the desired sandstone, and samples were extracted from some naturally formed caves along its sides where the required rock form was exposed. More Greensands were found at Ghajn Tuffieha (GT) and from a block of displaced sandstone at Mgarr. Furthermore, sand suspected to be of the same material was sampled from a beach called *'Ramla l-Hamra'* (RB). Yellow/red-brown Ooid nodules were easily identifiable where they unmistakably showed up against the dull Blue Clay outcrops (Figure 4-27) and were collected from the coastal areas of Marsalforn (Gozo), Ghajn Tuffieha and Mgarr.

All chosen sources were easily accessible and all the samples had a distinctive ochre colour, which facilitated their selection. Samples were carefully extracted using a

hammer and chisel when necessary, and care was taken to sample from undisturbed areas where possible. Multiple fragments were taken of the same material, and the best samples were carefully selected under a microscope. Powdering of the sample was also executed under a microscope from both the exterior and interior of the sample to avoid the occurrence of inclusions or other rock formations.

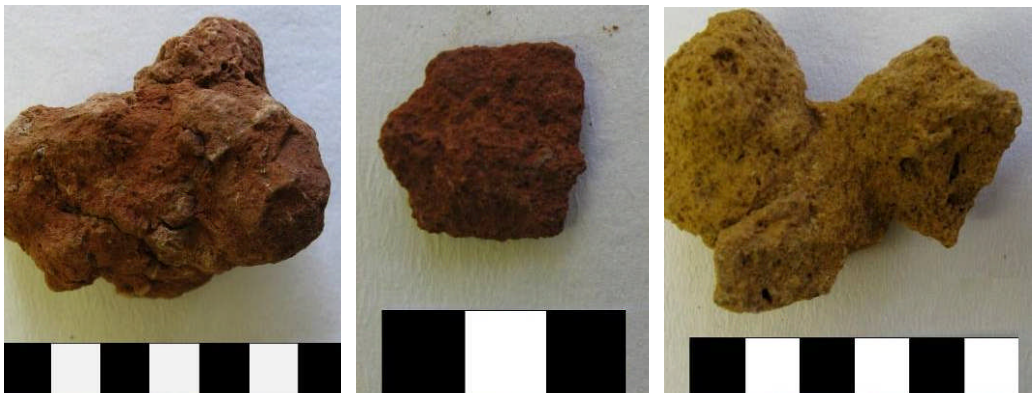

Figures 4-25a-c. Photographic documentation of samples Cwa 1002, G 1002 and G 1005 (ref. Table 1) Scale 1: 1cm (Photos: author)

Although sampling from the Maltese soils has been described elsewhere (Vella, 2006 – technical report), a brief description of the operations undertaken is listed below:

° Performing a reconnaissance survey to identify the major soil landscapes, and correlating these with existing soil maps,

° Planning and executing a precise grid survey of the Maltese Islands at 1 km by 1 km grid intervals, totalling a significant 331 survey points;

° Sampling the target sites by digging shallow pits, recording the profile data and collecting 1.5 kg of samples using spade, screw and/or gouge augers;

° Analysing samples and storing surplus material in an archive facility with controlled environmental conditions at the Agricultural Services Labs in Malta.

The soils for this project were sampled at this facility, and were chosen on the basis of soil type and location, obtaining as widespread a sample group of the most relevant

samples as possible (Figure 4-26). More Leptosols and Luvisols were collected as these were expected to be more iron-rich (refer back to Chapter 2)

Sample group	Location	Sample Nº. Analysed	Nº.
Calcitic Red (CR)	Cirkewwa	Cwa 1001, Cwa 1002, Cwa 1003, Cwa 1004	4
	Ghadira	Gh 1001, Gh 1002, Gh 1003	3
	Mistra village	Mv 1001	1
	Mgarr	MG 1101, MG 1201, MG 1301, MG 1401, MG 1501, MG 1601	6
		Total	14
Greensands (Gr)	Gelmus	G 1001, G 1002, G 1003, G 1004, G 1005, G 1006, G 1007, G 1008	8
	Ghajn Tuffieha	GTG 1001, GTG 1002, GTG 1003	3
	Ramla Bay	RB 1001	1
	Mgarr	MG 1009, MG 1100	2
		Total	14
Ooids (O)	Marsalforn	Mfn 1001, Mfn 1002, Mfn 2002, Mfn 2003, Mfn 2004	5
	Ghajn Tuffieha	GT 1001, GT 1002, GT 1003, GT 1004, GT 1005, GT 1006	6
	Mgarr	MG 1001, MG 1006, MG 1008, MG 1701	4
		Total	15
Terra Rossa (TR)	Gozo region	G 037, G 042 (leptosols), G 057 (calcisol)	3
	North Malta	G 073 (cambisol), G 113, G 129 (leptosols), G 132 (vertisol), G 135 (luvisol)	5
	South Malta	G 266 (cambisol), G 269, G 299 (luvisols)	3
	West Malta	G 178 (leptosol), G 254 (luvisol)	2
	Central Malta	G 223 (regosol), G 312 (luvisol)	2
		Total	15

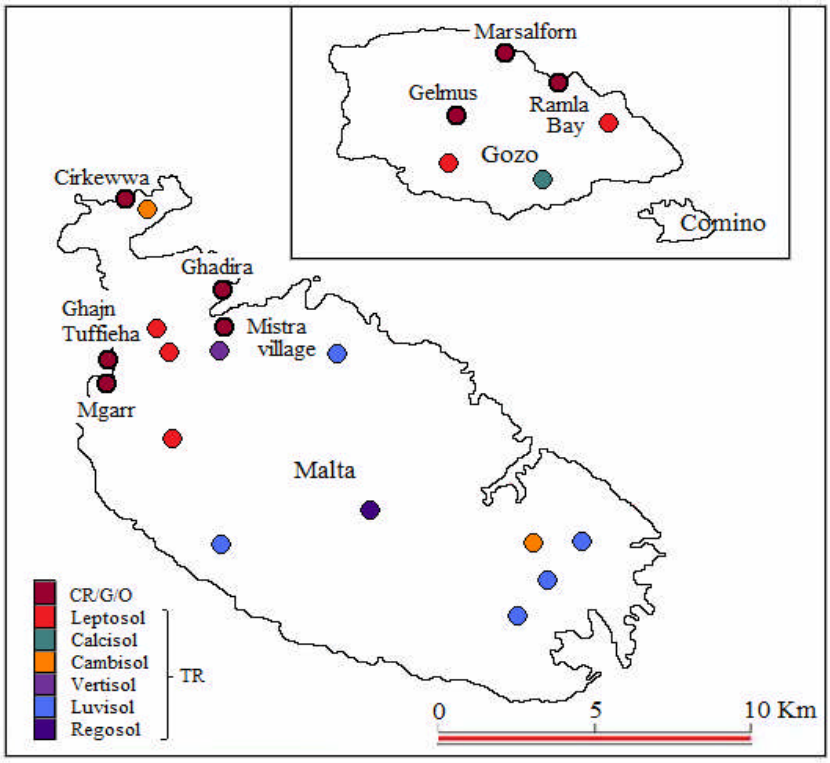

Table 4-9 and **Figure 4-26**. Samples selected for analysis and location of extraction

Figures 4-27a, b. (a)'Ooid' nodules in Blue Clay at Ghajn Tuffieha before extraction, (b) section through a nodule. Scale bar 1 : 1 cm

4.2.2. Maltese archaeological samples

In the pilot studies it was ascertained that ICP-AES was the ideal method for ochre differentiation for provenancing purposes. This technique was, however, destructive, as it necessitated complete sample digestion. Acquisition of the archaeological samples was therefore a lengthy process due to the ethical factors involved when authentic materials of historical and cultural significance were to be irretrievably lost. It was decided, nevertheless, that the benefits of the study – in terms of information obtained – prevailed over the ultimate loss of the required cultural material(s). Conditions dictating sample acquisition included the following:

i. That controlled but sufficient amounts of samples were to be taken where possible (pure ochre samples could not be in excess of 0.77 g);
ii. That the quantities of the remaining cultural material(s) significantly outweighed the total amount of sample to be consumed.

All the samples acquired were carefully photographed and documented. It was borne in mind that these samples may have been mixed with some other material at some point following extraction from their geological environment: either by the prehistoric peoples themselves, or following burial, post-excavation or during storage. Relatively pure samples were taken from the National Museum of Archaeology (NMA) in Valletta. Deposits of sediment material were also obtained from the Hal-Saflieni Hypogeum, which was chosen as the only known prehistoric site in Malta with deposit material left *in situ* following excavation. Although it was first thought that the sediment material from the Hypogeum should be rich in ochre remains (refer back to Chapter 2), on extraction samples indicated poor ochre quality as a result of being intermixed with large quantities of unconsolidated deposits. It was therefore decided to take samples from areas where the material was considered to be most useful (selected burial chambers and/or untouched deposits) and where it was found in abundance for both practical and ethical purposes. Bone samples were also acquired as these were thought to have been sprinkled with ochre as a part of the burial practice of these Neolithic people. The deposits were left to dry out in a fan oven at 26ºC (+/- 2 ºC) for 5 days, and were left to cool to room temperature.

Figures 4-28a, b. MA 001 and MA 005 ochre from the NMA before extraction (Photos: author)

From the eleven samples taken from the NMA, only seven good quality archaeological ochre remains were found. This is because MA 003, MA 006, MA 008 and MA 010 were merely lumps extracted from the same ochre finds box as their powder-form counterparts, namely samples MA 002, MA 005, MA 007 and MA 009 respectively. Furthermore, some samples were obtained in quantities below the desired weight and therefore could not be analysed via ICP-AES. A total of 13 deposits were obtained from the Hypogeum (HYPD), along with 12 bone pieces. The bones were collected from the disturbed deposits and unused material was to be returned on completion of the project. An overview of all the samples obtained from the Hypogeum is given in Figures 4-29 and 4-30 and are listed in Table 4-10 below.

Overview of samples obtained

	Sample Nº.	Description	Weight (g)	Estimated Phase (BC)	Analysis
1	MA 001	Red powder	0.1346	Zebbug: 4100-3800	SEM-EDS
2	MA 002	Red lump	0.5844	? Zebbug: 4100-3800	ICP-AES
3	MA 003	Red powder	0.7498	? Zebbug: 4100-3800	ICP-AES
4	MA 004	Orange powder	0.1594	Tarxien: 3000 - 2500	SEM-EDS
5	MA 005	Yellow lump	0.2369	Tarxien: 3000 - 2500	SEM-EDS
6	MA 006	Yellow powder	0.1764	Tarxien: 3000 - 2500	ICP-AES
7	MA 007	Yellow lump	0.379	Tarxien: 3000 - 2500	ICP-AES
8	MA 008	Yellow powder	0.2734	Tarxien: 3000 - 2500	ICP-AES
9	MA 009	Red lump	0.2541	Ggantija: 3600-3000	ICP-AES
10	MA 010	Red powder	0.4322	Ggantija: 3600-3000	ICP-AES
11	MA 011	Red powder	0.5151	Buqana burial: ~3000	ICP-AES
12	HYPD 1001	Deposit, C5	8.8704	Saflieni: 3300 - 3000	ICP-AES
13	HYPD 1002	Deposit, C5	9.3781	Saflieni: 3300 – 3000	ICP-AES
14	HYPD 1003	Deposit, C5	9.812	Saflieni: 3300 – 3000	ICP-AES
15	HYPD 1004	Deposit, C5	11.353	Saflieni: 3300 – 3000	ICP-AES
16	HYPD 2001	Deposit, C8	13.489	Saflieni: 3300 – 3000	ICP-AES
17	HYPD 3001a	Deposit, C9	10.595	Saflieni: 3300 – 3000	ICP-AES
18	HYPD 3001b	Deposit, C9	Subsample	Saflieni: 3300 – 3000	ICP-AES
18	HYPD 7001	Deposit, C18	3.19	Saflieni: 3300 – 3000	ICP-AES
20	HYPB 2003	Finger bone, C8	0.789	Saflieni: 3300 – 3000	ICP-AES
21	HYPB 4004	Foot bone, C14	3.597	Saflieni: 3300 - 3000	ICP-AES

Table 4-10. A description of the samples chemically analysed (via SEM-EDS/ICP-AES) in this part of the study. Phases are approximate, but all samples date back to the Temple Period (Pace 2000). MA samples were obtained from the NMA; the HYPD and HYPB samples from the Hypogeum

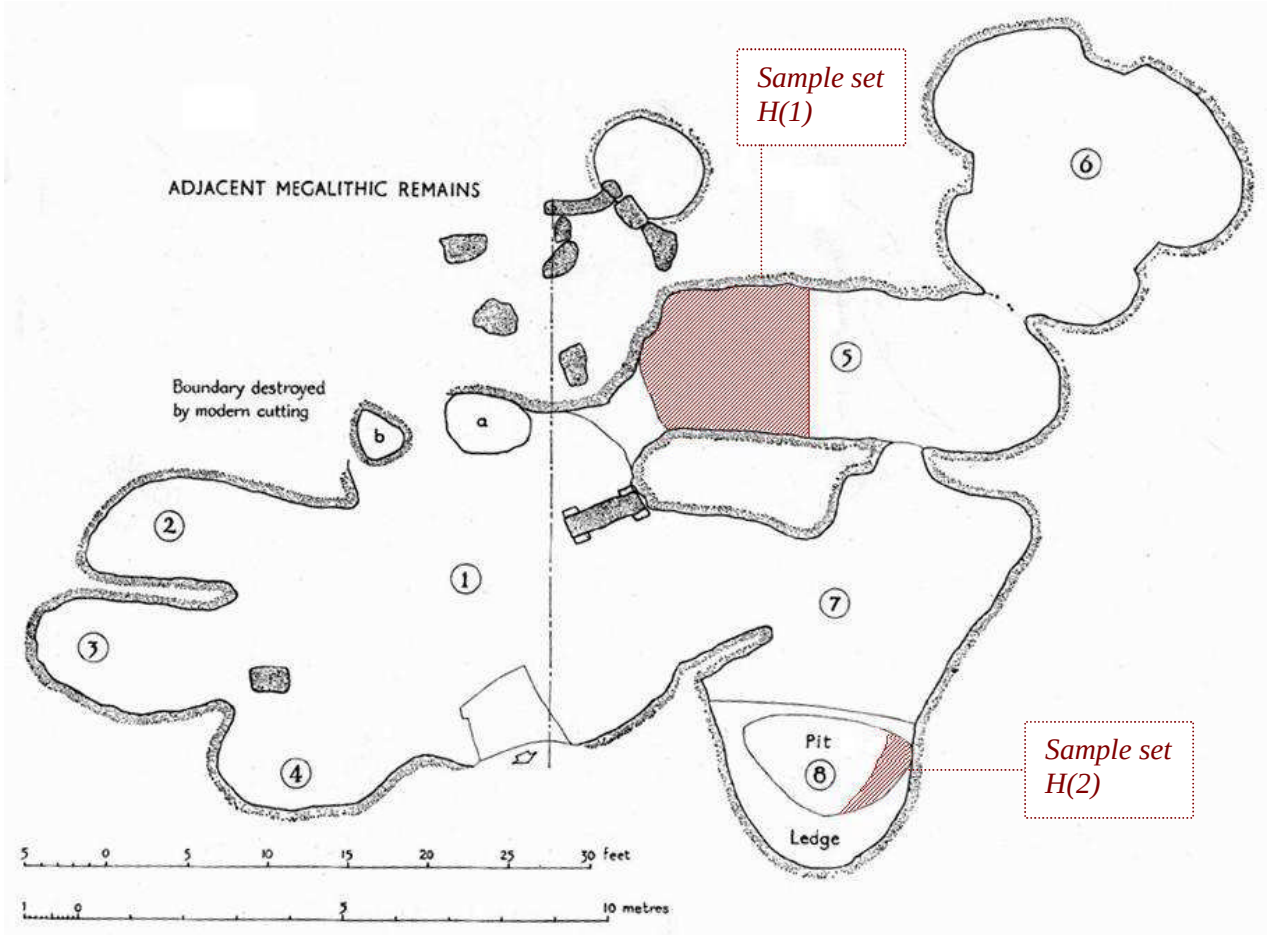

Figure 4-29. Plan of the Upper Level of the Hal-Saflieni Hypogeum, with sample sets obtained highlighted and numbered (Plans courtesy of Heritage Malta)

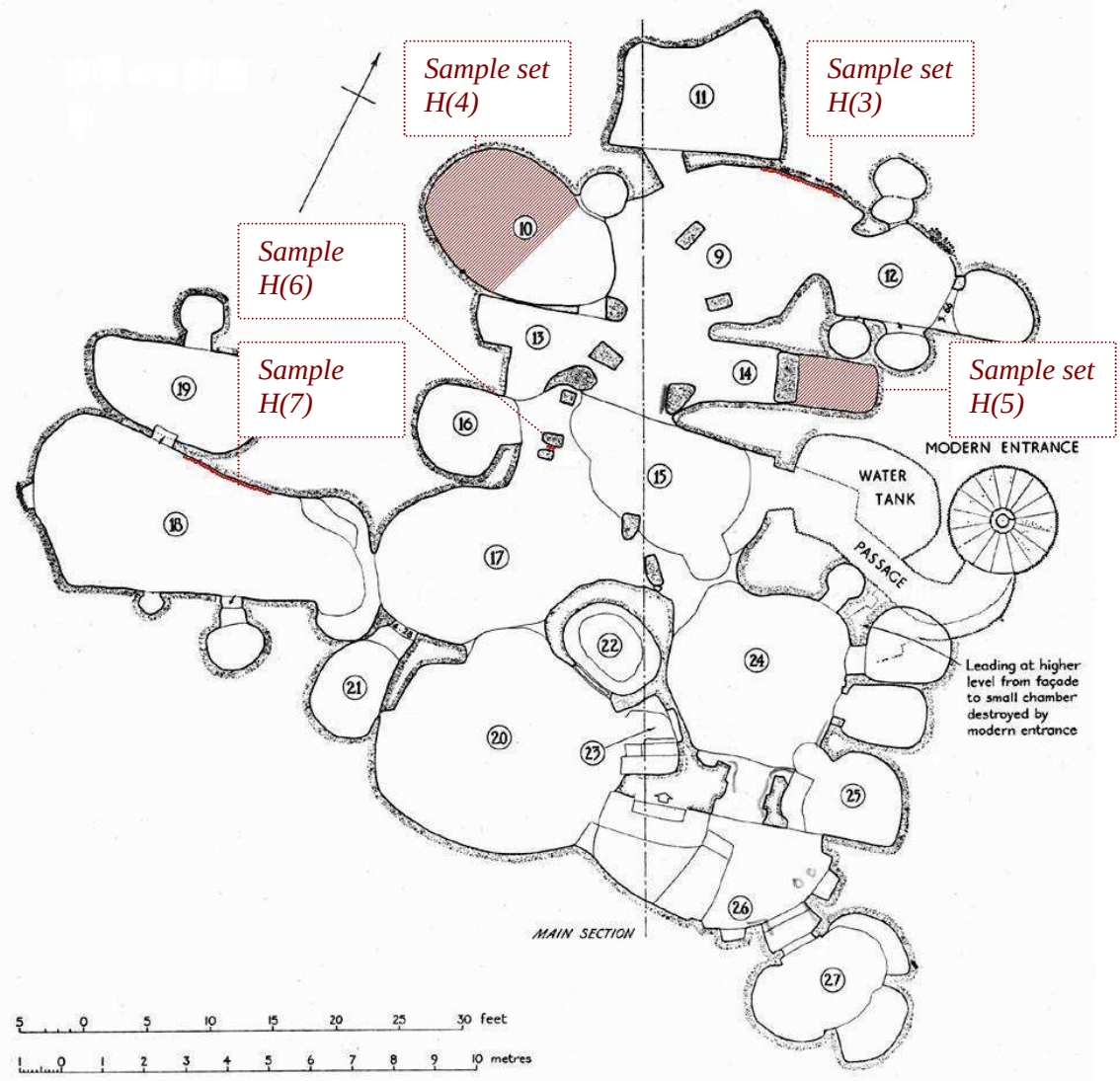

Figure 4-30. Plan of the Middle Level of the Hal-Saflieni Hypogeum, with sample sets obtained highlighted and numbered (Plans courtesy of Heritage Malta)

Sample Location	Samples
H(1)	*Deposits:* HYPD 1001, 1002, 1003, 1004
	Bone: HYPB 1001
H(2)	*Deposits:* HYPD 2001
	Bone: HYPB 2001, 2002, 2003
H(3)	*Deposits:* HYPD 3001
H(4)	*Deposits:* HYPD 4001, 4002
	Bone: HYPB 4001, 4002, 4003, 4004
H(5)	*Deposits:* HYPD 5001, 5002
	Bone: HYPB 5001, 5002, 5003, 5004
H(6)	*Deposits:* HYPD 6001
H(7)	*Deposits:* HYPD 7001, 7002

Table 4-11. The sample locations and respective samples obtained from each area

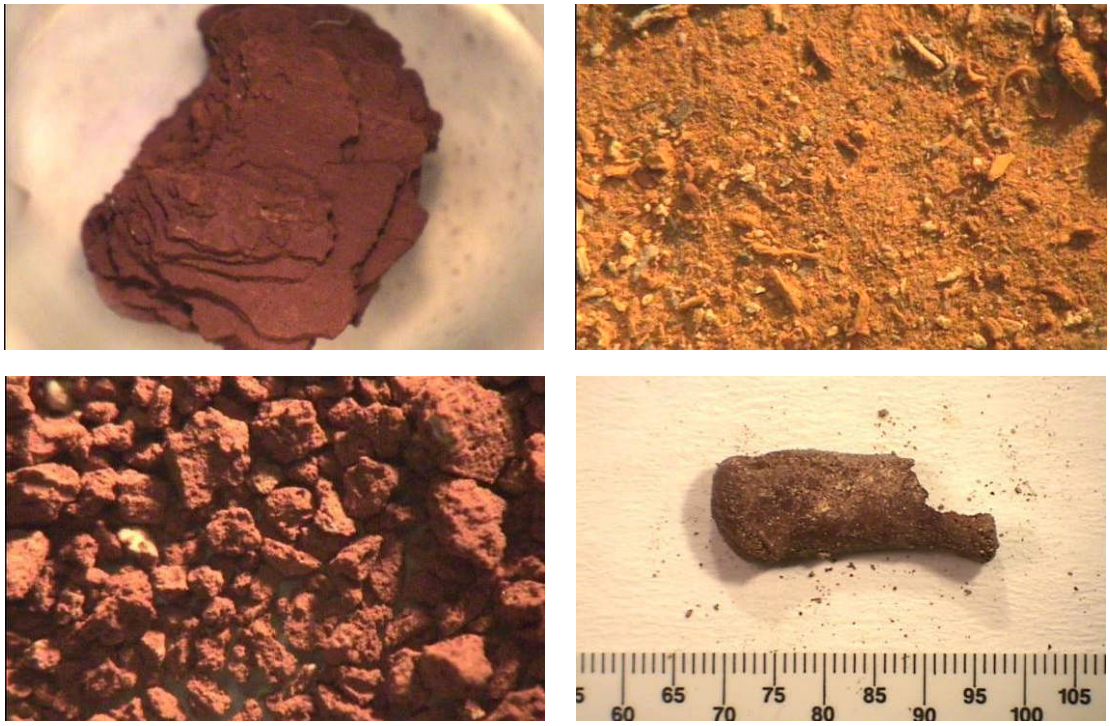

Figures 4-31a-d. Microphotographs of samples MA 002, MA 006, MA 010, HYPB 2003

4.2.3. Amarna samples

The next archaeological samples were obtained for the comparative Amarna study, a site selected on account of the renowned artistic skills of its inhabitants and its well-defined period of occupancy; because of sample availability and because samples were expected to be different from the Maltese ochres because of Egypt's dissimilar geology. Two sets of archaeological samples were acquired, both of which had been brought over from Egypt following an expedition to Amarna on separate occasions.

The first group (BLN 001-009) consisted of a total of nine samples - five yellow and four red pigments thought to be yellow and red ochres - obtained from Bolton Museum and Archives. Sampling was carried out through careful scraping of small amounts of powder off the larger lumps of archaeological samples in the presence of the curator.

Care to avoid sample contamination was taken by removing superficial dirt and sampling off 'cleaner' regions of material. This sampling technique was destructive, therefore it was only possible to obtain minimal amounts of pigment for ethical reasons (described earlier). Samples obtained weighed between 0.0139 and 0.0924 g.

Figure 4-32. Source lumps of BLN 003 and BLN 006 respectively before samples were taken

Overview of samples obtained

	Sample Nº.	Description	Weight (g)	Analysis
1	BLN 001	Light yellow powder	0.0924	SEM-EDS
2	BLN 002	Light yellow powder	0.0739	SEM-EDS
3	BLN 003	Light yellow powder	0.0139	SEM-EDS
4	BLN 004	Yellow powder	0.0240	SEM-EDS
5	BLN 005	Bright yellow lump	0.0208	PLM only
6	BLN 006	Red powder	0.0152	SEM-EDS
7	BLN 007	Bright red powder	0.0170	SEM-EDS
8	BLN 008	Deep red powder	0.0284	SEM-EDS
9	BLN 009	Deep red powder	0.0202	SEM-EDS
10	AMN 002	Yellow powder	0.0168	SEM-EDS
11	AMN 003	Yellow powder	0.0247	SEM-EDS
12	AMN 005	Red powder	0.0108	SEM-EDS
13	AMN 006	Red powder	0.0129	SEM-EDS
14	AMN 007	Yellow powder and lumps	0.0242	SEM-EDS
15	AMN 008	Red powder and lumps	0.0887	SEM-EDS
16	AMN 009	Yellow powder	0.1351	SEM-EDS
17	AMN 011	Light yellow lump	0.2272	ICP-AES
18	AMN 012	Deeper yellow lump	0.3330	ICP-AES
19	AMN 013	Bright red lump	0.9941	ICP-AES
20	AMN 014	Bright red lump	0.0930	SEM-EDS

Table 4-12. A description of the samples chemically analysed (via PLM/SEM-EDS/ICP-AES) in this part of the study. BLN samples were obtained from Bolton Museum; AMN samples were those donated to the project.

The second group (AMN 002-003; 005-009; 011-014) was donated to the project and consisted of a total of eleven pigment samples, six yellow and five red samples which were thought to be ochres, all of which were either in grains or in small blocks. A list of all these samples is given in Table 4-12.

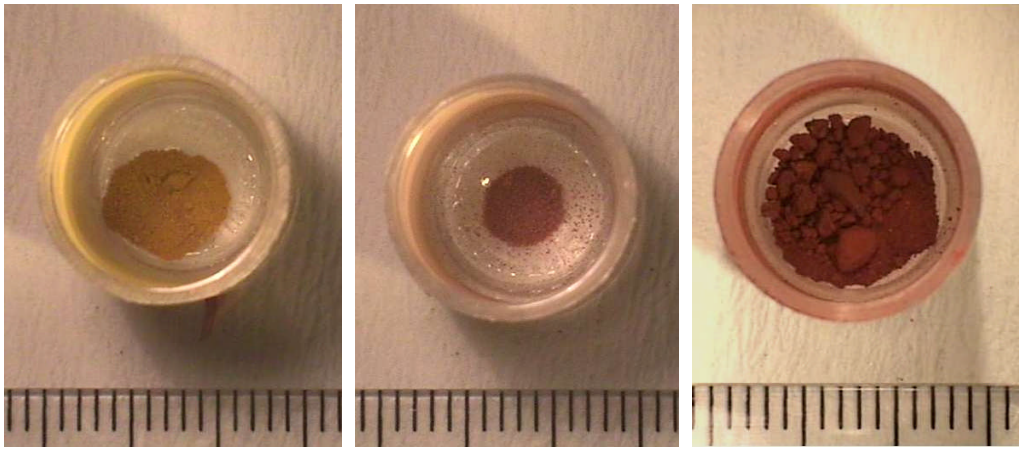

Figures 4-33a-c. Microphotographs of samples AMN 002, AMN 006, AMN 008

4.2.4. Sample preparation and analysis for Maltese and Egyptian samples

PLM, XRD, ICP-AES, SEM-EDS analysis

The analytical methodology described at the beginning of this chapter was therefore adopted for this project. Dispersions of each sample were first prepared, and each was analysed visually under a microscope in PPL and XPL. The selected geological specimens and those archaeological samples available in sufficient quantities for ICP-AES (most of the Malta samples, and AMN 011, AMN 012 and AMN 013) were pulverized in an agate mortar and sent to Royal Holloway college for analysis. Remaining 'Ooid' samples were also analysed via the X'Pert PRO PANalytical powder diffractometer. This technique was also tested on some other sample groups.

MA 001, MA 004 and MA 005 and the majority of the ancient Egyptian samples were prepared on a stub for investigation under the SEM-EDS in the LEO 435VP, which was operated under variable pressure conditions. A new set of parameters were adopted for the study of these small sample sizes, particularly to preclude particle-induced electron scattering and the X-ray absorption geometric effects normally experienced (Goldstein, Newbury et al. 2003: 462-480). A series of tests indicated that the best-suited conditions included operating the gun at 15 kV, with a beam current of 300 µA and an I probe value of 1.6 nA. The working distance was kept at 24 mm for BSE EDS measurements, which were collected by means of the GENESIS EDAX INC. advanced microanalysis solutions energy analyser at 300 seconds livetime (real time acquisition). Magnification was kept at X300 and an area of 100 μm^2 was scanned for every measurement. These conditions gave a reasonably high deadtime of approximately 13% with around 8000 counts per second. EDS values off known materials were cross-checked prior to analysis of the unknowns.

Non-invasive analysis on archaeological ochres in situ

Since there was little archaeological ochre left on the Maltese Islands and few examples were present in sufficient quantities that allowed for acquisition for laboratory analysis (SEM-EDS/ICP-AES), a non-invasive investigative method was attempted to analyse the ochre traces remaining on Neolithic artefacts. A successful application to Innov-X systems allowed for the analysis of traces of these prehistoric ochres *in situ* using an Innov-X Alpha Series XRF. Full instrumental details are described elsewhere (Chapter 4: 91) in this study.

The XRF was calibrated on an internal standard whenever the system was restarted. Background scans were also carried out on ochre-deficient areas of each area/object analysed, and measurements were taken off a series of 'standards' selected for this project. These essentially consisted of a set of earth samples of relatively uniform composition that had been analysed prior to this investigation via the ICP-AES. Livetime acquisition was 40 seconds, and the instrument was suspended at ~ 5 mm from the object. The gun emission area was also padded with a synthetic cloth to preclude damage in case involuntary contact was made, and a suitably sized aperture left to avoid any interference with the emission and detection of X-rays. An overview of the materials analysed and their respective locations are given in the table below:

Location/stored at	Chambers / objects analysed	Source	Phase
Ħal-Saflieni	Chamber 4, Upper level, Chamber 6, Intermediate level, Chamber 17, Walkway area, Chamber 18, Oracle Chamber, Chamber 20, Decorated room, Chamber 23, Stepped area, Chamber 26, Main hall	Hypogeum	Saflieni
Total number of readings	117		
National Museum of Archaeolgy (NMA)	Plate shard #1	Skorba	Ghar Dalam
	Plate shard #2	Mgarr	
	MA 002, shell, plate shard #3	?	Zebbug
	Large pot, Sleeping lady, reclining figure, large statue, alabaster fat goddess, Venus of Malta, pot shards #1 - #5	Hypogeum	Saflieni
	Phallic figures, single phallus, clay statuette, MA 004 – 007, MA 009 - 011	Tarxien	Tarxien
	MA 009 - 010	Ggantija	Ggantija
	MA 011	Buqana	?
Total number of readings	134 [1]		
Gozo Museum of Archaeology (GMA)	Shells #1 - #5, spoon, necklace beads #1 - #2, button, pendant, 12 beads forming necklace, Twin Seated figurine, miniature bowl, small pot, ochre pot, bones #1 - #3	Xaghra Stone Circle	Tarxien
	Pot shards #1 - #4	S. Verna	Zebbug
	Plaster samples #1 - #2, pebble, pottery shards #5 - #7	Ggantija	Ggantija
Total number of readings	169		

Table 4-13. Outline of XRF analytical work on Maltese archaeological materials

[1] Some data was lost owing to an instrument malfunction

Figures 4-34a, b. Collecting XRF data from the ochre wall paintings in the Hal-Saflieni Hypogeum

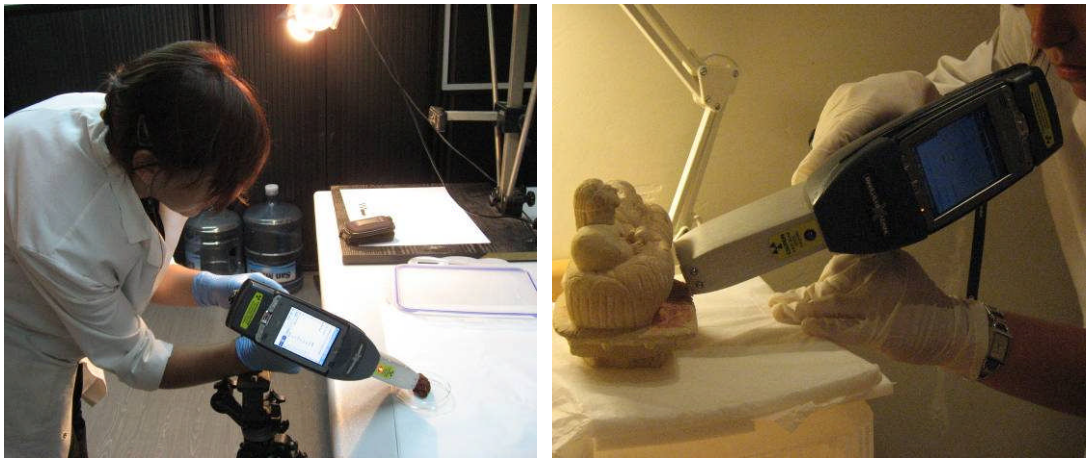

Figures 4-35a, b. XRF analysis in labs set up with restricted access in the NMA (a) and the GMA (b)

Figures 4-36a, b. Analysing immovable artefacts in cordoned off areas in the museum

4.3. Statistical methods employed for the provenancing of ochre

As it was concluded that elemental analysis was key to the sourcing of ochre; it was necessary to identify which statistical methods to implement on the acquired data in this provenancing study. This entailed using and adapting various statistical methods used in the provenancing of other materials to ochre (Earle and Ericson, 1977; Erlandson, Robertson et al., 1999; Glascock and Neff, 2003; MacDonald, Hancock et al., 2008). Iron oxides and/or iron hydroxides are the main colorants of these pigments, therefore it is important to establish which elements were directly linked to these minerals. Often, however, a large difference in concentration of Fe (III) is noted between ochres, even between ochres obtained from the same source; therefore it is customary to ratio the element to Fe, and log-normalise the data for comparative purposes (Popelka-Filcoff, Robertson et al., 2007; Popelka-Filcoff, Miksa et al., 2008). Further data examination in this study included extracting the main accessory element detected, Ca, out of the dataset. All these transformations make relationships between variables more distinct, were not expected to affect the resulting interpretation (Aitchison, Barcelo-Vidal et al., 2002).

Further statistical methods were applied to both the raw and transformed data, and those utilised in this project are described briefly below

i. Scatter plots and matrix plots: are both visuals way of showing trends between two elements. Matrix plots allow the simultaneous observation of the two-variable relationships among several variables, and have been used extensively in Chapter 5.

ii. Principle components (PC), biplots and loading plots: PC tests are simple multivariate techniques used to show relationships between variables by transforming them into a smaller number of variables known as principle components (Glascock and Neff, 2003): Only two PCs were used in this study. Biplots and loading plots are different ways of showing the trends in this PC space, by seeing how the variables correlate with each other.

iii. Pearson's tests, R^2 and P values: are also different methods used in this project to analyse correlations between data. The information given in these tests, is, however, numerical, and these methods are therefore more precise than the plots mentioned above. These tests were used to assess the degree of correlation between the elements, and when assessing accuracy of instrumental techniques (e.g. SEM-EDS/XRF and ICP-AES).

iv. Cluster analysis and hierarchical dendrograms. The dendrograms in particular have been used extensively in Chapter 5, and have also been used to classify data based on their similarities; as well as to assess the correlation and therefore grouping between observations. These are non-subjective methods and link data based on the statistical correlation between them.

Chapter 5.

Results

5.1. Maltese geological and archaeological samples

5.1.1. Polarising light microscopy (PLM)

The following photographs were chosen as the representative examples of the Maltese geological and archaeological sample groups. All the images were taken at a magnification of x400 under plane polarised light (PPL), unless stated otherwise.

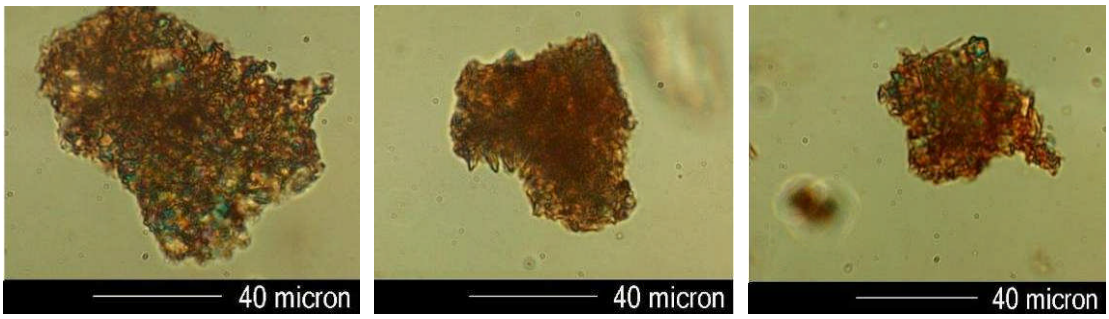

Figures 5-1a-c. PLM images of Calcitic reds*:* (a) Cwa 1001, (b) Gh 1001, (c) Mv 1001

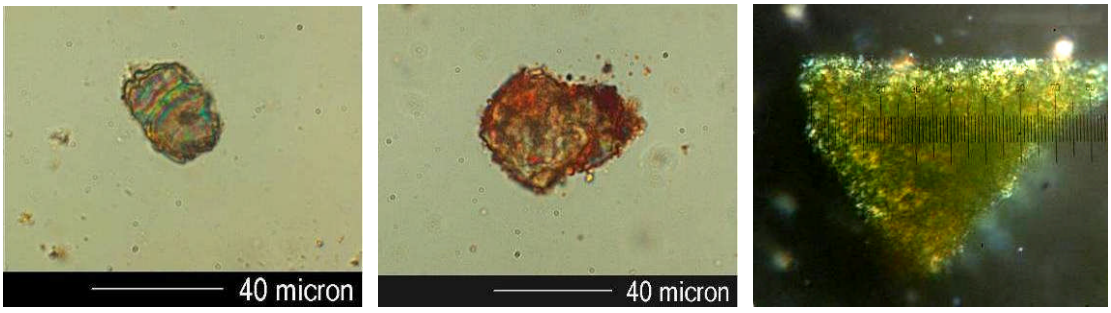

Figures 5-2a-c. PLM images of Greensands: (a) G 1001, (b) GTG 1002, (c) G 1008 (XPL)

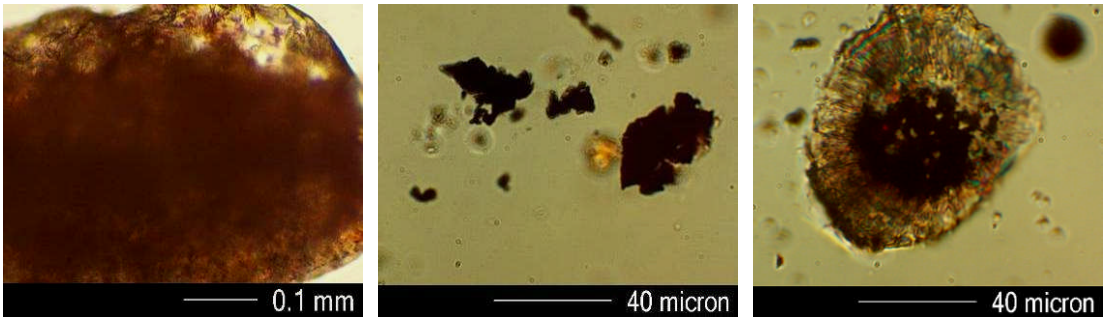

Figures 5-3a-c. PLM images of (a) RB 1001 (Mag x50), (b, c) *'Ooids'*: Mfn 1001, Mfn 2002

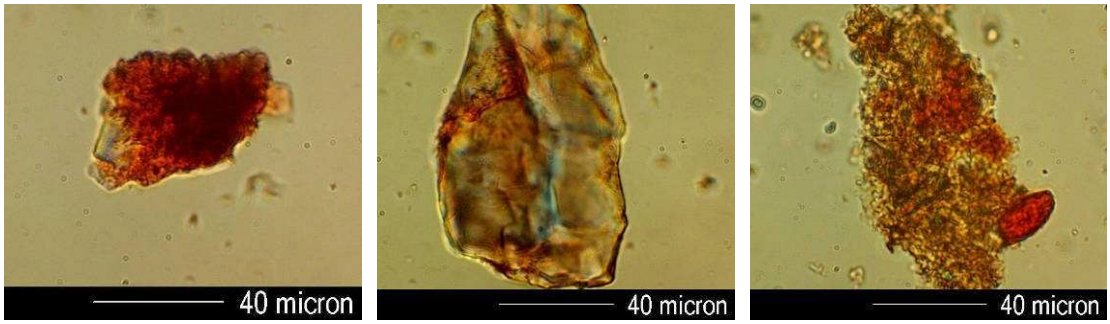

Figures 5-4a-c. PLM images of the Terra rossae: (a) G 037, (b) G 129 (c) G 132

Material	In samples	Fig. Nº.	Observations
Goethite	Most, not much in the MA (reds)	5-1a-c, 5-2a,b, 5-3c, 5-4a,c, 5-8a,c,	Yellow, yellow-brown to brown, generally fine to very fine particles. Shape: rounded, moderate relief. Refractive index (RI) > medium. Strong, yellow body colour so pleochrosim is not obvious. Particles are birefringent and clump together or onto an accessory material
Hematite	Most samples, apart from the MA (yellows)	5-1c, 5-2b, 5-4a-c, 5-7b, 5-9a-c, 5-10b,c	Deep red to reddish brown particles, mostly quite fine but in some cases were larger. Shape: smooth and rounded, sometimes angular to subhedral. Moderate to high relief, RI > medium, birefringent, with masked pleochrosim. Clumping is also observed.
Glauconite	Greensands, some Ooids	5-2a, 5-6	Colour: olive-green to brown ('rusted'). Particles are fine grained and rounded, with a low relief. RI < medium, moderate birefringence, and bright green pleochrosim.
Calcite	All	5-1a,c, 5-2a, 5-3c, 5-4c, 5-7a, 5-9a,c	Very fine, colourless, particles, with extremely variable relief, therefore varying refractive index. Shape: varies, euhedral/subhedral, sometimes microfossils were observed (see text) Particles extinguished when stage rotated under XPL Highly pleochoric and birefringent, with third order interference colours.
Gypsum	Ooids, MA (reds)	5-3b,c	Colourless, varying particle sizes, moderate relief with RI < medium. Commonly contain inclusions, low birefringence, grains still colourless, shape is typically subhedral with first order interference colours

Table 5-1. Summary of PLM observations, size scale: coarse (>10 μm), large (10 – 3 μm), medium (3 – 1 μm), fine (1 – 0.3 μm) and very fine (< 0.3 μm). (Comparisons were made to establish identities with descriptions in: Gribble and Hall, 1992; Eastaugh, Walsh et al., 2004; Helwig, 2007)

Material	In samples	Fig. N$^{o.}$	Observations
Quartz	All (less predominant than calcite)	5-3a, 5-7c	Larger particle sizes, ranging from medium to coarse, grains still colourless, shape is typically subhedral. Relief is variable though typically low. RI < medium, low birefringence with first order interference colours
Fibres	MA (yellows)	5-8a-c	Intense yellow to yellow-brown to brown, varying in size, generally quite large fibres, appear highly oxidised with low relief, and little pleochrosim. RI < medium, low birefringence, complete extinction
Bone	HYPD and HYPB	5-9b, 5-10a,c	Also intense yellow colour, and varying in size, generally quite large and rectangular-shaped with low relief No apparent pleochrosim. RI < medium, no birefringence

Table 5-1. Summary of PLM observations, continued (Gribble and Hall 1992; Eastaugh, Walsh et al. 2004; Trueman, Behrensmeyer et al. 2004; Helwig 2007)

Geological ochres

PLM observations showed that the samples presented similar characteristics. The predominance of calcite was observed from the unmistakable pleochroic effect (Figure 5-2a) exhibited by the particles when viewed in plane polars (PPL), as well as by the characteristically high third order interference colours observed under crossed polars (XPL) on rotation of the microscope stage (Gribble and Hall, 1992: 156). Various forms and dimensions of calcite particles were observed, including angular and broken grains of varying thicknesses (therefore varying birefringence), and microfossils such as coccoliths. G 2005 was an excellent example of a coccolith-full slide, with microfossil species thought to be Discoaster pentaradiatus and dimensions reaching up to 5 μm. All samples also had high quantities of both red and yellow ochre. These were present in varying proportions and sizes, and were typically clumped around the accessory minerals (calcite and quartz particles).

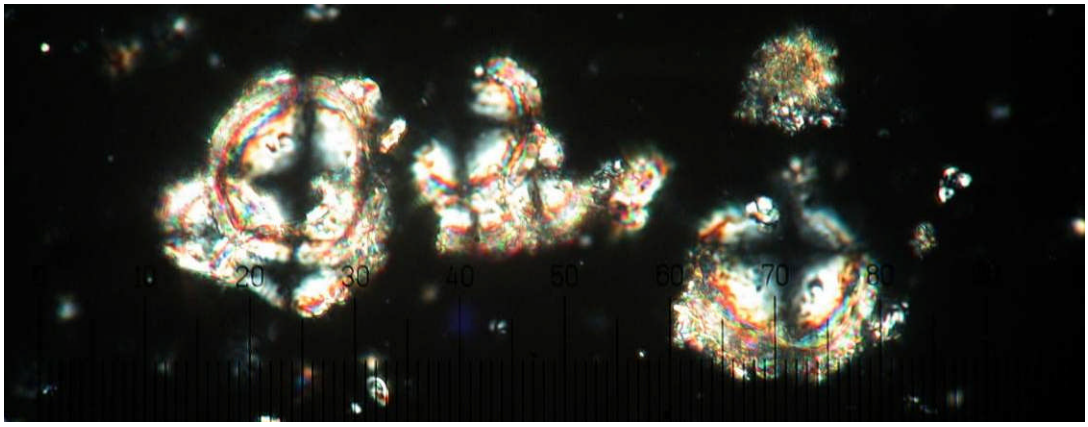

Figure 5-5. Coccoliths in G 2005, viewed under crossed polars. Mag. X1000

Although all the geological samples had many similarities, differences were also observed between the sample groups, although there were no obvious intra-group differences perceivable under the light microscope. The Calcitic red (CR) group predominated in red ochre (and calcite) and also contained few goethite, quartz and clay particles. The Greensands samples, like the CRs predominated in red/yellow ochre and calcite. They did, however, contain glauconite, whose particles varied both in size and in colour: these appeared to be green in certain dispersions (Figure 5-2c), whereas in other examples the mineral appeared to be 'rusting' to a reddish-brown colour, as was observed in G 2004 (Figure 5-6 below). The RB sample comprised large particles of quartz/calcite with smoothened, though irregular surfaces, probably indicating a prolonged exposure as a grain to the environment and its subsequent weathering effects. The relatively thick constitution of these sand grains enhanced the birefringent properties of the material, which were clearly observable under XPL. The inclusions and striations along the grains were probably a mixture of clay and/or some iron-based material, although this was difficult to certify with confidence.

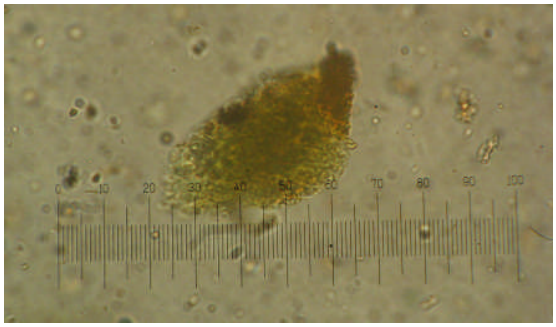

Figure 5-6. 'Rusting' glauconite grains in dispersion sample G 2004

The 'Ooid' group possibly constituted the most obviously dissimilar set of samples, and appeared to exhibit a higher quartz content in comparison with the other sample groups, with some glauconite, calcite (coccoliths were observed in these samples too, e.g. in Mfn 2004), gypsum and a clear abundance of iron oxides. Other interesting observations included some micro-scale ooids (Figure 5-4c). The final group of 'Terra rossae' were quite similar to the 'Calcitic reds' containing significant amounts of red ochre and calcite. These however also appeared to have a larger amount of quartz and organic materials in addition to the other mineral constituents (Conklin, 2005).

Archaeological ochres

The archaeological ochres were divisible into four groups: the MA 'reds' consisting of MA 001 – MA 004 and MA 009 – MA 011; the MA yellows, namely MA 005 –MA 008; the Hypogeum deposits (HYPD) and the bone scrapings (HYPB).

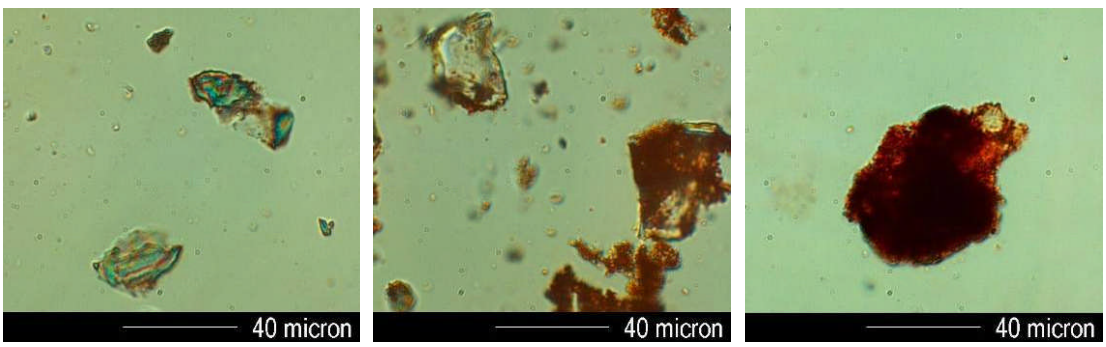

Figures 5-7a-c. PLM images of archaeological samples (a) MA 003, (b) MA 004, (c) MA 010

Figures 5-8a-c. (a) MA 006, (b) MA 007, (c) MA 008

Figures 5-9a-c. (a) HYPD 1002, (b) HYPD 4001, (c) HYPD 5001

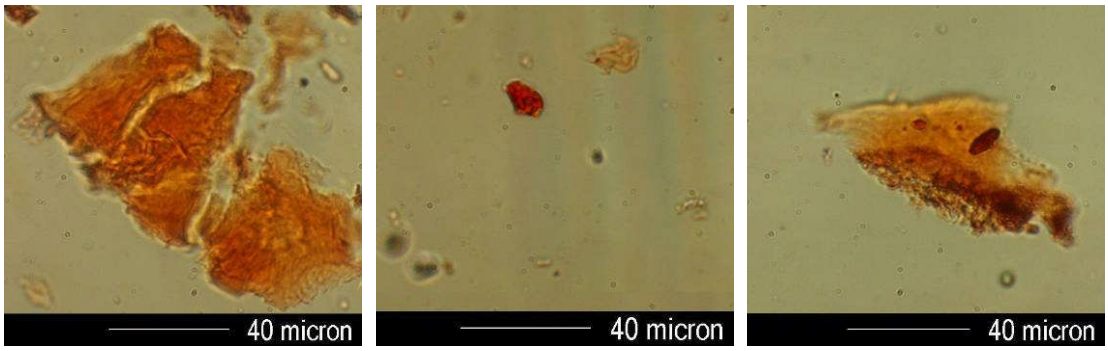

Figures 5-10a-c. (a) HYPB 1001 (b,c) HYPB 4001

The red archaeological ochres consisted of relatively pure grains of hematite that varied in grain shape and size. Some appeared as fine, rounded particles, whereas others were larger, more discrete, platy crystals. These particles were typically found clumped onto grains of highly pleochoric calcite (Figure 5-9c), and in certain cases, hematite was also observed coating larger grains of quartz (Figure 5-7b). Accessory material quantities varied considerably, with MA 001 – MA 003 possibly being the

purest ochres (lower quantity of accessory material). The chief colorant in these ochres was therefore hematite, with the main accessory mineral being calcite, and some quartz.

Goethite predominated in the yellow samples, and appeared as orangey-yellow, rather fine, pure, particles often clumped onto fibrous-looking yellow-brown (probably heavily oxidized) material of varying dimensions that extinguished under cross-polars (Figure 5-8 a,c). Although positive identification of the fibrous material could not be ascertained by means of PLM, it was assumed to be a collection of textile fibres, possibly flax/jute/hemp owing to the complete, parallel extinction observed (Petraco and Kubic, 2004). The goethite particles themselves also varied in size and very few accessory minerals were observed apart from the remote calcite and/or quartz particle.

The HYPD dispersions were all similar with minor differences in amounts of calcite, organic material, overall purity and ochre type. In some examples red ochre appeared to predominate as the main colorant, observed in HYPD 1001, 1003, 2001 and 7002; whereas in other dispersions goethite was present in higher amounts (HYPD 1002 and 5001). Although the iron oxides/hydroxides varied in particle sizes, they were essentially small and clumped together or onto accessory minerals (Figure 5-9 b, c). HYPD 3002 and 4002 were particularly rich in organic matter and humic material. The calcite content was invariably high, and varied in grain size. Some samples were also relatively rich in ascidian microfossils and other coccoliths. Other accessory materials included quartz, some gypsum and clays. Many samples also contained traces of oxidised bone, as was expected from this burial environment (Trueman,

Behrensmeyer et al., 2004). The control sample HYPD 8001 was difficult to distinguish from the other HYPD samples. It essentially consisted of red and yellow ochre, and calcite; but lacked the microfossil features that were observed in the other samples, as well as humic material, bone and quartz.

The samples extracted from bone obtained from Hal-Saflieni contained a mixture of various ochres, calcite (few microfossils), quartz and yellow-brown oxidized, bone material (Figures 5-10a, c, 5-11a). Less accessory materials (other than bone) were observed in these samples in comparison to the HYPD dispersions.

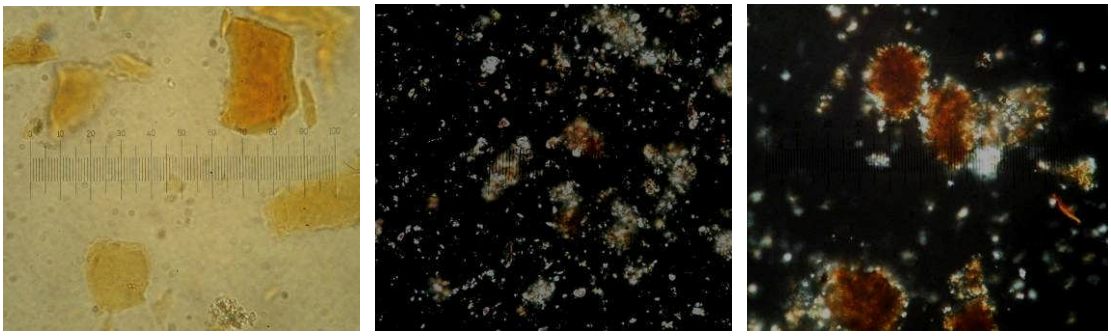

Figures 5-11a-c. The bone in sample HYPD 4001 (PPL), and images showing the predominance of calcite and hematite in samples HYPD 6001 and HYPB 2001 (XPL)

5.1.2. X-ray diffraction (XRD)

The diffractograms reproduced on the following pages are examples selected from those obtained from the XRD tests carried out on the *geological* sample groups from the Maltese islands. The final diffractogram is an overlay of a number of the results obtained from the 'Ooid' group, which was the more interesting of materials. A summary of the chief constituent materials based on the corresponding peaks is given in Table 5-2 below.

Mineral	Major 2-Theta peaks (High intensity)	Observed in sample groups
Calcite	29.363, 35.961, 39.401, 43.166, 47.508, 48.517	Calcitic reds, Terra rossae, Greensands
Quartz	20.826, 26.568, 42.447, 59.953, 68.141	Calcitic reds, Terra rossae, Ooids
Hematite	28.091, 38.651, 41.597, 58.076, 63.633, 73.942, 75.908	(Terra rossae, Ooids – poor quality)
Goethite	24.65, 38.779, 42.924, 62.686	Terra rossae, Ooids
Gypsum	11.633, 20.731, 29.116, 31.09, 33.367, 43.32, 50.333	Ooids

Table 5-2. Summary of XRD results

XRD tests carried out on the 'Calcitic reds' and the 'Greensands' failed to confirm the presence of iron oxides and/or hydroxides. Diffractograms showed the predominance of calcite, as was expected, and some samples additionally contained some quartz. Diffraction profiles of the 'Terra rossa' group indicated the presence of hematite, albeit in small amounts.

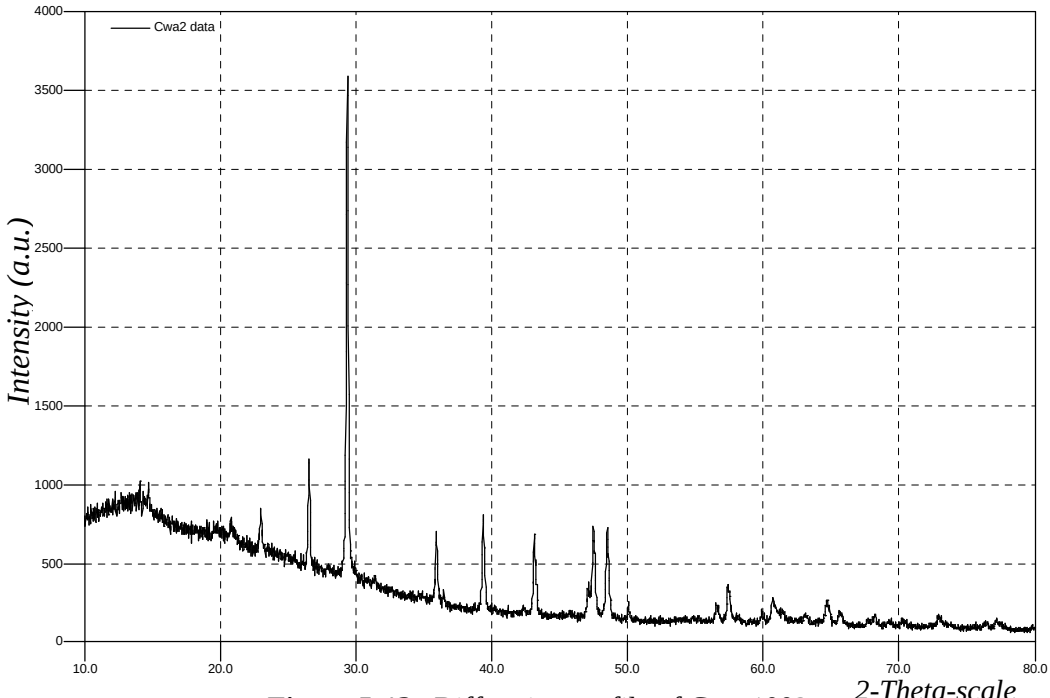

Figure 5-12. Diffraction profile of Cwa 1002

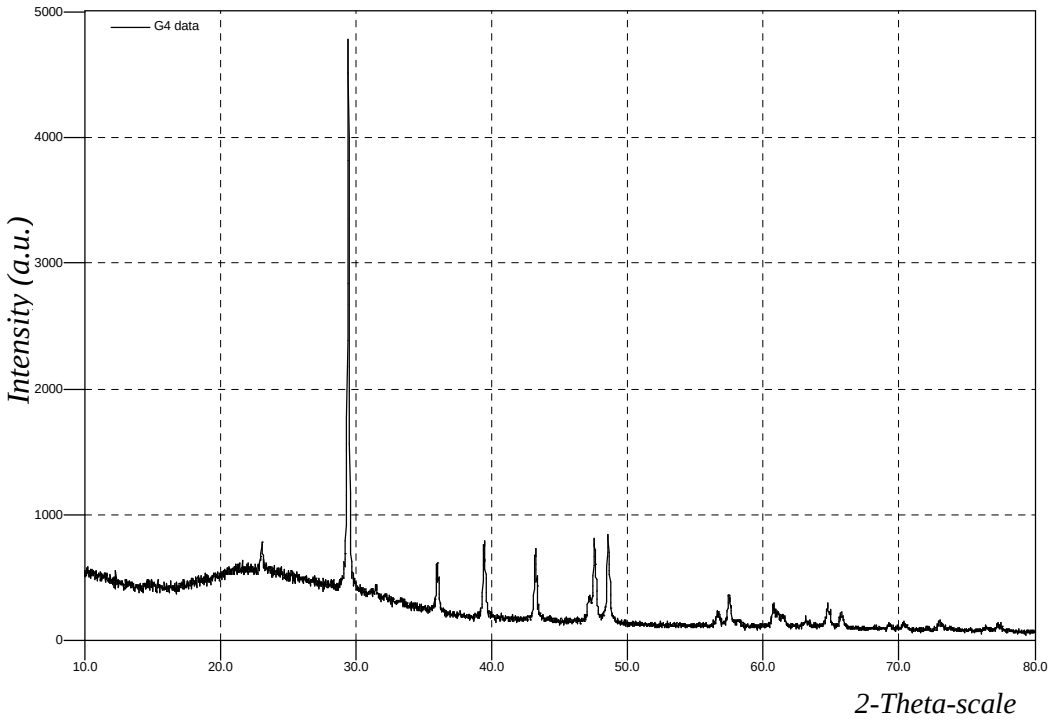

Figure 5-13. Diffraction profile of G 1004

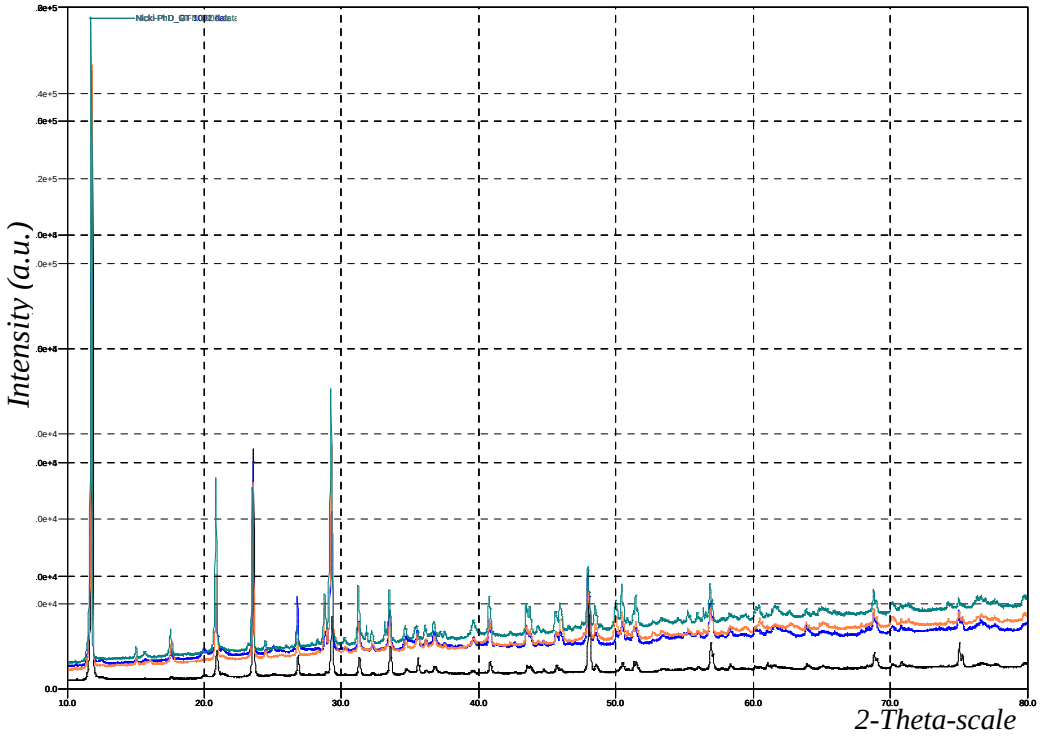

Figure 5-14. An overlay of the diffraction profiles of a number of 'Ooid' samples, namely GT 1001 (black), GT 1002 (blue), GT 1004 (orange) and Mfn 2002 (teal)

This technique, however, imparted useful information pertaining to the 'Ooid' group, although actual identification of constituent minerals was difficult. It was evident that the nodules consisted of a mixture of minerals, including crystalline and poorly crystalline phases, which also showed some preferential orientation. Although interpretation was tentative for several reasons as described below, the most likely material present appeared to be gypsum (calcium sulphate, $CaSO_4.2H_2O$), whose peaks prevailed in the diffractograms. Also present were calcite ($CaCO_3$), quartz (SiO_2), goethite (FeOOH) and possibly hematite (Fe_2O_3) and/or bernalite [$Fe(OH)_3(H_2O)$].

In the majority of these 'Ooid' group diffractograms it was apparent that the gypsum peaks were consistently shifted slightly towards higher 2θ angles. Quartz, although showing preferential orientation, was used as the internal standard and all peaks were corrected for this material. The gypsum shift, was, however, still present, indicating a shift in the lattice parameter that was probably the result of some internal substitution (possibly strontium substituting for the calcium) and/or a variance in the amount water of crystallisation present.

It was also clear that the peak heights (e.g. 20.7 2θ) did not correspond particularly well at times (with, e.g. gypsum), and that the main iron-containing minerals appeared to be present only in minor amounts when element analysis (see later) showed Fe to predominate in these samples. The goethite (and hematite) peaks were, moreover, poorly defined, indicative of poor crystallinity.

5.1.3. Inductively coupled plasma – Atomic emission spectroscopy (ICP-AES)

Geological samples

	%	%	%	%	%	%	%	%	%	(ppm)	(ppm)	(ppm)	(ppm)	(ppm)	(ppm)
sample	**Al_2O_3**	**Fe_2O_3**	**MgO**	**CaO**	**Na_2O**	**K_2O**	**TiO_2**	**P_2O_5**	**MnO**	**Ba**	**Co**	**Cr**	**Cu**	**Li**	**Ni**
Cwa 1001	0.68	0.34	0.70	49	0.22	0.12	0.03	0.07	0.01	51	51	1	12	8	3
Cwa 1002	6.4	2.9	0.94	34	0.19	0.84	0.30	0.06	0.04	137	137	11	58	13	41
Cwa 1003	3.8	1.5	0.74	40	0.19	0.69	0.21	0.05	0.02	103	103	4	30	10	17
Cwa 1004	6.2	2.3	0.87	36	0.18	0.82	0.30	0.07	0.02	123	123	6	54	16	35
Gh 1001	3.1	1.3	1.06	40	0.43	0.62	0.16	0.03	0.02	70	70	4	20	12	12
Gh 1002	2.1	0.88	0.94	46	0.33	0.43	0.11	0.04	0.01	96	96	2	8	8	7
Gh 1003	1.7	0.66	0.55	47	0.13	0.28	0.05	0.02	0.00	45	45	1	16	11	7
Mv 1001	4.01	1.7	0.67	38	0.38	0.49	0.20	0.03	0.03	92	92	5	32	14	13
MG 1101	1.5	0.62	0.56	52	0.03	0.19	0.05	0.03	0.01	20	20	2	19	7	7
MG 1201	3.6	1.5	0.75	47	0.23	0.49	0.13	0.04	0.02	61	61	4	35	13	17
MG 1301	1.9	0.86	0.52	50	0.11	0.28	0.07	0.04	0.01	28	28	2	22	9	10
MG 1401	1.5	0.62	0.42	50	0.04	0.19	0.05	0.02	0.01	22	22	2	13	8	9
MG 1501	2.5	1.04	0.57	48	0.18	0.34	0.10	0.04	0.02	39	39	3	26	11	12
MG 1601	2.3	0.86	0.53	48	0.09	0.33	0.08	0.04	0.01	32	32	3	24	9	10

	(ppm)	(ppm)	(ppm)	(ppm)	(ppm)	(ppm)	(ppm)	(ppm)	(ppm)	(ppm)	(ppm)	(ppm)	(ppm)	(ppm)
sample	**Sc**	**Sr**	**V**	**Y**	**Zn**	**Zr**	**La**	**Ce**	**Nd**	**Sm**	**Eu**	**Dy**	**Yb**	**Pb**
Cwa 1001	1	250	10	6	14	9	3	13	3	0.6	0.2	0.6	1.2	2
Cwa 1002	9	130	56	89	35	61	63	63	69	15.9	3.9	10.7	4.5	9
Cwa 1003	3	120	28	13	26	41	12	30	13	2.1	0.6	1.8	1.6	5
Cwa 1004	7	120	43	68	54	49	41	43	46	11.0	3.1	7.6	3.3	10
Gh 1001	3	130	21	7	43	40	10	27	10	1.6	0.4	0.9	0.4	1
Gh 1002	2	280	15	7	30	33	9	18	9	1.0	0.3	0.6	0.7	0
Gh 1003	1	105	10	4	35	11	4	6	4	0.7	0.1	0.2	0.3	1
Mv 1001	4	86	36	15	24	35	13	34	14	2.9	0.8	1.8	1.6	2
MG 1101	2	43	10	7	15	12	9	27	9	0.4	0.1	0.9	0.8	4
MG 1201	3	67	33	8	24	28	6	26	7	1.0	0.2	1.4	0.9	6
MG 1301	2	66	17	7	18	16	8	20	8	0.5	0.0	0.8	0.8	2
MG 1401	1	35	12	6	14	12	12	7	12	2.1	0.1	0.9	0.9	2
MG 1501	2	50	24	8	19	21	5	10	6	1.5	0.1	1.2	1.1	3
MG 1601	2	49	17	8	18	17	8	4	8	1.8	-0.1	1.2	0.7	3

Table 5-3a, b. *'Calcitic red'* data (all data rounded off to 2 significant figures)

	%	%	%	%	%	%	%	%	%	(ppm)	(ppm)	(ppm)	(ppm)	(ppm)	(ppm)
sample	**Al_2O_3**	**Fe_2O_3**	**MgO**	**CaO**	**Na_2O**	**K_2O**	**TiO_2**	**P_2O_5**	**MnO**	**Ba**	**Co**	**Cr**	**Cu**	**Li**	**Ni**
G 1001	1.3	4.6	0.76	45	0.07	0.46	0.08	0.41	0.02	24	4	62	11	1	14
G 1002	0.58	3.7	0.64	46	0.05	0.12	0.04	0.15	0.02	13	3	26	22	1	14
G 1003	0.94	5.1	0.75	44	0.17	0.29	0.06	0.23	0.02	21	4	55	25	1	17
G 1004	0.35	1.9	0.54	49	0.14	0.07	0.02	0.09	0.02	13	2	22	18	1	12
G 1005	0.55	1.6	0.53	50	0.18	0.12	0.03	0.11	0.02	12	2	23	16	0	18
G 1006	0.65	2.9	0.56	48	0.09	0.15	0.05	0.17	0.02	14	3	49	23	3	10
G 1007	0.93	5.9	0.75	44	0.20	0.26	0.06	0.24	0.02	16	6	51	30	3	19
G 1008	0.99	3.0	0.67	46	0.59	0.44	0.07	0.35	0.01	16	2	29	11	4	4
GTG 1001	2.5	4.0	0.86	44	0.20	0.89	0.10	0.53	0.04	28	3	52	12	7	23
GTG 1002	2.3	3.6	0.92	43	1.00	0.86	0.09	0.47	0.03	28	3	46	9	7	21
GTG 1003	2.2	3.6	0.90	44	1.04	0.88	0.09	0.50	0.02	26	3	45	9	6	15
RB 1001	0.47	1.6	1.01	47	0.12	0.14	0.02	0.30	0.01	18	1	17	5	1	8
MG 1009	1.0	6.4	0.72	49	0.03	0.16	0.05	0.10	0.01	14	0	20	12	2	8
MG 1100	0.89	5.5	0.74	49	0.02	0.14	0.04	0.09	0.01	20	0	19	10	3	7

	(ppm)	(ppm)	(ppm)	(ppm)	(ppm)	(ppm)	(ppm)	(ppm)	(ppm)	(ppm)	(ppm)	(ppm)	(ppm)	(ppm)
sample	**Sc**	**Sr**	**V**	**Y**	**Zn**	**Zr**	**La**	**Ce**	**Nd**	**Sm**	**Eu**	**Dy**	**Yb**	**Pb**
G 1001	1	62	97	20	27	17	9	25	11	4.2	0.9	2.9	2.0	5
G 1002	1	41	64	9	29	7	5.4	12	8.6	2.2	0.45	1.6	0.6	26
G 1003	2	56	86	17	33	12	9.0	21	14	3.5	0.77	2.5	1	23
G 1004	1	71	33	7	16	4	2	16	3	1.7	0.2	0.7	1.0	15
G 1005	0	47	34	13	16	6	3	13	5	1.7	0.6	1.8	1.2	2
G 1006	2	59	66	10	41	7	6	15	7	2.5	0.4	1.4	0.7	19
G 1007	2	48	93	14	48	10	7	11	8	3.3	0.6	1.7	1.2	22
G 1008	1	81	46	14	45	10	7	14	8	3.4	0.9	1.8	0.6	1
GTG 1001	4	280	86	33	58	12	16	32	19	6.1	1.9	4.1	1.2	2
GTG 1002	4	290	76	28	54	10	14	32	16	5.2	1.3	3.4	1.1	6
GTG 1003	4	290	72	32	54	8	15	34	18	5.2	1.6	3.9	1.2	4
RB 1001	2	380	25	14	26	4	7.4	13	9.9	2.3	0.51	1.9	0.77	6
MG 1009	1	64	22	5	20	9	4	15	5	2.3	0.6	0.6	0.8	3
MG 1100	1	63	17	5	19	8	8	7	8	2.7	0.5	0.6	0.8	6

Table 5-4a, b. *'Greensands'* data

	%	%	%	%	%	%	%	%	%	(ppm)	(ppm)	(ppm)	(ppm)	(ppm)	(ppm)
sample	**Al_2O_3**	**Fe_2O_3**	**MgO**	**CaO**	**Na_2O**	**K_2O**	**TiO_2**	**P_2O_5**	**MnO**	**Ba**	**Co**	**Cr**	**Cu**	**Li**	**Ni**
Mfn 1001	1.7	34	0.37	8.7	0.61	0.45	0.09	0.07	0.01	20	2	16	13	3	81
Mfn 1002	1.5	19	0.31	18	0.94	1.4	0.08	0.13	0.00	22	1	17	10	5	19
Mfn 2002	1.6	19	0.35	16	0.91	1.6	0.08	0.13	0.00	20	2	12	13	5	32
Mfn 2003	1.7	19	0.47	19	0.95	1.4	0.08	0.13	0.00	27	4	15	19	5	46
Mfn 2004	2.0	22	0.40	15	0.87	2.0	0.10	0.14	0.00	31	3	20	14	6	38
GT 1001	5.3	10	0.65	22	0.10	1.0	0.25	0.07	0.01	61	11	29	12	18	54
GT 1002	8.0	11	1.09	16	0.22	1.8	0.35	0.11	0.01	109	6	41	13	27	25
GT 1003	12	16	1.5	9.2	0.26	2.04	0.52	0.17	0.02	180	8	69	19	37	43
GT 1004	9.4	13	1.2	12	0.14	1.7	0.42	0.13	0.01	140	6	55	18	33	26
GT 1005	5.4	3.8	0.59	18	0.09	0.97	0.26	0.03	0.00	130	3	21	10	17	8
GT 1006	8.9	23	1.2	7.01	0.19	2.3	0.40	0.13	0.01	130	6	59	17	29	37
MG 1001	2.5	20	0.47	18	0.79	1.3	0.12	0.20	0.01	32	3	29	9	7	42
MG 1006	3.5	20	0.43	13	0.31	3.2	0.17	0.07	0.01	51	3	38	9	12	20
MG 1008	2.7	16	0.52	21	0.05	0.72	0.13	0.13	0.01	46	5	33	8	10	57
MG 1701	2.9	14	0.44	24	0.06	0.46	0.14	0.07	0.02	44	11	30	15	11	49

	(ppm)	(ppm)	(ppm)	(ppm)	(ppm)	(ppm)	(ppm)	(ppm)	(ppm)	(ppm)	(ppm)	(ppm)	(ppm)	(ppm)
sample	**Sc**	**Sr**	**V**	**Y**	**Zn**	**Zr**	**La**	**Ce**	**Nd**	**Sm**	**Eu**	**Dy**	**Yb**	**Pb**
Mfn 1001	1	180	35	4	46	21	6	5	4	6.0	2.4	1.4	2.3	6
Mfn 1002	2	360	26	2	59	15	6	3	6	7.0	1.9	0.7	0.9	14
Mfn 2002	2	330	24	3	59	15	7	9	7	5.4	1.8	0.5	0.9	20
Mfn 2003	2	320	26	4	75	16	8	9	8	6.4	1.6	0.3	1.0	24
Mfn 2004	2	420	30	3	78	25	9	9	9	7.8	1.8	0.5	1.3	24
GT 1001	5	350	45	5	62	33	13	18	13	2.0	0.9	0.4	0.7	16
GT 1002	7	430	66	7	62	46	19	28	18	3.4	1.0	0.5	0.9	11
GT 1003	10	180	91	11	98	69	27	41	27	5.2	1.5	1.3	1.4	17
GT 1004	9	200	80	9	72	55	22	36	21	4.0	1.1	0.8	1.0	14
GT 1005	4	370	38	4	35	30	13	22	13	0.4	0.3	0.3	0.6	1
GT 1006	8	307	85	8	73	52	22	31	21	*	*	0.6	1.3	16
MG 1001	2	710	31	5	34	24	9	11	10	6.3	2.1	0.3	1.7	17
MG 1006	3	406	38	2	31	29	9	10	10	5.3	1.8	0.0	1.5	22
MG 1008	3	730	31	6	40	24	8	13	9	4.8	1.7	0.6	1.3	21
MG 1701	3	470	27	4	47	23	7	14	8	4.0	1.3	0.2	1.3	32

Table 5-5a, b. *'Ooid'* data (* indicates that the element was present in concentrations below the detection limit of the instrument)

	%	%	%	%	%	%	%	%	%	(ppm)	(ppm)	(ppm)	(ppm)	(ppm)	(ppm)
sample	**Al_2O_3**	**Fe_2O_3**	**MgO**	**CaO**	**Na_2O**	**K_2O**	**TiO_2**	**P_2O_5**	**MnO**	**Ba**	**Co**	**Cr**	**Cu**	**Li**	**Ni**
G037	17	6.9	1.5	5.4	0.34	2.6	0.75	0.40	0.08	320	15	120	55	72	48
G042	14	6.03	1.5	12	0.33	2.1	0.64	0.45	0.08	320	15	97	56	50	41
G113	9.0	3.9	1.3	18	0.30	1.5	0.46	1.04	0.07	250	10	90	41	37	30
G129	13	5.8	1.3	4.6	0.42	2.0	0.75	0.17	0.10	370	15	100	30	51	36
G178	15	6.6	1.5	3.8	0.37	2.1	0.77	0.22	0.09	350	16	110	33	60	42
G135	15	6.3	1.3	11	0.29	1.8	0.70	0.34	0.09	330	15	110	37	68	46
G254	20	8.04	1.5	3.7	0.22	2.3	0.80	0.12	0.07	304	18	120	41	85	73
G269	13	5.5	1.2	15	0.27	1.4	0.60	0.37	0.06	270	14	110	44	55	49
G299	7.5	3.3	1.0	27	0.24	1.0	0.40	0.63	0.05	230	9	73	71	29	33
G312	11	4.6	1.1	17	0.30	1.3	0.59	0.26	0.07	308	12	91	27	42	44
G073	16	7.0	1.2	1.5	0.40	2.3	0.77	0.14	0.07	380	17	83	25	68	42
G057	5.8	2.7	1.1	32	0.21	0.9	0.31	0.61	0.04	250	11	108	24	42	41
G266	10.4	4.5	1.2	22	0.25	1.1	0.53	0.29	0.06	150	7	57	23	21	22
G132	11	4.7	1.3	19	0.13	1.6	0.53	0.15	0.02	150	10	59	21	36	30
G223	3.1	1.5	0.84	38	0.13	0.5	0.17	0.76	0.02	110	4	43	38	14	20

	(ppm)	(ppm)	(ppm)	(ppm)	(ppm)	(ppm)	(ppm)	(ppm)	(ppm)	(ppm)	(ppm)	(ppm)	(ppm)	(ppm)
sample	**Sc**	**Sr**	**V**	**Y**	**Zn**	**Zr**	**La**	**Ce**	**Nd**	**Sm**	**Eu**	**Dy**	**Yb**	**Pb**
G037	15	103	120	39	130	140	50	91	52	9.1	2.2	5.7	3.2	65
G042	12	170	97	36	120	109	40	71	42	7.4	1.7	4.8	2.2	39
G113	9	205	67	28	150	95	32	54	33	5.8	0.9	4.2	2.3	49
G129	12	110	90	34	110	130	46	87	48	8.7	1.7	5.0	2.7	45
G178	14	105	106	41	108	140	48	94	50	9.3	2.1	5.6	3.3	62
G135	13	140	120	40	130	130	47	89	49	9.2	2.1	5.4	3.0	44
G254	17	82	150	42	107	150	51	93	53	9.8	2.0	5.9	3.6	30
G269	12	180	97	47	110	110	48	78	51	9.8	2.4	6.4	3.2	109
G299	7	190	62	35	130	71	31	54	33	6.5	1.7	4.6	2.4	83
G312	10	180	83	44	100	106	42	71	45	7.7	1.9	5.5	2.3	53
G073	16	102	130	46	107	130	56	103	59	11	2.5	6.5	3.8	36
G057	10	260	82	43	65	106	40	72	41	6.6	1.0	5.8	3.1	24
G266	6	270	42	21	84	53	22	39	23	5.2	1.2	2.8	1.4	27
G132	10	290	86	19	85	76	30	56	31	5.3	1.1	2.8	1.5	11
G223	3	480	29	23	140	32	15	23	16	2.6	0.9	2.3	1.2	104

Table 5-6a, b. *'Terra rossa'* data

Archaeological data

	%	%	%	%	%	%	%	%	%	(ppm)	(ppm)	(ppm)	(ppm)	(ppm)	(ppm)
sample	**Al_2O_3**	**Fe_2O_3**	**MgO**	**CaO**	**Na_2O**	**K_2O**	**TiO_2**	**P_2O_5**	**MnO**	**Ba**	**Co**	**Cr**	**Cu**	**Li**	**Ni**
MA 002	9.5	51	1.03	1.4	0.23	1.6	0.48	0.51	0.01	580	14	69	29	20	140
MA 003	8.8	43	1.02	6.4	0.19	1.4	0.43	0.71	0.01	440	16	80	29	21	130
MA 006	5.6	9.5	1.8	23	0.73	1.8	0.27	4.6	0.07	290	8	35	220	20	26
MA 007	6.1	13	2.4	26	0.83	1.9	0.31	3.20	0.06	420	7	42	250	24	33
MA 008	6.9	13	2.01	23	1.0	2.3	0.34	4.06	0.07	330	9	52	340	24	31
MA 009	12	28	1.4	0.97	0.36	2.8	0.60	0.63	0.01	350	11	90	22	25	54
MA 010	13	29	1.9	1.9	0.32	3.0	0.62	0.68	0.01	380	12	106	24	27	60
MA 011	7.3	21	0.98	23	0.24	0.85	0.42	1.6	0.01	200	8	68	38	39	90
HYPD 1001	3.2	3.0	0.88	35	0.32	0.56	0.19	6.3	0.02	65	4	60	29	15	39
HYPD 1002	2.9	2.8	0.81	37	0.32	0.53	0.17	7.07	0.01	71	4	55	27	13	35
HYPD 1003	2.9	2.9	0.94	37	0.46	0.52	0.17	5.4	0.02	87	4	51	25	12	30
HYPD 1004	2.6	2.7	0.74	36	0.37	0.46	0.15	8.8	0.02	73	3	44	24	12	29
HYPD 2001	2.2	1.8	0.93	47	0.36	0.38	0.14	4.2	0.01	40	4	33	33	9	50

	(ppm)	(ppm)	(ppm)	(ppm)	(ppm)	(ppm)	(ppm)	(ppm)	(ppm)	(ppm)	(ppm)	(ppm)	(ppm)	(ppm)
sample	**Sc**	**Sr**	**V**	**Y**	**Zn**	**Zr**	**La**	**Ce**	**Nd**	**Sm**	**Eu**	**Dy**	**Yb**	**Pb**
MA 002	8	1700	140	10	120	72	32	31	30	*	*	0.5	3.5	82
MA 003	8	1600	130	11	140	58	30	41	28	*	*	0.2	3.0	87
MA 006	5	410	81	25	307	11	25	47	26	6.4	1.0	3.0	1.8	30
MA 007	6	600	108	32	150	35	31	47	33	4.8	1.9	3.9	2.3	19
MA 008	6	460	104	30	200	22	31	57	33	7.6	1.7	3.9	2.6	25
MA 009	11	940	130	12	86	88	35	52	34	*	*	0.9	2.7	53
MA 010	11	1040	140	12	103	79	36	54	35	*	*	0.8	2.5	61
MA 011	6	507	109	16	120	24	23	33	23	*	*	1.2	1.9	33
HYPD 1001	4	440	48	40	230	22	19	29	21	3.9	0.9	3.3	1.9	3
HYPD 1002	3	480	42	40	240	7	19	25	21	3.9	1.1	3.2	1.9	7
HYPD 1003	3	560	41	33	209	19	17	27	19	4.0	0.8	3.1	1.5	11
HYPD 1004	3	570	38	30	220	27	16	22	17	3.2	0.8	2.6	1.6	5
HYPD 2001	2	590	35	26	140	7	12	18	13	1.8	0.7	2.3	1.4	3

Table 5-7a, b. Archaeological ICP-AES data (* indicates that the element was present in concentrations below the detection limit of the instrument)

	%	%	%	%	%	%	%	%	%	(ppm)	(ppm)	(ppm)	(ppm)	(ppm)	(ppm)
sample	**Al_2O_3**	**Fe_2O_3**	**MgO**	**CaO**	**Na_2O**	**K_2O**	**TiO_2**	**P_2O_5**	**MnO**	**Ba**	**Co**	**Cr**	**Cu**	**Li**	**Ni**
HYPD 3001 #1	1.8	2.3	0.76	43	0.33	0.29	0.12	15	0.03	54	21	44	139	7	407
HYPD 3001 #2	2.7	1.9	0.92	43	0.21	0.47	0.16	2.04	0.03	70	8	45	50	11	72
HYPD 7001	2.0	1.7	0.96	40	0.21	0.34	0.17	1.00	0.03	250	7	99	101	8	96
HYPB 2005	0.27	0.57	0.48	38	1.00	0.06	0.02	23	0.02	35	3	15	27	2	54
HYPB 4005	0.22	0.44	0.36	37	0.75	0.04	0.01	24	0.01	41	4	16	16	2	29

	(ppm)	(ppm)	(ppm)	(ppm)	(ppm)	(ppm)	(ppm)	(ppm)	(ppm)	(ppm)	(ppm)	(ppm)	(ppm)	(ppm)
sample	**Sc**	**Sr**	**V**	**Y**	**Zn**	**Zr**	**La**	**Ce**	**Nd**	**Sm**	**Eu**	**Dy**	**Yb**	**Pb**
HYPD 3001 #1	2	600	53	27	302	15	13	21	14	2.5	0.5	2.1	1.3	24
HYPD 3001 #2	3	543	35	27	130	14	15	20	16	2.8	0.9	2.4	1.2	80
HYPD 7001	2	509	50	23	200	25	14	22	15	2.5	0.7	2.1	1.0	790
HYPB 2005	0	415	11	4	260	7	3	5	3	0.3	0.0	0.6	0.5	1
HYPB 4005	0	340	10	4	370	4	2	2	2	0.7	0.1	0.4	0.6	8

Table 5-8a, b. Archaeological ICP-AES data continued

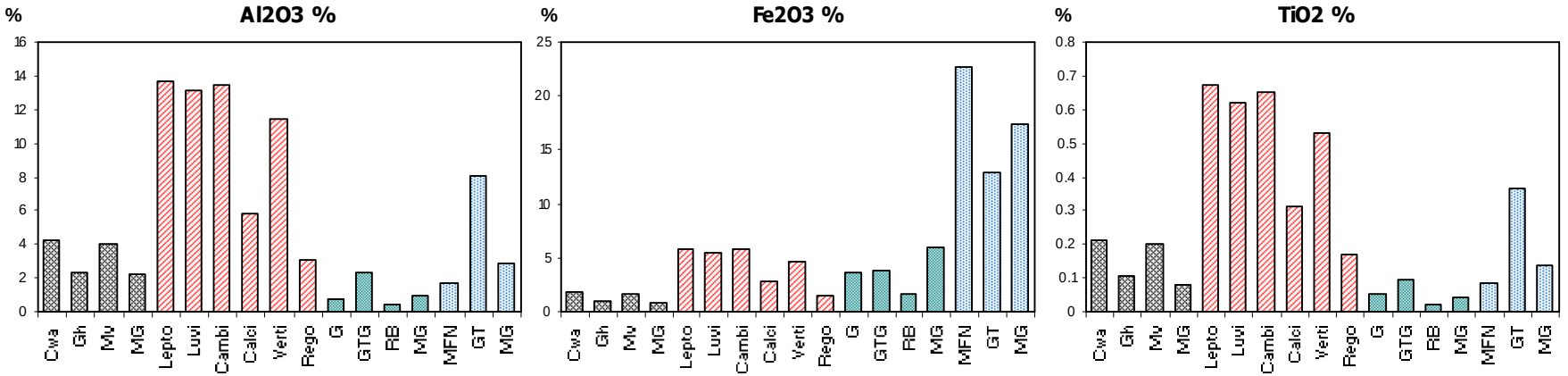

Figures 5-15a-c. Un-transformed data, showing distinct inter-site and inter-group differences between some elements: Intra-site values have been averaged

Data analysis and statistical tests for ICP-AES results

All the data was converted to ppm, and for most statistical operations was also log-normalised for display purposes. Statistics were necessary to identify the trends between datasets, with the multivariate statistical methods applied to assess group or source associations based on pattern recognition. Statistical methods used have been described previously in section 4.3 and include matrix plots, Pearson's correlation tests, biplots of principle components, hierarchical cluster analysis and confidence ellipses to understand and assess correlations. The majority of these assessments were made using the statistics package Minitab.

A difficulty encountered when observing the data was the substantial number of variables (the elements) obtained per sample (observation); an aspect deemed necessary because of the novel data obtained in this study and the indefinite (unknown) correlations. Matrix plots were therefore drawn as these facilitated the simultaneous observation of the two-variable relationships. The plots were divided as shown in Table 5-9 for initial observations, and several plots have been included in Appendix III for further reference.

Matrix plot	Variables	Elements (observed in ppm)
A	Major	Al, Fe, Mg, Ca, Na, K, Ti, P, Mn
B	Minor (1)	Ba, Co, Cr, Cu, Li, Ni, Sc
C	Minor (2)	Sr, V, Y, Zn, Zr, Pb
D	Rare earths	La, Ce, Nd, Sm, Eu, Dy, Yb
Total No. of elements (variables) examined per sample: 29		

Table 5-9. Matrix plots devised per set of observations

Comparison of the different geological groups

Since all groups (groups ≡ different sources) contained samples from different sites (same geological source), it was necessary to examine the inter-site and therefore the intra-group element variation between the same and the different groups in order to satisfy the provenance postulate theory mentioned in Chapter 1. It was essential to firstly show that (1) the sites clustered into definite groups (not much intra-source variation), indicative of their geological source and that (2) the various sources (groups) were distinctly separate, therefore enabling the (3) identification of whether inter-source variation was actually greater than the intra-source variation.

The observations described here are aimed at illustrating the relationships of element concentrations with respect to one another per sample and per sample site, to analyse the intra- and inter- source differences, and to identify any obvious discordant outliers within the sample groups from simple matrix plots and from the results data. The matrix plots show comparisons of un-normalised data as the compared variables were on a similar scale.

Group Nº.	Group name	Sites (and number of samples)
1	Calcitic Red	Cwa (4), Gh (3), Mv (1), MG (6)
2	Terra Rossa	Vary, divided into leptosols (5), luvisols (5), cambisols (2), calcisols (1), vertisols (1), regosols (1)
3	Greensands	G (8), GTG (3), RB (1), MG (2)
4	Ooids	Mfn (5), GT (6), MG (4)
Total No. of geological samples: 58		

Table 5-10. Source groups and samples: Samples from Cirkewwa (Cwa), Ghadira (Gh), Mistra village (Mv), Mgarr (MG), Gelmus (G), Ramla Bay (RB), Marsalforn (Mfn) and Ghajn Tuffieha (GT)

Intra- and inter- site variation in the Calcitic reds

The largest degree of intra-site variation was exhibited in the Cwa samples, with least variation in the MG samples. Element concentrations in the MG samples were also consistently lower than those observed in the other Group 1 samples as these appeared to predominate in Ca. The opposite effect was observed in samples Cwa 1002 and Cwa 1004, which exhibited a rather large, recurrent discrepancy between variables, owing to lower levels of Ca resulting in elevated concentrations of other elements, showing the high variability of this element. An example of this discrepancy is shown in the REE matrix plot in Figure 5-16. Spread in this source group was therefore limited to a cluster and/or to an analogous correlation.

Interpretations of the results were based on the assumption that the elements correlating with Fe were related to the Fe oxide signature and to the sample origin, whereas the elements not associated with, or negatively correlated with, Fe were related to accessory minerals associated with the Fe mineral, and therefore were acting as diluents to the ochre (see later). This characteristic was clearly exhibited in all the Ca graphs, which showed a highly negative correlation, not only with Fe but with all the other major element observations, therefore illustrating this diluent effect. The majority of the other elements presented a linear regression with a positive gradient, and a distinct relationship especially exhibited between Al and Fe, Al and K, Al and Ti; as well as between Fe and Mn, Fe and K, and Fe and Ti. These elements were analysed further by means of multivariate and PC statistical analysis, as will be discussed later. This positive correlation was also marked in the minor element plots; conversely the data in the REE plots formed obvious clusters, apart from the two unmistakable Cwa outliers.

Variation between the analysed soil units in the Terra rossa group

A similar positive correlation with most elements apart from Ca was exhibited in these Terra rossae as was observed with the first group (Calcitic reds). However, certain differences were also noted, including an inversely proportional relationship of all elements with P and Sr, as well as a larger concentration of heavy metals and other trace elements; and scattered data points for trace metals Cu, Zn and Pb. There was also a larger spread of data, which, although still showing correlation trends, was not as clear-cut as the Group 1 set. The regosol (G 223) was the only sample that gave a definite series of outlying data points; appearing to be calcium-rich, and therefore containing a lower concentration of other elements with respect to this diluent (Figure 5-17). This regosol also had a higher proportion of Sr in comparison to the other samples, indicating that the two were directly related and substituted for each other. Furthermore, the REEs did not form clusters but plotted as straight lines with a positive gradient, with the regosol exhibiting the lower REE concentration (ppm) and the calcisol G 073 the higher amount of REEs.

Intra- and inter- site variation of the Greensands

Group 3 samples appeared to have a wider spread of data, albeit displayed on a smaller scale range than in the other two sample groups (Figure 5-18). Data clustering was, nevertheless, apparent although linear correlations were not as pronounced, indicating a relationship between the samples but not a clear-cut relationship with the element variables. The scatter was especially prominent with the majority of the minor element plots, although positive correlations with some clustering were evident in most of the REE plots (apart from Yb). Consistent ‘outliers’ in this sample group included the

GTG samples, which all had a lower Ca content and therefore unsurprisingly almost invariably plotted at higher ppms in the graphs, with the exceptions of Ca, Cr, Cu, Zr and Pb. RB had a significantly higher Mg and a lower Fe content, with an overall composition nevertheless approximating that of the G samples.

Intra- and inter- site variation of the Ooids

These samples gave the largest data spread of all the three groups (Figure 5-19). The samples extracted from Marsalforn (Mfn) and Mgarr (MG) generally clustered together, while the samples from Ghajn Tuffieha (GT) appeared to correlate with each other, either positively in most cases, or occasionally negatively. The latter relationship was observed, once again, in the Ca plots, confirming its predominance and its diluent effect on overall material composition. Positive correlations were particularly pronounced in graphs between Al and Ti, Al and Mg, Ti and Mg, Sc and Ba, as well as the plots between Cr and Li. The most interesting and atypical relationships were those observed in the REE plots of both Sm and Eu against La, Ce and Nd (Figure 5-20), where a higher concentration than expected of Sm and Eu was exhibited in relation to the other five lanthanides for the Mfn and the MG samples. These lanthanides will be discussed in their entirety later on in the text (refer to P.190-191).

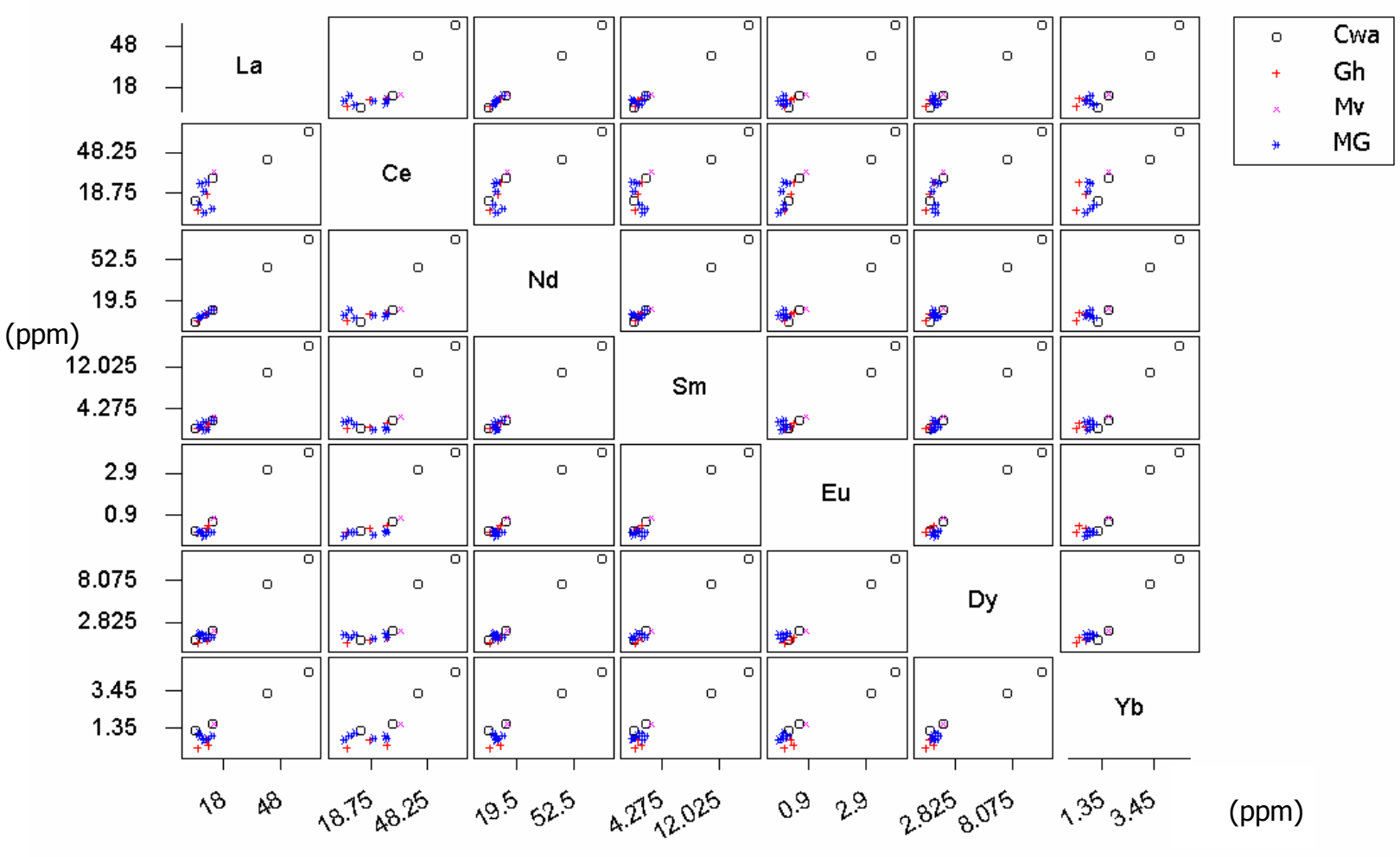

Figure 5-16. Matrix plot of REE Group 1 'Calcitic red' samples, showing the outlying samples Cwa 1002 and Cwa 1004

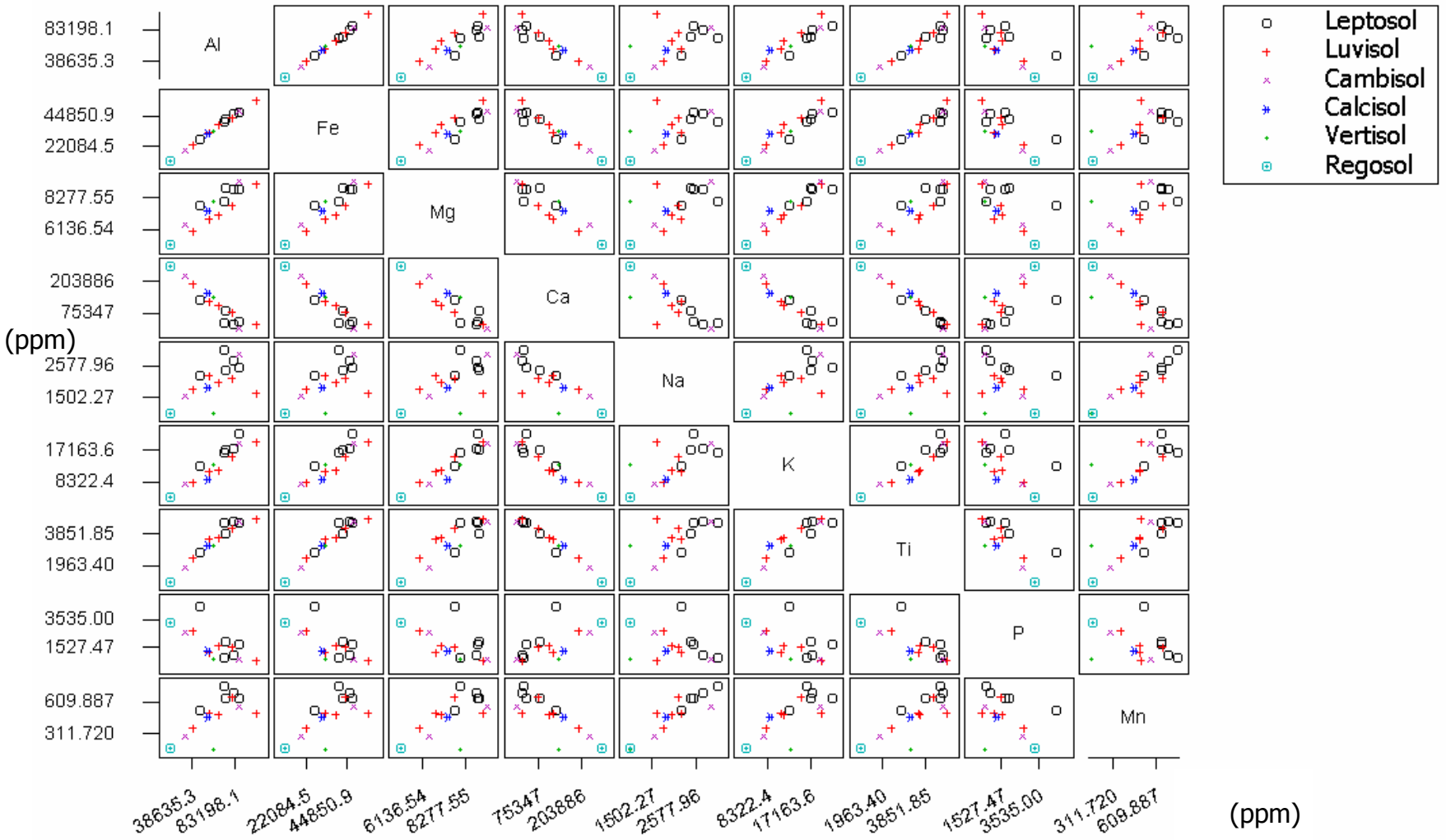

Figure 5-17. Matrix plot of major elements in Group 2 'Terra rossa' samples, showing the positive and negative correlations between the elements

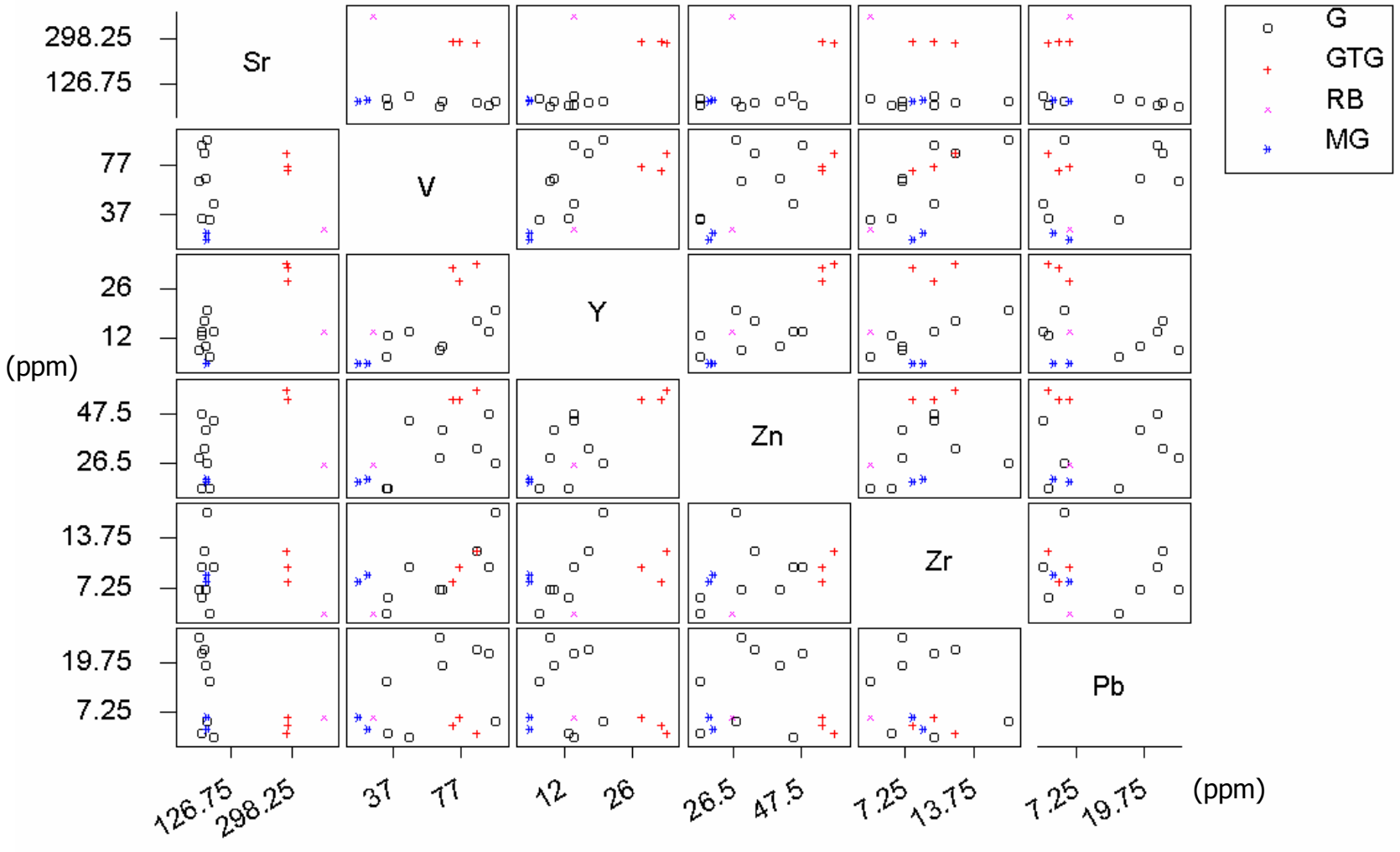

Figure 5-18. Trace element matrix plots showing the GTG outliers

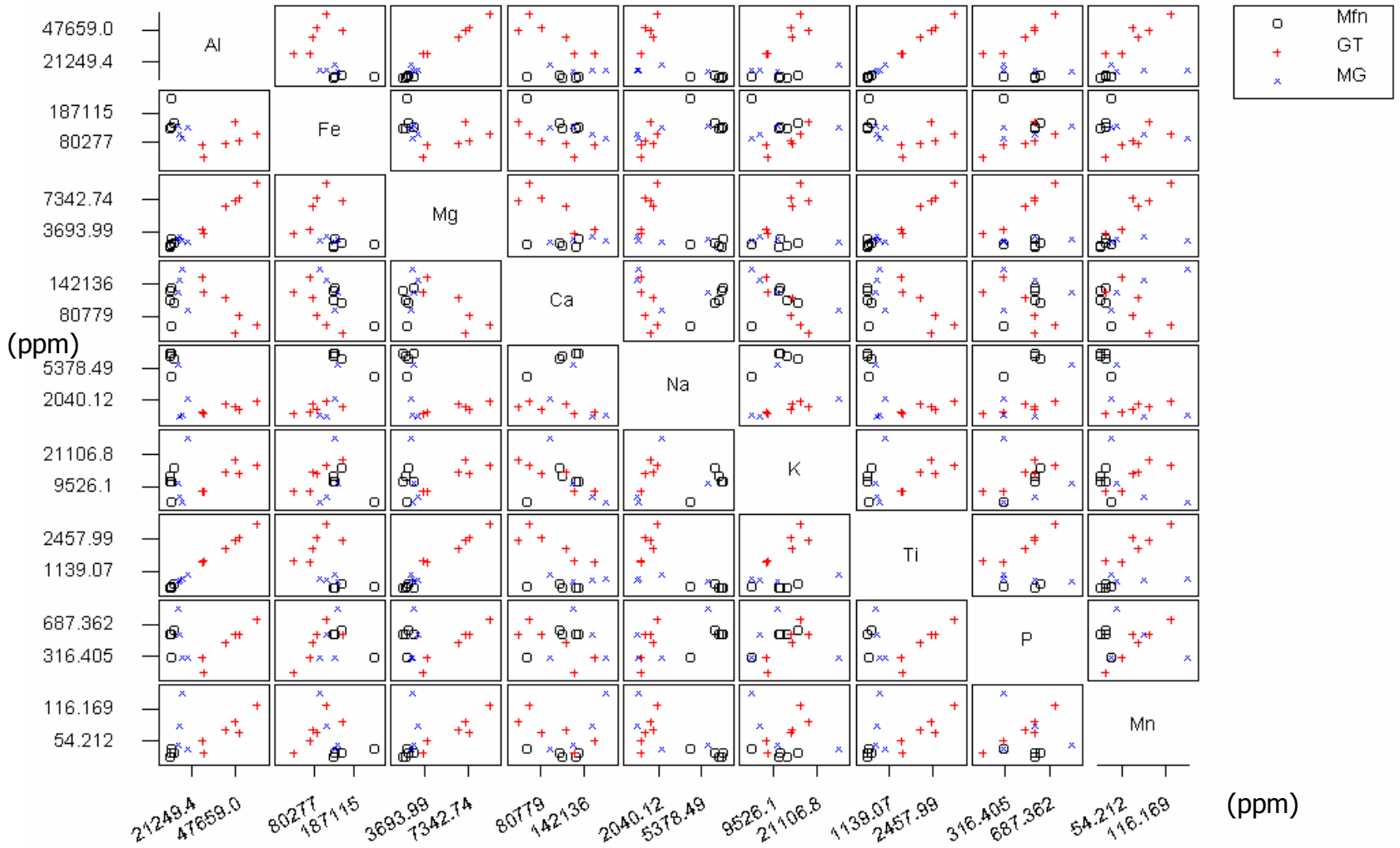

Figure 5-19. Matrix plot of the major elements in the Ooid samples

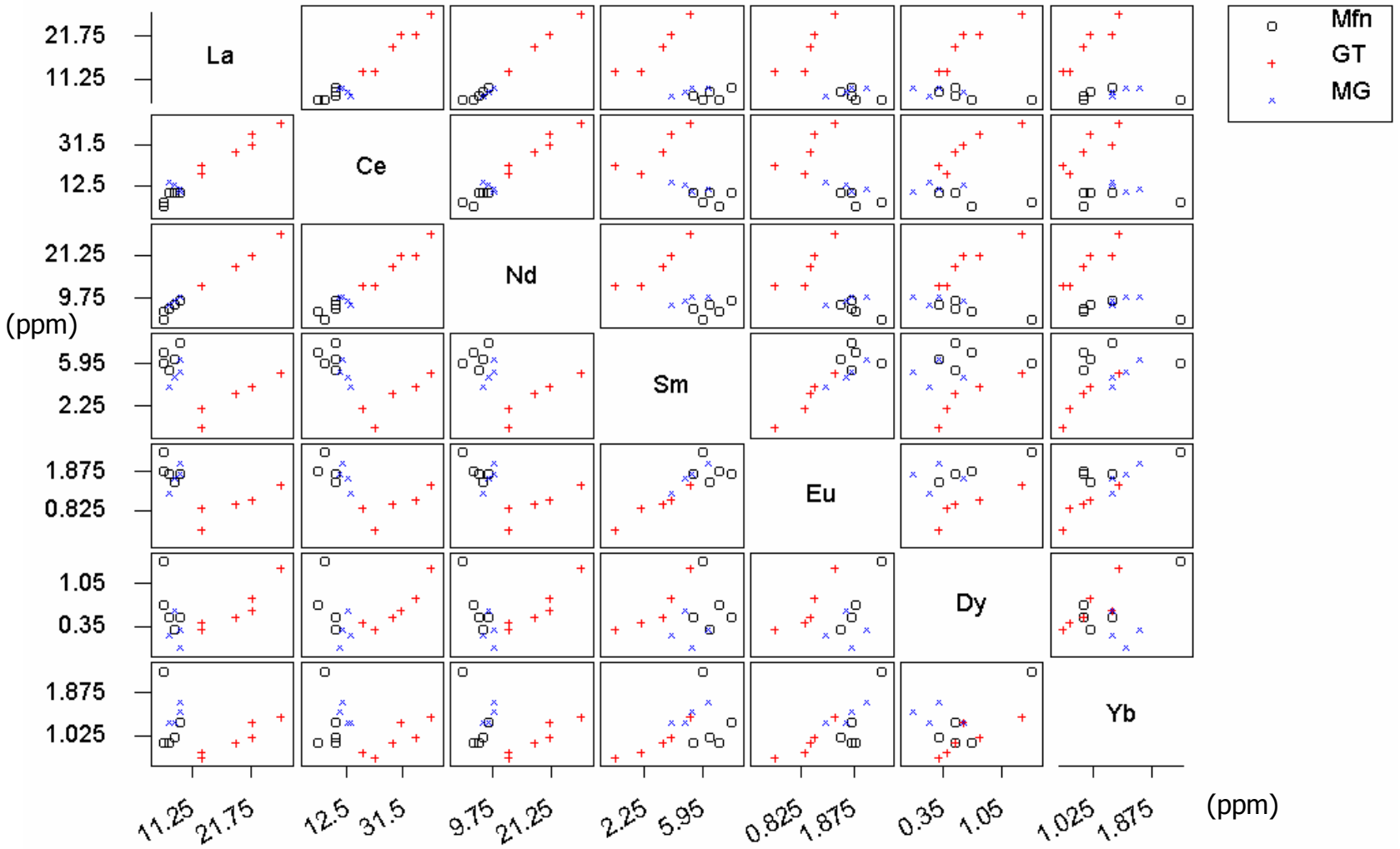

Figure 5-20. Matrix plot showing the relationship between the REEs in the Ooid group

Group variations.

Though site and source group averages of data illustrated that several variables showed intra-group similarities and inter-source differences, conjectures based on this data were deemed inadequate and further data analysis was necessary.

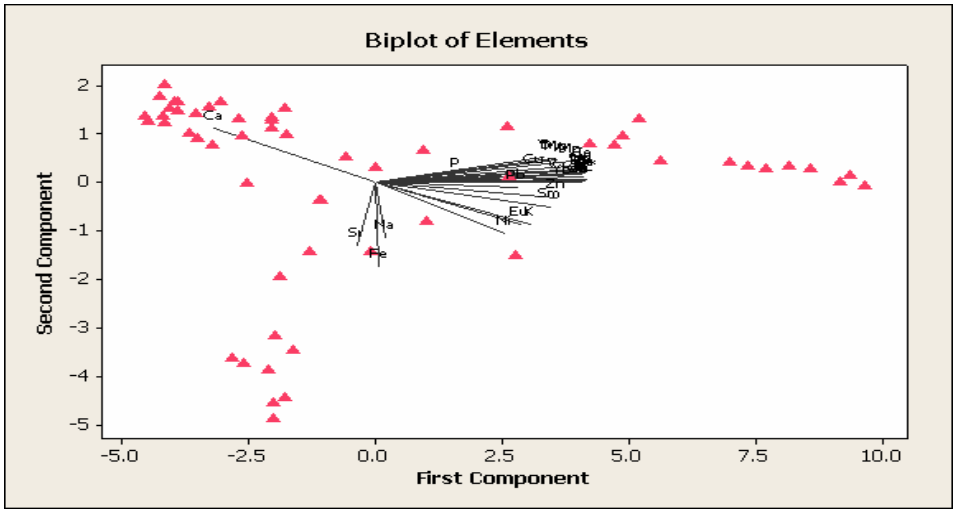

Figure 5-21. Biplot, showing the significant negative correlation of the variables with Ca (components established using Minitab 15)

Examples of these trends can be observed in the histograms in Figures 5-15a-c above which show the mean site variables for each group. Initial data analysis indicated that the majority of the elements showed a distinct positive correlation with each other, and that the Fe concentrations varied considerably. The latter factor also appeared to be affecting the variance of the total data set content and therefore the interpretation. Ca also clearly contributed to the overall dilution effect. These relationships are shown in the biplot above, which was drawn to identify patterns in the dataset within a principle component (PC) space: here the samples are displayed as points whereas the element variables are illustrated as vectors. These PC tests are simple multivariate techniques principally used to describe the variation between the elements by transforming them into a smaller number of variables (two were used in this case).

A mathematical adjustment was therefore made to the data for statistical analysis of the ochre samples. This involved extracting respective Ca values from the total, and presenting all resultant data as ratios to Fe to mitigate the influence of large concentration differences in Fe across the entire data set. Consequently, relationships become relative rather than absolute allowing for the dilution effect of both Ca and Fe, allowing the trace element data relative to Fe for each sample to be better observed (Erlandson, Robertson et al., 1999; Glascock and Neff, 2003; Popelka-Filcoff, 2006; Popelka-Filcoff, Robertson et al., 2007; MacDonald, Hancock et al., 2008; Popelka-Filcoff, Miksa et al., 2008). The log-transform normalisation was then applied to these values. The operation is described in Equation 1, and the vectors for the modified datasets are plotted in the loading plot below (Figure 5-23), which shows the strong correlation the variables have with one another.

$$\log\left(\frac{\frac{10^6}{10^6 - [Ca]}}{[Fe]}\right) \times [element]$$

Equation 5-1

Matrix scatter plots were subsequently drawn using this analysed data, which included all data points to preclude inaccurate inferences from these results. The aims of these observations were therefore to (i) assess the possibility of group discernment by mere visual observation of the graphs, (ii) to recognize those variables that could potentially distinguish between these sources, and (iii) to identify whether there were any other interesting correlations that could provide further insight to the character of these geological groups and potentially help differentiation.

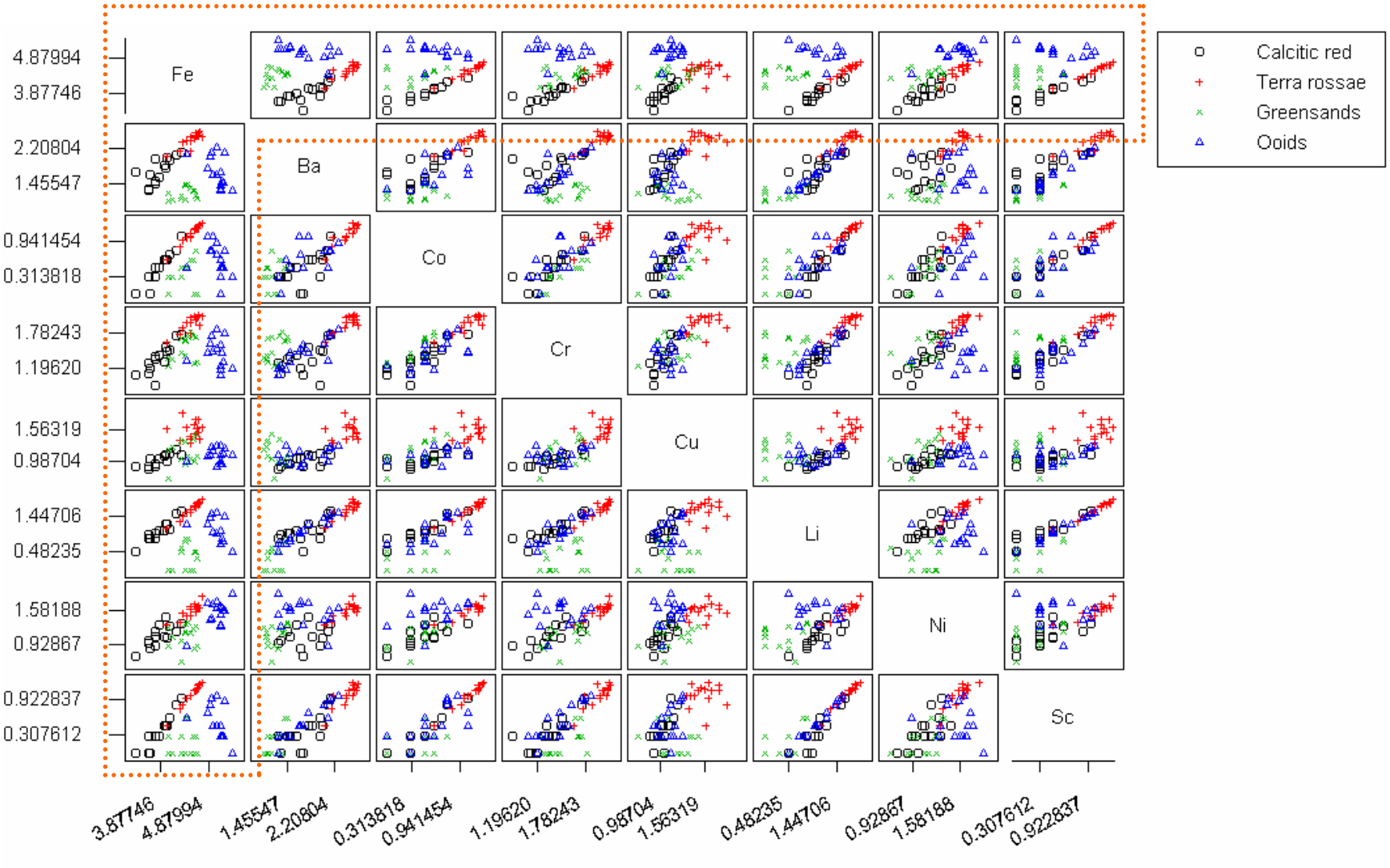

Figure 5-22. Log_{10} normalised data of minor elements (1st set) plotted to show the relationship exhibited with Fe (highlighted)

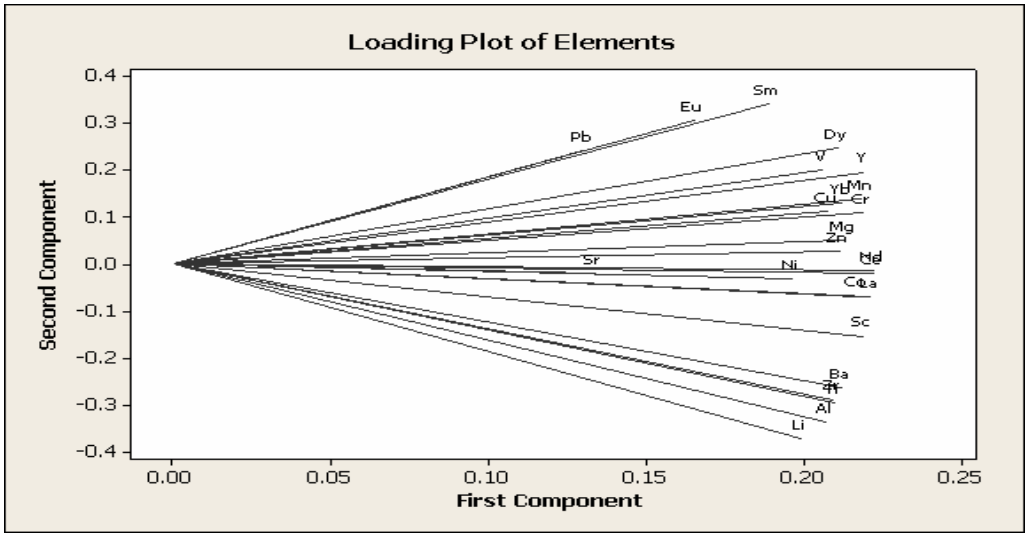

Figure 5-23. Loading plot, showing a strong covariance between the variables in the analysed dataset (components established using Minitab 15)

On observation of these matrix plots, the first prominent aspect was the clustering between the Calcitic reds and the Terra rossae groups in all plot comparisons between major, minor and rare earth variables, making them difficult to differentiate when compared to each other on a scale that included the other two geological groups (Figure 5-24).

Positive correlation trends were remarkably distinct in the vast majority of the graphs between all the geological groups (also shown in the loading plot above), although a broader scatter was exhibited in plots of Na, P, Sr and Pb, probably as a result of the effects of pollution. It was also evident that the distinction between the three groups was more pronounced in certain scatter plots than in others. This was observed in a number of graphs between major elements, particularly those between Al and Mg, Al and Mn, Mn and Ti, and Ti and Mg; as well as between the minor elements, namely Ba and Cr, Cr and Li, Zr and V, and Zr and Y.

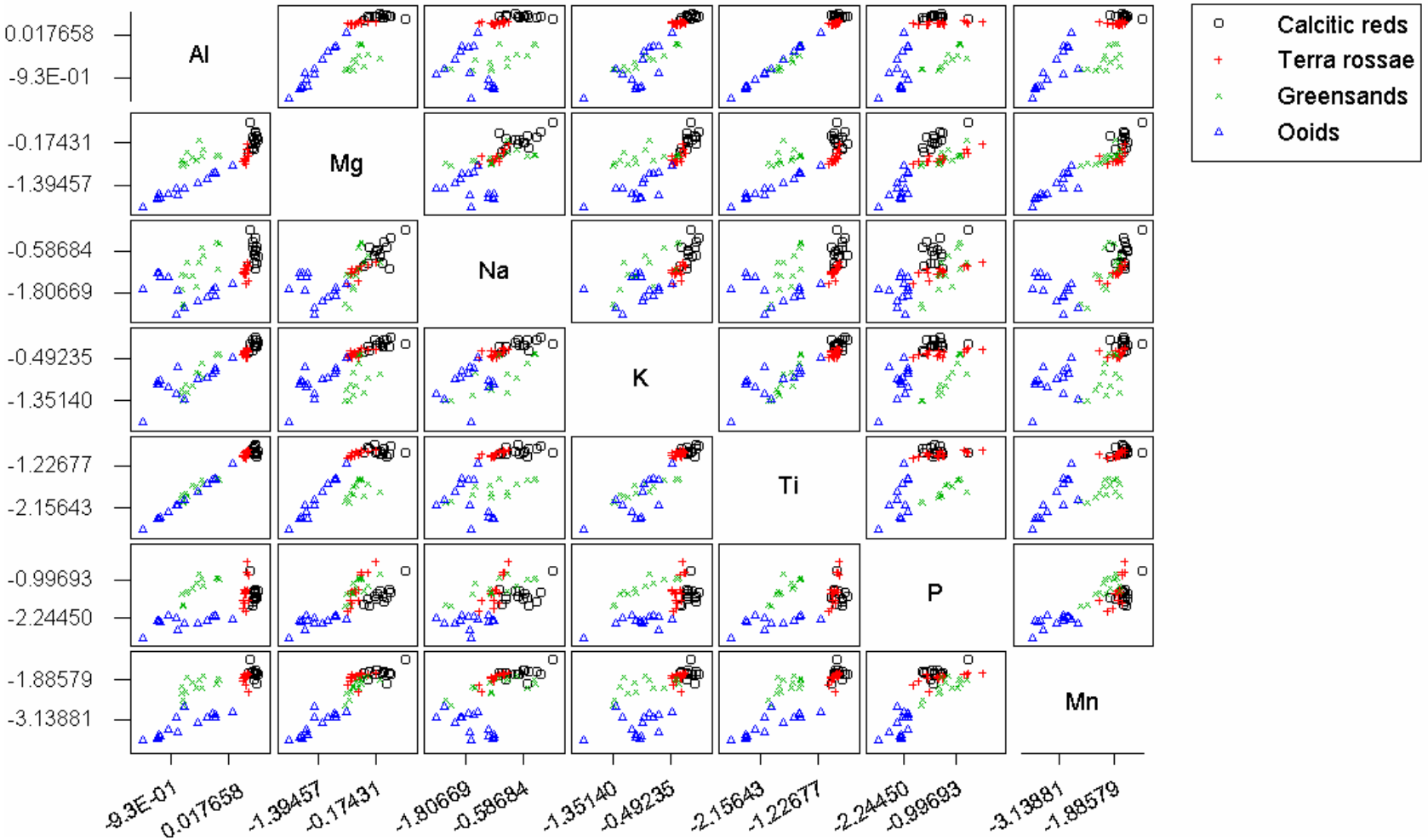

Figure 5-24. Comparison of major elements in different source groups after applying element transformation equation [$\log_{10}(\{10^6/10^6$-Ca}/Fe)*element] to each variable

No definite distinctions could be made from REE relative concentrations or ratios, as most of these trace elements appeared to exhibit strong, linear, positive correlations with one other, as is expected for REE amounts in materials forming in similar geological environments. A quotient trend, however, is apparent, with the Ooids having the highest REE ratio and the Calcitic reds-Terra rossae unanimously having the smallest ratio.

Further data examination: Correlation with Fe^{III}

As Fe is the key component of interest in ochre, an essential operation prior to cross comparing sets of data from source groups included observing which elements exhibited a distinctly direct dependence on the Fe concentration by showing a positive, ideally linear relationship when plotted against Fe. The correlation was assessed by applying the Pearson's correlation (r) statistical test between Fe and the selected variable (all the elements, individually) to determine the degree of proportionality and appropriate measure of the strength of the association between the two elements. This correlation coefficient is defined by the following equation,

$$r_{xy} = \frac{\Sigma(x_i - \bar{x})(y_i - \bar{y})}{(n-1)\sigma_x \sigma_y} \qquad \text{Equation 5-2}$$

where x_i and y_i are individual measurements; $\bar{x}$ and $\bar{y}$ are the sample means, and σx and σy are the standard deviation of the data sets (Rees, 2001: 213). Incident values were the raw data, and all values, including the correlations with the archaeological samples (which will be described later) are tabulated in Table 5-11 below.

Pearson's correlation coefficient is represented by the symbol *r* (rho), which ranges between -1 and 1, where -1 represents a perfect negative (inverse) correlation, 0 indicates no correlation, whereas 1 is the highest, perfect, positive correlation. Pearson's results were assessed for significance on a 95% confidence interval (α=0.05), and the results are given as the P-value. A P-value of less than 0.05 indicates that there is a statistically significant relationship between the two variables, and that the null hypothesis can be rejected in favour of the alternative hypothesis. The archaeological samples were also tested for comparative purposes.

The results indicated that while some geological groups, namely the Calcitic reds and the Terra rossae, showed clear correlation trends with Fe, correlations were much less distinct with the Ooids, and particularly even less so in the Greensands group. The definite correlations have been highlighted in the same table. Many scores were close to 0; therefore a clear determination of correlation was difficult. Those elements with a consistent negative Pearson's coefficient were eliminated from further statistical analysis.

Correlation	Calcitic reds		Terra rossae		Greensands		Ooids		MA (reds)		MA (yellows)		HYPD	
between Fe&:	r	P-value	r	P-value	r	P-value	r	P-value	r	P-value	r	P-value	r	P-value
Al	0.990	0.000	0.998	0.000	0.238	0.412	-0.371	0.174	-0.118	0.850	0.796	0.414	0.730	0.040
Mg	0.588	0.027	0.907	0.000	0.146	0.619	-0.269	0.332	-0.336	0.581	0.748	0.462	-0.435	0.281
Ca	-0.909	0.000	-0.955	0.000	-0.265	0.360	-0.505	0.055	-0.541	0.347	0.391	0.744	-0.840	0.009
Na	0.294	0.308	0.582	0.023	-0.159	0.586	0.536	0.039	-0.524	0.365	0.803	0.406	0.628	0.096
K	0.927	0.000	0.932	0.000	0.081	0.784	0.051	0.857	-0.138	0.825	0.686	0.519	0.715	0.046
Ti	0.966	0.000	0.973	0.000	0.350	0.220	-0.380	0.162	-0.249	0.686	0.929	0.241	0.408	0.315
P	0.448	0.109	-0.691	0.004	-0.038	0.896	0.275	0.322	-0.677	0.209	-0.756	0.454	0.409	0.314
Mn	0.908	0.000	0.714	0.003	-0.131	0.656	-0.199	0.477	0.770	0.128	-0.179	0.886	-0.488	0.220
Ba	0.846	0.000	0.821	0.000	0.210	0.471	-0.455	0.088	0.948	0.014	0.731	0.478	-0.381	0.352
Co	0.959	0.000	0.981	0.000	0.151	0.605	-0.435	0.105	0.855	0.065	0.063	0.960	-0.279	0.504
Cr	0.938	0.000	0.793	0.000	0.304	0.290	-0.178	0.524	-0.295	0.630	0.846	0.358	-0.180	0.670
Cu	0.804	0.001	0.030	0.915	0.244	0.400	0.078	0.781	-0.159	0.798	0.720	0.488	-0.483	0.226
Li	0.957	0.000	0.972	0.000	0.144	0.624	-0.423	0.116	-0.847	0.070	0.998	0.040	0.769	0.026
Ni	0.607	0.021	0.841	0.000	0.065	0.825	0.588	0.021	0.801	0.103	0.941	0.219	-0.229	0.586
Sc	0.972	0.000	0.992	0.000	0.066	0.822	-0.385	0.157	-0.083	0.895	0.998	0.040	0.753	0.031
Sr	-0.010	0.972	-0.863	0.000	-0.327	0.254	-0.157	0.576	0.977	0.004	0.647	0.552	-0.390	0.340
V	0.979	0.000	0.981	0.000	0.266	0.358	-0.156	0.579	0.781	0.119	0.980	0.128	0.115	0.787
Y	0.885	0.000	0.655	0.008	-0.074	0.803	-0.191	0.495	-0.853	0.066	0.941	0.219	0.858	0.006
Zn	0.654	0.011	-0.063	0.823	0.109	0.712	0.047	0.867	0.477	0.416	-0.930	0.239	0.523	0.184
Zr	0.934	0.000	0.953	0.000	0.570	0.033	-0.255	0.359	0.312	0.609	0.805	0.404	0.215	0.609
Pb	0.804	0.001	-0.291	0.293	0.166	0.571	0.103	0.716	0.921	0.026	-0.825	0.382	-0.553	0.155
La	0.878	0.000	0.929	0.000	0.174	0.552	-0.314	0.255	0.246	0.690	0.998	0.040	-0.105	0.012
Ce	0.896	0.000	0.944	0.000	-0.017	0.954	-0.435	0.105	-0.389	0.517	0.554	0.627	0.831	0.011
Nd	0.881	0.000	0.923	0.000	0.146	0.619	-0.350	0.201	0.119	0.848	0.998	0.040	0.837	0.010
Sm	0.888	0.000	0.894	0.000	0.235	0.420	0.788	0.001	/	/	-0.022	0.986	0.884	0.004
Eu	0.903	0.000	0.742	0.002	0.121	0.680	0.939	0.000	/	/	0.966	0.167	0.481	0.228
Dy	0.898	0.000	0.765	0.001	-0.068	0.817	0.443	0.098	-0.856	0.064	0.998	0.040	0.857	0.007
Yb	0.870	0.000	0.825	0.000	0.145	0.621	0.820	0.000	0.953	0.012	0.950	0.202	0.848	0.008

Table 5-11. Pearson's correlation coefficient values: r, and their respective P-values or the significance level

Various elements are known to substitute for Fe in ochres; and the tests and plots above show which variables were likely to have experienced this substitution within the samples analysed in this study. These are summarised in the table below:

Elements	Pearson's tests	Literature	Graphs
Major elements	Al, Mg, K, Ti, Mn,	Al, Ti, Mn	Al, Mg, Ti, Mn
Minor elements	Ba, Co, Cr, Cu, Li, Ni, Sc, V, Zr, Pb	Co, Cr, Cu, Ni, V, Sc, Zn, Pb	Ba, Cr, Cu, Li, Zr, V, Y
REE	All	All	/

Table 5-12. Comparison between the elements exhibiting a positive correlation with Fe from the Pearson's results; and elements known to substitute for Fe^{III} from literature sources (Cornell and Schwertmann, 2003: 47; Dawood, El-Naby et al., 2004; Wells, Fitzpatrick et al., 2006), as well as the potentially discriminating variables obtained from the [$\log_{10}(\{10^6/10^6$-Ca}/Fe)*element] graphs.

The elements therefore expected to co-vary in relation to Fe^{III} and potentially differentiate between the groups were plots of Al, Ti, Mn, Cr, Cu and V. Other possible variables also included K, Ni, Li, Zr and Zn. Discrimination by means of REEs was debatable, although links between these trace elements would indicate geological associations. Sc and Pb were likely to have been pollutant-associated elements, therefore trends within these variables were questionable and these elements were eliminated from further statistical tests along with the rest of the 'unrelated' variables.

Hierarchical cluster analysis using the agglomerative method was used to classify the variables on the basis of data similarity. The method in this study was set on a single linkage cluster algorithm, which assesses the two most similar samples in the data matrix based on the Euclidian distance between data points. Consequently, individuals that linked together within a single group in a cluster were expected to be most similar

and/or exhibit a comparable relationship. All the samples were automatically grouped together and linked through a dendrogram, therefore allowing for a direct visualisation of how the variables related to each other by their clustering. Although it is not recommended that the validity of these groupings be established by this statistical representation alone, this method identifies potentially inter-related variables, and was actually used to further confirm hypotheses of similarities discussed above between variables and observations within the groups (Everitt, Dunn et al., 1991: 67, 102).

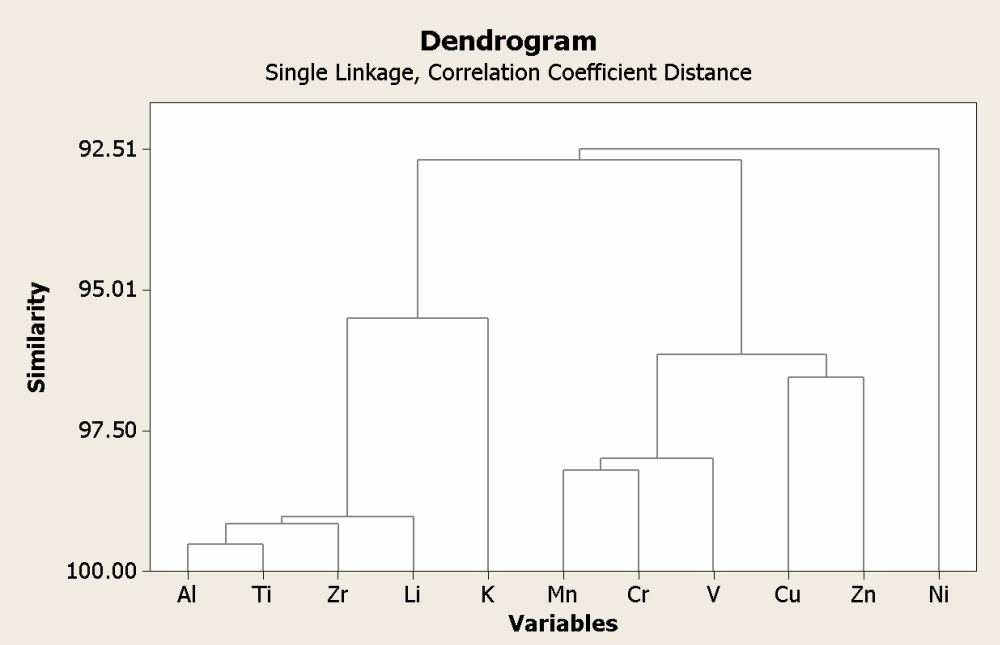

Figure 5-25. Dendrogram showing the hierarchical clustering between the selected variables off all geological observations (program used: Minitab 15)

It would appear that, in the dendrogram of the selected potential inter-related variables Al, K, Ti, Mn, Cr, Cu, Li, Ni, V and Zn, for example, Al and Ti were co-related for all observations, yet it was debatable well how well K and Ni integrated into these variable groups. The dendrogram, however, was suggestive of two main element divisions: Al, Ti, Zr, Li (variable set A) and Mn, Cr, V, Cu and Zn (variable set B).

Hierarchical clusters were subsequently used to analyse whether the selected variables could be used to identify the different source groups. Various clusters were attempted, using a varying number of variables to test whether any distinction between groups was coincidental or actually related to those elements substituting for Fe. Dendrograms were therefore charted using Al, Ti, Zr, Li, Mn, Cr, V, Cu, Zn, La, Ce, Nd and Yb (13 variables), Al, Ti, Zr, Li, Mn, Cr, V, Cu, Zn (no REE: 9 variables) and Al, Ti, Mn, Cr, Cu, V and Zr (7 variables). The first 'observations-based' cluster analysis (Figure 5-26 below) is an example of the 9-variable dendrogram, and included all the *geological* samples.

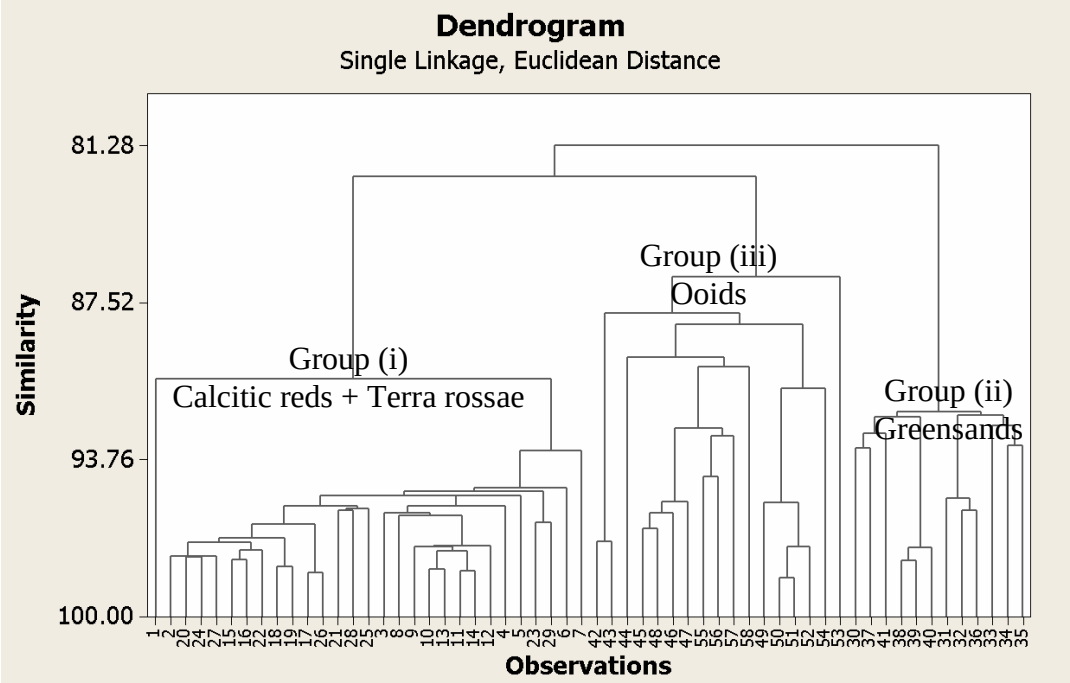

Figure 5-26. A hierarchical cluster showing the algorithm-based division of the *geological* samples into groups based on the correlation between the values of the 9 chosen variables. For a key to the observation numbers (x-axis) refer to Table 5-13.

These cluster analyses indicated that, based on the 13, 9 and 7 variables chosen for this test, three main groups were recognised, namely the Calcitic reds and the Terra rossae (CR-TR): Group (i), the Greensands: Group (ii) and the Ooids, shown as Group (iii) on

the dendrogram below. Two samples from the Greensands group, however, namely MG 1009 and 1100, were consistently associated with the Ooids in Group (iii) rather than with the rest of the Greensands. Notwithstanding this irregularity, the method generally corroborated the observations from the matrix plots of the geological groups described earlier, and also substantiated the validity of the chosen element variables. A key to the numerical connotation of the observations on the x-scale is given in Table 5-13.

Numbers	Groups
1 – 14	Calcitic reds (CR)
15 – 29	Terra rossae (TR)
30 – 43	Greensands (Gr)
44 – 58	Ooids (O)
59 – 63	MA (reds)/MA (r)
64 – 66	MA (yellows)/ MA (y)
67 – 74	HYPD
75 – 76	HYPB

Table 5-13. Key to the numbers in dendrograms in Figures 5-26 and 5-27

Archaeological data

A similar set of dendrograms using the same three sets of variables was used to assess how the archaeological groups fitted in with the geological groups and an example using the same 9-variable set (Al, Ti, Zr, Li, Mn, Cr, V, Cu, Zn) is shown in Figure 5-27 below. This statistical algorithm method effectively identified four overall groups within the sample lots, although certain sub-groups were also observed. Group (i) included the HYPD and the HYPB samples, which fitted in with the Calcitic reds and the Terra rossae geological sample sets; Group (ii) consisted of the Greensands; Group (iii) primarily comprised the Ooids and all the red MA archaeological ochres; whereas Group (iv) indicated that the yellow MA ochres, unlike all the other archaeological samples, did not fall into any particular source group but formed a separate cluster.

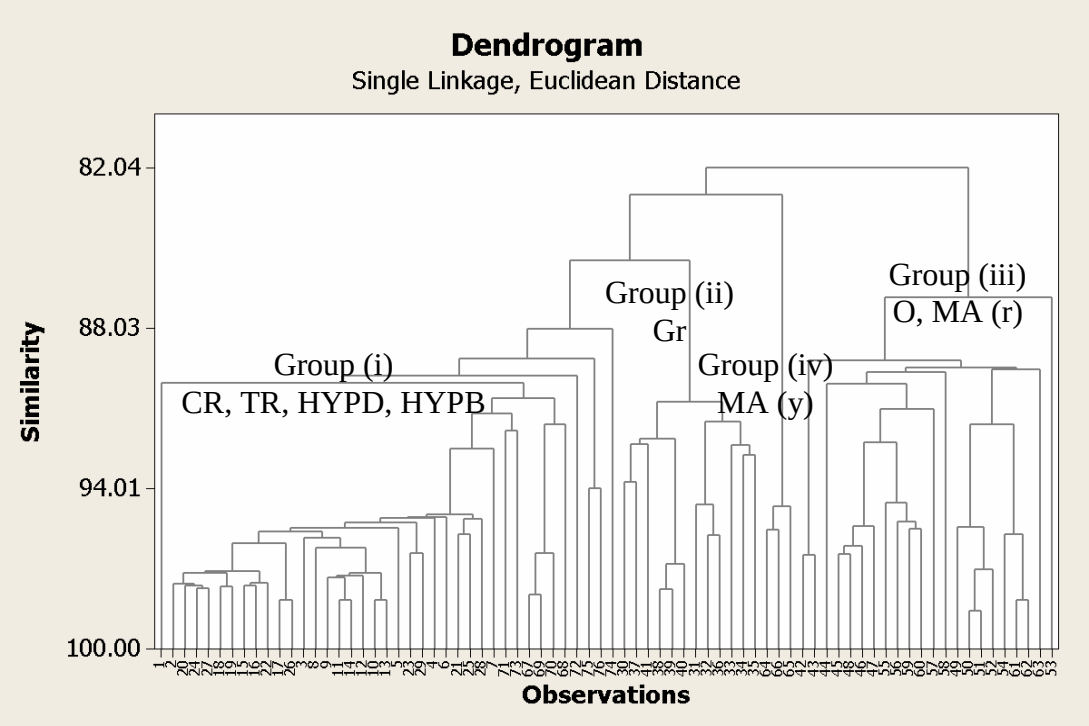

Figure 5-27. Hierarchical cluster of geological and archaeological samples based on correlations between the selected variables. A key to the observations is given in Table 5-13.

Group	Numbers	Group Identities
(i)	1 – 29 67 – 76	Calcitic reds (CR) and Terra rossae (TR) HYPDs and HYPBs
(ii)	30 - 41	Greensands (Gr)
(iii)	42 – 43 44 – 48, 55 – 60 49 – 54 61 – 63	Greensands MG 1009, 1100 Ooids (O), some MA (reds) Ooids Rest of the MA (reds)
(iv)	64 - 66	MA (yellows)

Table 5-14. An outline of the correlations and groups described in the dendrogram above

This hierarchical dendrogram therefore showed that the HYPD samples exhibited a distinct similarity between the variables in the CR-TR. The HYPB samples also exhibited similar trends to these three data sets but were a separate sub-group to these clusters and could therefore almost be considered as outliers to the group. This dendrogram additionally showed that while the Greensands and the MA (yellows) showed some correlation with the other sample sets (more so with the CR-TR in Group

[i] than with the Ooids in Group [iv]), trends between the data points were not as pronounced; hence they were statistically clustered as different groups. Finally, and probably most importantly, the red archaeological ochres (MA red) presented comparable trends in the data sets with the Ooids. This demonstrated a similarity in composition that potentially showed that the two sample sets might be linked, and that the Ooid group could be the likely source for these red MA samples.

To confirm these hypotheses, more matrix plots were compiled that included all major, minor and rare earth elements of the $\log_{10}$ transformed data ratios of all the geological and archaeological samples to assess these trends on a visual basis. Sample ellipses using a sample confidence ellipse at 75% confidence levels were also drawn around the groups to show the probability of the overlying of data and groups in two-dimensions, using Systat 13 software. Some examples of these tests are given on the following pages and in the Appendix III. The results of these tests are discussed in the following chapter.

Description of archaeological data, and comparison with the geological groups

An overview of the relative amounts of the major element to be found in each of the archaeological ochres is displayed in the histograms in Figure 5-28 with averages (including series line connectors) shown in Figure 5-29 below. Differences were noted between each set of samples, with more similarities being exhibited between the HYPDs and the HYPBs than between any other group. Key differences were observed between the elements P, Ca and Fe.

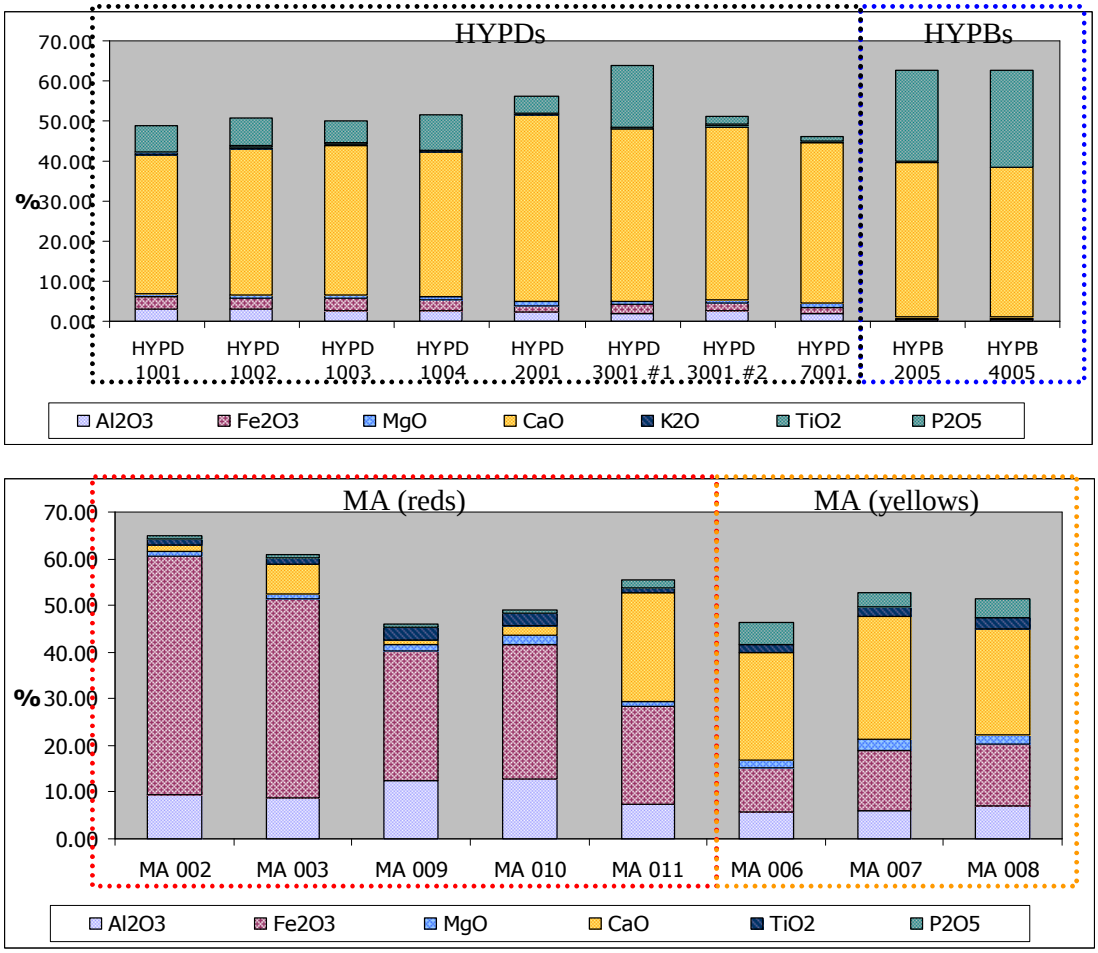

Figures 5-28 a, b. Histograms showing the relative abundances (weight %) of the major and some minor elements present in each sample

P_2O_5 levels were very high in the HYPBs and relatively (though less) high in the HYPDs. In the latter group levels varied from 1 wt-% in HYPD 7001 to 15 wt-% in HYPD 3001 #1. Some P_2O_5 was also observed in the MA (yellows), but averaged to less than 1 wt-% in the MA (reds). Amounts of calcium were similar in the HYPDs and the HYPBs (~39 wt-%) ; and were also considerably high in the MA yellows (24 wt-%). The calcium content of the MA reds differed somewhat between samples from 1 wt-% in MA 009 to 23% in MA 011. Fe_2O_3 (wt-%) also differed between samples, and the MA (reds) were clearly more iron-rich and displayed a wider degree of variation than any of the other archaeological samples.

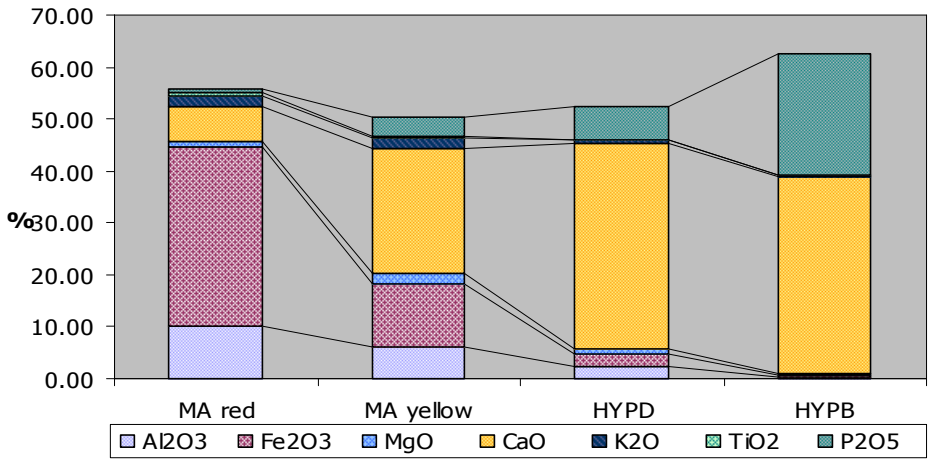

Figure 5-29. A histogram comparing the average quantities of (weight %) of the major and some minor elements present between sample groups: The graphs include series lines.

It was therefore possible to distinguish between archaeological sample groups through evaluation of these histograms: while CaO and P_2O_5 predominated in both HYPDs and HYPBs, analysis showed that the HYPDs contained higher quantities of iron-rich material. The MA samples had more Fe_2O_3 in comparison with the other samples, with the highest occurrence detected in the MA (reds). These MAs appeared to have similar % ratios of these selected oxides, although the yellow samples had much larger amounts of calcium and phosphorous oxides present.

Differences were evaluated by comparing scatter plots (Figure 5-30): here archaeological data has been plotted with geological data for comparative purposes. All archaeological groups formed tight clusters and/or exhibited similar element ratios, the majority of which correlated with certain geological groups, as was observed in the statistical tests, and will be discussed later. Element plots also confirmed differences between these four archaeological groups. Similar trends between certain elements as have already been observed in the geological matrix plots: these were therefore also noted in these archaeological samples between Al and Ti/ Mg/K, Mg and Na/Ti.

Results showed that: The Hypogeum archaeological samples correlated with the aforementioned CR-TR groups. Relationships experienced between elements in these geological groups were therefore reflected in these deposit samples from Hal-Saflieni, and examples of these relationships can be observed in the matrix plots in Figure 5-33, 5-35, 5-36, and in the scatter plot in Figure 5-31a. Noted differences between these archaeological and geological samples included slightly lower concentrations of both the major and the minor elements in the HYPD samples, and, as was also observed above, high levels of phosphorous, which averaged at 27374 ppm: almost 16 times greater than the average phosphorous levels in the Terra rossae (Figure 5-30a).

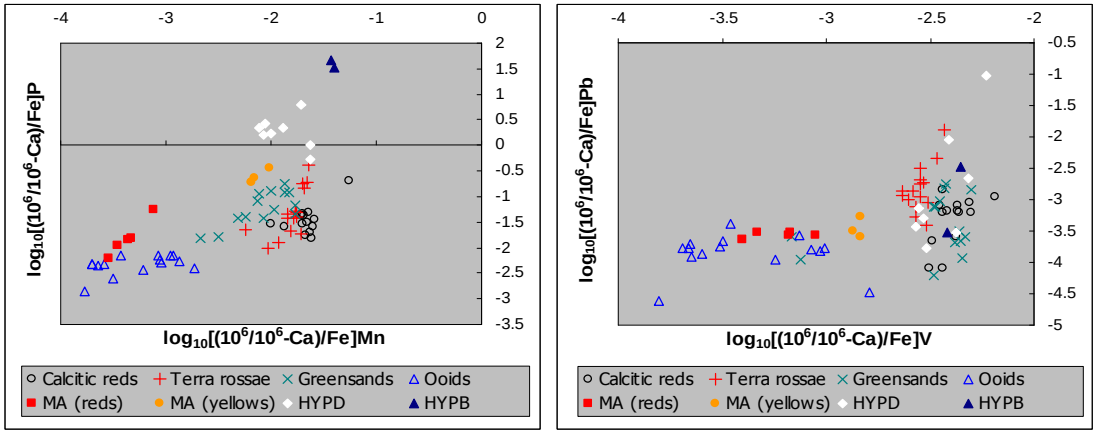

Figures 5-30 a, b. (a) showing high concentration of P in the HYPD and HYPB samples (b) example of correlation between groups, showing high Pb value in HYPD 7001

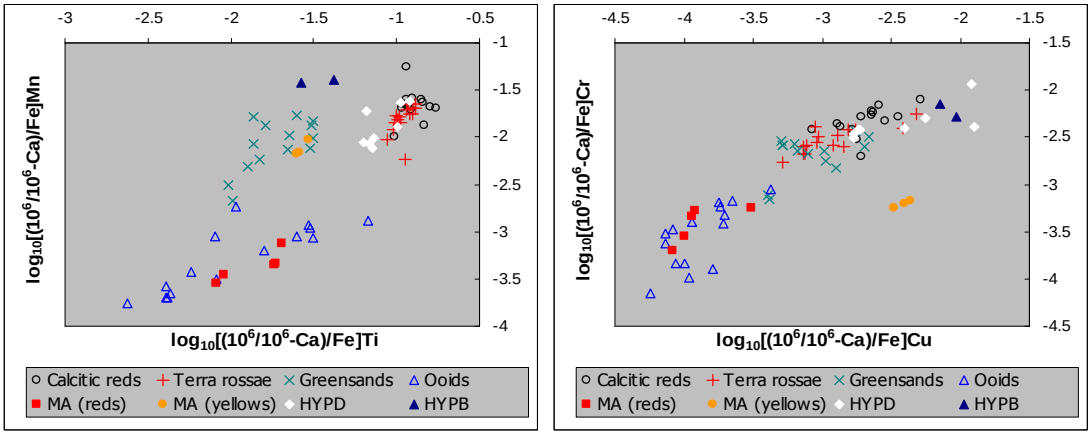

Figures 5-31 a, b. (a) similarities between the MA (yellows) and the Greensands, (b) MA (yellows) as obvious outliers

The ratio of Zr to the other elements also differed in relation to the CR-TR groups: points were more scattered and had lower values in the archaeological set. Certain HYPD samples also had higher concentrations of particular elements in comparison with the rest of the HYPD sample group. HYPD 3001 #1, for example, had much higher amounts of several minor elements, particularly of Ni (407 ppm in comparison to the average of 50 ppm). HYPD 7001 had a particularly high value of Pb (Figure 5-30b). These elevated concentrations of P and Ni were also seen in the HYPB samples, which also exhibited high amounts of Sr and Zn. The HYPB samples were somewhat different in composition, but more related to this CR-TR geological group than to any other.

The MA yellows were dissimilar to the other archaeological ochres. They additionally did not correspond well with any geological sample group, although they did exhibit similarities with the Greensands (Figure 5-31a). Trends were observed between several major element plots, such as Al vs. Mn, Mg vs. Ti, Mn vs. Ti. The associations between most of the minor elements, however, were dissimilar. The MA (yellow) Cr vs. Cu plot, for example (Figure 5-31b), was very different to the other samples, as were the plots between Cr vs. Li, Ni vs. Cu, V vs. Zr.

Although the MA reds had the largest degree of variation between major elements of the archaeological samples, data analysis of scatter plots not only showed that all MA reds exhibited similar trends, though MA 002 and MA 003 appeared to correlate together more, and MA 009–MA 011 formed a tighter cluster together. MA 002 and

MA 003 had higher concentrations of Fe, and several other elements, as shown in Table 5-15 below:

Element											
Higher	Al	Fe	Ti	Ba	Co	Cr	Ni	Sr	V	Zr	Pb
Lower	Mg	Mg	Ca	Na	K	P	Mn	Cu	Y	Zn	

Table 5-15. Elements more (higher) and less (lower) abundant in MA red samples 002 and 003; and vice versa for samples MA 009 – 011

Furthermore, the element plots of these archaeological samples almost invariably indicated a correlation with the Ooid geological group. This was exhibited in the vast majority of the scatter plots (Figures 5-34, 5-35), apart from those graphs with the variable Ba. This discrepancy was more distinct between this element and Cr (Figure 5-32b), Cu, Li and Sc. The variable ratios between the MA reds and the Ooids are given in Table 5-16 below.

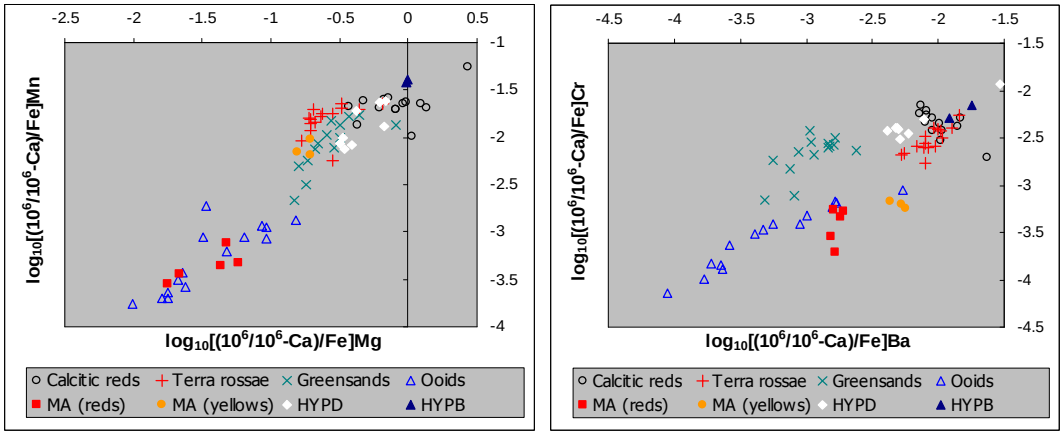

Figures 5-32a, b. (a) similarities between the MA (reds) and the Ooids, (b) shows the discrepancy between the Ba/Cr ratio in the MA reds

Average	Ba/Cr	Ba/Cu	Ba/Li	Ba/Sc
Ooids	0.92	0.84	0.83	0.73
MA 002, 003	0.77	0.69	0.67	0.61
MA 009 – 011	0.84	0.73	0.74	0.64

Table 5-16. A comparison between the Ba/selected variable ratios for the geological Ooids and the MA samples

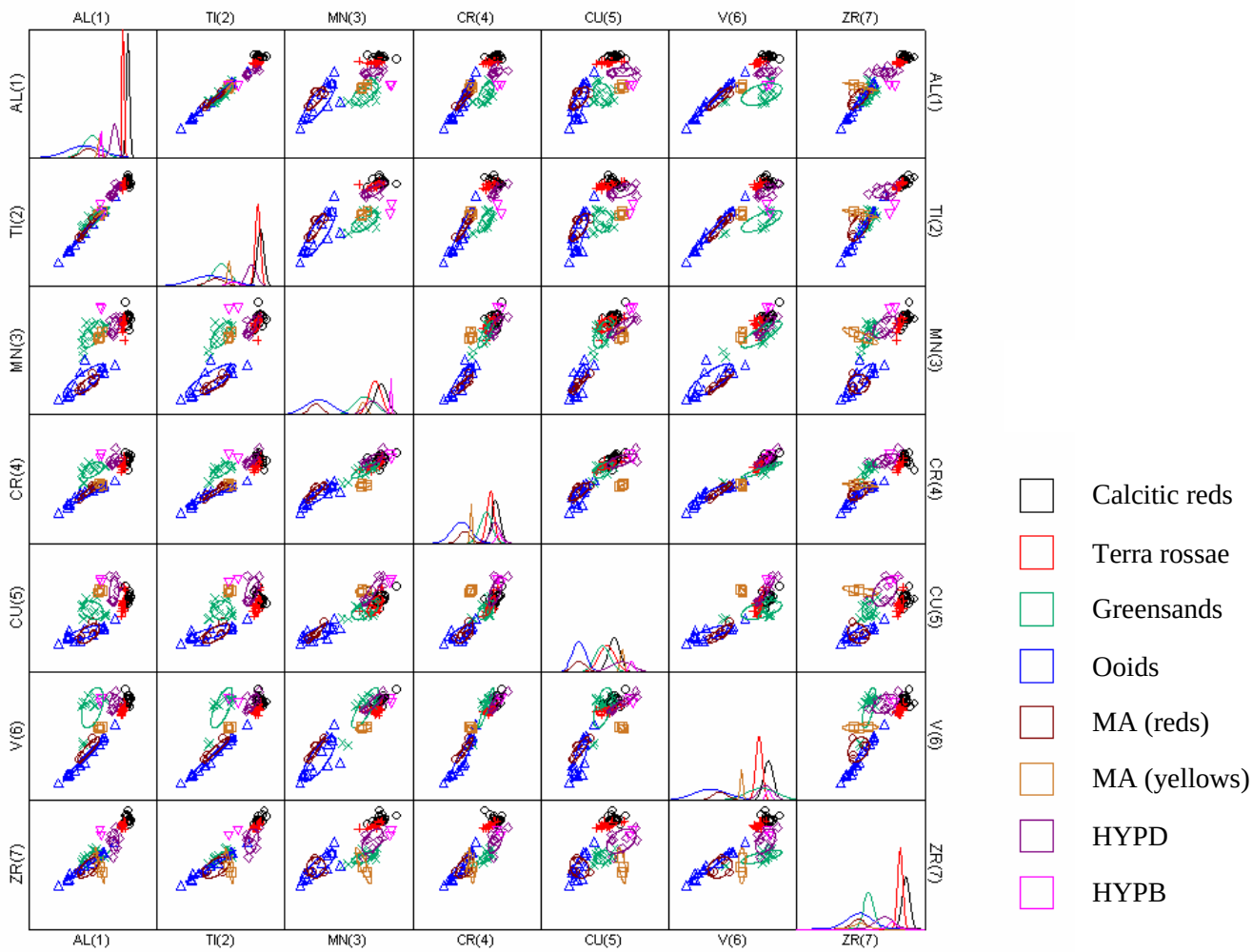

Figure 5-33. Sample ellipses around selected clusters of variables, where each colour is representative of a different geological/archaeological group. The graphs plotted within these matrix plots are normal distribution curves of each sample data series (Program used: Systat 13)

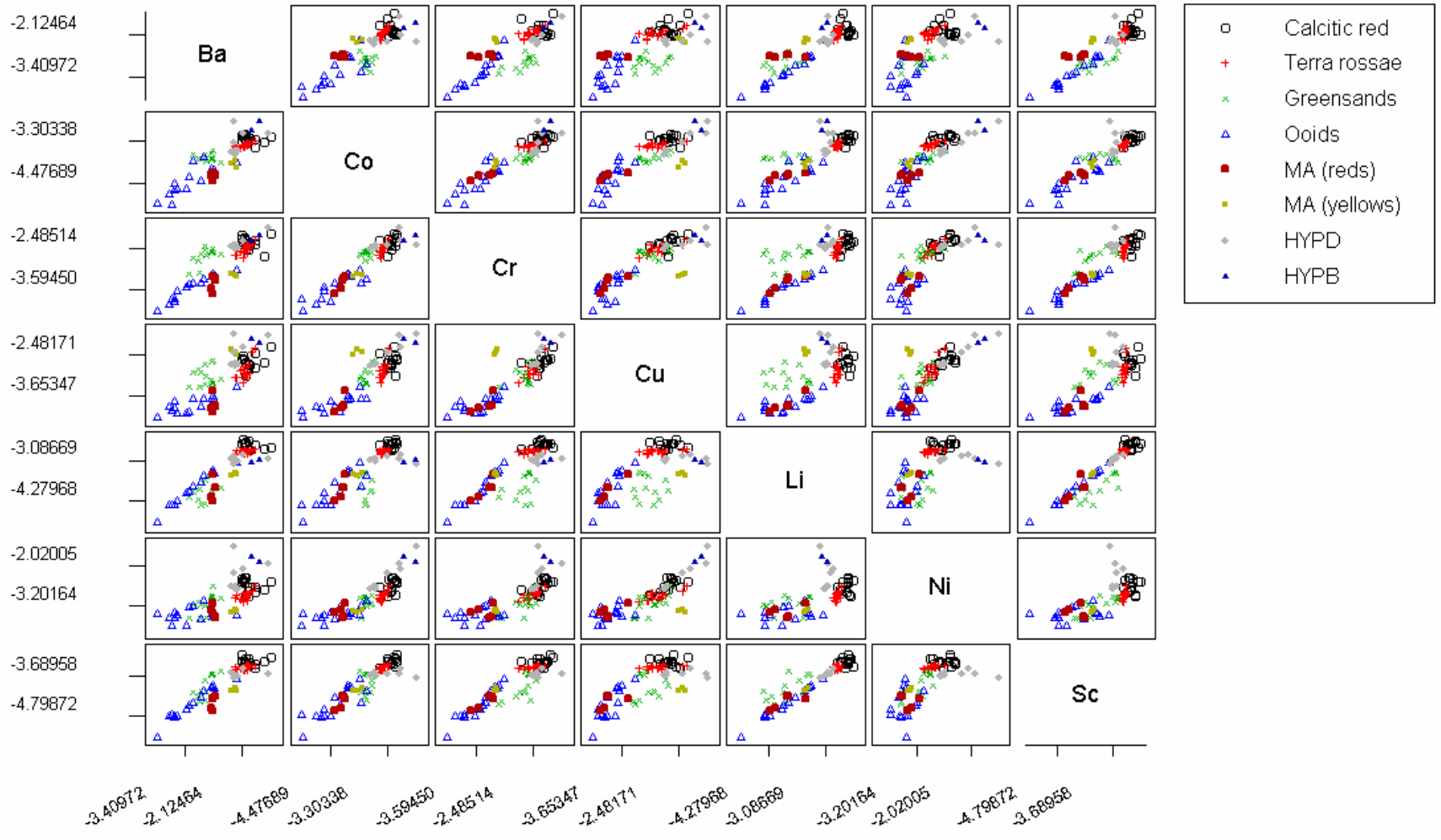

Figure 5-34. Matrix plot (using Minitab 13) comparing geological and archaeological data for some of the minor elements: All values here and in the ellipse plots above have been corrected using the transformation equation [$\log_{10}(\{10^6/10^6\text{-Ca}\}/\text{Fe})$*element]

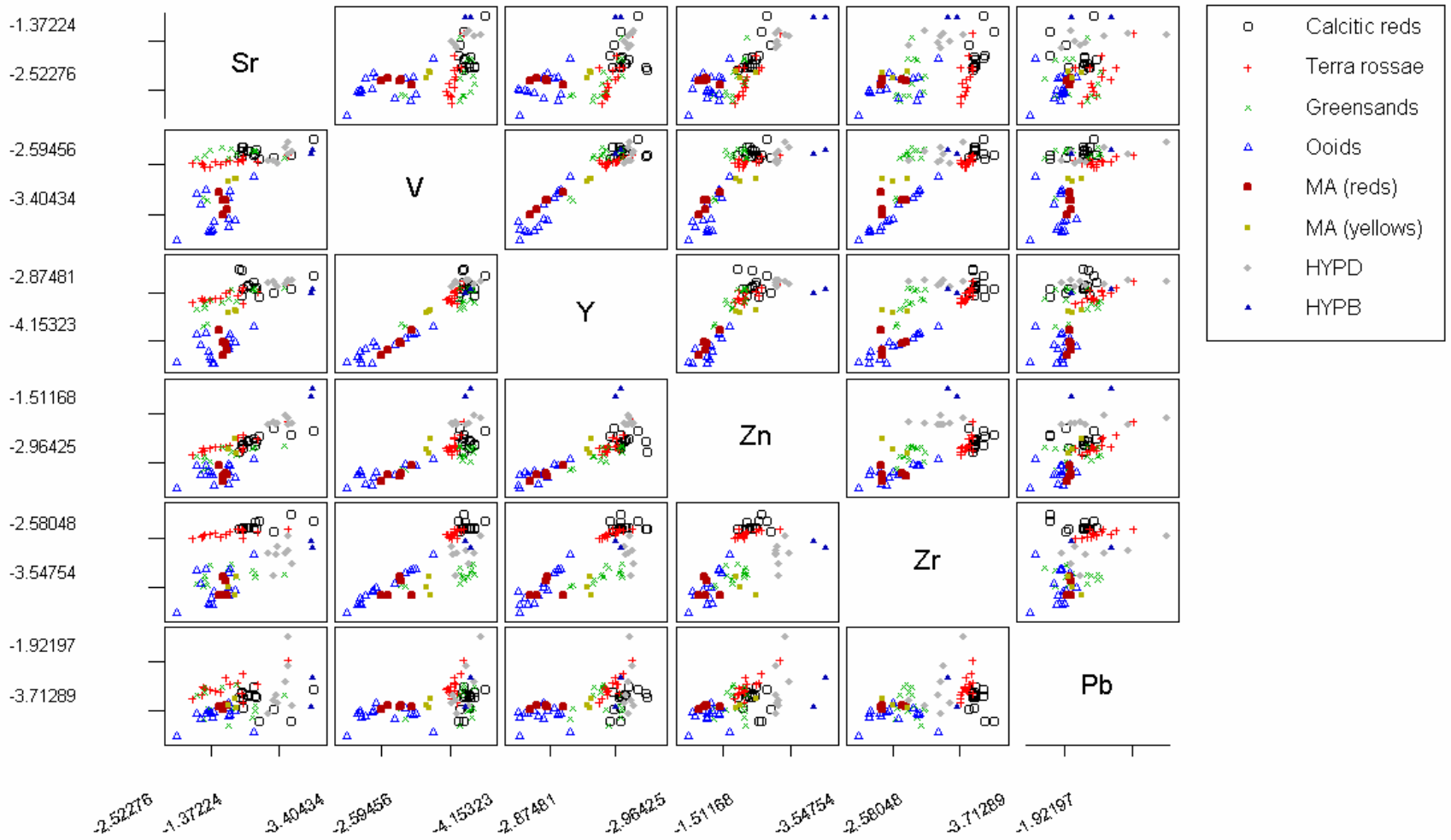

Figure 5-35. Matrix plots for the rest of the minor elements

Rare earth elements (REE)

The REE data is also known to provide an insight into the chemical behaviour of natural systems. Their abundance as well as their relative distribution in sedimentary rocks has been used to help define geologic environments and processes (Nakamura, 1974; Kato, Ohta et al., 1998; Dawood, El-Naby et al., 2004; Basta, Ryan et al., 2005; Marmolejo-Rodríguez, Prego et al., 2007). The distribution of REEs in nature corresponds to the Oddo - Harkins rule, where a plot of concentration against atomic number shows striking differences in abundance between neighbouring REEs. For comparative purposes concentrations are usually normalised to a shale standard for sedimentary and related rocks, which makes the y-scale more functional by removing apparent differences between neighbouring REEs and emphasises any relative fractionation of elements (Piper, 1974).

The plots of REE concentrations on a shale-normalised diagram are illustrated on the following page (Figures 5-36): these include examples of the geological and archaeological sample groups. Shale standard values were obtained from Piper (1974). These REEs resulted in a smooth correlation profile, with the exception of that for Eu. This was indicative of an obvious correlation between the geological and the archaeological samples; and the smooth pattern of REE concentrations was an additional assessment of analytical accuracy (Jarvis, 1989). It was, however, not possible to observe the Eu anomaly on the MA (red) plots and on those of the Calcitic red MG 1601 because the element (Eu) was not detected in these samples owing to instrument limitations relating to the high amount of Fe present[1].

[1] Personal communication from Dr Walsh (analyst)

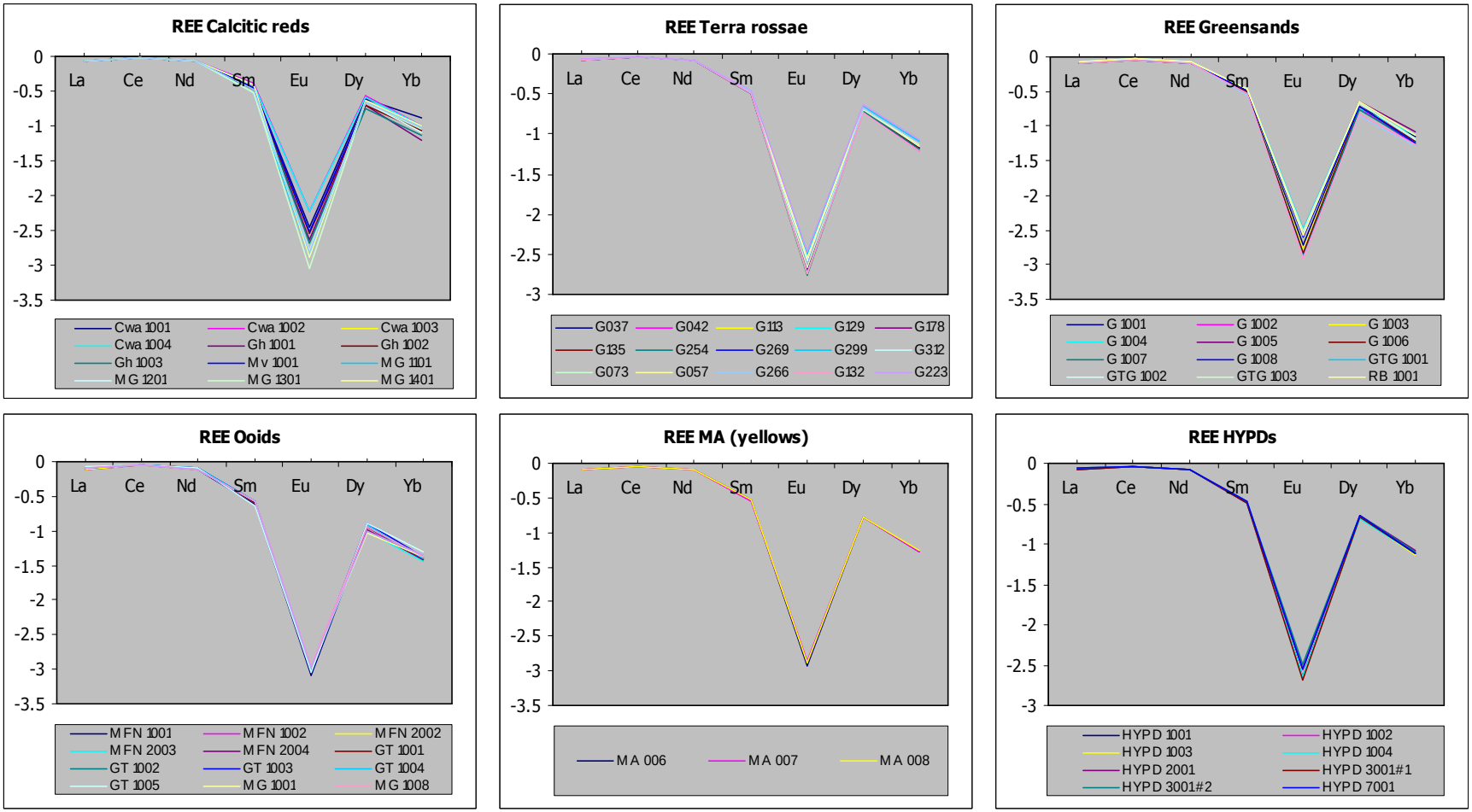

Figures 5-36a-f. Concentration plots of shale-normalised REE values of the geological and the archaeological samples

5.1.4. Scanning electron microscopy-energy dispersive X-ray spectroscopy (SEM-EDS) results

	%	%	%	%	%	%	%	%	%	%	%	%
sample	**Al_2O_3**	**Fe_2O_3**	**MgO**	**CaO**	**Na_2O**	**K_2O**	**TiO_2**	**P_2O_5**	**SiO_2**	**SO_3**	**Cl**	**Cr_2O_3**
MA 001	9.6	62	0.83	2.8	0.28	1.01	1.08	0.47	22	0.32	0.22	0.0
MA 004	0.6	0.34	0.17	31	0.16	0.34	0.00	0.00	1.3	59	0.25	6.5
MA 005	6.1	22	1.8	27	0.61	2.19	0.21	2.2	38	0.09	0.06	0.0

Table 5-17. Archaeological SEM-EDS data, conventionally displayed as an oxide in wt%

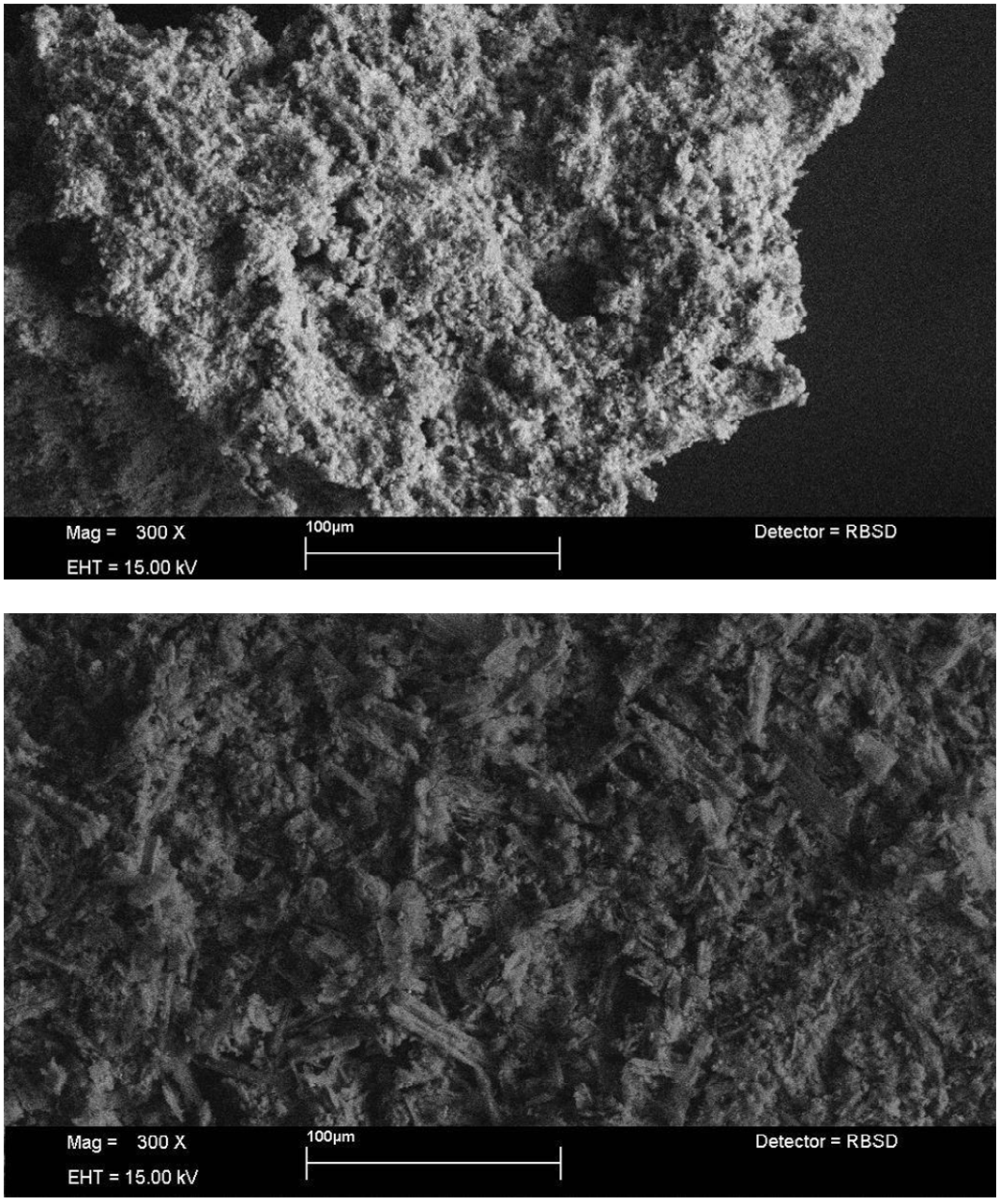

Figures 5-37a, b. SEM (BSE) images of MA 001 and MA 005

The SEM images did not give much information about the samples, except that MA 001 and MA 004 appeared to consist of minute grains of approximately 1.25 μm, whereas MA 005, the yellow ochre, included some fibrous-like material of varying size and lengths reaching up to 38 μm.

All calibration check results obtained off the standard materials (and off the samples analysed) indicated a good correlation of data with the results obtained from the more accurate ICP-AES technique. Any discrepancies were attributable to the auto-normalisation of all the values to 100, but these were not considered problematic as ratios were good and the element data of the archaeological samples compared well for the majority of the elements. Data was, however, still rounded off to 2 significant figures and given an average error of ~20%. The correlation between ICP-AES and SEM-EDS values is shown in the example given for Fe (ppm) below, and in Table 5-18, which lists the R^2-values and the gradient for each element.

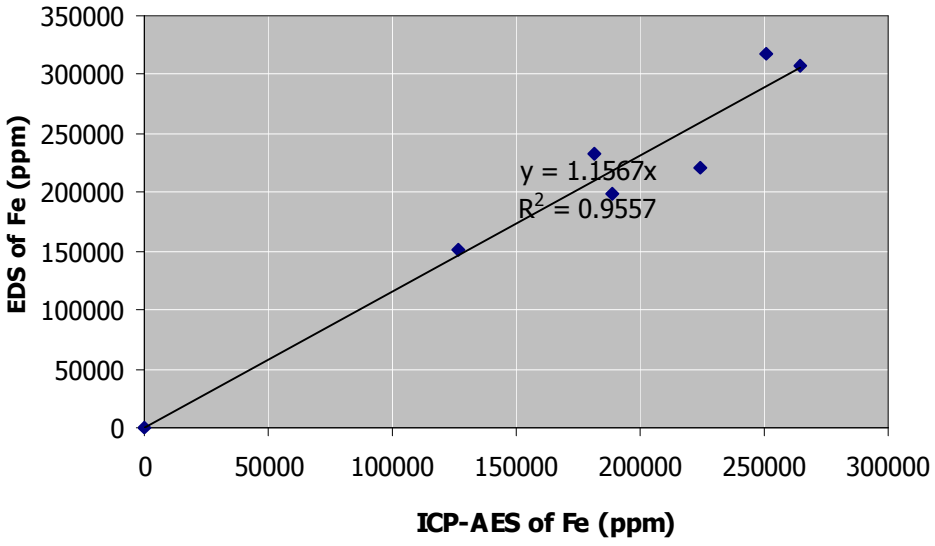

Figures 5-38. Correlation between SEM-EDS and ICP-AES in the measurement of Fe

Element	Al	Fe	Ca	Mg
R^2-value	0.9064	0.9557	0.8358	0.7123
Gradient	y = 1.0285x	y = 1.1567x	y = 0.8641x	y = 1.0526x
Element	**Na**	**K**	**Ti**	
R^2-value	0.8015	0.9851	0.2197	
Gradient	y = 0.5195x	y = 1.0236x	y = 1.2688x	

Table 5-18. R^2 values and gradients for some of the analysed variables

The three samples analysed using this technique have been included in the matrix plot in Figure 5-40 below. MA 001 was categorised as an MA (red), MA 005 was one of the yellow ochres whereas MA 004 was classed separately as an MA (orange).

Although the SEM-EDS was not as sensitive a method as ICP-AES, it imparted useful information by giving the concentrations (in oxide wt-%) of the major and of some of the minor elements when these were present in sufficient amounts. It also identified the presence and relative quantities of Si, S and Cl in the archaeological ochres, elements that were not measured by ICP-AES owing to the limitations of the method.

The SEM-EDS results therefore confirmed that the results for MA 001 and MA 005 fitted well with the ICP-AES data for the archaeological reds and yellows respectively; and therefore further corroborated the ICP-AES discussion pertaining to the material sources by increasing the number of data points. It also showed that Si was an important component in these materials, whereas S and Cl were only present in minor amounts.

This technique also showed that MA 004 appeared to consist of a mixture that predominated in Ca, S and Cr with only minor amounts of Fe (< 0.34%) present. Although it may be that some support had inadvertently been included in the sample

mixture as the orange pigment had to be scraped off the surface of the artefact; conclusions regarding the actual identity of the pigment were uncertain, particularly as chromium (III) oxide is green pigment, not an orange one. This sample undoubtedly required a further in-depth study, but establishing its identity was beyond the objective of this project.

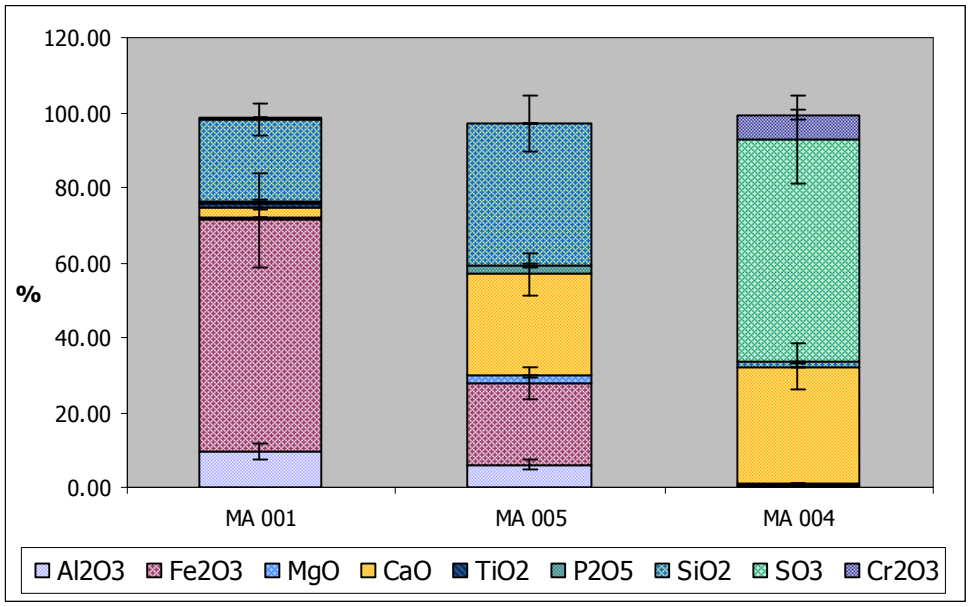

Figure 5-39. Weight % of some of the variables showing the differences in composition between samples. Error bars at 20%

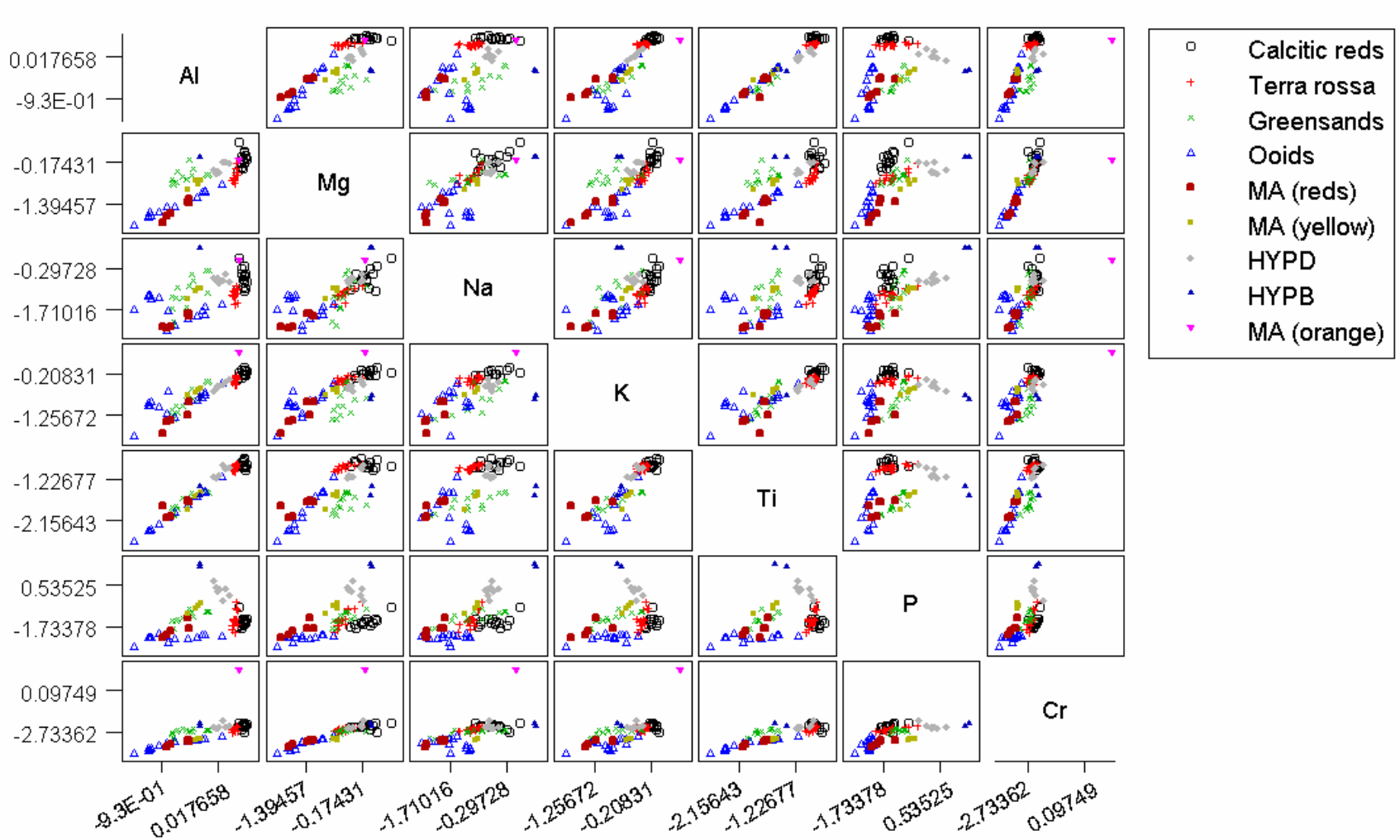

Figure 5-40. Matrix plots comparing geological and archaeological data from ICP-AES and SEM-EDS samples

5.1.5. X-ray fluorescence spectroscopy (XRF) data

Archaeological data

A considerably large number of readings were taken, and element variables assumed to be of significance included Fe, Ti, Mn, Zn and Zr. Variants taken into consideration included the type of support (limestone/clay/alabaster/shell), and the Neolithic site the artefacts were originally obtained from. Error bars varied per element and per reading, and average % errors are listed per element in Table 5-25. All readings copied here were assumed to be readings off the ochre, because the artefact background readings (XRF reading of an area on the object with no ochre on it) were subtracted from the ochre + support values.

	(ppm)	(ppm)	(ppm)	(ppm)	(ppm)		
Sample	**Fe**	**Ti**	**Mn**	**Zn**	**Zr**	**Source**	**Support**
HOC18R4	9300	1700	140	*	3	HYP	Wall
HOC18R5	15000	1900	790	9	1	HYP	Wall
HOC18R6	12000	*	960	7	11	HYP	Wall
HOC18R7	15000	*	*	*	5	HYP	Wall
HOC18R8	5800	*	130	*	1	HYP	Wall
HOC18R9	9500	*	*	*	3	HYP	Wall
HOC18R10	13000	2000	200	*	12	HYP	Wall
HOC18R11	6800	1600	*	1	3	HYP	Wall
HOC18R12	5500	1800	170	9	3	HYP	Wall
HOC18R13	28000	*	*	9	11	HYP	Wall
HOC18R14	11000	1900	240	6	10	HYP	Wall
HOC18R15	21000	2500	630	33	11	HYP	Wall
HOC18R16	12000	1900	340	6	19	HYP	Wall
HOC18R17	11000	2700	200	14	8	HYP	Wall
HOC18R18	24000	*	980	17	10	HYP	Wall
HOC18R19	15000	*	210	7	*	HYP	Wall
HOC18R22	3800	*	270	*	*	HYP	Wall
HOC18R23	2100	*	*	*	*	HYP	Wall
HOC18R24	16000	*	320	7	3	HYP	Wall
HOC18R25	13000	*	270	8	6	HYP	Wall
HOC18R26	11000	*	400	17	5	HYP	Wall
HOC18R27	13000	*	310	10	*	HYP	Wall
HOC18R28	25000	2200	2200	28	21	HYP	Wall

Table 5-19. Archaeological XRF data (HYP = Hal-Saflieni Hypogeum). * indicates that the element was present in concentrations below the detection limit of the instrument

	(ppm)	(ppm)	(ppm)	(ppm)	(ppm)		
Sample	**Fe**	**Ti**	**Mn**	**Zn**	**Zr**	**Source**	**Support**
HOC18R29	18000	*	780	28	2	HYP	Wall
HOC18R30	11000	*	210	23	11	HYP	Wall
HAO18R31	*	2000	180	16	*	HYP	Wall
HAO18R32	2200	*	*	20	*	HYP	Wall
HAO18R33	1100	*	260	32	*	HYP	Wall
HAO18R34	680	*	*	36	*	HYP	Wall
HAO18R35	*	*	*	41	*	HYP	Wall
HAO18R36	1200	2000	*	10	*	HYP	Wall
HAO18R37	*	*	*	17	*	HYP	Wall
HAO18R38	*	*	*	17	*	HYP	Wall
HAO18R39	*	*	*	12	*	HYP	Wall
HILC6R41	13000	2600	440	3	63	HYP	Wall
HILC6R42	20000	2200	210	2	51	HYP	Wall
HILC6R43	14000	*	700	3	53	HYP	Wall
HILC6R44	2800	1800	190	10	3	HYP	Wall
HILC6R45	2100	1400	*	2	1	HYP	Wall
HILC6R46	1600	*	110	*	*	HYP	Wall
HULC4R47	4800	*	180	22	5	HYP	Wall
HULC4R48	3600	1400	*	*	*	HYP	Wall
HULC4R49	3100	1600	*	3	8	HYP	Wall
HULC4R50	5600	*	*	6	*	HYP	Wall
HULC4R51	5100	*	*	*	17	HYP	Wall
HDRC20R53	5900	1700	*	9	6	HYP	Wall
HDRC20R54	520	1600	*	*	2	HYP	Wall
HDRC20R55	3300	*	1100	21	2	HYP	Wall
HDRC20R56	3700	*	*	*	4	HYP	Wall
HDRC20R57	2800	1700	*	*	*	HYP	Wall
HDRC20R58	1800	*	*	*	3	HYP	Wall
HDRC20R61	300	*	170	*	*	HYP	Wall
HDRC20R62	*	1500	*	*	*	HYP	Wall
HDRC20R63	2400	1800	*	*	3	HYP	Wall
HDRC20R64	2500	*	*	*	4	HYP	Wall
HDRC20R65	*	*	*	8	*	HYP	Wall
HDRC20R66	5000	1500	*	*	10	HYP	Wall
HDRC20R71	9600	1900	140	12	19	HYP	Wall
HDRC20R72	3600	*	400	*	1	HYP	Wall
HDRC20R74	*	1500	*	*	*	HYP	Wall
HDRC20R75	6100	*	200	7	*	HYP	Wall
HDRC20R76	4500	1600	*	*	6	HYP	Wall
HDRC20R77	6700	1800	*	*	4	HYP	Wall
HDRC20R78	2100	*	*	190	*	HYP	Wall
HDRC20R80	5200	1800	200	130	9	HYP	Wall
HDRC20R81	1800	*	*	220	10	HYP	Wall
HDRC20R82	5800	*	460	86	*	HYP	Wall
HDRC20R83	8800	*	*	2	7	HYP	Wall
HSAC23R84	9400	1800	200	2	20	HYP	Wall

Table 5-20. Archaeological XRF data (HYP=Hal Saflieni Hypogeum). * indicates that the element was present in concentrations below the detection limit of the instrument

	(ppm)	(ppm)	(ppm)	(ppm)	(ppm)		
Sample	**Fe**	**Ti**	**Mn**	**Zn**	**Zr**	**Source**	**Support**
HSAC23R85	5000	2200	360	1	7	HYP	Wall
HHoHC26R86	5600	*	*	11	48	HYP	Wall
HHoHC26R87	13800	1800	160	22	37	HYP	Wall
HHoHC26R90	3100	*	170	*	9	HYP	Wall
HHoHC26R91	6000	2600	300	13	10	HYP	Wall
HHoHC26R92	9000	*	260	*	8	HYP	Wall
HMHC26R93	4000	1600	200	*	7	HYP	Wall
HMHC26R94	460	*	*	*	*	HYP	Wall
HMHC26R95	7700	*	140	8	11	HYP	Wall
HMHC26R96	6000	1600	240	6	1	HYP	Wall
HMHC26R97	17000	2100	220	24	14	HYP	Wall
HMHC26R98	19000	2200	150	*	8	HYP	Wall
HMHC26R99	3100	*	*	*	6	HYP	Wall
HMHC26R100	3600	*	*	3	11	HYP	Wall
HMHC26R101	6400	1400	280	*	5	HYP	Wall
HWC17R106	5900	*	*	2	5	HYP	Wall
HWC17R107	630	*	*	*	*	HYP	Wall
HWC17R108	13000	*	*	*	*	HYP	Wall
HWC17R109	8300	*	*	*	8	HYP	Wall
HWC17R110	470	*	*	*	*	HYP	Wall
HWC17R111	1300	*	140	*	1	HYP	Wall
HWC17R112	6200	*	*	*	*	HYP	Wall
HWC17R113	6100	*	*	*	1	HYP	Wall
HLSR19	2300	1500	*	*	11	HYP	Stone
HLSR20	2100	*	*	*	24	HYP	Stone
HLSR21	3100	*	*	*	*	HYP	Stone
TPFR34	1400	450	130	32	*	TAR	Stone
TPFR35	1800	420	110	44	*	TAR	Stone
TPFR36	1600	700	*	21	*	TAR	Stone
TPFR37	830	*	140	8	*	TAR	Stone
TSPR40	2100	*	*	130	110	TAR	Stone
TSPR41	880	*	*	220	80	TAR	Stone
GPR70	5400	1600	110	17	*	GTA	Stone
GPR71	3700	630	*	*	*	GTA	Stone
XSCTSR95	23000	*	*	*	1	XSC	Stone
XSCTSR96	7900	*	*	*	*	XSC	Stone
XSCTSR97	4600	*	*	*	*	XSC	Stone
XSCTSR98	30000	830	*	*	*	XSC	Stone
XSCBR107	1700	*	*	*	*	XSC	Stone
XSCBR108	3100	*	*	*	*	XSC	Stone
SS1R27	14000	3100	12	31	17	SKB	Clay
SS1R29	7700	900	*	27	9	SKB	Clay
TCSR44	16000	2100	*	53	22	TAR	Clay
TCSR46	22000	1700	*	44	17	TAR	Clay
TCSR47	15000	2300	*	42	22	TAR	Clay
TCSR48	13000	230	160	55	10	TAR	Clay

Table 5-21. Archaeological XRF data (GTA = Ggantija temples, SKB = Skorba, TAR = Tarxien, XSC = Xaghra Stone Circle): * indicates that the element was present in concentrations below the detection limit of the instrument

	(ppm)	(ppm)	(ppm)	(ppm)	(ppm)		
Sample	**Fe**	**Ti**	**Mn**	**Zn**	**Zr**	**Source**	**Support**
HSLR2	13000	1300	46	9	25	HYP	Clay
HSLR3	8600	1500	*	76	14	HYP	Clay
HSLR4	6400	*	*	30	27	HYP	Clay
HSLR5	21000	2700	*	88	36	HYP	Clay
HSLR6	17000	2300	*	78	34	HYP	Clay
HSLR7	6900	530	*	54	11	HYP	Clay
HPS2R67	2200	*	*	82	14	HYP	Clay
HPS2R68	3300	*	*	82	8	HYP	Clay
HPS5R80	3700	680	260	10	3	HYP	Clay
HPS5R82	*	*	170	40	*	HYP	Clay
HPS6R2	*	*	390	*	*	HYP	Clay
HPS6R4	*	*	530	*	*	HYP	Clay
HPS6R5	*	*	210	*	*	HYP	Clay
HPS6R7	*	*	280	4	18	HYP	Clay
GPS5R113	52000	480	40	*	3	GTA	Clay
GPS5R114	46000	1000	*	*	2	GTA	Clay
GPS5R115	65000	1200	*	*	2	GTA	Clay
GPS5R116	31000	160	30	*	7	GTA	Clay
GPS6R120	51000	7200	240	60	75	GTA	Clay
GPS6R121	51700	6300	*	54	48	GTA	Clay
GPS6R122	62000	4200	*	46	34	GTA	Clay
GPS7R126	*	*	43	19	*	GTA	Clay
GPS7R127	2600	*	*	32	*	GTA	Clay
GPS7R128	*	*	*	19	*	GTA	Clay
XSCSPR133	23000	*	*	13	*	XSC	Clay
XSCSPR134	10000	1400	*	43	29	XSC	Clay
XSCOPR137	170000	*	*	*	*	XSC	Clay
XSCOPR138	180000	*	*	*	8	XSC	Clay
XSCOPR139	130000	*	*	*	*	XSC	Clay
SVPS1R29	20000	1000	150	30	49	STA V	Clay
SVPS1R30	52000	1100	210	180	25	STA V	Clay
SVPS2R32	1400	350	*	3	*	STA V	Clay
SVPS2R33	2100	120	*	5	*	STA V	Clay
SVPS2R34	300	*	14	10	*	STA V	Clay
SVPS2R35	7000	*	20	11	*	STA V	Clay
?GNBR109	1600	*	*	*	*	?GOZO	Clay
?GNBR112	4600	*	*	7	*	?GOZO	Clay
XSCB1R142	2400	*	*	34	*	XSC	Bone
XSCB2R145	27000	*	*	15	*	XSC	Bone
XSCB3R148	11000	1500	*	*	*	XSC	Bone
XSCB3R147	*	*	*	25	*	XSC	Bone
HAFGR25	3600	*	*	380	*	HYP	Alabaster
HAFGR26	1700	1800	*	140	*	HYP	Alabaster
HAFGR28	500	*	*	40	*	HYP	Alabaster
XSCS1R11	6800	*	*	*	*	XSC	Shell
XSCS1R12	3800	*	*	*	*	XSC	Shell

Table 5-22. Archaeological XRF data (STA V = Santa Verna, ?GOZO = unknown Neolithic site in Gozo): (* indicates that the element was present in concentrations below the detection limit of the instrument

	(ppm)	(ppm)	(ppm)	(ppm)	(ppm)		
Sample	**Fe**	**Ti**	**Mn**	**Zn**	**Zr**	**Source**	**Support**
XSCS2R14	2600	*	170	*	*	XSC	Shell
XSCS3R16	*	38	*	*	*	XSC	Shell
XSCS4R19	5300	*	*	250	20	XSC	Shell
XSCS4R20	6700	*	*	270	*	XSC	Shell
XSCS5R23	2300	*	*	*	*	XSC	Shell

Table 5-23 Archaeological XRF data

As has already been discussed, portable XRF was the only methodology available for the analysis of the Neolithic ochres remaining on the surfaces of objects *in situ* from which sampling was impossible for ethical reasons. As Ca was amongst the elements beyond the detection limits of the loaned XRF, all data was merely plotted as a $\log_{10}$ normalised ratio to Fe, with the transformation factor being $\log_{10}$(element/Fe). Data was compared on the basis of the original artefact location (excavation site/temple/burial ground) and of the support material. Both sets of data gave equally broad spreads, therefore results from the archaeological and geological datasets were plotted on the matrix plots on the basis of the support material (stone vs. clay vs. alabaster vs. shell) owing to the greater likelihood of error based on residual support signature (Table 5-25).

Although the values obtained from the reference materials correlated very well with the ICP-AES data (an example is given in Figure 5-41), the attempts to make this technique as non-invasive/non-destructive as possible on site appeared to have compromised the quality of the data. Lowest % error (Table 5-25) was also noted in the standards.

Element	Fe	Ti	Mn	Zn	Zr
R^2-value	0.983	0.8772	0.8937	0.9281	0.8217
Gradient	y = 0.8773x	y = 1.1776x	y = 0.7722x	y = 0.7875x	y = 1.9944x

Table 5-24. R^2 values and gradients for the analysed variables

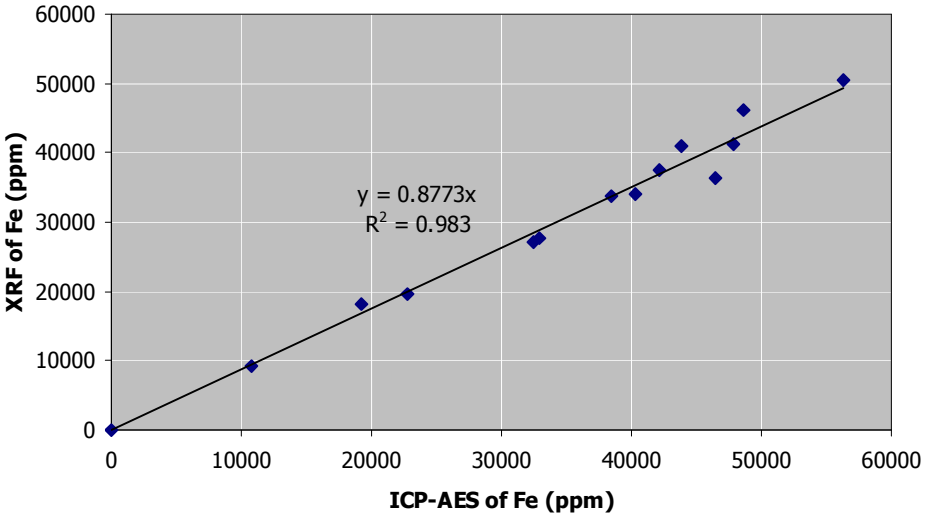

Figure 5-41. Correlation between XRF and ICP-AES in the measurement of Fe

	% error per element				
Ochre on:	**Fe**	**Ti**	**Mn**	**Zn**	**Zr**
Stone	2	26	15	13	16
Clay	1	14	16	8	4
Other	2	30	27	8	29
In standards	1	12	12	8	2

Table 5-25. % error calculated by averaging +/- error bars and values per element per support/group of materials

Errors affecting counts and values probably included artefact surface irregularities, the slight 5 mm distance kept between the spectrometer and the object to avert damage, and the relatively short acquisition times. All these factors undoubtedly contributed to the loss of emitted and reflected X-rays, and therefore affected the results output. Further probable inaccuracies included the assumptions taken when analysing datasets, such as subtracting a supposed consistent composition of the support, which was averaged from three readings, from the ochre plus support values.

Observation of matrix plots showed a wide spread of points although some correlation was observed. This included significant clustering of the stone-support readings towards a smaller element/Fe ratio that appeared to correspond to the Calcitic red and Terra rossa data points. The XRF of the ochre applied to the clay objects also appeared to correlate well with these two geological groups. The best trend was observed between the $\log_{10}$ ratios of Ti and Mn, whereas the largest scatter was experienced in plots between Zn and Zr.

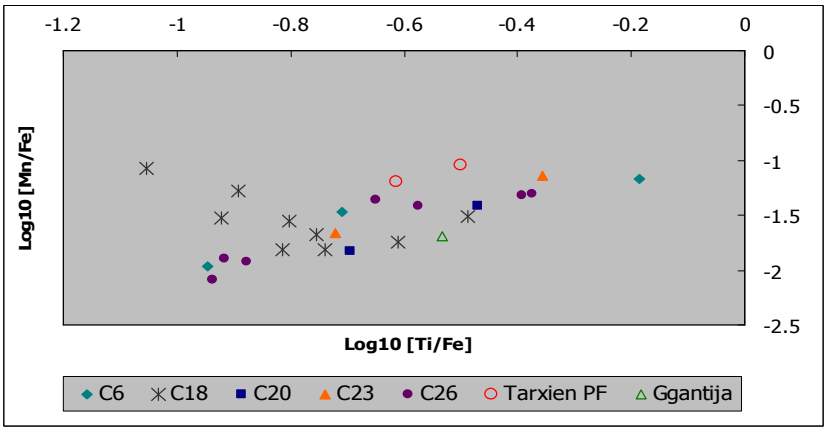

Figure 5-42. Example of a scatter plot within the datasets: C represents the chamber from which the readings were taken in the Hypogeum, PF are the phallic figures from Tarxien (TPFR34, 35), and Ggantija refers to some readings taken off ochre-doused pebbles found in Ggantija (GPR70). Support material: stone

The scatter plot above (Figure 5-42), for example, shows that variation between data from a particular site and support materials does not show any particular disparities and/or trends. The positive correlation between Mn and Ti is still apparent. Results, however, were inconclusive for this particular provenancing study and discussions have therefore been left open for further debate.

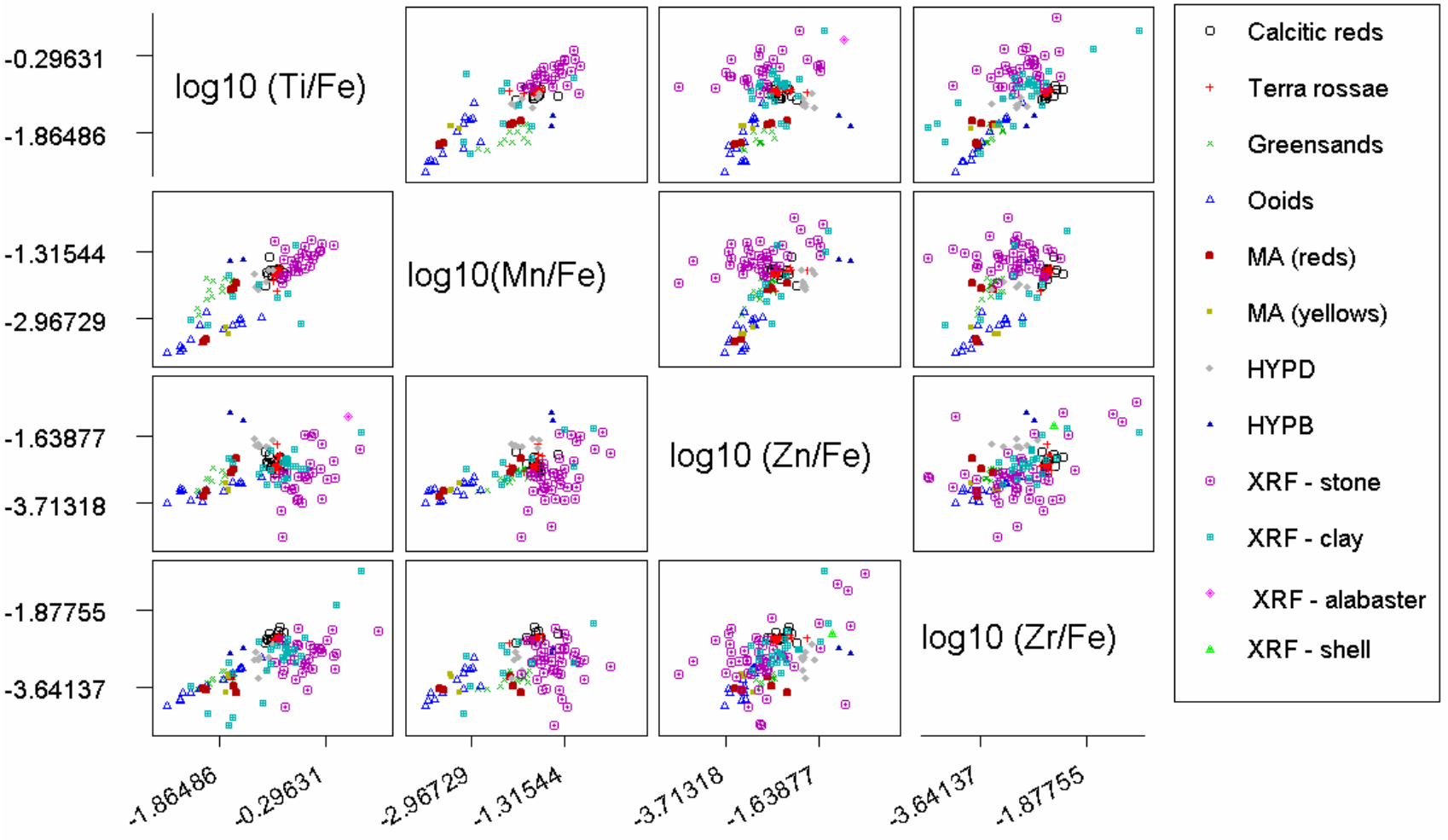

Figure 5-43. Matrix plots comparing geological and archaeological data for ICP-AES and XRF results

5.2. Comparative study: Amarna archaeological samples

5.2.1. Polarising light microscopy (PLM)

All the images reproduced below were chosen as representative photographs of the relevant Amarna archaeological samples, taken at a magnification of x400 under PPL, unless stated otherwise.

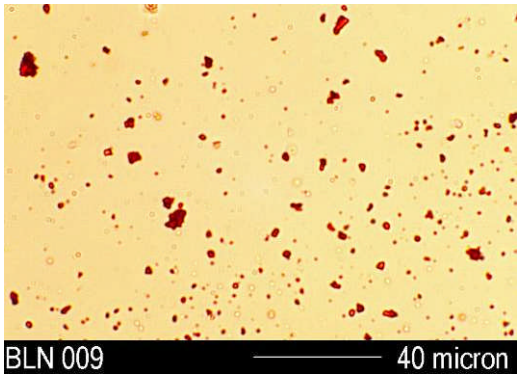

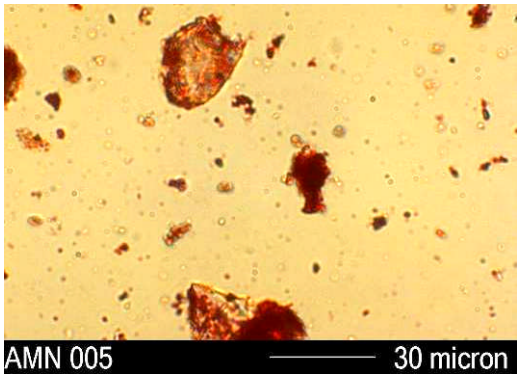

Figures 5-44a, b. Examples of red ochres: BLN 009 and AMN 005

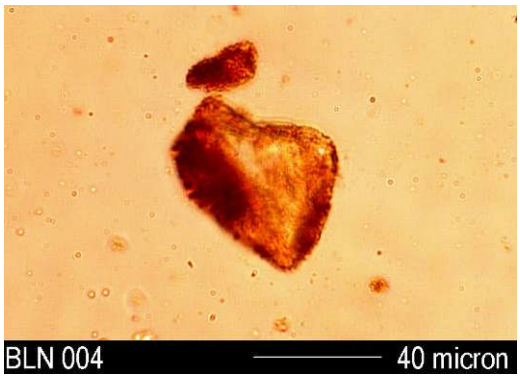

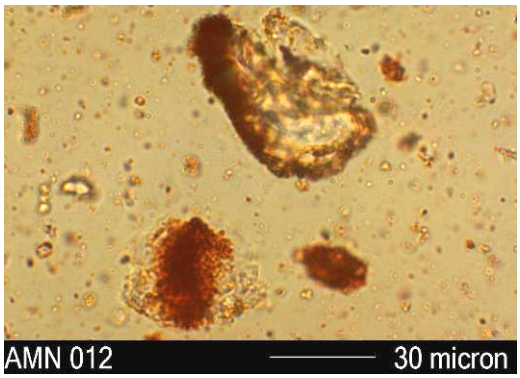

Figures 5-45a, b. Yellow ochres: BLN 004, AMN 012

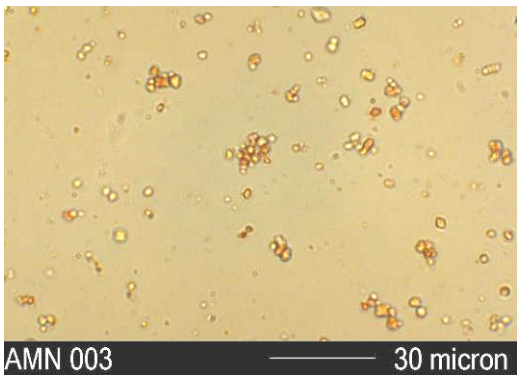

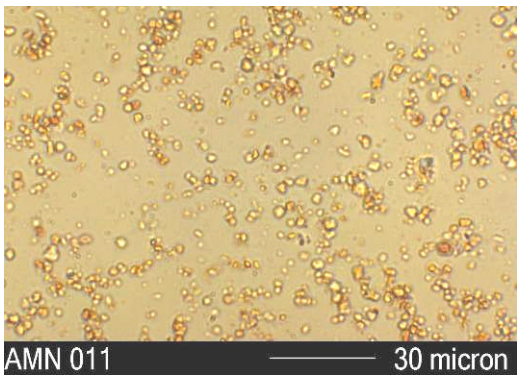

Figures 5-46a, b. Examples of the jarosites/natrojarosites: AMN 003, AMN 011

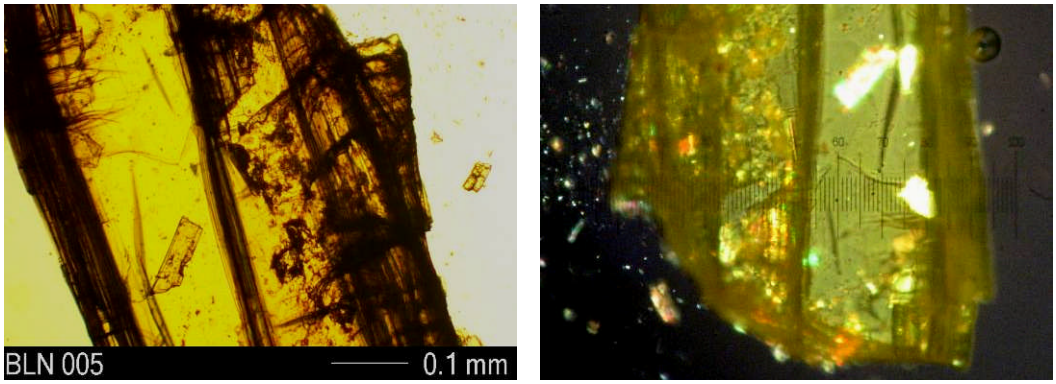

Figures 5-47a, b. BLN 005 under PPL and XPL, Mag x100

Observation of BLN 005 under the PLM showed that this sample was not an ochre. Characteristics observed included platy/micaceous-looking crystals, a bright-yellow colour, high relief and strong birefringence. These all indicated that the pigment was most likely to be a sample of orpiment (arsenic sulphide) of excellent quality [highly crystalline] (Eastaugh, Walsh et al., 2004: 127).

Visual and PLM observations used for distinguishing between the ochres, and enabled the division of samples into their constituent groups. Three main groups of pigments were identified and are outlined in Table 5-26 below.

Group	Pigment	Sample numbers	Total
1	Red ochres	BLN 006 – 009, AMN 005 – 006, AMN 008 and AMN 013 – 014	9
2	Yellow ochres	BLN 004, AMN 002, AMN 007, AMN 009 and AMN 012	5
3	Jarosites / natrojarosites	BLN 001 – 003, AMN 003 and AMN 011	5

Table 5-26. The groups of pigments as identified under the light microscope

The observations showed a similarity between the red and the yellow ochre samples: Both sets consisted of pure, fine, pigment particles, typically clustered together or onto some accessory material (Figures 5-44, 5-45). Calcite and quartz were also present in

the majority of the samples (refer back to Table 5-1 for a full list of discriminating optical properties). A foraminifera was also observed in BLN 004 (Figure 5-48 below). The major differences between the yellow and red ochres, was obviously the colour, and the abundance of iron hydroxide/oxide minerals in the ochres: the iron oxide (red) pigments appeared to be purer than the iron hydroxide-dominant pigments. These yellow ochres appeared to contain more accessory minerals, as well as traces of other pigments; including some red ochre (e.g. BLN 004 and AMN 002: Figure 5-45a) and minor traces another mineral, identified as jarosite/natrojarosite (AMN 007, description below).

The final group of pigments was clearly distinguishable from the ochres when observed under the optical microscope. The particles had approximately hexagonal to subhedral habits, and appeared as fine, discrete, transparent, pale-yellow to light green grains. Birefringence was moderate to high, but interference colours were of the first order and ranged mostly from white to grey (Figure 5-48b). These pigments were therefore identified as jarosites/natrojarosites: the two cannot be distinguished under a microscope (Eastaugh, Walsh et al., 2004: 151). Although they could arguably be unrelated to this study as they are clearly not ochres, their chemistry shows that they are iron-rich complexes, albeit also rich in sulphur and potassium/sodium. Previous studies additionally indicate that the ancient Egyptians often used these pigments as replacements for yellow ochre (Davies, 2001: 2). These iron-rich complexes were therefore analysed further, purely for comparative purposes.

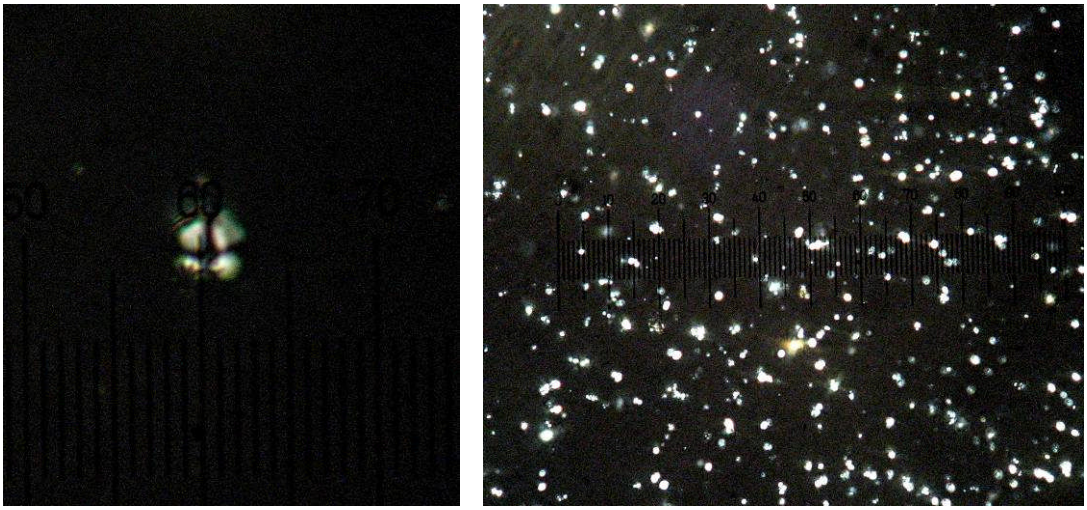

Figures 5-48 a, b. The foraminifera in BLN 004, and the jarosite/natrojarosite particles under crossed polars. Mag. X1000 (oil immersion) for (a), X400 for (b)

5.2.2. Scanning electron microscopy-energy dispersive X-ray spectroscopy SEM-EDS results

All SEM images showed surface irregularities. Particles were more distinct in the jarosites/natrojarosites, and measured approximately 1.2 μm. The red and yellow ochres formed tight agglomerates of particles, with grains of approximately 1.3 μm. Examples of a sample from the BLN Group 1 samples and the AMN Group 2 samples for the red and yellow ochres, and for the jarosites/natrojarosites are given below. Magnification of the images here is the magnification used for EDS measurements.

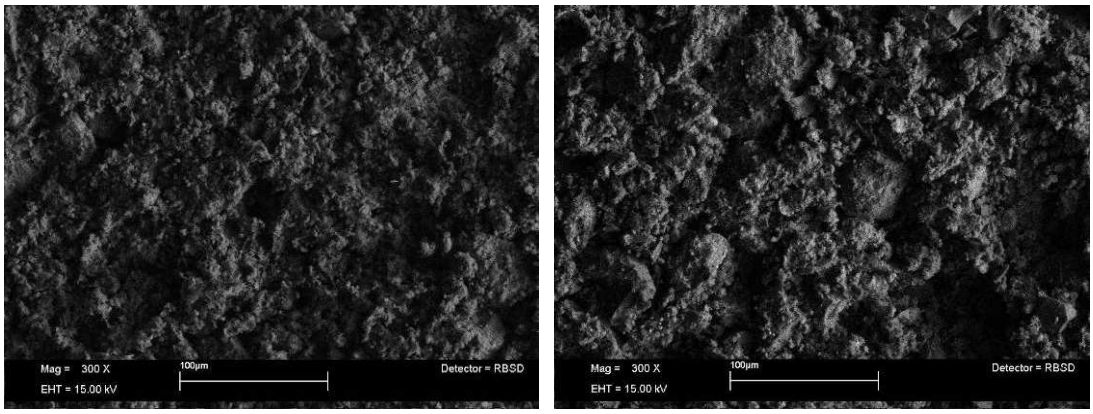

Figure 5-49a, b. SEM backscattered electron (BSE) images of examples of red ochres BLN 007 and AMN 005

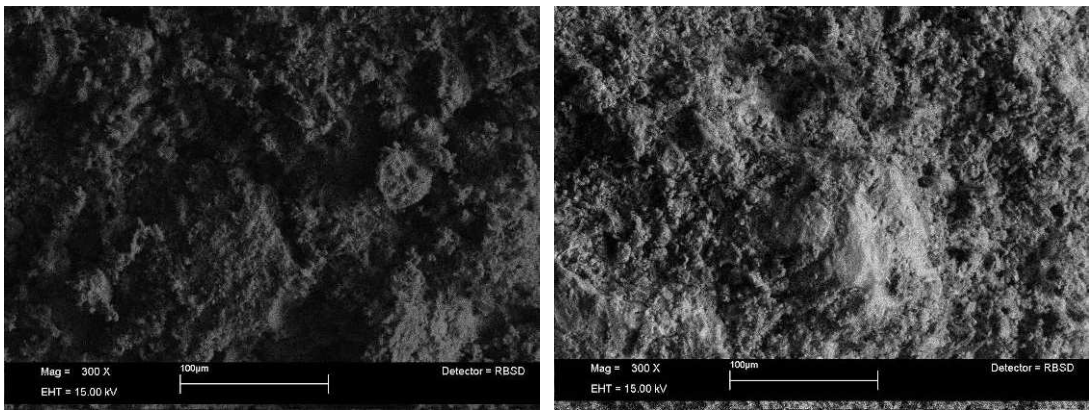

Figures 5-50a, b. BSE images of examples of yellow ochres BLN 004 and AMN 002

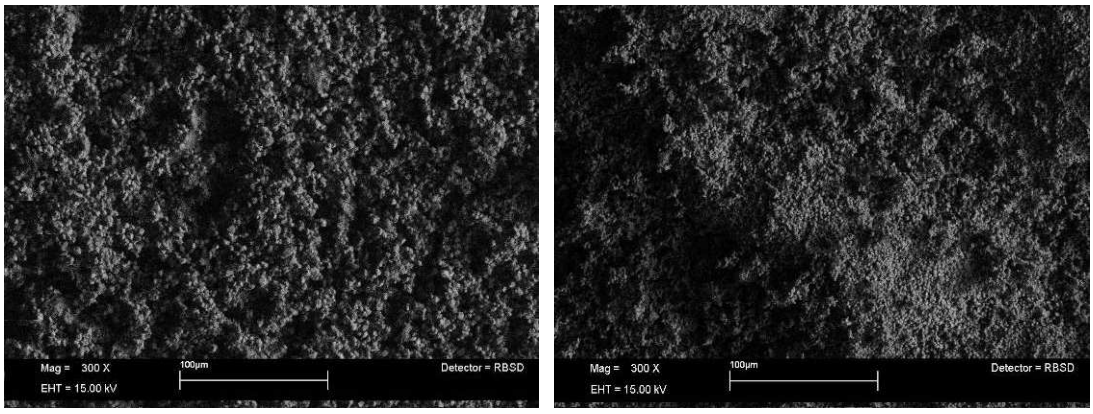

Figures 5-51a, b. BSE images of the jarosites/natrojarosites BLN 001 and AMN 003

EDS data

	%	%	%	%	%	%	%	%	%	%	%	%
sample	**Al_2O_3**	**Fe_2O_3**	**MgO**	**CaO**	**Na_2O**	**K_2O**	**TiO_2**	**P_2O_5**	**MnO**	**SiO_2**	**SO_3**	**Cl**
BLN 001 (a)	12	38	0.2	*	3.7	0.7	0.54	0.22	*	12	32	0.15
BLN 001 (b)	9.6	46	0.1	*	3.5	0.7	0.35	0.1	*	7.8	32	0.12
BLN 001 (c)	11	45	0.2	*	4.1	0.7	0.32	0.18	*	8.7	30.2	0.06
BLN 002 (a)	17	29	0.4	*	6.5	0.9	0.12	0.53	*	8.8	36	1.80
BLN 002 (b)	16	26	1.0	*	7.6	1.0	0.4	1.2	*	9.4	33	4.30
BLN 002 (c)	17	30	0.2	*	7.9	1.0	0.44	0.25	*	5.8	32	5.30
BLN 003 (a)	16	35	0.2	*	4.1	1.2	0.12	0.25	*	5.1	38	0.16
BLN 003 (b)	16	35	0.2	*	4.3	1.5	0.13	0.29	*	3.7	39	0.19
BLN 003 (c)	15	38	0.2	*	3.9	1.3	0.3	0.26	*	4.1	37	0.17
BLN 004 (a)	23	29	0.2	0.3	0.1	0.3	2.06	0.24	*	45	0.06	0.08
BLN 004 (b)	26	22	0.3	0.5	0.1	0.2	1.7	0.16	*	48	0.43	0.08
BLN 004 (c)	21	20	0.2	0.5	0.1	0.4	2.5	0.18	*	55	0.23	0.11
BLN 006 (a)	6.1	78	0.8	0.1	0.5	0.5	0.32	0.14	0.53	13	0.46	0.41
BLN 006 (b)	9.2	69	1.0	0.1	0.5	0.5	0.35	0.21	0.51	18	0.55	0.51
BLN 006 (c)	5.2	78	0.7	0.2	0.4	0.6	0.57	0.27	0.96	12	0.71	0.52
BLN 007 (a)	22	25	0.3	0.6	0.2	0.5	4.8	0.5	0.11	45	0.32	0.14
BLN 007 (b)	25	21	0.3	0.6	0.2	0.5	2.09	0.22	0.03	50	0.26	0.15
BLN 007 (c)	23	24	0.3	0.7	0.2	0.9	2.3	0.2	0.13	49	0.23	0.18
BLN 008 (a)	3.5	85	0.6	*	0.3	0.2	0.19	0.31	1.1	7.6	0.94	0.38
BLN 008 (b)	3.8	83	0.7	*	0.4	0.3	0.36	0.29	1.02	9.06	0.94	0.41
BLN 008 (c)	4.9	79	0.8	*	0.4	0.3	0.39	0.33	1.08	11	1.04	0.48
BLN 009 (a)	3.4	31	0.7	23	0.5	0.3	0.16	0.29	0.31	7.8	32	0.30
BLN 009 (b)	4.6	31	1.0	21	0.7	0.4	0.18	0.16	0.31	10.2	31	0.42
BLN 009 (c)	4.3	45	0.9	16	0.5	0.4	0.19	0.39	0.4	10.5	21	0.38

Table 5-27. BLN SEM-EDS data, all quoted to 2 significant figures (error bars at 20%) -* indicates that the element was present in concentrations below the detection limit of the instrument

	%	%	%	%	%	%	%	%	%	%	%	%
sample	**Al_2O_3**	**Fe_2O_3**	**MgO**	**CaO**	**Na_2O**	**K_2O**	**TiO_2**	**P_2O_5**	**MnO**	**SiO_2**	**SO_3**	**Cl**
AMN 002 (a)	23	33	0.26	0.45	2.6	0.27	1.03	0.12	0.11	35	0.55	4.0
AMN 002 (b)	14	42	0.12	0.44	8.06	0.22	0.95	0.12	0.27	22	0.71	11
AMN 002 (c)	18	24	0.1	0.39	9.6	0.22	0.78	0.15	0.23	27	0.73	18
AMN 003 (a)	12	50	0.09	0.27	4.2	0.69	*	0.2	0.07	1.1	32	*
AMN 003 (b)	11	49	0.11	0.36	3.4	0.84	*	0.28	0.20	1.1	33	0.1
AMN 003 (c)	14	40	0.15	0.28	4.9	0.71	*	0.3	0.06	2.4	37	0.07
AMN 005 (a)	15	45	0.28	0.58	0.76	0.3	1.2	0.11	0.20	36	0.38	0.12
AMN 005 (b)	11	34	0.28	2.4	0.49	0.45	0.93	0.03	0.22	49	1.2	0.13
AMN 005 (c)	13	29	0.24	0.58	0.56	0.35	1.2	*	0.21	55	0.58	0.07
AMN 006 (a)	26	8.8	0.41	1.4	0.14	0.92	*	0.09	0.03	60	0.87	0.58
AMN 006 (b)	27	9.9	0.43	1.7	0.24	1.08	*	0.12	0.11	58	0.82	0.71
AMN 006 (c)	19	14	0.40	1.03	0.13	1.04	*	0.04	*	63	1.1	0.49
AMN 007 (a)	1.3	93	0.35	0.47	0.26	0.24	*	0.24	0.37	3.3	0.4	0.44
AMN 007 (b)	1.3	92	0.4	0.40	0.32	0.23	*	0.24	0.47	3.4	0.5	0.44
AMN 007 (c)	3.7	84	0.73	0.12	0.24	0.79	*	0.06	0.38	9.1	0.27	0.4
AMN 008 (a)	6.2	88	0.35	0.11	0.66	0.39	*	0.27	0.30	1.2	2.09	0.14
AMN 008 (b)	6.3	87	0.25	0.13	0.68	0.58	*	0.16	0.49	1.7	2.9	0.09
AMN 008 (c)	4.9	87	0.17	0.07	0.64	0.64	*	0.2	0.45	2.2	3.4	0.11
AMN 009 (a)	1.8	60	2.6	14	5.3	0.87	*	5.5	0.33	5.09	1.06	4
AMN 009 (b)	1.6	84	0.79	4.5	1.2	0.3	*	0.58	0.41	4.4	0.69	1.05
AMN 009 (c)	5.6	66	0.86	2.9	1.3	2.0	*	0.43	0.28	19	0.66	0.58
AMN 014 (a)	27	17	0.43	1.2	0.31	0.65	*	0.05	3.5	48	0.08	1.3
AMN 014 (b)	22	10	0.31	0.85	0.43	0.71	*	0.07	1.5	63	0.17	1.2
AMN 014 (c)	22	32	0.58	1.01	0.47	0.60	*	0.17	2.3	40	0.19	1.02

Table 5-28. AMN SEM-EDS data (error bars at 20%)

As mentioned earlier, most sample quantities were insufficient for ICP-AES analysis, consequently the majority of the pigments were analysed via SEM-EDS. Although this limited the amount of information obtained per sample, it nevertheless gave useful data that allowed for analogies between samples. The results were also compared to the Maltese prehistoric MA red and MA yellow ochres, and will be described towards the end of this section.

Initial data examination included calculating the mean and the standard deviation for each set of points taken from each sample (total of three [a-c] per sample) during SEM-EDS analysis. The standard deviation, a statistical measure of dispersion within a normal distribution (Rees, 2001: 89), differed per element; with observed variability usually being proportional to the percentage quantity of the element present, albeit with some exceptions. Iron oxide (wt-%) was the most variable oxide in question, followed by silicon and aluminium oxide respectively. Furthermore, although the concentration of sulphur clearly differed per sample (the reason for its presence in the selected samples will be explained later), each set of values was similar per observation; consequently the standard deviation was low even when the quantities of this variable were high (Table 5-29). Another important observation was made when comparing the average standard deviations of the BLN samples, and the AMN set (Table 5-31): the latter consistently gave a slightly higher divergence from the mean, possibly indicating that these samples were somewhat less pure. This was, nevertheless, an expected statistical result owing to the fact that while the BLN samples were extracted from lumps of ochre, the majority of the AMN pigments were obtained in smaller quantities in powdered form, indicating probable sample handling prior to this study.

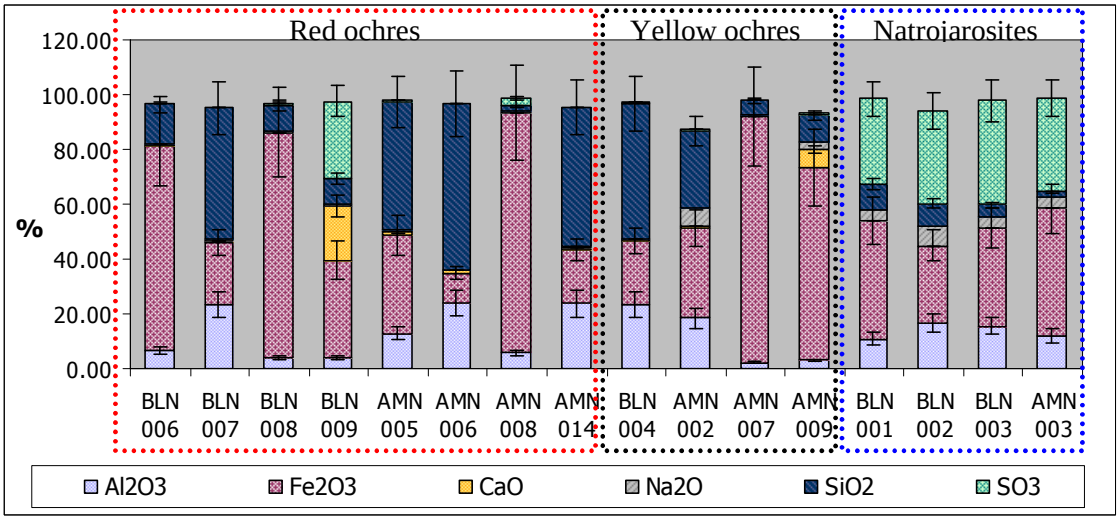

Figure 5-52. A histogram showing the relative abundances (weight %) of the major elements present in relation to one another. Error bars at 20%

Although the ochres had similar major constituents, the ratios of these oxides varied between observations. Samples BLN 006, BLN 008, AMN 008 (red ochres) and AMN 007 (yellow ochre), for example, had a high relative proportion of Fe_2O_3 that ranged between 75 – 90% and was indicative of ochres with little accessory minerals and therefore colorant-rich. The high concentration of sodium also indicated that the non-ochre yellows were actually natrojarosites rather than jarosites. These had a markedly more consistent composition than the ochres, as shown in the histogram in Figure 5-52 above.

The sample grouping of ochres and jarosites/natrojarosites established through optical observations was therefore confirmed by means of both SEM-EDS and ICP-AES analysis: the abundance of S and Na were the major elements present that dictated the prevalence of natrojarosite.

Sample	Al_2O_3	Fe_2O_3	MgO	CaO	Na_2O	K_2O	TiO_2	P_2O_5	MnO	SiO_2	SO_3	Cl
BLN 001	10.93	42.99	0.14	0.00	3.77	0.72	0.40	0.17	0.00	9.45	31.33	0.11
Sd	1.56	4.42	0.05	0.00	0.33	0.06	0.13	0.05	0.00	1.84	0.92	0.08
BLN 002	16.75	28.06	0.49	0.00	7.31	0.97	0.32	0.66	0.00	8.02	33.63	3.79
Sd	0.25	2.47	0.44	0.00	0.75	0.10	0.18	0.37	0.00	1.74	1.82	3.00
BLN 003	15.65	35.73	0.16	0.00	4.10	1.29	0.18	0.27	0.00	4.32	38.13	0.17
Sd	0.72	2.00	0.01	0.00	0.29	0.23	0.11	0.02	0.00	0.62	0.92	0.03
BLN 004	23.37	23.47	0.23	0.43	0.10	0.28	2.09	0.19	0.00	49.52	0.24	0.09
Sd	2.30	5.28	0.02	0.12	0.05	0.13	0.46	0.03	0.00	4.97	0.14	0.03
BLN 006	6.82	74.83	0.81	0.13	0.49	0.52	0.41	0.21	0.66	14.07	0.57	0.48
Sd	1.79	4.26	0.15	0.09	0.07	0.08	0.12	0.05	0.29	2.50	0.08	0.10
BLN 007	23.16	23.09	0.29	0.62	0.20	0.61	3.03	0.31	0.09	48.19	0.27	0.15
Sd	1.58	2.59	0.02	0.08	0.02	0.31	1.62	0.13	0.08	2.76	0.03	0.04
BLN 008	4.09	82.17	0.68	0.00	0.36	0.25	0.31	0.31	1.08	9.35	0.97	0.42
Sd	0.59	2.42	0.06	0.00	0.04	0.10	0.10	0.02	0.06	1.41	0.04	0.09
BLN 009	4.09	35.49	0.88	19.77	0.54	0.36	0.18	0.28	0.34	9.49	28.22	0.37
Sd	0.52	8.73	0.15	5.12	0.13	0.04	0.02	0.08	0.06	1.07	4.43	0.10
AMN 002	18.55	33.03	0.17	0.43	6.59	0.24	0.93	0.13	0.20	28.11	0.66	10.98
Sd	4.89	9.49	0.10	0.06	3.92	0.06	0.17	0.01	0.09	6.15	0.04	10.47
AMN 003	12.01	46.34	0.11	0.30	4.16	0.75	0.00	0.26	0.11	1.54	34.36	0.06
Sd	1.61	5.56	0.04	0.06	1.04	0.11	0.00	0.04	0.11	0.65	2.46	0.09
AMN 005	12.99	35.67	0.27	1.18	0.60	0.37	1.10	0.04	0.21	46.76	0.71	0.11
Sd	1.46	8.31	0.02	1.30	0.16	0.13	0.16	0.04	0.02	8.98	0.29	0.05
AMN 006	24.04	10.94	0.41	1.01	0.17	0.59	1.37	0.08	0.05	60.39	0.00	0.93
Sd	4.82	3.77	0.02	0.11	0.08	0.18	0.38	0.04	0.09	1.96	0.00	0.26
AMN 007	2.11	89.66	0.50	0.33	0.27	0.42	0.00	0.18	0.41	5.31	0.38	0.43
Sd	1.08	3.65	0.19	0.19	0.04	0.40	0.00	0.06	0.06	2.35	0.05	0.02
AMN 008	5.77	87.46	0.25	0.10	0.66	0.54	0.00	0.21	0.41	1.70	2.78	0.12
Sd	0.60	0.58	0.08	0.04	0.02	0.17	0.00	0.04	0.12	0.37	0.38	0.04
AMN 009	3.03	70.08	1.40	7.00	2.64	1.07	0.00	2.16	0.34	9.60	0.80	1.88
Sd	1.91	11.39	0.92	6.27	2.63	1.11	0.00	1.89	0.06	5.99	0.14	2.81
AMN 014	23.68	19.56	0.44	1.01	0.40	0.66	2.40	0.10	0.00	50.46	0.15	1.15
Sd	3.26	13.09	0.13	0.20	0.11	0.13	1.37	0.05	0.00	12.33	0.04	0.28

Table 5-29. Averages and standard deviation (Sd) per sample (values determined via SEM-EDS analysis)

Sample	Al_2O_3	Fe_2O_3	MgO	CaO	Na_2O	K_2O	TiO_2	P_2O_5	MnO	SiO_2	SO_3	Cl
BLN	2.4	6.6	0.25	1.3	0.65	0.38	0.33	0.39	0.07	4.64	0.17	0.86
AMN	1.9	7.0	0.29	1.5	0.74	0.41	0.33	0.45	0.06	5.09	0.20	0.96

Table 5-30. Average standard deviation per set of samples (BLN and AMN)

Sets	Al_2O_3	Fe_2O_3	MgO	CaO	Na_2O	K_2O	TiO_2	P_2O_5	MnO	SiO_2	SO_3	Cl
BLN	14	51	0.50	0.3	0.29	0.42	1.4	0.25	0.46	30.2	0.51	0.29
AMN	12	52	0.54	1.8	0.79	0.61	0.81	0.46	0.23	29	0.8	0.77
Colour	Al_2O_3	Fe_2O_3	MgO	CaO	Na_2O	K_2O	TiO_2	P_2O_5	MnO	SiO_2	SO_3	Cl
RO	14	48	0.45	0.58	0.41	0.51	1.2	0.18	0.36	33	0.78	0.5
YO	9.5	61	0.71	2.6	1.0	0.59	0.7	0.85	0.25	21	0.47	0.8

Table 5-31. Average % of variable per set (BLN and AMN) and per colour (RO = red ochre, YO = yellow ochre)

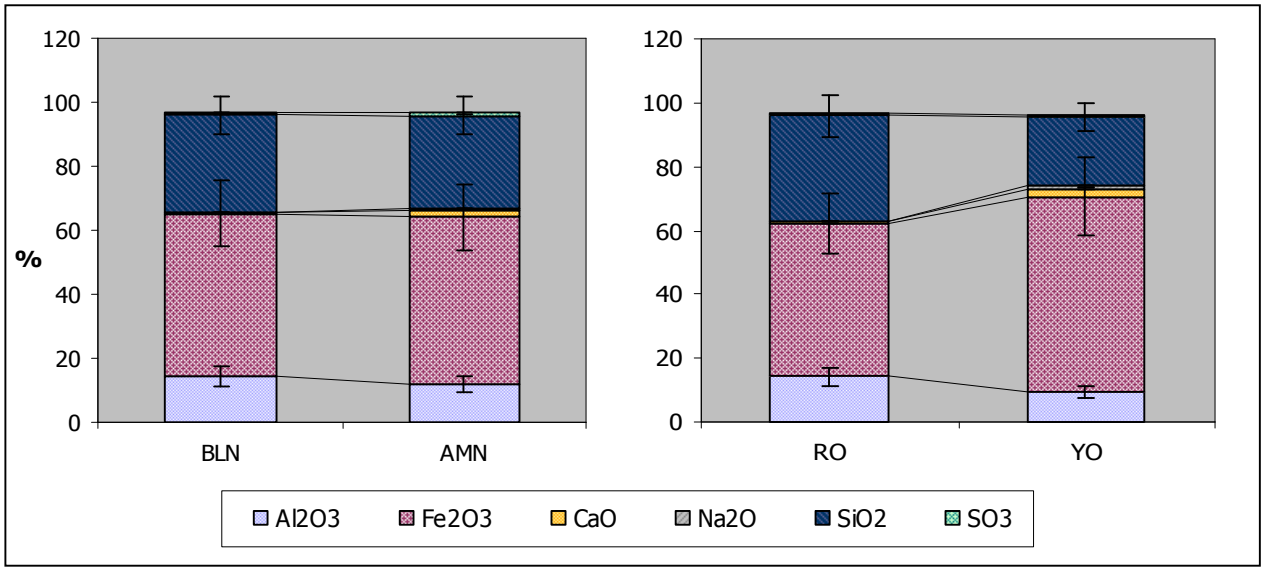

Figure 5-53. Histograms showing the average quantities (%) of the major and some minor elements present in relation to one another. The graphs include series lines and error bars (20%)

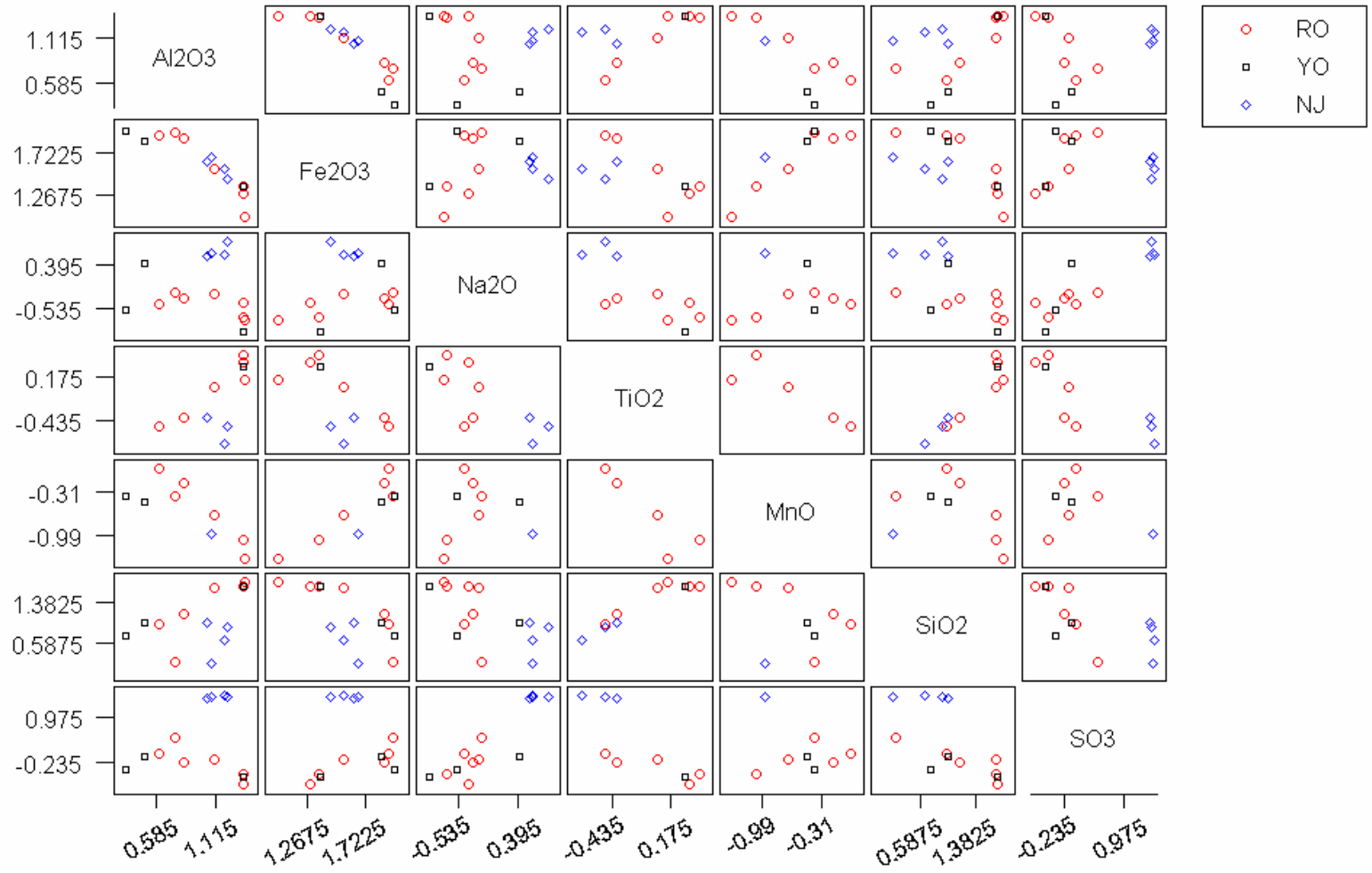

Figure 5-54. Matrix plots of some of SEM-EDS results (values have been $\log_{10}$ normalised, and data excludes BLN 009 and AMN 002)

The main accessory mineral in all these Amarna samples was quartz. CaO was only present in minor amounts, although BLN 009 and AMN 009 indicated a prevalence of the element in the pigment. The red ochre sample BLN 009 gave particularly inconsistent results that included high quantities of both CaO (20 wt-%) and SO_3 (28 wt-%). Concentrations of these components within the sample were rather high and could have been indicative of the presence of gypsum in the material. This was construed particularly as there was no Na_2O to offset the SO_3, therefore indicating that the sulphur present was not due to the occurrence of natrojarosite. Another exception was observed in sample AMN 002, which showed an inconsistency in the chlorine content with values ranging between 18 wt-% and 4 wt-% (Table 5-28). The higher amount of sodium present suggested that these elements indicated the presence of common salt, sodium chloride (NaCl). Because all the oxide % values were normalised, the presence of these elements was found to have a statistically significant effect on the values of the other elements present in the material ($P > 0.05$), therefore necessitating their removal from the sample set.

Both the differences between the averages of the elements present in the two main sample sets, as well as the differences between the averages of the red and the yellow ochres were assessed. The data taken into consideration excluded the natrojarosites and the discordant outliers BLN 009 and AMN 002 mentioned earlier. The results are shown in Table 5-30 and an outline of the comparisons are shown in the histograms (Figures 5-53) above.

It appears that there was no major difference between the BLN and the AMN sample sets, apart from there being a slightly higher percentage of CaO and SO_3 in the latter set that may have been indicative of sample handling prior to this investigation. The discrepancy, however, could arguably also be attributed to a difference in source. A greater difference was observed on comparing the red to the yellow ochres, with the latter yellow ochres appearing to have more Fe_2O_3 and less SiO_2. These observations, however, were difficult to ascertain and statistical tests at a 95% level of confidence showed that these differences in variable values were unlikely to have been of significance. It is probable that these statistical results were affected by the small sample size for yellow ochres (total of three samples), and by the exceptionally pure yellow ochre AMN 007. SEM-EDS studies therefore indicated that the major elements did not offer enough information to distinguish between the red and the yellow ochres, and that if their source was different, this factor could not be identified by this analytical method alone.

5.2.3. Inductively coupled plasma – atomic emission spectroscopy (ICP-AES) data

	%	%	%	%	%	%	%	%	%	(ppm)
sample	**Al_2O_3**	**Fe_2O_3**	**MgO**	**CaO**	**Na_2O**	**K_2O**	**TiO_2**	**P_2O_5**	**MnO**	**Ba**
AMN 011	14	29	0.11	0.83	6.0	0.71	0.04	0.06	0.007	29
AMN 012	14	18	0.14	0.23	1.03	0.17	0.93	0.13	0.02	89
AMN 013	14	26	0.23	0.39	0.75	0.23	1.04	0.10	0.11	210

	(ppm)	(ppm)	(ppm)	(ppm)	(ppm)	(ppm)	(ppm)	(ppm)	(ppm)
sample	**Co**	**Cr**	**Cu**	**Li**	**Ni**	**Sr**	**V**	**Y**	**Zn**
AMN 011	1	72	10	0	0	9	680	70	0
AMN 012	14	77	29	8	61	14	95	132	9
AMN 013	26	66	108	4	99	14	96	173	28

	(ppm)	(ppm)	(ppm)	(ppm)	(ppm)	(ppm)	(ppm)	(ppm)	(ppm)
sample	**Zr**	**La**	**Ce**	**Nd**	**Sm**	**Eu**	**Dy**	**Yb**	**Pb**
AMN 011	15	5	3	4	*	*	1.1	1.5	10
AMN 012	130	34	48	33	2.0	1.9	1.0	2.3	15
AMN 013	120	11	290	15	*	*	5.4	4.0	37

Tables 5-32a –c. ICP-AES data of AMN 011 – AMN 013

The ICP-AES results from the three samples analysed, namely AMN 011, AMN 012 and AMN 013, compared well with the SEM-EDS results and included a natrojarosite, a yellow ochre and a red ochre respectively, therefore providing an example of each sample group. Matrix plots of the results that included the MA yellow and red archaeological samples from the Maltese islands were used to compare data from these two completely different sites, and an example of a matrix plot for the REEs is given below.

On analysis of these REE plots, the results suggested that the Egypt red ochres could be outliers, while the yellow ochres possibly fitted into the MA (red) group. Comparison of some element concentrations corroborated the observations for the red ochres, but also showed that Egypt's yellow ochres were potentially different from the MA samples. The natrojarosites were recurrent outliers, as was expected. Nevertheless, although there appears to be a difference between the Maltese and Egyptian pigments, this observation is difficult to ascertain as the analysed ICP-AES sample set for Egypt was small owing to the limited sample quantities, therefore any dissimilarities could be coincidental.

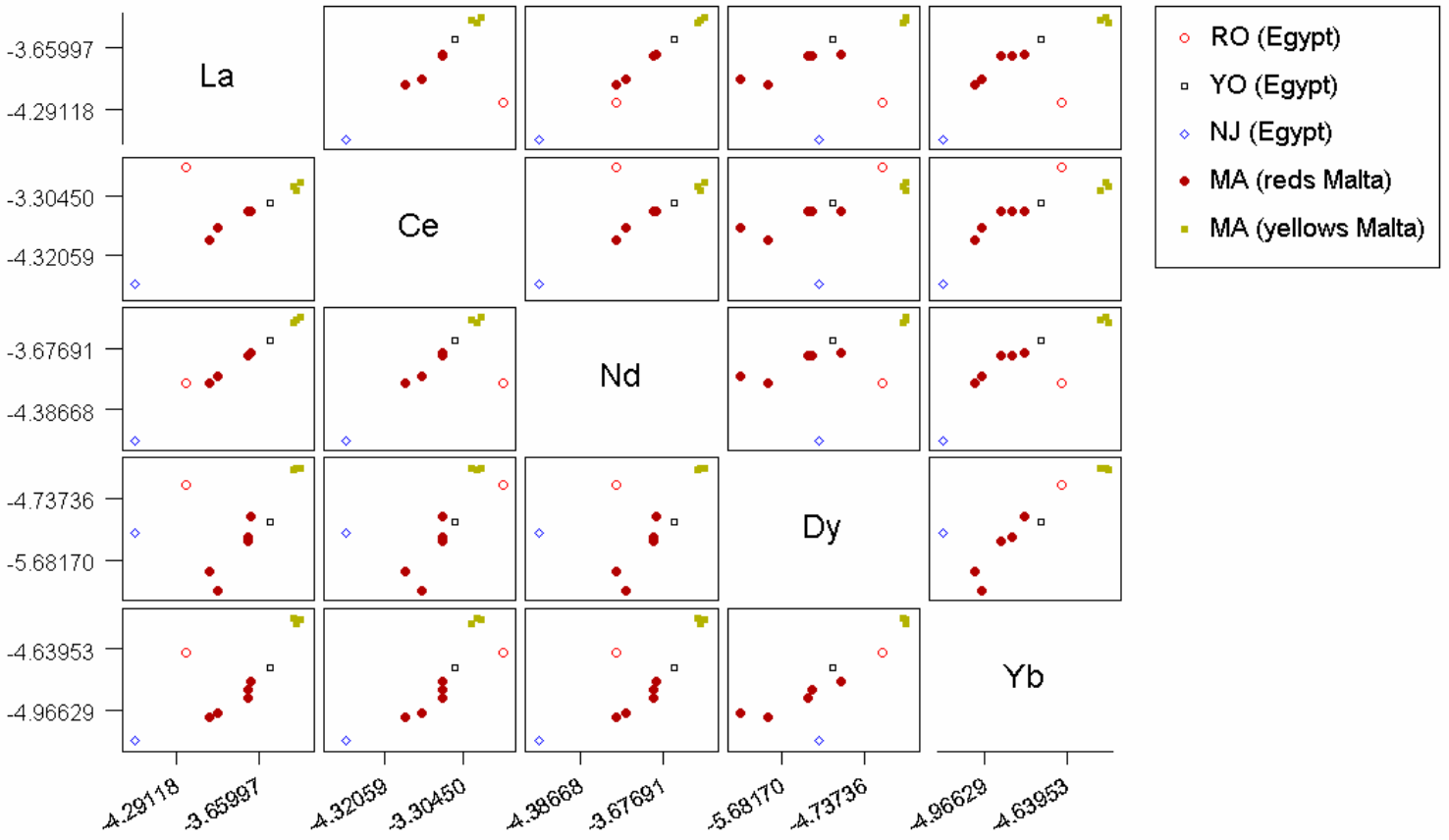

Figure 5-55. Matrix plot of REEs for samples of red and yellow ochre from Egypt (RO and YO), and the MA (red and yellow) samples. Eu and Sm were not included in the plots as some of the data was missing

Data analysis for differentiation/provenancing purposes

All SEM-EDS and ICP-AES data values were transformed using the mathematical adjustment described in the previous chapter (also refer to Erlandson, Robertson et al., 1999; Glascock and Neff, 2003; Popelka-Filcoff, 2006; Popelka-Filcoff, Robertson et al., 2007; MacDonald, Hancock et al., 2008; Popelka-Filcoff, Miksa et al., 2008). Oxide values were therefore converted to their element ppm and further transformed using the following equation: $(\{10^6/10^6\text{-Ca}\}/\text{Fe})*\text{element}$. The log-transform normalisation was then applied to the result. Although it is arguable as to whether it was necessary to remove the Ca from the total as it was clear that the major accessory material in these samples was Si-based, the 'extraction' was deemed necessary mainly for two purposes: (i) For comparison with the ICP-AES as detection of Si with the ICP-AES was not possible. (ii) For eventual comparison with the MA samples, which were clearly Ca-rich

The subtraction was not expected to affect the results other than allowing for more efficient observation of the relevant data, i.e. data pertaining to the iron oxides/iron hydroxides themselves (described previously). It was therefore merely performed as a systematic procedure in this study. The correlation between all the elements before and after this statistical analysis of data to show the relationship between the variables in a principal component space is shown in the loading plots below.

Results indicate that, apart from the Mn and Cl, most elements show a positive correlation, indicating that the Fe was having the same dilution effect observed in the Maltese samples as described previously.

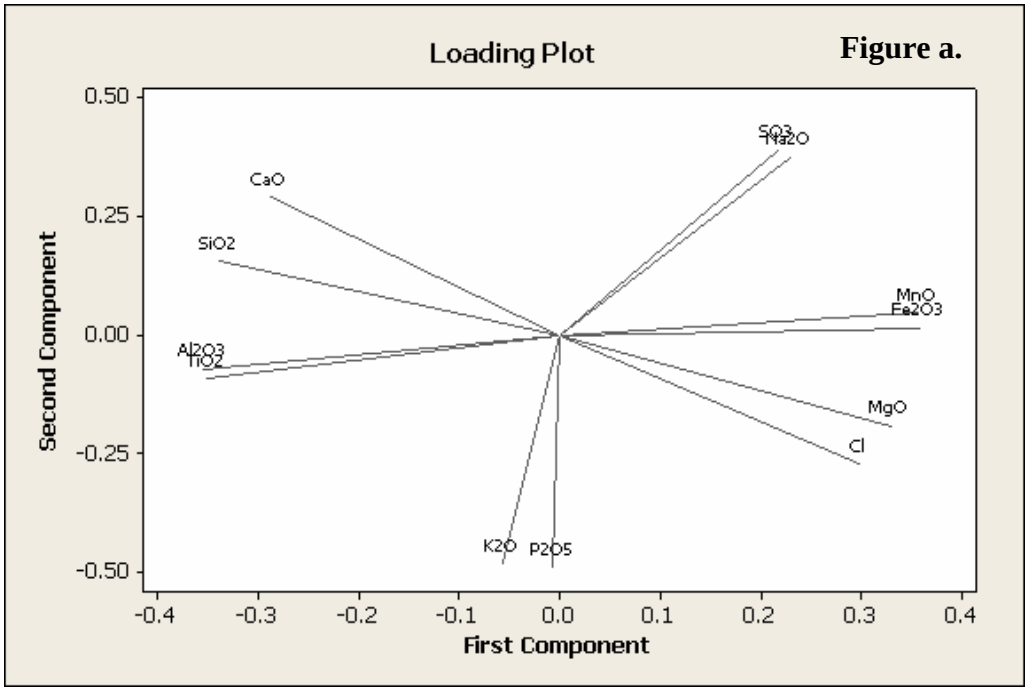

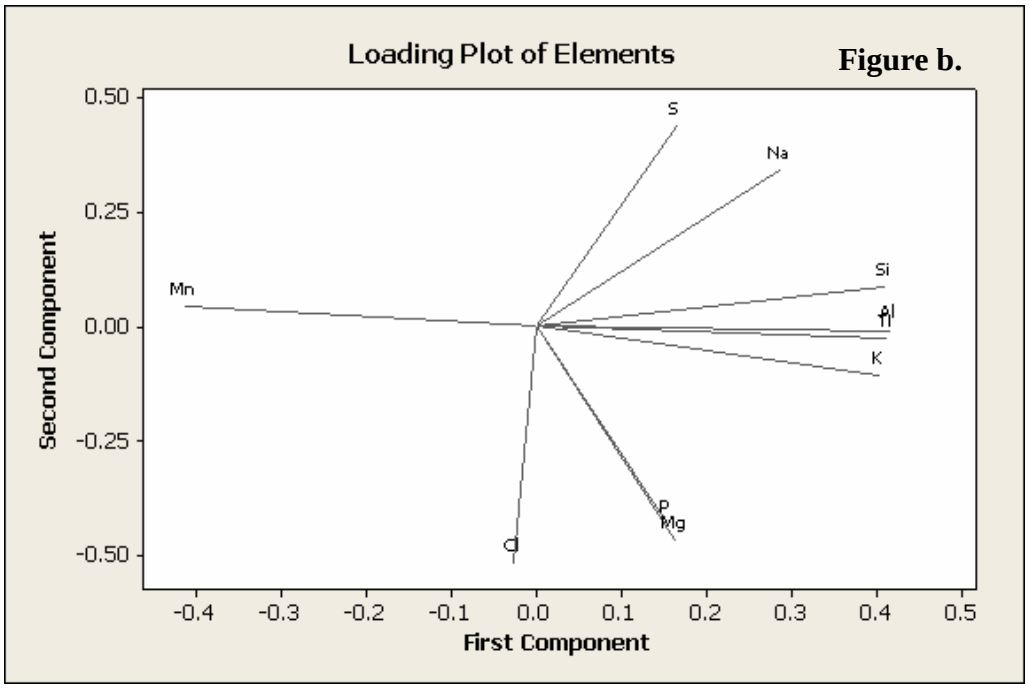

Figures 5-56a, b. PC (Minitab 15) loading plots of ochre components (natrojarosite and discordant outliers have been removed from the dataset for these plots) (a) before and (b) after the mathematical adjustment

Hierarchical cluster analysis of variables and observations

In the previous chapter, various tests (Pearson's tests and matrix plots) were used to assess which elements co-varied with Fe and which were subsequently likely to serve as discriminating variables between groups. In this sub-study, however, the number of elements detected was limited owing to the lower sensitivity of the SEM-EDS. Breakdown of data following transformation and normalisation indicated that the only variables available for comparison included Al, Mg, Na, K, Ti, Mn and P; and that Ti, Mn and P were present in quantities below the detection limit in certain samples. As a result, on constructing the hierarchical cluster using the single linkage algorithm method to compare the variables, P was omitted from the cluster because of problems experienced when working with too many missing variables. Here the number of missing values could not exceed the number of elements for hierarchical clusters of variables: It was assumed (from the previous study) that Ti and Mn were the more likely elements to substitute for and therefore be dependant on Fe, rather than P.

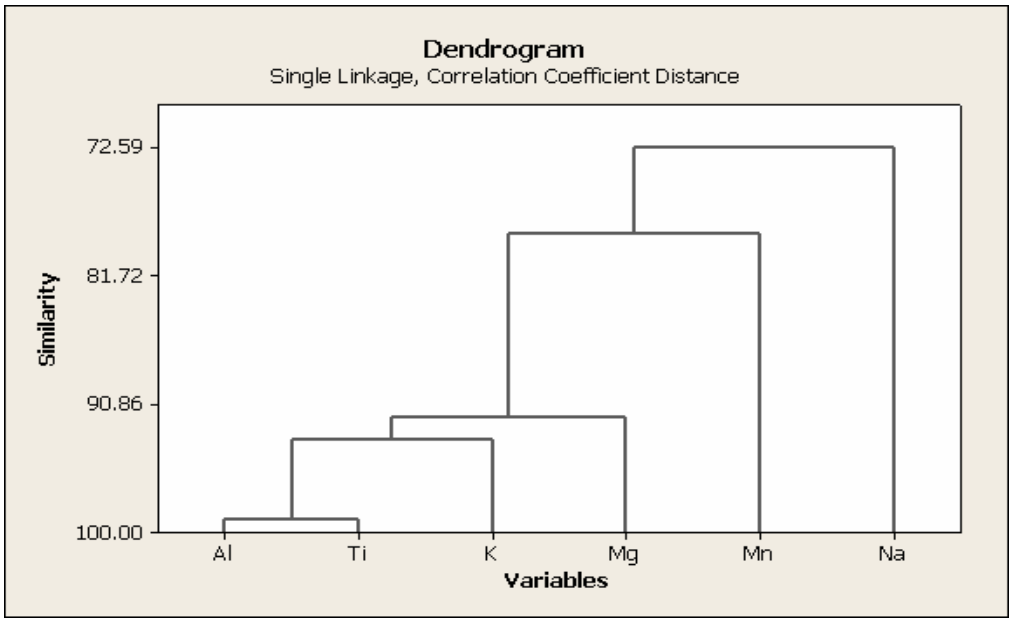

Figure 5-57. Dendrogram showing the hierarchical clustering between the selected variables off the ancient Egyptian ochres

The dendrogram showed that the elements most likely to co-vary with Fe in these ancient Egyptian ochres were Al, Ti, K and Mg.

Similar hierarchical dendrograms were used to compare the samples (or observations) based on this Euclidian distance clustering methodology. Hierarchical clusters of observations, however, require an entire set of data for each variable; consequently the number of elements compared here was limited even further. The first dendrogram was used to assess the relationship between the red and yellow ancient Egyptian ochres based on the association between the variables Al, Mg, Na, K, Mn. Here, observations 1-8 are representative of the red ochres, while 9-12 correspond to the yellow ochres (refer to key below). Results from this dendrogram showed that there did not appear to be any clear distinction between the yellow and red ancient Egyptian ochres.

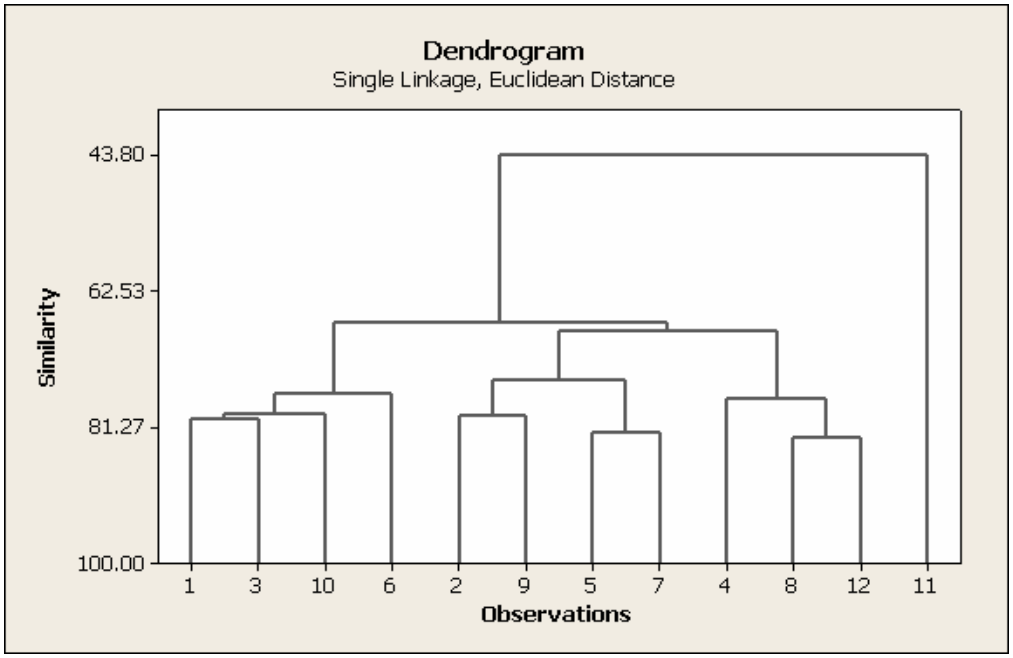

Figure 5-58. A hierarchical cluster to show the similarity between the red and yellow Egyptian ochres: a key to the numbers (observations) is given in Table 5-33

Group	Numbers	Observations (sample numbers)
Egypt: red ochres	1 – 3 4 – 6 7 – 8	BLN 006 – 008 AMN 005 – 006, AMN 008 AMN 014 – 013
Egypt: yellow ochres	9 10 – 12	BLN 004 AMN 007, AMN 009, AMN 012
Malta: red ochres	13 – 14 15 – 17	MA 002 – MA 003 MA 009 – MA 011
Malta: yellow ochres	18 – 20	MA 006 – MA 008

Table 5-33. Key to numbers and their corresponding observations for Figure 5-58, 5-59

There did, however, appear to be a discrepancy between the variables in AMN 009 and the variables in the other samples as this yellow ochre appeared to correlate to a much lesser extent. This was a feature also observed earlier when comparing the major elements present (histogram in Figure 5-52), where the presence of a high amount of CaO (%) was noted. This discrepancy could be indicative of a variation in source, or of some degree of sample handling prior to this study.

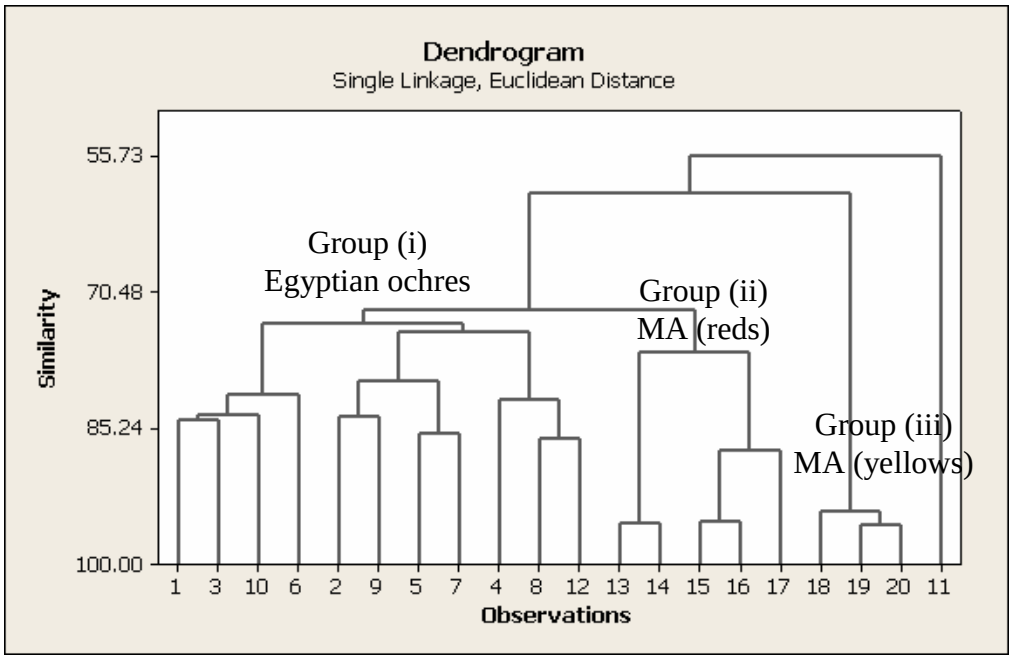

Figure 5-59. A hierarchical cluster showing the groups Egyptian ochres vs. Maltese ochres. A key to the numbers (observations) is given in Table 5-33.

A second cluster (Figure 5-59) was used to compare the Egypt and the MA samples. It includes the majority of the MA samples, with the exception of MA 001 and MA 005 which were omitted because (a) they would have contributed to the exclusion of another potentially key variable, Mn and (b) despite the omission of these two samples there were still enough remaining (representative) observations of the red archaeological MAs.

The cluster analysis did pick out three groups, in addition to the AMN 009 outlier. The observed groups included: the ochres from ancient Egypt (Group i), the red ochres (Group ii) and the yellow ochres (Group iii) from the Maltese islands. The hierarchical cluster within Figure 5-59 featuring the Egyptian ochres was identical to the dendrogram in Figure 5-58, as was expected. The whole correlation dendrogram nevertheless indicated that the MA reds from the Maltese islands approached the composition of the ancient Egyptian ochres much more than the MA (yellows), which in turn formed quite a discrete cluster.

The relationship between these variables can be observed, to some extent, in the matrix plot below (Figure 5-60), which features all common variables between the SEM-EDS and ICP-AES results. This plot illustrates the characteristics recognized in the hierarchical cluster by showing: (a) that the Neolithic yellow ochres from Malta do form quite a distinct cluster, and that the MA reds show similar trends, as was described in the previous chapter, and (b) that there is a wider spread in the ancient Egyptian ochres, although identical correlations with the MA samples are observed between certain elements; such as Al and Ti, but that the element ratio is relatively different between the ochres from the two countries.

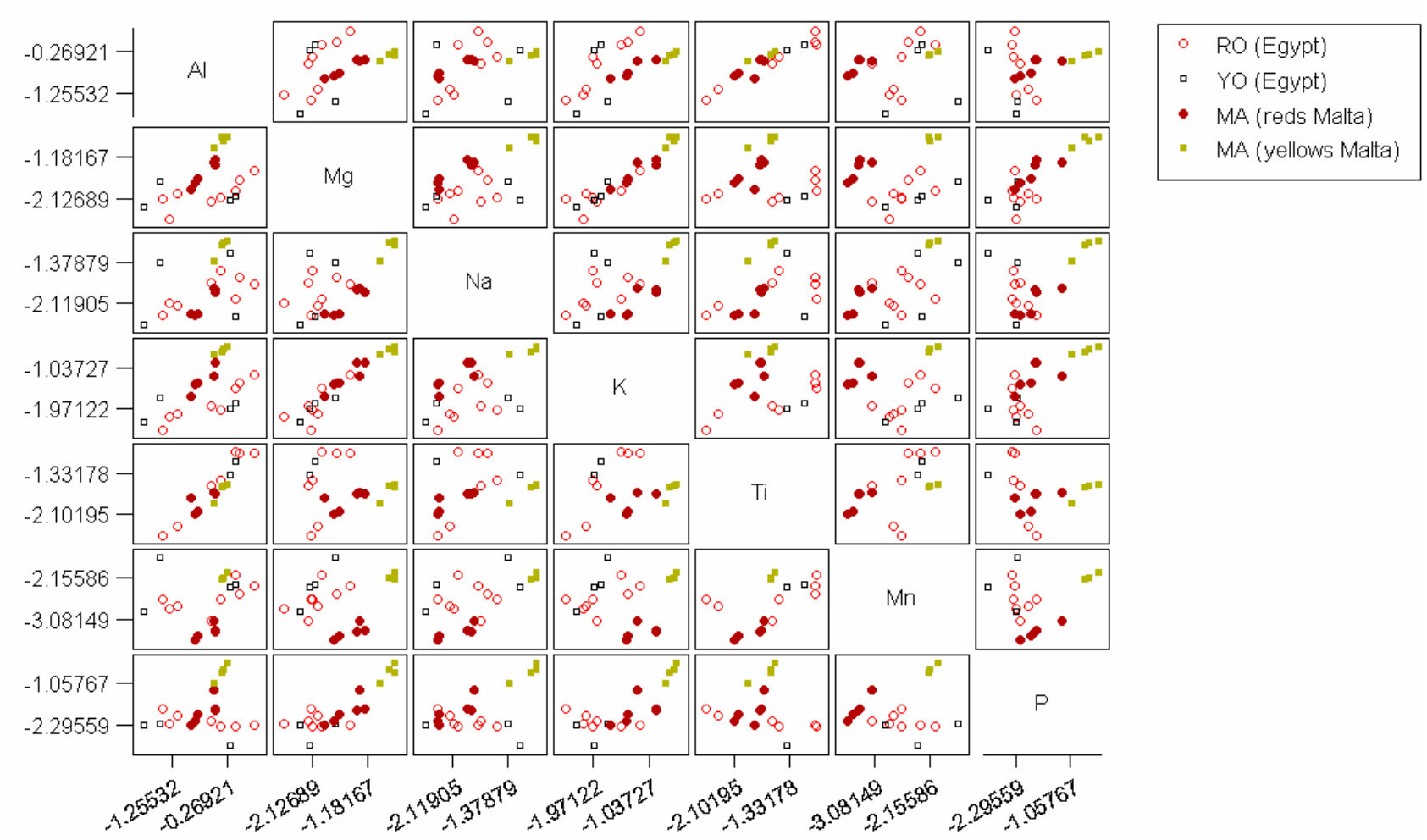

Figure 5-60. Matrix plot showing joint results for the Egyptian and the Neolithic Maltese ochres

Chapter 6.

Discussion

6.1. Characterisation of ochres for provenancing purposes

As it was necessary to establish which instrumental techniques would be most useful to analyse the samples in this characterisation and provenancing study, a comparison of techniques was carried out and the overall discussion has been described elsewhere (Chapter 4). The PLM and XRD were, however, selected and used for the analysis of the geological and/or the archaeological Maltese and Amarna samples, and the results obtained will be critically appraised in this section. Both techniques indicated the potential of distinguishing between geological sources, and the PLM study also brought to light differences between all the archaeological sample groups.

PLM revealed a number of aspects that could not be determined by any other technique implemented in this study. This is because it facilitated the user's capacity to observe and study the sample constituents, their respective colours and optical properties at close proximity. A summary of the PLM findings include the following:

i. The ochres present were similar to published studies in terms of their optical properties (Eastaugh, Walsh et al. 2004: 146);
ii. All the geological and archaeological ochres contained iron oxides and/or hydroxides and accessory minerals (characteristic of ochres, refer to Chapter 1);
iii. There were similarities between all the Maltese geological samples, such as the abundance of calcite, hematite and goethite;
iv. Differences were observed between all the geological samples. These included a higher amount of organic material in the Terra rossae, which nevertheless

compared well to the Calcitic reds; the presence of glauconite in the Greensands, and the larger quantities of gypsum and quartz in the Ooids;

v. There were various interesting aspects to the Maltese archaeological samples, including: the good ochre quality exhibited by the red MAs (fewer accessory materials/ochre impurities) in comparison to the poorer quality HYPDs; the unusual fibres present in the MA (yellows), and the bone in the HYPBs, HYPDs and yellow MA samples;

vi. There were discriminating factors between the Amarna samples: it was possible to tell which samples were mainly jarosites/natrojarosites. This method also showed whether samples contained traces of other pigments and was found to have a higher specificity at qualitatively distinguishing between red and yellow ochres than the elemental techniques. It was also a much simpler technique to implement.

Since a larger quantity of sample was required for XRD analysis than for PLM and SEM-EDS studies, and the ability to identify the poorly crystalline iron oxides was unsuitable (minimum detection limit of about 15-20%), only the Maltese geological samples were analysed using this method. The identities of the major phases present were readily determined, and were found to be predominantly calcite and quartz. Certain results, however, were difficult to interpret owing to (i) the peak shifts observed in the Ooid samples and (ii) the broadened diffraction profiles exhibited by the natural iron oxides, a characteristic experienced even when these were present in relatively high quantities (15-20%).

Results obtained during the pilot studies and previous publications have shown that iron oxides and hydroxides actually exhibit poor crystallinity as a result of their small size, non-stoichiometry and the presence of H_2O and/or OH^- ions introduced into the crystal lattice in a disordered way. This results in line broadening of the corresponding XRD reflections (Schwertmann, Cambier et al. 1985). These natural iron oxides/hydroxides also have the tendency to exhibit isomorphous substitution of Fe^{3+} by other cations, as described in Chapter 1. These substitutions may be quite high, resulting in obvious deviations from the theoretical composition and therefore affect the resultant diffraction pattern. The substitutions and the poor diffraction experienced could therefore account for the irregularities in peak positions, and for the low quantities of iron-containing minerals detected in the diffraction spectra of all the geological groups.

This method therefore showed:

i. The high quantity of calcite in the Calctic reds and the Greensands, whose constituent peaks masked all other peaks;
ii. The presence of both calcite and quartz in the Terra rossae, with calcite being the more abundant accessory mineral;
iii. The abundance of calcite, gypsum and quartz, in the Ooid group;
iv. The presence of goethite and hematite in the Terra rossae and the Ooids, with goethite appearing to have better crystallinity as the peaks were more defined.

6.2. Provenancing: Elemental analysis

Elemental analysis corroborated the results obtained through PLM and XRD investigations. ICP-AES, in particular, was used in the Malta provenancing study to enable the characterisation and quantification of the elemental components, and by extrapolation, the use of relationships between 'signature' elements to try and establish the source of these materials. Characterisation and provenancing will therefore be discussed simultaneously below.

6.2.1. Comparative study

The methods implemented in this study were used in a comparative study between ancient ochres from Amarna. The aims were to establish (a) how well the method employed in this study could distinguish between ochres, (b) to ascertain that the method does work, and (c) to show that archaeological ochres obtained from different locations are not identical. Though the results have been described elsewhere (refer to P.204), the data showed that the implemented methods (PLM, elemental analysis and statistics) allowed for the discrimination between the yellow ochres, and what was identified, by means of light microscopy and elemental analysis, as jarosite/ natrojarosite, $K/NaFe_3(SO_4)_2(OH)_6$.

Since most Amarna sample quantities were insufficient for ICP-AES analysis, ochre elemental data for statistical testing using the variables established as key for ochre discrimination (Chapter 5) was limited to a total of four elements (Al, Mg, Na and K). The results using these variables showed that the Amarna ochres were significantly different from the Maltese ochres, but that the red and yellow Egyptian ochres,

although visibly different, could not be differentiated statistically via ICP-AES analysis ($P < 0.05$), implying that a larger dataset of variables was required to successfully distinguish between these ochres. Although the method worked, therefore, the limitations experienced were a result of the use of the SEM-EDS and not through a flaw in the method. Scatter plots indicated a wider spread of data points in comparison with the Maltese archaeological ochres, which probably indicated that the source of these ochres was not as chemically distinct as those from the Maltese islands, and could also explain why the hierarchical analysis could not find auxiliary trends in the Amarna dataset.

6.2.2. The Maltese islands

The concept of provenancing materials by satisfying the 'provenance postulate' has been described in section 1.5. In summary, if an archaeological material is to be linked to a particular geological source, the inter-source variation between the potential sources must be greater than the intra-source variation within a given source (Glascock and Neff, 2003).

Though differentiation between ochres has been conducted using a number of approaches (which justifies the necessity of establishing an analytical methodology), perhaps the most commonly exploited method of characterising sources, establishing the association between them and analysing the correlation between these sources and the archaeological materials, is through elemental analysis (Erlandson, Robertson et al., 1999; Glascock and Neff, 2003; Popelka-Filcoff, 2006; Popelka-Filcoff, Robertson et al., 2007; MacDonald, Hancock et al., 2008; Popelka-Filcoff, Miksa et al. 2008).

Minor (or trace) elemental distribution, for example, is often used in the interpretation of the history of formation and diagenesis of both igneous rocks and geological sediments, mainly because different elements have varied affinities for certain specific environments (Basta, Ryan et al., 2005).

In provenance studies, the abundances and relative distribution of the minor and rare earth elements are also used to define the parent material. This, however, is limited by the premise that post-depositional processes, such as weathering, re-suspension, re-deposition and material extraction for human use, do not significantly alter the elemental composition; hence, any correlation between the geology and the material prior to and post extraction is retained (Abanda and Hannigan, 2006). Various studies have shown that trace elements (lanthanides in particular) do not fractionate significantly during diagenesis due to their lack of mobility in post-depositional processes; or during post extraction processes, such as water loss through material heating. They are accordingly often used to explain geochemical processes occurring in natural environments, such as the origin of sediments, acting as chemical "fingerprints" (Nakamura, 1974; Kato, Ohta et al., 1998; Dawood, El-Naby et al., 2004; Basta, Ryan et al., 2005).

As expected, however, other studies have shown that there are exceptions to these assertions, and that some element mobilisation may occur, albeit in a predictable manner (Pattan, Pearce et al., 2005; Abanda and Hannigan, 2006). Many trace elements, especially metals, have also become increasingly problematic pollutant groups as a result of urbanisation, as has been discussed in Chapter 5 (Adriano, 2001: 2, 4).

Although the association of ochre with other materials not really relating to its actual composition (such as binders/source variation) may be an issue in provenance studies (Chapter 1: 44), there appears to be no evidence of the problem in this study, apart from a couple of anomalous results in the Greensands data. This lack of fractionation, alteration and/or contamination was supported by the fact that there was no significant difference between the external and internal composition of the geological samples. Particular challenges included limited archaeological sample sizes, both in quantity (g) and as separate observations (number of samples); and due to the inadequacies of the non-invasive XRF method (P.201-202). There is also limited research on the effects of diagenesis and the environment on ochres. Though these materials are known to be amongst the most stable of pigments, exhibiting a remarkable resistance to environmental agents of degradation (Helwig, 2007), few studies actually address the chemistry of ochres, and the possible effects of time on the overall concentration of constituent (/signature) elements present.

6.2.2.1. Sourcing of Maltese archaeological ochres: The geological groups

All geological samples had high concentrations of Ca, and variable quantities of Fe, therefore corroborated the PLM and XRD observations. Average oxide concentrations of CaO included: 46 wt-% for Greensands, 44 wt-% for the Calcitic reds, 16 wt-% for the Ooids and 15 wt-% for the Terra rossae. The iron oxide content ranged between 0.3 wt-% to 34 wt-% (refer to histogram Figure 5-15b), therefore also justifying the data analysis using the equation 5-1 and method described on P.169 for statistical testing.

The evaluation of data described in the elemental analysis (ICP-AES and SEM-EDS) results section in Chapter 5 has been structured to help qualify and quantify this intra- and inter-source variation. The matrix scatter plots were used to observe the similarities on a visual basis, whilst the hierarchical clusters proved associations by means of an impartial statistical method.

The results from these geological samples showed that various elements showed strong correlations with each other, as displayed in the PC tests in Figure 5-23 on P.171. Especially notable trends are those seen between certain bivariate plots of elements, namely: Al vs. Ti, Zr, and Li, which all appeared to associate well together; Mn vs. Cr, Co and V, which also correlated with the previous set of variables; and Cu vs. Zn (refer to matrix plots between geological groups in Chapter 5, and in Appendix III). Dendrograms between elements also displayed these associations (Figure 5-25): all variables also showed a strong covariance with Fe. Other strong trends were observed between Mg, Na, K, Ba, Ni, Sc, Y, Zn, though correlations were less pronounced in certain groups, such as the Greensands (e.g. Figure 5-18). The REEs also displayed similar trends, as was expected, and will be discussed later on P.244.

All these elements have a strong tendency to substitute for Fe, and for each other (Chapter 1). Substitution is likely to be dictated by Goldschmidt's rules, where two ions with the same valency and radius are expected to exchange easily and/or enter into solid solution in amounts equal to their overall proportions (Suess, 1988). Substitution can thus be expected between Fe and elements with similar ionic radii and cation valencies, such as Mn (cationic radius of 0.83) and Fe (cationic radius of 0.78),

Mn and Mg (radius of 0.72) and Fe and Mg (Pettijohn, 1975: 289). Furthermore, when a compatible trace element substitutes for a lattice Fe in the material structure, the concentration of the element can be predicted by means of its distribution coefficient, and should plot on a reasonably straight line in a scatter plot between elements, as was observed in the results in Chapter 5. The ratio of the likely substitution elements, such as Al/Fe, may also represent similarities in geochemistry and reflect the environment in which the oxides were formed (Manceau, Schlegel et al., 2000).

These trends observed in the Malta geological samples therefore indicate a similar geochemical origin, as should be expected on a small archipelago. This factor was considered as important in determining the relationship between these geological groups and the archaeological material. The correlation between elements in the Calcitic reds and the Terra rossae, for example (Figure 5-24), was probably because the former sample group was the likely/closely associated to the parent material to these red soils (Terra rossae). This also explains why the Calcitic reds were more abundant in Ca, and why the Terra rossae were richer in Fe and the other minerals (see Cornell and Schwertmann 2003: 437). The higher proportions of Al and Mg in these Terra rossae could also be representative of the presence of clay minerals, such as kaolinite ($Al_2Si_2O_5(OH)_4$) and/or chlorite group clay minerals ($Mg_5(Al,Fe)(OH_8)(AlSi)_4O_{10}$) which are often present in soils and ochres (Hradil, Grygara et al., 2003; Helwig, 2007: 60; Iriarte, Foyo et al., 2008). These variables were also high in the Ooid group, but much lower in the Calcitic reds and Greensands respectively.

The broader scatter of data points at higher concentration levels was observed for some trace elements and heavy metals in the Terra (soil) group, and was attributed to the presence of some pollutants (Figure App.III-5). Soils are, in fact, often referred to as "pollutant sinks", accumulating in contaminants resulting from the release of fertilisers, human wastes and landfills into the environment, therefore this feature was expected (Adriano, 2001: 2, 4, 29).

The clusters formed by the Calcitic reds and the Terra rossae in the scatter plots plotted at lower or higher ppm levels with respect to one another. Examples of the average log normalised data of some elements are given below. Although it appeared possible to distinguish between these two source groups through observation of their element concentration levels on the clusters in the scatter plots, the elemental ratios were found to be similar and the difference was therefore not considered to be statistically significant (P-value <0.05). This was also observed in the hierarchical cluster as shown on P.169.

	Mean element concentration							
Source	**Al**	**Ti**	**Mn**	**Cr**	**Cu**	**V**	**Zr**	**Li**
CR	0.43	-0.90	-1.67	-2.34	-2.68	-2.39	-2.33	-2.64
TR	0.29	-0.96	-1.81	-2.53	-2.92	-2.55	-2.48	-2.83

Table 6-1. Examination of the Fe ratio log normalised data for some of the elements in the Calcitic reds and the Terra rossae

The other two geological groups (Greensands and Ooids), exhibited significantly different element ratios (P >0.05) to the previous two sample groups and to each other (Table 5-11). They were thus distinguishable on the majority of the bivariate scatter plots as they formed discrete clusters. This feature was also confirmed statistically and has been discussed earlier on P.179. Consequently, only three main geological groups

were confidently identified as being statistically chemically distinct. Intra-source correlation was also attributable to mineral composition and not to sampling proximity as sample acquisition was carried out from the same geological source in very different localities (Figure 4-26).

In summary, these results showed that:

i. Certain elements exhibited strong, statistically significant correlations with each other (P.177);
ii. The geological groups were distinct as separate clusters in a large number of graphs, especially on those scatter plots of elements expected to exhibit positive trends with Fe. Some formations were tighter than others, as stronger trends were seen between several elements in each of these groups (P.172);
iii. The Calcitic reds and the Terra rossae exhibited patterns in data element ratios, though the latter sample group had higher concentrations of minor elements. These two groups were not recognised as separate groups from statistical tests (P.178);
iv. Three of the geological groups therefore satisfied the provenance postulate for this method; where the variation between the different sample groups was greater than the intra-source variation within a given geological source. The groups were divided as follows: CR-TR, Greensands and Ooids (P.178).

6.2.2.2. Sourcing of Maltese archaeological ochres: The archaeological groups

Histograms, graphical representations and statistical tests including both archaeological and/or geological data suggested various factors pertaining to the archaeological samples.

(*a) Differences between archaeological samples.* Inter-group differences in element concentrations were observed between samples as has been highlighted earlier (Chapter 5). Noticeable features included the elevated levels of P_2O_5 observed in the HYPB (mean: 23 wt-%), HYPD (mean: 6.3 wt-%) and yellow MAs (mean: 4 wt-%). This reflected the large quantity of bone mineral, carbonate-hydroxylapatite $Ca_{10}(PO_4)_{6-x}(CO_3)_x(OH)_{2+x}$ (Reiche, Favre-Quattropani et al., 1999), present at the burial site at Hal-Saflieni in these Hypogeum samples. This also suggested that bone was a component of the yellow MA ochres.

The histograms given in Figure 5-29 (P.183) also illustrated the relative weight percent values of some other the major elements of these Maltese Neolithic samples, and showed the correlations and differences in composition between these sample groups. Similarities were observed between the HYPDs and the HYPBs, in the calcium oxide content, for example, although for completely different reasons. While the calcium oxide content in the HYPBs (38 wt-%) reflected bone mineral chemistry, that in the HYPDs (40 wt-%), reflected the calcite from the calcium carbonate-dominant environment and some bone material. The HYPBs were found to consist of very little, if any, ochre. These histogram 5-29 also showed which HYPD samples were richer in bone mineral remains, namely those obtained from chambers C5 and C9 (refer to

Figures 4-29, 4-30), and therefore indicated that these chambers were probably burial chambers. None of these Hypogeum samples, however, appeared to have enough ochre (Fe content >10 wt-%) to support the statement given by Soddart (1999: 183), who claimed that vast amounts of ochre were sprinkled on the bones and reburied in this underground necropolis.

The Fe content also varied significantly and showed that the MA (reds) were ochres of higher quality, based on the assumption that higher ratios of iron and less amounts of other accessory materials implied a better quality of ochre (defined in Chapter 1). Values of iron oxide in these archaeological samples ranged between 51 wt-% and 21 wt-%. These were followed by the yellow MAs (13 – 9.4 wt-%), the HYPDs (<3 wt-%) and lastly by the HYPBs (mean of 0.5 wt-% iron oxide). The yellow MA samples also appeared to contain features characteristic to the other archaeological groups, containing some bone, a good amount of Ca, and reasonably high levels of Fe, yet the relative proportions of elements indicated that this set of archaeological samples was chemically distinct from all the rest. All bivariate plots also showed that these four sets of archaeological samples exhibited good intra-sample data clustering, but had different chemical compositions, therefore inter-group differences were clear.

(b) Archaeology vs. geology. The statistical tests were used to observe how the archaeological sample data fitted in with the geological groups. The results showed that the archaeological MA (reds) consistently coincided with the Ooid data points, with one exception. The Ba scatter plots exhibited slight discrepancies which were more pronounced when the variable was plotted against Cr (Figure 5-32b P.186), Cu,

Li and Sc, and also where Fe was present in higher concentrations (refer to Table 5-15/16). Samples MA 002 and MA 003 therefore experienced a greater divergence of this element from the norm, implying an indirectly proportional relationship with Fe. Although the reason for this discrepancy is uncertain as publications to date do not mention any particular incongruity in Ba amounts, it is possible that substitution of Ba with Ca reflecting the growth environment of the Ooids could be an underlying cause (Pettijohn 1975: 295). It was assumed that the removal of samples from their natural environment resulted in a discontinuation of exchange and fractionation between the constituent elements and their geological environment (Glover, Eick et al. 2002; Miro, Hansen et al. 2005). If the environment experienced an increase in the Ba-Ca content for some particular reason, this would be reflected when comparing samples extracted from the geological environment today to archaeological samples that had been extracted several millennia ago.

The MA (yellows) did not coincide particularly well with any source groups, though this archaeological sample set correlated better with the Greensands than with any other geological source (Figure 5-31a). These trends, however, were not consistent (P-value >0.5) and results suggested that the MA (yellows) were obtained from an alternative source to the Maltese islands. The difference in composition, however, could have also been a result of possible 'contamination' with other materials, such as the bone and the fabric that were undoubtedly present in with the ochre, consequently changing the nature of the material to a certain extent.

A consistent pattern was observed between the major and minor elements of the Calcitic reds-Terra rossae and the HYPD samples. The elemental relationships were

similar, but the major and some minor variables appeared to be present in smaller amounts in the archaeological data when compared with the geological material. This factor was attributed to the observed high levels of phosphorous (Figure 5-30a P.184), which have also been described above. The elements which differed slightly in comparison to the geological groups, namely the variables Ni and Zr, were associated with the bone present within their composition since similarly elevated concentrations were also observed in the HYPBs.

HYPB samples appeared as near-identical discordant outliers in a number of plots, as was expected from this bone-dominant material. The ppm observations of some of the major and minor elements in the bone were also found to approximate those of PIXE studies carried out on emerged archaeological bone, therefore indicating that the two bone samples analysed had probably been disturbed prior to this investigation (Reiche, Favre-Quattropani et al., 1999).

The HYPD (and HYPB) results confirmed that these samples were not particularly ochre-rich. The proximity of their element values to the Terra rossae data however showed that they had undergone only minor changes in material chemistry. These deposits were therefore unlikely to have experienced significant changes in composition, even though the HYPD and Terra rossae were the most likely of the sample groups to have suffered the effects of pollution (as was described earlier). This observation was used to further emphasize the unlikelihood of Terra rossae being the incident source of Neolithic Maltese ochres.

The tests therefore showed various correlations and discrepancies between certain archaeological samples and the Maltese geological groups, as summarised below:

i. The MA (reds) showed definite analogies with the Ooids group, indicating that this could be a likely source for this archaeological ochre.
ii. The MA (yellows) did not correspond well to any geological source.
iii. The HYPDs and the HYPBs exhibited similar trends as the CR-TR. The HYPBs had a different composition, but were closer to this other archaeological and geological group than to any other.

6.2.2.3. Sourcing of Maltese archaeological ochres: The REEs

REEs have often been used in provenancing studies to establish relationships between the archaeological data and geological sources (Glascock and Neff, 2003; Popelka-Filcoff, Robertson et al., 2007; Iriarte, Foyo et al., 2008). All REE data following normalisation (Piper, 1974) indicated that the geological and archaeological ochre groups had formed from very similar environments owing to the near-identical trends observed (Figure 5-36a-f). Although the Eu concentration for the MA (reds) could not be detected (see previously), all the other samples showed a strong negative Eu-anomaly. This was attributed to extensive fractionation of Eu relative to the other REEs possibly because of suspected suboxic/anoxic (Eu^{3+} reduced to Eu^{2+}) conditions in the Maltese and/or Mediterranean terrestrial environment when the sedimentary rocks were being formed (Jarvis, 1989). This paleoindicator factor therefore strongly suggests that even the MA (yellows), which data presented as being the most likely outliers, were related to the geological environment (either the same environment or a similar one) of the Maltese islands.

6.2.2.4. SEM-EDS and XRF

The final two methods used to characterise, to a limited extent, the materials in this study were exploited because of the limited sample quantities and difficulties (ethics) associated with sample acquisition. Although there was a good agreement between the measurements and the ICP-AES data, certain interpretations remain debatable: It has already been established that limiting the number of variables limits the sensitivity of this provenancing method (P.233)

SEM images of the MA red sample (001) and of MA 004 were similar to published results as particle sizes appeared similar (Helwig, 2007: 75-76). MA 005 consisted a mixture of ochre and large quantities of some fibrous material. The EDS values showed that MA 004 was not an ochre, and that MA 001 and MA 005 oxide percentages fitted well with the ICP-AES results from red and yellow ochres respectively.

The XRF data was more difficult to work with, mainly because the number of variables was reduced to a total of five owing to (a) the instrument limitations and percentage errors and (b) the presence of certain elements within the support and their similarities with the ochre-support composition and (c) the assumptions taken when working with the data, including that the support composition was uniform. Bivariate plots of these variables also gave a combination of distinct clusters and less defined groups, which showed potential relationships between element ratios.

The trends observed between the $\log_{10}$(Ti/Fe) - $\log_{10}$(Mn/Fe) in the XRF-stone scatter plots (Figure 5-43 P.204) appeared to correlate particularly well with the CR-TR clusters. Although this could imply an alternative source (other than the Ooids) for these ochres, it is more likely that the values were experiencing an overall dilution effect because of the measurements of the background (support). These reflect the limitations of this non-invasive method, as has been mentioned earlier in section 5.1.5. This justification could also explain the inconsistent relationships experienced in other scatter plots, and why certain points, such as the XRF-clay ratios, matched the Ooids and/or the MA (reds) better (richer support, lower dilution effect experienced). This similarity observed between the XRF-clays and the Ooids/MA (reds), was also inconsistent, and although this could show that ochres on certain artefacts were different to others, it appeared that data was more dependant on the composition of the support, once again confirming that this as a consistent limitation.

The chemical signature of the ochres analysed in this XRF study was, therefore, not well defined, and results were not definitive enough for use in this provenancing study. Although published studies elsewhere have suggested otherwise (Popelka-Filcoff, Robertson et al., 2007), it appears that sampling may be required for this purpose, as XRF analyses in this study were carried out on ground (powdered and prepared) samples of the selected ochres. This sampling method precludes the problematic dilution effect resulting from the background material, but is destructive, and therefore unethical.

6.3. Implications of findings

The characterisation studies also showed a similarity in the composition between the red MA ochres, even though these were obtained from different archaeological sites across the islands. This indicated that these pigments, which had been used so profusely throughout the islands during the Neolithic period (refer to Chapter 2), were probably extracted from the same and/or similar geological source.

The evidence provided in this thesis also suggested that the Ooids, or a source group inherently similar to the Ooids, was the source for these MA reds. Although it is difficult to dismiss the possibility of these ochres as being imported products, the meta-theoretical principle of Occam's razor denotes that the simplest solution is frequently the most probable explanation. These findings thereby suggest that:

i. Sources of ochre on the Maltese islands do exist, therefore disproving conventional belief which claims that there are no such sources on the islands (Tilley, 2004: 140 – also refer to Chapter 2);
ii. The presence and use of ochre in Malta cannot be used to support the theory of trade between the archipelago and mainland Europe during the Neolithic period;
iii. Robb's (2001) arguments of Malta being linked to the rest of Europe through a wide regional network based on the ochre debate are put in question: the use of this pigment cannot be the definite proof for contact (Chapter 2)
iv. Contact with mainland Europe may have been more limited than was commonly believed, and this could help to explain the uniqueness of the Neolithic temples. This also strengthens the hypothesis that biogeography and

the insularity of the islands resulted in the observed cultural differences and could explain why the Neolithic temple architecture remains unparalleled by any of the contemporaries of the Neolithic Maltese.

v. If the Neolithic Maltese understanding of architecture was thought extraordinary, their knowledge of materials was not less so. It is clear that Neolithic Maltese painstakingly not only sourced the purer forms of the ochre, but also sought to prepare the material for use.

The yellow archaeological ochre (MA yellow) sourced for this study was also an important discovery. Further research showed it may have been found and documented in the early twentieth century as a yellow textile that had been wrapped around various bodies in the Bronze Age ancient Tarxien cremation cemetery (Evans, 1971). The find was recorded, albeit briefly, as an unusual discovery in the museum annual reports, and the yellow colour was thought to have been '…perhaps a reddish colour turned yellow through burning' (Annual Report of Valletta Museum, 1916). This statement therefore further emphasised the unusualness of the discovery of this colour associated with ancient burials. The analysis in this study has shown that these MA yellows were a clear mixture of several components, including yellow ochre, deteriorating textile and bone; therefore coherently linking these samples to the reported find. The ochre used, however, could never have been red ochre, as dehydroxylation (by calcination) is an irreversible reaction (Chapter 1) and it is only possible to dehydrate yellow ochre (iron hydroxide) into red ochre (iron oxide). This statement was therefore invalidated. REE measurements showed that this yellow ochre was also obtained from a geological context that was similar to the geology of

the Maltese islands, but minor and trace element analysis either indicated that the nature of the sample had changed, and/or that the source of this material was not the Maltese archipelago. It therefore appears that this yellow ochre find might not be of Neolithic origin, and is definitely not representative of the red ochre used extensively in the Temple period (Mifsud and Ventura, 1999: 14).

This study also showed that the red ochre remains in the Hal-Saflieni Hypogeum were only present in the paintings on the chamber walls. This therefore contradicted the popular belief about burial customs adopted by these Neolithic peoples in relation to the Hypogeum, which claimed that bones were doused in ochre and reburied in the necropolis (Stodart, 1999: 183). There additionally did not appear to be much difference in composition between the ochres from the different chambers in the Hypogeum. No concrete conclusions, however, could be made by comparing element concentrations of ochre on different artefacts as the XRF data was subjective to the support of the ochre in question.

CONCLUSIONS

The results indicated that the methods employed in this thesis satisfied the provenance postulate theory and could be used to characterise and provenance ochre, as was shown through the case study of the ochre on the Maltese islands. Elemental analysis is the key to this, though the final results are compromised when fewer element variables are obtained (observed with results from SEM-EDS and XRF results analysis). PLM and XRD were useful to observe respective optical and structural differences between materials, and the microscopy technique in particular allowed for material grouping and pigment documentation prior to the irreversible process of sample digestion for ICP-AES. The ideal analytical methodology therefore involved combining ICP-AES analysis and statistical tests to identify the elements that correlated positively with the main elemental component of the ochres: Fe. These 'signature' or 'fingerprint' elements were also determined statistically, and included Al, Ti, Zr, Li, Mn, Cr, V, Cu, Zn, La, Ce, Nd and Yb. It was found that limiting the number to 9 or even 7 of these variables (Al, Ti, Mn, Cr, Cu, V and Zr) was sufficient for efficient clustering for provenancing purposes.

Test results therefore identified common patterns between ochre source groups and showed that three geological sources of ochre on the Maltese islands satisfied the provenance postulate. These included the Calcitic reds-Terra rossae (1), the Greensands (2) and the Ooids (3). Applying the same method to the archaeological samples indicated how these samples corresponded to the geological groups. Results showed that the red MA ochres, which were used profusely throughout the Maltese Neolithic/Temple Period, were almost entirely consistent with the Ooid group. This

showed that the Ooids were the most likely source for these MA reds; and that these ochres were probably obtained from the Maltese islands. The MA yellows did not correspond well to any geological source, and further evidence indicated that these ochres may have been Bronze Age finds, rather than Neolithic material. The HYPD and the HYPB samples from the Hal Saflieni Hypogeum also showed that there was little ochre present in these samples. This indicated that apart from its application as artwork on the walls, there was no definite proof that ochre was extensively used during burial practices at this underground necropolis.

The evidence provided in this project therefore shows that there is a consistent correlation between the signature elements in the geological iron-rich Ooid nodules, and the red archaeological ochres from the Maltese islands. Although it is possible that similar Ooid nodules from a near-identical geological environment (e.g. Sicily perhaps?) may have been an alternative source, the findings in this thesis, coupled with archaeological evidence (described below) strongly support the fact that the ochre used extensively in Neolithic Malta was of local origin (Occam's razor) rather than an import during the Temple era (Robb, 2001).

This study therefore provides scientific evidence to show that Malta was probably a physically isolated space during the Temple period. This evidence is also supported by the vast majority of archaeological evidence that highlights this missing link to mainland Europe, thus clearly supporting the argument for a "local evolution" (Evans 1953). Corroborating archaeological evidence includes (1) the absence of any similarity between the Megalithic Temples and other architecture in Sicily and/or in

Europe. The analogy observed by Robb between the rock-cut tomb in Calaforno and Hal Saflieni in Malta, though presenting a good argument, cannot possibly equal the complexity and abundance of the above-ground temples constructed on the Maltese islands in any way. (2) Further archaeological evidence is provided by the difference observed in ceramic-ware, which was very specialised and local on the archipelago, presenting obvious gaps in ceramic evidence for trade. (3) Finally, the decrease in quantities of imported products also supports this argument for isolation, although it is suggested that further studies should be carried out on other (few) suspected imports, such as the flints and/or hardstones.

"The ancient Maltese culture, which, despite local variations, had hitherto marched step by step with that of Sicily, now continued to develop on its own, showing scarcely a trace of connections with Sicily until it was finally swept away by a new influx of people from abroad some centuries later (Evans, 1953: 80)

This project therefore helps us reconstruct a satisfactory picture of Maltese Neolithic prehistory by providing evidence that undeniably fills gaps in our knowledge. Although current evidence cannot explain the reason for the break between the archipelago and mainland Europe, this study is definitely a start to the unravelling the mystery surrounding these tiny but all important group of islands.

This study is a first in its kind in that it provides an in-depth investigation of Maltese ochres, and supplies a valuable dataset for forthcoming research. Future projects to support the arguments and hypotheses discussed in this thesis with regards to trade

during the Maltese Temple period could include looking for further evidence by applying the same method to similar ochre deposits possibly present in Sicily. The study could also be broadened by examining sources further afield in southern Italy, and in other localities Malta was suspected to have been trading with during the pre- and post-Temple era. A full, in-depth comparison between geological sources is suggested, with Sicily, however, being the most likely source, owing to a similar geology to that of the Maltese islands (Schembri, 1993: 28). Further studies would include comparing the ochre used in Neolithic Sicily and southern Italy to the Neolithic ochre from Malta. It is also recommended that the results are corroborated with provenancing studies carried out on other items that could have been traded during the Maltese Temple Period, such as hardstones and flint. Future work could therefore additionally include applying the same or a similar methodology to ochres found at other ancient sites and comparing the elemental data to their suspected sources, thereby possibly also mapping ochre trade across Europe and further afield.

References

Abanda, P. A. and R. E. Hannigan (2006). "Effect of diagenesis on trace element partitioning in shales." Chemical Geology **230** 42–59.

Action (2004). Non-destructive analysis and testing of museum objects. COST Action G8. M. C. o. t. Action**:** 17.

Adriaens, A. (2005). "Non-destructive analysis and testing of museum objects: An overview of 5 years of research." Spectrochimica Acta **Part B**(60): 1503-1516.

Adriano, D. C. (2001). Trace elements in terrestrial environments: Geochemistry, bioavailability and risks of metals. N.Y., Springer-Verlag.

Afia, M. S. and A. A. H. (trans) (1996). Extraction and use of minerals and rocks along the Egyptian civilizations. Egypt, Egyptian Geological Survey.

Aitchison, J., C. Barcelo-Vidal, et al. (2002). "Some comments on compositional data analysis in archaeometry, in particular the fallacies in Tangri and Wright's dismissal of logratio analysis." Archaeometry **44**(2): 295-304.

Aldred, C. (1994). Akhenaten: King of Egypt. London, Thames and Husdon Ltd.

Aldred, C. (1994). Egyptian art in the days of the pharaohs. London Thames and Hudson Ltd.

Aldred, C. (1994). The Egyptians. London, Thames and Hudson Ltd.

Aloupi, E., A. Karydas, et al. (2000). "Pigment analysis of wall paintings and ceramics from Greece and Cyprus. The optimum use of X-ray spectrometry on specific archaeological issues." X-ray Spectrometry **29**: 18-24.

Alvarez, M., E. H. Rueda, et al. (2007). "Simultaneous incorporation of Mn and Al in the goethite structure." Geochimica et Cosmochimica Acta **71**: 1009–1020.

Ambers, J. (2004). "Raman analysis of pigments from the Egyptian Old Kingdom." Journal of Raman Spectroscopy **35**: 768-773.

Andel, T. H. v. (1998). "Paleosols, red sediments, and the old Stone Age in Greece." Geoarchaeology: An International Journal **13**(4): 361-390.

Andrikopoulos, K. S., S. Daniilia, et al. (2006). "*In vitro* validation of a mobile Raman-XRF micro-analytical instrument's capabilities on the diagnosis of Byzantine icons." Journal of Raman Spectroscopy **37**: 1026-1034.

Ashok, R., ed. (1993). Artists' pigments, a handbook of their history and characteristics. Washington, National Gallery of Art.

Aslanov, L. A., G. V. Fetisov, et al. (1998). Crystallographic instrumentation. New York, Oxford University Press.

Barba, L., J. Blancas, et al. (2008). "Provenance of the limestone used in Teotihuacan (Mexico): A methodological approach." Archaeometry **50**.

Barbe, J. G. and K. J. Smith (2001). Raman spectroscopy and art authentication. 29th Annual Meeting of the AIC, Dallas, Texas, Paintings Speciality Group.

Barber, C. (1974). "Major and trace element associations in limestones and dolomites." Chemical Geology **14**: 273-280.

Baronti, S., A. Casini, et al. (1997). "Principal component analysis of visible and near-infrared multispectral images of works of art." Chemometrics and Intelligent Laboratory Systems **39** 103-114.

Barrowclough, D. A. and C. Malone (2007). Cult in context: Reconsidering ritual in archaeology, Oxbow books.

Bartick, E. (2002). Forensic analysis by Raman spectroscopy: An emerging technology. 16th Meeting of the International Association of Forensic Sciences, Monduzzi Editore S.p.A. - Medimond Inc.

Basta, N. T., J. A. Ryan, et al. (2005). "Trace element chemistry in residual-treated soil: Key concepts and metal bioavailability." J. Environ. Qual **34**: 49–63.

Bednarik, R. (1994). "A taphonomy of Palaeoart." Antiquity **68**: 68-74.

Berger, R., ed. (1970). Scientific methods in Medieval archaeology. California, University of California Press.

Bernal, J. P., S. M. Eggins, et al. (2006). "Dating of chemical weathering processes by in situ measurement of U-series disequilibria in supergene Fe-oxy/hydroxides using LA-MC-ICPMS." Chemical Geology **235**: 76-94.

Bersani, D., P. P. Lottici, et al. (2004). "Pigments and binders in the wall paintings of Santa Maria della Steccata in Parma (Italy): the ultimate technique of Parmigianino." Journal of Raman Spectroscopy **35**: 694-703.

Beveridge, A., T. Fung, et al. (2001). Use of infrared spectroscopy for the characterisation of paint fragments. Forensic Examination of Glass and Paint. B. Caddy. London, Taylor&Francis**:** 183-241.

Bieber, A. M., D. W. Brooks, et al. (1976). "Application of multivariate techniques to analytical data on Aegean ceramics." Archaeometry **18**(1): 59-74.

Bischof, G. (1854). Chemical and physical geology, Cavendish society.

Blanckenburg, F. v., M. Mamberti, et al. (2008). "The iron isotope composition of microbial carbonate." Chemical Geology **249** (2): 113–1.

Boivin, N. (2004). From veneration to exploitation: Human engagement with the mineral world. Soils, Stones and Symbols: Cultural Perceptions of the Mineral World. N. Boivin and M. A. Owoc. London, UCL**:** 1-29.

Bonanno, A. (1986). A socio-economic approach to Maltese prehistory. The temple builders. Malta Studies of its Heritage and History. Malta, Mid Med Bank.

Bonanno, A. (1991). Malta's changing role in Mediterranean cross-currents. From prehistory to Roman times. Malta: a Case Study in International Cross-currents. S. Fiorini and V. M. Milanes. Malta**:** 1-12.

Boschian, G. (1997). "Sedimentology and soil micromorphology of the late pleistocene and early holocene deposits of Grotta dell'Edera (Trieste Karst, NE Italy)." Geoarchaeology: An International Journal **12**(3): 227-249.

Brenner, M., J. O. Lill, et al. (2004). "PIXE analyses of pigments in eighteenth-century furniture and interior painting." Studies in Conservation **49**: 99-106.

Brill, R. H. (1999). Chemical analysis of early glasses - the catalogue. New York, The Corning Museum of Glass.

Brissaud, I., G. Lagarde, et al. (1996). "Study of multilayers by PIXE technique. Application to paintings." Nuclear Instruments and Methods in Physics Research **117**: 179-185.

Broadhurst, A. (2002). A novel approach to non-destructive depth profiling. Department of Materials and Medical Sciences. Shrivenham, Cranfield University. **MPhil/PhD**.

Brundle, C. R., C. A. Evans, et al. (1992). Encyclopedia of materials characterization, surfaces, interfaces, thin films. Oxford, Batterworth-Heinemann.

Budzyń, B., C. J. Hetherington, et al. (2008). "Application of electron probe microanalysis Th–U–total Pb geochronology to provenance studies of sedimentary rocks: An example from the Carpathian flysch." Chemical Geology **254** 148–163.

Burgio, L. (2000). Analysis of pigments on art objects by Raman microscopy and other techniques. London, University College. **PhD:** 225.

Burgio, L., D. A. Ciomartan, et al. (1997). "Raman microscopy study of the pigments on three illuminated mediaeval latin manuscripts." Journal of Raman Spectroscopy **28**: 79-83.

Burrafato, G., M. Calabrese, et al. (2004). "ColoRaman project: Raman and fluorescence spectroscopy of oil, tempera and fresco paint pigments." Journal of Raman Spectroscopy **35**: 879-886.

Buxbaum, G. and G. Pfaff (2005). Industrial inorganic pigments. Weinheim, Wiley-VCH Verlag GmbH & Co KGaA.

Buzzini, P., G. Massonnet, et al. (2006). "The micro Raman analysis of paint evidence in criminalistics: case studies." Journal of Raman Spectroscopy **37**: 922-931.

Campbell, J. L., J. A. Cookson, et al. (1983). "Uncertainties in thick-target PIXE Analysis." Nuclear Instruments and Methods **212**: 427-439.

Campbell, R. (1936). A dictionary of assyrial chemistry and geology. London, Thompson Clarendon Press.

Carney, M. D. and P. J. Mienie (2003). "A geological comparison of the Sishen and Sishen South (Welgevonden) iron ore deposits, Northern Cape Province, South Africa." Applied Earth Science **112** (B): 81-87.

Cassar, J. and S. Vannucci (2001). "Petrographical and chemical research on the stone of the megalithic temples." Malta Archaeological Review(5).

Castro, K., M. Perez-Alonso, et al. (2004). "Pigment analysis of a wallpaper from the early 19th century: *Les Monuments de Paris*." Journal of Raman Spectroscopy **35**: 704-709.

Castro, K., M. D. Rodriguez-Laso, et al. (2001). "Fourier transform Raman spectrscopic study of pigments present in decorative wallpapers of the middle nineteenth century from the Santa Isabel Factory (Vitoria, Basque Country, Spain)." Journal of Raman Spectroscopy **33**: 17-25.

Centeno, S. A., V. Llado Buisan, et al. (2006). "Raman study of synthetic organic pigments and dyes in early lithographic inks (1980-1920)." Journal of Raman Spectroscopy **37**: 1111-1118.

Centeno, S. A., D. Mahon, et al. (2004). "Examination of a Spanish medieval processional crucifix substantially reworked in the 20th century." Journal of Raman Spectroscopy **35**: 774-780.

Cesareo, R., A. Castellano, et al. (2004). "Giotto in the chapel of the Scrovegni: EDXRF analysis of the golden haloes with portable equipment." X-ray Spectrometry **33**: 289-293.

Cesareo, R., A. Castellano, et al. (1998). "Energy dispersive X-ray fluorescence analysis of thin and intermediate environmental samples." X-ray Spectrometry **27**: 257-264.

Chalmin, E., C. Vignaud, et al. (2004). "Palaeolithic painting matter: natural or heat-treated pigment?" Appl. Phys. A **79**: 187-191.

Chiari, G. and M. Leona (2005). "The state of conservation science." Conservation, the GCI Newsletter **20**(2): 5-9.

Chitrakar, R., S. Tezuka, et al. (2006). "Phosphate adsorption on synthetic goethite and akaganeite." Journal of Colloid and Interface Science **298** 602-608.

Clark, R. J. H. and J. Van der Weerd (2004). "Identification of pigments and gemstones n the Tours Gospel: the early 9th century Carolingian paletter." Journal of Raman Spectroscopy **35**: 279-283.

Clout, J. M. F. (2006). "Iron formation-hosted iron ores in the Hamersley Province of Western Australia." Applied Earth Science **115**(4): 115 – 125.

Coates, J. (2000). Interpretation of infrared spectra, A practical approach. Encyclopedia of Analytical Chemistry. R. A. Meyers. Chichester, John Wiley & Sons Ltd**:** 10815–10837.

Colinart, S., E. Delange, et al. (1996). Colours and pigments of the Ancient Egypt.

Colman, T. B. and D. C. Cooper (2000). Exploration for metalliferous and related minerals in Britain: A guide. British Geological Survey, NERC.

Colombini, M. P., G. Giachi, et al. (2003). "The characterization of paints and waterproofing materials from the shipwrecks found at the archaeological site of the Etruscan and Roman harbour of Pisa (Italy)." Archaeometry **45**: 659-674.

Conklin, A. R. (2005). Chemical analysis: A series of monographs on analytical chemistry and its applications. Introuction to Soil Chemistry: Analysis and Instumentation. J. D. Winefordner. New Jersey, John Wiley & Sons, Inc. **167**

Cookson, J. A. and J. L. Campbell (1983). "Specimen surface effects in thick-target PIXE analysis." Nuclear Instruments and Methods **216**: 489-495.

Cope, J. (2004). The megaltithic European. London, Element, Harper Collins Publishers.

Cornell, R. M. and U. Schwertmann (2003). The iron oxides: structure, properties, reactions, occurrences, and uses. Weinheim, Wiley-VCH.

Costa, G. M. D. and M. F. D. J. Filho (1992). "X-ray differential line broadening on tabular haematites." Journal of materials science **27**: 6116-6122.

Coupry, C., A. Lautie, et al. (1994). "Contribution of Raman spectroscopy to art and history." Journal of Raman Spectroscopy **25**: 89-94.

Creagh, D. C., M. E. Kubik, et al. (2007). "On the feasibility of establishing the provenance of Australian Aboriginal artefacts using synchrotron radiation X-ray diffraction and proton-induced X-ray emission." Nuclear Instruments and Methods in Physics Research A **580** 721-724.

Cudennec, Y. and A. Lecerf (2006). "The transformation of ferrihydrite into goethite or hematite, revisited." Journal of Solid State Chemistry **179** 716–722.

Cullity, B. D. (1978). Elements of X-ray diffraction. Philippenes, Addison-Wesley Publishing Company, Inc.

D.Stafford, M., G. C.Frison, et al. (2003). "Digging for the color of life: Paleoindian red ochre mining at the Powars II Site, Platte County, Wyoming, U.S.A." Geoarchaeology: An International Journal **18**(1): 71-90.

D'Andrea Cennini, C. (1954). The craftsman's handbook: Il libro dell' arte. New York, Dover.

Damiani, D., E. Gliozzo, et al. (2003). "Pigments and plasters discovered in the house of Diana (*Cosa*, Grosseto, Italy): An integrated study between art history, archaeology and scientific analyses." Archaeometry **45**: 341-354.

Danielson, A., P. Moller, et al. (1992). "The europium anomalies in banded iron formations and the thermal history of the oceanic crust." Chemical Geology **97** 89-100.

Daniilia, S., D. Bikiaris, et al. (2002). "An extensive non-destructive an micro-spectroscopic study of two post-Byzantine overpainted icons of the 16th century." Journal of Raman Spectroscopy **33**: 807-814.

Davey, R., D. J. Gardiner, et al. (1994). "Examples of pigments from fine art objects by raman microscopy." Journal of Raman Spectroscopy **25**: 53-57.

Davies, W. V. (2001). Colour and painting in ancient Egypt. London, The Trustees of the British Museum.

Dawood, Y., H. A. El-Naby, et al. (2004). "Influence of the alteration processes on the origin of uranium and europium anomalies in trachyte, central Eastern Desert, Egypt." Journal of Geochemical Exploration **81**(1-3): 15-27.

de Gelder, J., P. Vandenabeele, et al. (2005). "Forensic analysis of automotive paints by Raman spectroscopy." Journal of Raman Spectroscopy **36**: 1059-1067.

Deer, W. A., R. A. Howie, et al. (1966). An introduction to the rock-forming minerals U.K., Longmans, Green and Co. Ltd.

Delhez, R., T. H. de Keijser, et al. (1988). "Structure and properties of surface layers: X-ray diffraction studies." Aust. J. Phys. **41**: 261-282.

Derbyshire, A. and R. Withnall (1999). "Pigment analysis of portrait miniatures using raman microscopy." Journal of Raman Spectroscopy **30**: 185-188.

Derrick, M. R., D. Stulik, et al. (1999). Infrared spectroscopy in conservation science. Los Angeles, The J. Paul Getty Trust.

Domenech, A., M. T. Domenech-Carbo, et al. (2007). "Identification of earth pigments by applying hierarchical cluster analysis to solid state voltammetry. Application to severely damaged frescoes." Electroanalysis **19**(18): 1890 – 1900.

Drake, A. and K. Moore (2006). "Ways of seeing: Fourier transform Raman spectroscopy in the examination of artist's materials." The Internet Journal of Vibrational Spectroscopy **2**(2): 1-22.

Eastaugh, N., V. Walsh, et al. (2004). Pigment compendium: A dictionary of historical pigments. Oxford, Butterworth-Heinemann.

Eastaugh, N., V. Walsh, et al. (2004). Pigment compendium: optical microscopy of historical pigments. Oxford, Gulf Professional Publishing.

Edwards, H. G. M., C. J. Brooke, et al. (1997). "Fourier transform Raman spectrscopic study of pigments from English mediaeval wall paintings." Journal of Raman Spectroscopy **28**: 95-98.

Edwards, H. G. M., L. Drummond, et al. (1999). "Fourier transform Raman spectrscopic study of prehistoric rock paintings from the Big Bend Regon, Texas." Journal of Raman Spectroscopy **30**: 421-428.

Edwards, H. G. M., D. W. Farwell, et al. (1999). "Raman spectroscopic study of red pigment and fresco fragments from Kinf Herod's Palace at Jericho." Journal of Raman Spectroscopy **30**: 361-366.

Edwards, H. G. M., D. W. Farwell, et al. (1999). "Spanish mediaeval frescoes at Basconcillos sel Tozo: a fourier transform Raman spectroscopic study." Journal of Raman Spectroscopy **30**: 307-311.

Edwards, H. G. M., E. R. Gwyer, et al. (1997). "Fourier transform Raman analysis of paint fagments from biodeterioratied Renaissance frescoes." Journal of Raman Spectroscopy **28**: 677-684.

Edwards, R. and K. Atkinson (1986). Ore deposit geology and its influence on mineral exploration. London, Chapman and Hall.

Einsele, G. (2000). Sedimentary basins: evolution, facies, and sediment budget. U.K., Springer.

Einwögerer, T., H. Friesinger, et al. (2006). "Upper Palaeolithic infant burials." Nature **444**(16): 285.

Eremin, K., J. Stenger, et al. (2006). "Raman spectroscopy of Japanese artists' materials: *The Tale of Genji* by Tosa Mitsunobu." Journal of Raman Spectroscopy **37**: 1119-1124.

Erlandson, J. M., J. D. Robertson, et al. (1999). "Geochemical analysis of eight red ochres from western North America." American Antiquity **64**(3): 517-526.

Evans, A. M. (1993). Ore geology and industrial minerals an introduction. U.K., Blackwell Scientific Publications.

Evans, E. D. (1953). The prehistoric culture- sequence in the Maltese archipelago. Prehistoric Society.

Evans, J. D. (1971). Prehistoric antiquities of the Maltese islands. London, Athlone.

Evans, J. D. (1976). "Archaeological evidence for religious practices in the Maltese Islands during the Neolithic and Copper Ages." Kokalos **22**: 130 - 146.

Evans, J. D. (1977). "Island archaeology in the Mediterranean: problems and opportunities." World Archaeology **9**(12-25).

Evans, J. D. (1984). Maltese prehistory: a reappraisal. The Deya Conference of Prehistory: Early Settlement in the Western Mediterranean Islands and their Peripheral Areas. W. Waldren. Oxford, British Archaeological Reports**:** 490 – 497.

Everitt, B. S., G. Dunn, et al. (1991). Applied multivariate data analysis. Great Britain, A divivsion of Hodder & Stoughton.

Fan, H., B. Song, et al. (2006). "Thermal behavior of goethite during transformation to hematite." Materials Chemistry and Physics **98** 148–153.

Feller, R. L., ed. (1986). Artists' pigments, a handbook of their history and characteristics. Washington, National Gallery of Art.

Fenech, K. (2007). Human-induced changes in the environment and landscape of the Maltese islands from the Neolithic to the 15th century AD as inferred from a scientific study of sediments from Marsa, Malta. Oxford, BAR International Series 1682.

Ferrero, J. L., C. Roldan, et al. (2002). "Analysis of pigments from Spanish works of art using a portable EDXRF spectrometer." X-ray Spectrometry **31**: 441-447.

Ferretti, M. (1993). Scientific investigations of works of art. Rome, ICCROM.

Forenbahe, S. (1993). "Radiocarbon dates and absolute chronology of the central European Early Bronze Age." Antiquity **67**(218-20): 235-56.

Fremout, W., S. Saverwyns, et al. (2006). "Non-destructive micro-Raman and X-ray fluorescence spectroscopy on pre-Eyckian works of art - verification with the results obtained by destructive methods." Journal of Raman Spectroscopy **37**: 1035-1045.

Friedel, J. and U. Schwertmann (1996). "Aluminium influence on iron oxides: XVIII. The effect of Al substitution and crystal size on magnetic hyperfine fields of natural goethites." Clay Minerals **31**: 455-464.

Fritzsche, A., B. Pagels, et al. (2006). "Interferences on reductive dissolution and precipitation of iron (hydr)oxides in soils." Geophysical Research Abstracts **8**: 1-2.

Frost, R. L., Z. Ding, et al. (2003). "Thermal analysis of goethite: relevance to Australian indigenous art." Journal of Thermal Analysis and Calorimetry **71** 783–797.

Gardiner, W., M. Grasso, et al. (1995). "Plio-pleistocene fault movement as evidence for mega-block kinematics within the Hyblean-Malta plateau, central Mediterranean " J. Geodynamics **19**(1): 35-51.

Glascock, M. D. and H. Neff (2003). "Neutron activation analysis and provenance research in archaeology." Meas. Sci. Technol. **14** 1516–1526.

Goldstein, J. I. (1992). Scanning electron microscopy and X-ray microanalysis London and New York, Plenum.

Gombrich, E. H. (1995). The story of art. London, Phaidon Press.

Goni-Elizalde, S. and M. E. Garcia-Clavel (1990). "Characterization studies of goethite samples of varying crystallinity obtained by the homogeneous precipitation method." J. Am. Ceram. Soc. **73**(1): 1-26.

Goodall, R. A., J. Hall, et al. (2006). "Raman microscopic investigation of paint samples from the *Rosalila* building, Copan, Honduras." Journal of Raman Spectroscopy **37**: 1072-1077.

Goodhew, P. J., J. Humphreys, et al. (2001). Electron microscopy and analysis. London, Taylor & Francis.

Goss, C. J. (1987). "The kinetics and reaction mechanism of the goethite to hematite transformation." Mineralogical Magazine **51**: 437–51.

Grassi, N., A. Migliori, et al. (2004). "Identification of lapis-lazuli pigments in paint layers by PIGE measurements." nuclear Instruments and Methods in Physics Research **219 - 220**: 48 - 52.

Grassi, N., A. Migliori, et al. (2005). "Differential PIXE measurements for the stratigraphic analysis of the painting *Madonna dei fusi* by Leonardo da Vinci." X-ray Spectrometry **34**: 306-309.

Gualtieri, A. and P. Venturelli (1999). "In situ study of the goethite-hematite phase transformation by real time synchrotron powder diffraction." American Mineralogist **84**: 895–904.

Guthrie, R. D. (2005). The nature of Palaeolithic art. USA, University of Chicago Press.

Hahn, O., B. Kannigieber, et al. (2005). "X-ray fluorescence analysis of iron gall inks, pencils and coloured crayons." Studies in Conservation **50**: 23-32.

Hahn, O., D. Oltrogge, et al. (2004). "Coloured prints of the 16th century: Non-destructive Analysis on coloured engravings from Albrecht Durer and contemporary artists." Archaeometry **46**: 273-282.

Hainsworth, S. (2004). "Paint tribology." 2004.

Hall, K., I. Meiklejohn, et al. (2007). "The thermal responses of rock art pigments: Implications for rock art weathering in southern Africa." Geomorphology **91** 132–145.

Hammond, C. (1990). Introduction to crystallography. Oxford, Royal Microscopy Society.

Hanke, L. D. (2001). Handbook of analytical methods for materials. Plymouth, Materials Evolution and Engineering, Inc.

Hansen, E. F., S. Walston, et al. (1994). Matte paint: its history and technology, analysis, properties, and conservation treatment with special emphasis on ethnographic objects. Los Angeles, Getty Trust Publications.

Hawkesworth, C. J. and A. I. S. Kemp (2006). "The differentiation and rates of generation of the continental crust." Chemical Geology **226** 134- 143.

Helwig, K. (2007). Iron oxide pigments: Natural and synthetic. Artists' Pigments: A Handbook of Their History and Characteristics. B. H. Berrie. Oxford, Archetype Publications. **4:** 39 – 109.

Herbst, W., K. Hunger, et al. (2004). Industrial organic pigments: Production, properties, applications. Weinheim, WILEY-VCH Verlag GmbH & Co. KGaA.

Hernanz, A., J. Gavira-Vallejo, et al. (2006). "Introduction to Raman microscopy of prehistoric rock paintings from the Sierra de las Cuerdas, Cuenca, Spain." Journal of Raman Spectroscopy **37**: 1054-1062.

Hernanz, A., M. Mas, et al. (2006). "Raman microscopy and IR spectrosopy of prehistoric paintings from Los Murcielagos cave (Zuheros, Cordoba, Spain)." Journal of Raman Spectroscopy **37**: 492-497.

Houot, S. and J. Berthelin (1992). "Submicroscopic studies of iron deposits occurring in field drains: formation and evolution." Geoderma **52** 209-222.

Hovers, E., S. Ilani, et al. (2003). "An early case of color symbolism: Ochre use by modern humans in Qafzeh cave." Current Anthropology **44**(4): 491-522

Hradil, D., T. Grygara, et al. (2003). "Clay and iron oxide pigments in the history of painting." Applied Clay Science **22** 223- 236.

Hsu, C. P. S. (2002). Infrared spectroscopy. Handbook of Instrumental Techniques for Analytical Chemistry.

Hu, Z. and S. Gao (2008). "Upper crustal abundances of trace elements: A revision and update." Chemical Geology **253** 205–221.

Ida, H. and J. Kawai (2005). "Portable X-ray fluorescence spectrometer with a pyroelectric X-ray generator." X-ray Spectrometry **34**: 225-229.

Iriarte, E., A. Foyo, et al. (2008). "The origin and geochemical characterization of red ochres from the Tito Bustillo and Monte Castillo Caves (Northern Spain)." Archaeometry.

James, T. G. H. (1979). An introduction to ancient Egypt. London, The Trustees of the British Museum Publications Ltd.

Jarvis, K. E. (1989). "Determination of rare earth elements in geological samples by inductively coupled plasma mass spectrometry." Journal of analytical atomic spectometry **4**.

Jones, A. (2004). "Archaeometry and materiality: Materials-based analysis in theory and practice." Archaeometry **46**: 327-338.

Jorge Villar, S. E., H. G. M. Edwards, et al. (2006). "Raman spectroscopic analysis of medieval wall paintings in the Palencia region, Spain." Journal of Raman Spectroscopy **37**: 1078-1085.

Juliá, C. G. and C. P. Bonafé (2004). "The use of natural earths in picture: study and differentiation by thermal analysis." Thermochimica Acta **413** 185–192.

Kalish, R. and G. Bahir (1983). "PIXE analysis of compound materials." Nuclear Instruments and Methods in Physics Research **218**: 415-419.

Kaminska, A., M. Sawczak, et al. (2006). "Pigment identification of a XIV/XV c. wooden crucifix by means of the Raman spectroscopic technique." Journal of Raman Spectroscopy **37**: 1125-1130.

Kannigieber, B., W. Malzer, et al. (2005). "Three-dimensional micro-XRF investigations of paint layers with a tabletop setup." Spectrochimica Acta Part B **60**: 41-47.

Kato, Y., I. Ohta, et al. (1998). "Rare earth element variations in mid-Archean banded iron formations: Implications for the chemistry of ocean and continent and plate tectonics." Geochimica et Cosmochimica Acta **62**(21/22): 3475–3497.

Kemp, B. J., S. Garfi, et al. (1993). A survey of the ancient city of El – 'Amarna. London, The Egypt Exploration Society.

Kendix, E., O. F. Nielsen, et al. (2004). "The use of micro-Raman spectroscopy in architectural paint analysis." Journal of Raman Spectroscopy **35**: 796-799.

Kerschner, M., H. Mommsen, et al. (1993). "Neutron activation analysis of bird bowls and related archaic ceramics from Miletus." Archaeometry **35**(2): 197-210.

Kiddera, D. L., R.Krishnaswamy, et al. (2003). "Elemental mobility in phosphatic shales during concretion growth and implications for provenance analysis." Chemical Geology **198** 335– 353.

Kimberley, M. (1979). "Geochemical distinctions among environmental types of iron formations." Chemical Geology **25** 185-212.

Klockenkamper, R., A. von Bohlen, et al. (2000). "Analysis of pigments and inks on oil paintings and historical manuscripts using total reflection X-ray fluorescence spectrometry." X-ray Spectrometry **29**: 119-129.

Krekel, C. and K. Polborn (2003). "Lime blue - A medieval pigment for wall paintings?" Studies in Conservation **48**: 171-182.

Lambourne, R. and T. A. Strivens (1999). Paint and surface coatings. USA, William Andrew Publishing Ltd.

Lang, D. M. (1960). Soils of Malta and Gozo. London, HMSO.

Lawrence, M. G., A. Greig, et al. (2006). "Direct quantification of rare earth element concentrations in natural waters by ICP-MS." Applied Geochemistry **21** 839–848.

Leakley, L. S. B. (1962). "The Olduvai discoveries." Antiquity **34**: 119-122.

Learner, T. J. S. (2004). Analysis of modern paints. Los Angeles, J.Paul Getty Trust.

Leona, M., F. Casadio, et al. (2004). "Identification of the pre-Colombian pigment Maya blue on works of art by non-invasive UV-VIS and Raman spectroscopic techniques." JAIC **43**: 39-54.

Lepot, L., S. Denoel, et al. (2006). "The technique of the mural paintings of the Tournai Cathedral." Journal of Raman Spectroscopy **37**: 1098-1103.

Lill, J. O., M. Strom, et al. (2002). "Ion beam characterisation of paint layers made according to late 18th century techniques." Nuclear Instruments and Methods in Physics Research **189**: 303-307.

Lines, S. R. (2006). "Examination of a "Velasco" signature on an oil painting." J Forensic Sci **51**(4): 929-933.

Loffler, L. and W. Mader (2006). "Anisotropic X-ray peak broadening and twin formation in hematite derived from natural and synthetic goethite." Journal of the European Ceramic Society **26** 131–139.

Lombard, M. (2007). "The gripping nature of ochre: The association of ochre with Howiesons Poort adhesives and later Stone Age mastics from South Africa." Journal of Human Evolution **53** 406-419.

Lucas, A. and J. R. Harris (1999). Ancient Egyptian materials and industries. USA, Dover Publications.

Luo, J. and J. Tao (1996). "Quantitative X-ray diffraction analysis of surface layers by computed depth profiling." Thin Solid Films **279**: 53-58.

Lyman, C. E., et al. (1990). Scanning electron microscopy, X-ray microanalysis, and analytical electron microscopy, a laboratory workbook New York, Plenum Press.

Macdonald, A. M. and P. Wyeth (2006). "On the use of photobleaching to reduce fluorescence background in Raman spectroscopy to improve the reliability of pigment identification on painted tectiles." Journal of Raman Spectroscopy **37**: 830-835.

MacDonald, B., R. G. V. Hancock, et al. (2008). "Neutron activation analysis of archaeologcail ochres from coastal British Columbia." Antiquity **82**(316).

Mackay, A. and A. Welz (2007). "Engraved ochre from a middle Stone Age context at Klein Kliphuis in the western Cape of South Africa." Journal of Archaeological Science **35**(6): 1521-1532

Manceau, A., M. L. Schlegel, et al. (2000). "Crystal chemistry of trace elements in natural and synthetic goethite." Geochimica et Cosmochimica Acta **64**(21): 3643–3661.

Mando, P. A. (1994). "Advantages and limitations of external beams in applications to arts and archaeology, geology and environmental problems." Nuclear Instruments and Methods in Physics Research **85**: 815-823.

Maniscalco, L. (1989). "Ocher containers in the central Mediterranean Copper Age." American Journal of Archaeology **93**(4): 537-541.

Marmolejo-Rodríguez, A. J., R. Prego, et al. (2007). "Rare earth elements in iron oxy−hydroxide rich sediments from the Marabasco River-Estuary System (pacific coast of Mexico). REE affinity with iron and aluminium." Journal of Geochemical Exploration **94**(1-3): 43-51.

Maynard, J. B. (1983). Geochemistry of sedimentary ore deposits. New York, Springer-Verlag.

Mazeina, L. and A. Navrotsky (2007). "Enthalpy of water adsorption and surface enthalpy of goethite (r-FeOOH) and hematite (r-Fe2O3)." Chem. Mater. **19**: 825-833.

Mazzeo, R., P. Baraldi, et al. (2004). "Characterization of mural painting pigments from the Thubchen Lakhang temple in Lo Manthang, Nepal." Journal of Raman Spectroscopy **35**: 678-685.

Mazzeo, R., E. Joseph, et al. (2006). "Scientific investigations of the Tokhung-Ri tomb mural paintings (408 A.D.) of the Koguryo era, Democratic People's Republic of Korea." Journal of Raman Spectroscopy **37**: 1086-1097.

Merrifield, M. P. (2003). Medieval and Renaissance treatises on the arts of painting: Original texts with English translations (history of art). U.K., Dover Publications Inc.

Minzoni-Deroche, A., M. Menu, et al. (1995). "The working of pigment during the Aurignacian evidence from Ucagizli cave (Turkey)." Antiquity **69**: 153-8.

Mioc, U. B., P. Colomban, et al. (2004). "Ochre decor and cinnabar residues in Neolithic pottery from Vinca, Serbia." J. Raman Spectrosc. **35**: 843–846.

Moioli, P. and C. Seccaroni (2000). "Analysis of art objects using a portable X-ray fluorescence spectrometer." X-ray Spectrometry **29**: 48-52.

Mongelli, G. and P. Acquafredda (1999). "Ferruginous concretions in a Late Cretaceous karst bauxite: composition and conditions of formation." Chemical Geology **158**: 315–320.

Morris, R. C. (1998). "BIF-hosted iron ore deposits – Hamersley style." AGSO Journal of Australian Geology & Geophysics **17**(4): 207-211.

Moser, M., I. F. Bubb, et al. (1998). "Applications of external beam PIXE at RMIT." Nuclear Instruments and Methods in Physics Research **139**: 164-168.

Murad, E. and U. Schwertmann (1983). "The influence of aluminium substitution and crystallinity on the mossbauer spectra of goethite." Clay Minerals **18**: 301-312.

Nakai, I., S. Yamada, et al. (2005). "Development of a portable X-ray fluorescence spectrometer equipped with two monochromatic x-ray sources and silicon drift detector and field analysis of Islamic glasses at an excavation site in Egypt." X-ray Spectrometry **34**: 46-51.

Nakamura, N. (1974). "Determination of REE, Ba, Fe, Mg, Na and K in carbonaceous and ordinary chondrites." Geochimica e cosmochimica acta **38**: 757-775.

Napier, J. R. and J. S. Weiner (1962). "Olduvai gorge and human origins." Antiquity **36**: 41-47.

Neelmeijer, C., I. Brissaud, et al. (2000). "Paintings - a challenge for XRF and PIXE analysis." X-ray Spectrometry(101-110).

Neelmeijer, C. and M. Mader (2002). "The merits of particle induced X-ray emission in revealing painting techniques." Nuclear Instruments and Methods in Physics Research **189**: 293-302.

Nel, P., D. Lau, et al. (2006). "Non-destructive micro-X-ray diffraction analysis of painted artefacts: Determination of detection limits for the chromium oxide-zinc oxide matrix." Nuclear Instruments and Methods in Physics Research B **251**: 489-495.

Nicholson, P. T. (2007). Brilliant things for Akhenaten production of glass, vitreous materials and pottery at Amarna site 045.1. Oxford, Egypt Exploration Society.

Nicolaus, K. (1998). The restoration of paintings. Cologne, Könemann.

Nicolaysen, K. P. and L. W. Ritterbush (2005). "Critical thinking in geology and archaeology: Interpreting scanning electron microscope images of a lithic tool." Journal of Geoscience Education **53**(2): 166-172.

Nyquist, R. and R. O'Kagel (1971). Infrared spectra of inorganic compounds (3800 - 45 cm-1). London, Academic Press Inc.

Oliveira, S. M. M. d., R. A. L. Imbernon, et al. (1996). "Mössbauer spectroscopic study of iron oxides and oxyhydroxides in gossans." Geoderma **73**: 245-256.

Ospitali, F., D. C. Smith, et al. (2006). "Preliminary investigations by Raman microscopy of prehistoric pigments in the wall-painted cave at Roucadour, Quercy, France." Journal of Raman Spectroscopy **37**: 1063-1071.

Osticioli, I., A. Zoppi, et al. (2006). "Fluorescence and Raman spectra on painting materials: reconstruction of spectra with mathematical methods." Journal of Raman Spectroscopy **37**: 974-980.

Pace, A. (2004). Insight heritage guides: The Hal Saflieni Hypogeum, Paola. Malta, Heritage Books.

Pages-Camagna, S. and T. Calligaro (2004). "Micro-PIXE and micro-Raman spectrometry applied to a polychrome wooden altarpiece from the 16th century." Journal of Raman Spectroscopy **35**: 633-639.

Palacio-Perez, E. (2010). "Cave art and the theory of art: The origins of the religious interpretation of palaeolithic graphic expression." Oxford journal of archaeology **29**(1): 1-14.

Paterson, E. and R. Swaffield (1980). "Influence of adsorbed anions on the dehydroxylation of synthetic goethite." Journal of Thermal Analysis **18** 161-167.

Pattan, J. N., N. J. G. Pearce, et al. (2005). "Constraints in using cerium-anomaly of bulk sediments as an indicator of paleo bottom water redox environment: A case study from the Central Indian Ocean Basin." Chemical Geology **221** 260–278.

Pedley, M., M. H. Clarke, et al. (2002). Limestone isles in a crystal sea: The geology of the Maltese islands. Malta, Publishers Enterprises Group (PEG) Ltd.

Perez, J. M. and R. Esteve-Tebar (2004). "Pigment identification in Greek pottery by Raman microspectroscopy." Archaeometry **46**: 607-614.

Petrie, F. (1894). Tell El Amarna. London, Methuen & Co.

Petrie, F. (1996). The arts and crafts of ancient Egypt. London, Bracken Books reprint.

Petru, S. (2006). "Red, black or white: The dawn of colour symbolism." Documenta Praehistorica **32** 203-208.

Pettijohn, F. J. (1975). Sedimentary rocks. USA, Harper & Row, Publishers, Inc.

Piper, D. Z. (1974). "Rare earth elements in the sedimentary cycle: a summary." Chemical Geology **14**: 285-304.

Pocock, R. W. (1942). Wartime pamphlet no.21 ochres, umbers and other natural earth pigments of England and Wales. Lonson Crown.

Pollard, M. and C. Heron (2008). Archaeological chemistry. Cambridge, RSC publishing.

Ponting, M. (2004). "The scanning electron microscope and the archaeologist." Physics Education **39**(2): 166-170.

Popelka-Filcoff, R. S. (2006). Applications of elemental analysis for archaeometric studies: Analytical and statistical methods for understanding geochemical trends in ceramics, ochre and obsidian. Columbia, University of Missouri. **Doctor of Chemistry**.

Popelka-Filcoff, R. S., E. J. Miksa, et al. (2008). "Model for iron mineralisation in the middleback iron formations of the Hutchison Group Centrex Metals Ltd, mineralisation model." Journal of Archaeological Science **35**.

Popelka-Filcoff, R. S., E. J. Miksa, et al. (2008). "Elemental analysis and characterization of ochre sources from Southern Arizona." Journal of Archaeological Science **35**(3): 752-762.

Popelka-Filcoff, R. S., J. D. Robertson, et al. (2007). "Trace element characterization of ochre from geological sources." Journal of Radioanalytical and Nuclear Chemistry **272**(1): 17–27.

Pradell, T., N. Salvado, et al. (2006). "Physical processes involved in production of the ancient pigment, Egyptian blue." J. Am. Ceram. Soc. **89**(4): 1426-1431.

Prasad, P. S. R., K. S. Prasad, et al. (2006). "In situ FTIR study on the dehydration of natural goethite." Journal of Asian Earth Sciences **27** 503–511.

Priori, S., E. A. C. Costantini, et al. (2008). "Pedostratigraphy of terra rossa and quaternary geological evolution of a lacustrine limestone plateau in central Italy." J. Plant Nutr. Soil Sci. **171**: 509-523.

Rampazzi, L., L. Campo, et al. (2007). "Prehistoric wall painting: the case of the Domus de Janas Necropolis (Sardinia, Italy)." Archaeometry **49**(3): 559–569.

Rapp, G. R. (2002). Archaeomineralogy. New York, Springer-Verlag.

Redford, D. B. (1992). Akhentaten: The heretic King Donald. Egypt, The American University in Cairo Press.

Rees, D. G. (2001). Essential statistics. USA, Chapman & Hall/CRC.

Reiche, I., R. Britzke, et al. (2005). "An external PIXE study: Mughal painting pigments." X-ray Spectrometry **34**: 42-45.

Reiche, I., L. Favre-Quattropani, et al. (1999). "Trace element composition of archaeological bones and post-mortem alteration in the burial environment." Nuclear Instruments and Methods in Physics Research B **150** 656-662.

Rendle, D. F. (2003). "X-Ray Diffraction in forensic science." The Rigaku Journal **20**(1): 11-22.

Ricci, C., I. Borgia, et al. (2004). "The Perugino's palette: integration of an extended *in situ* XRF study by Raman spectroscopy." Journal of Raman Spectroscopy **35**: 616-621.

Rikers, R. A., P. Rem, et al. (1998) Characterization of heavy metals in soil by high gradient magnetic separation. Soil and Sediment Contamination **Volume**, 163-190 DOI:

Robb, J. (2001). "Island identites: ritual, travel and the creation of a difference in Neolithic Malta." European Journal of Archaeology **4**(2): 175-202.

Robertson, A. H. F. and A. J. Fleet (1976). "The origins of rare earths in metalliferous sediments of the Troodos Massif, Cyprus." Earth and Planetary Science Letters **28** 385-394.

Robinson, D. (2004). The Mirror of the Sun: Surface, mineral applications and interface in California rock-art. Soils, Stones and Symbols: Cultural Perceptions of the Mineral World. N. Boivin and M. A. Owoc. London, UCL**:** 91-105.

Rogers, F. R. and M. A. Rogers (1985). Painting and poetry: form, metaphor, and the language of literature. London, Bucknell University Press.

Rohrs, S. and H. Stege (2004). "Analysis of Limoges painted enamels from the 16th to 19th centuries using a portable micro X-ray fluorescence spectrometer." X-ray Spectrometry **33**: 396-401.

Rosalie David, A., H. G. M. Edwards, et al. (2001). "Raman spectroscopic analysis of ancient Egyptian pigments." Archaeometry **43**: 461-473.

Rosi, F., A. Burnstock, et al. (2008). "A non-invasive XRF study supported by multivariate statistical analysis and reflectance FTIR to assess the composition of modern painting materials." Spectrochimica Acta Part A: Molecular and Biomolecular Spectroscopy: 1-8.

Rosi, F., C. Miliani, et al. (2004). "Identification of nineteenth century blue and green pigments by *in situ* X-ray fluorescence and micro-Raman spectroscopy." Journal of Raman Spectroscopy **35**: 610-615.

Rouessac, A. and F. Rouessac (2000). Chemical analysis: Modern instrumental methods and techniques. London, John Wiley & Sons.

Rull Perez, F., H. G. M. Edwards, et al. (1999). "Fourier transform Raman spectroscopic characterization of pigments in the medieval frescoes at Convento de la Peregrina, Sahagun, Leon, Spain. Part 1 - preliminary study." Journal of Raman Spectroscopy **30**: 301-305.

Ryan, K. M. and D. M. Williams (2007). "Testing the reliability of discrimination diagrams for determining the tectonic depositional environment of ancient sedimentary basins." Chemical Geology **242** 103–125.

Sackler, A. M. (2005). Scientific examination of art: Modern techniques in conservation and analysis. Washington, D.C., National Academy of Sciences.

Samek, L., J. Injuk, et al. (2002). "Performance of a new compact EDXRF spectrometer for aerosol analysis." X-ray Spectrometry **31**: 84-86.

Sammut, S. (2004). MALSIS (Maltese Soil Information System) soil geographic database of the Maltese islands. Malta, National Soil Unit, Ministry for Rural Affairs and the Environment.

Sammut, S. (2005). State of the environment report for Malta – Background report on soil. Malta, MEPA.

Sammut, S. (2006). State of the environment report sub-report 5: Soil Malta environment & planning authority (MEPA).

San Andres, M., M. I. Baez, et al. (1997). "Transmission electron microscopy applied to the study of works of art: sample preparation methodology and possible techniques." Journal of Microscopy **188**(1): 42-50.

Scalarone, D. and O. Chiantore (2004). "Separation techniques for the analysis of artists' acrylic emulsion paints." J. Sep. Sci. **27**: 263-274.

Scardova, S., P. P. Lottici, et al. (2002). "A study of the external coloration of historic buildings in Parma (Italy) and surroundings by micro-Raman technique." Studies in Conservation **47**: 24-28.

Schembri, P. J. (1993). Physical geography and ecology of the Maltese islands: A brief overview options Méditerranéennes, Sér. B / n°7. Malta, Food, Agriculture, Fisheries and the Environment.

Schmandt-Besserat, D. (1980). Ocher in prehistory: 300,000 years of the use of iron ores as pigments by from: The coming of the age of iron. T. A. Wertime and J. D. Muhly. USA, Yale University**:** 127-150.

Schwertmann, U. and R. M. Cornell (2000). Iron oxides in the laboratory: preparation and characterization. Weinheim, Wiley-VCH.

Schwertmann, U., J. Friedl, et al. (1999). "From Fe(III) ions to Ferrihydrite and then to hematite." Journal of Colloid and Interface Science **209**: 215–223.

Sciuti, S., G. Fronterotta, et al. (2001). "A non-destructive analytical study of a recently discovered Roman wall painting." Studies in Conservation **46**: 132-140.

Scott, D. A. (2001). "The application of scanning X-ray fluorescence microanalysis in the examination of cultural materials." Archaeometry **43**: 475-482.

Scott, W. B. (1921). An introduction to geology. USA, The Macmillan Company.

Shackley, M. (1982). "The case for Neanderthal survival: fact, fiction or faction?" Antiquity **56**: 31-41.

Silbilia, J. P. (1996). A guide to materials characterization and chemical analysis. New York, Wiley-VCH.

Singer, R. (1957). "Evolution and man." Antiquity **31**: 188-198.

Singh, M. and I. M. Low (2002). "Depth-profiling of phase composition and preferred orientation in a graded alumina/mullite/aluminium-titanate hybrid using X-ray and synchrotron radiation diffraction." Materials Research Bulletin **37**: 1279-1291.

Singh, M., I. M. Low, et al. (2002). "Depth profiling of a functionally graded alumina/calcium-hexaluminate composite using grazing incidence synchrotron-radiation diffraction." Journal of the European Ceramic Society **22**: 2877-2882.

Skoog, D. A., F. J. Holler, et al. (1998). Principles of instrumental analysis. USA, Thomson Learning.

Smith, B. C. (1996). Fundamentals of fourier transform infrared spectroscopy. USA, CRC Press, Inc.

Smith, D. C. and A. Barbet (1999). "A preliminary Raman microscopic exploration of pigments in wall paintings in the roman tomb discovered at Kertch, Ukraine, in 1891." Journal of Raman Spectroscopy **30**: 319-324.

Smith, G. D. and R. J. H. Clark (2001). "Raman microscopy in art history and conservation science." Reviews in Conservation **2**: 92-103.

Smith, G. D., A. Derbyshire, et al. (2002). "*In situ* spectroscopic detection of lead sulphide on a blackened manuscript illumination by Raman microscopy." Studies in Conservation **47**: 250-256.

Smith, M. A. and S. Pell (1997). "Oxygen-isotope ratios in quartz as indicators of the provenance of archaeological ochres." Journal of Archaeological Science **24**: 773–778.

Spratt, T. A. B. (1854). On the geology of Malta and Gozo. Whitefriars, Bradbury and Evans.

Stevens, D. T. (2005). State of the environment report - short note on soil biodiversity. Floriana, Malta, MEPA.

Stoye, D. and W. Freitag (1998). Paints, coatings and solvents Weinheim, Wiley-VCH.

Suzuki, E. M. and M. X. McDermot (2006). "Infrared spectra of U.S. automobile original finishes. VII. Extended range FT-IR and XRF analyses of inorganic pigments *In Situ* - nickel titanate and chrome titanate." J Forensic Sci **51**(3): 532-546.

Szokefalvi-Nagy, Z., I. Demeter, et al. (2004). "Non-destructive XRF analysis of paintings." Nuclear Instruments and Methods in Physics Research **226**: 53-59.

Taçon, P. (2004). Ochre, clay, stone and art: The symbolic importance of minerals as life-force among aboriginal peoples of northern and central Australia. Soils, Stones and Symbols: Cultural Perceptions of the Mineral World. N. Boivin and M. A. Owoc. London, UCL**:** 31-42.

Thompson, D. V. (1956). The materials and technique of medieval painting. New York, Dover Publications.

Thorne, W. S., S. G. Hagemann, et al. (2006). "Hydrothermal alteration zonation and fluid chemistry of the southern ridge and north deposits at Mt Tom Price." Applied Earth Science **115**(4): 152-160.

Tilley, R. J. D. (2006). Crystals and crystal structures. Chichester, John Wiley & Sons Ltd.

Towell, D. G., R. V. Spirn, et al. (1969). "Europium anomalies and the generation of basalt: a discussion." Chem. Geol. **4** 461-465.

Trump, D. H. (2008). Malta prehistory and temples. Malta, Middlesea Books Ltd.

Trzeinska, B. (2006). "Classification of black powder toners on the basis of Integrated analytical information provided by fourier transform infrared spectrommetry and X-ray fluorescence spectrometry." J Forensic Sci **51**(4): 919-924.

Tucker, M. E. (2001). Sedimentary petrology: An introduction to the origin of sedimentary rocks. Oxford, Wiley-Blackwell.

Uda, M., G. Demortier, et al. (2005). X-rays for archaeology. The Netherlands, Springer.

Vallance, S. L. (1997). "Applications of chromatography in art conservation: Techniques used for the analysis and identification of proteinaceous and gum binding media." The Analyst **122**: 75R-81R.

van der Weerd, J., R. M. A. Heeren, et al. (2004). "Preparation methods and accessories for the infrared spectroscopic analysis of multi-layer paint films." Studies in Conservation **49**: 193-210.

van der Weerd, J., A. van Loon, et al. (2005). "FTIR Studies of the effects of pigments on the aging of oil." Studies in Conservation **50**: 3-22.

Vandenabeele, P. (2004). "Raman spectroscopy in art and archaeology." Journal of Raman Spectroscopy **35**: 607-609.

Vannucci, S., G. Alessandrini, et al. (1994). La conservazione dei monumenti nel bacino del Mediterraneo: Atti del terzo simposio internazionale. Prehistoric megalithic temples of the Maltese Archipelago: causes and mode of deterioration of Globigerina Limestone. V. Fassina. Venezia

van-San, E., E. D. Grave, et al. (2001). "Study of Al-substituted hematites prepared from the thermal treatment of lepidocrocite." Phys. Chem. Minerals **28**: 488-497.

Vassallo, B. (2007). Prehistoric Malta, Europe and Noth Africa. Prehistoric remains of Malta and Gozo, Europe, Anatolia and North Africa. Malta, Allied Publications Limited.

Wachowicz, E. and A. Kiejna (2008). "Effect of impurities on grain boundary cohesion in bcc iron." Computational Materials Science.

Wadley, L., B. Williamson, et al. (2003). "Ochre in hafting in middle Stone Age southern Africa: a practical role." Antiquity **78**(301): 661-675.

Walter, D. (2006). "Characterization of synthetic hydrous hematite pigments." Thermochimica Acta **445** 195–199.

Walter, D., G. Buxbaum, et al. (2001). "The mechanism of the thermal transformation from goethite to hematite." Journal of Thermal Analysis and Calorimetry **63**: 733-748.

Wang, Q. and K. C. Andrews (2002). "Technological investigation of the decorative coatings on Yangshao pottery from Henan, China." Archaeometry **44**(2): 241-250.

Wang, X., Q. Wang, et al. (2004). "Study of wall-painting pigments from Feng Hui Tomb by Raman spectroscopy and high-resolution electron microscopy." Journal of Raman Spectroscopy **35**: 274-278.

Watari, F., P. Delavignette, et al. (1983). "Electron microscopic study of dehydration transformation. Part III: High resolution observation of the reaction process FeOOH-Fe2O3." Journal of Solid State Chemistry **29**: 49–64.

Watterson, B. (1999). Amarna, ancient Egypt's age of revolution. U.K., Tempus Publishing Inc.

Weber, G., L. Martinot, et al. (2005). "Application of PIXE and PIGE under variable ion beam incident angle to several fields of archaeometry." X-ray Spectrometry **34**: 297-300.

Weihe, H., S. Piligkos, et al. (2009). "EPR of Mn2+ impurities in calcite: a detailed study pertinent to marble provenance determination." Archaeometry **51**(1): 43–48.

Weis, T. L., Y. Jiang, et al. (2004). "Toward the comprehensive spectrochemical imaging of painted works of art: a new instrumental approach." Journal of Raman Spectroscopy **35**: 813-818.

West, J. C. (1975). "Examination of paint smears on clothing by X-ray fluorescence spectrometry." X-ray Spectrometry **4**: 71-73.

Wolska, E. and U. Schwertmann (1989). "Nonstoichiometric structures during dehydroxylation of goethite." Zeitschrift für Kristallographie **189**: 69-75.

Wreschner, E. E. (1976). "The red hunters: Further thoughts on the evolution of speech." Current Anthropology **17**(4): 717-719.

Wreschner, E. E. (1980). "Red ochre and human evolution: A case for discussion." Current Anthropology **21**(5): 631-644.

Zammit, T. (1925). The Hal-Saflieni Hypogeum: A short description with plan illustrations. Malta.

Zammit-Maempel, G. (1977). An outline of Maltese geology and a guide to the geology hall of the National Museum of Natural History Mdina, Malta. Malta Unknown Binding.

Zhua, J., J. Shana, et al. (2004). "The multivariate statistical analysis and XRD analysis of pottery at Xigongqiao site." Journal of Archaeological Science **31**: 1685-1691.

Zuo, J., C. Xu, et al. (1999). "Identification of the pigment in painted pottery from the Xishan site by Raman microscopy." Journal of Raman Spectroscopy **30**: 1053-1055.